ALMA MATER STUDIORUM - UNIVERSITÀ DI BOLOGNA

DOTTORATO DI RICERCA IN
BENI CULTURALI E AMBIENTALI

CICLO 34

SETTORE CONCORSUALE: 03/A1 - CHIMICA ANALITICA

SETTORE SCIENTIFICO DISCIPLINARE: CHIM/12 - CHIMICA DELL'AMBIENTE E DEI BENI CULTURALI

RICORDACI: RESEARCH ON THE CONSERVATION, RESTORATION AND DIAGNOSIS OF CINEMATOGRAPHIC FILMS

PRESENTATA DA: MARCO VALENTE CHAVEZ LOZANO

COORDINATORE DOTTORATO
ROBERTO PASINI

SUPERVISORE
SILVIA PRATI

CO-SUPERVISORI
ROCCO MAZZEO
GIORGIA SCIUTTO
CHIARA SAMORÌ
MARIANNA DE SANCTIS

ESAME FINALE ANNO 2022

Gracias – Thank you

A mi familia, que nuevamente son la hermosa compañía con quien comparto la travesía de esta vida: mis amados Magali, Valente, Bruno y Franco, que aún en la distancia mantienen fuerte la cercanía interna, por su ayuda, admiración y cariño. Gracias de nuevo a mis tíos, primos y sobrinos de todo el clan Lozano.

***

Thank you my brothers in Ravenna, Luca and Agnese, and your families, who so often have opened your hearts and doors to a Mexican stranger to delight in your wonderful Microcosmos. You both remain my second family and your company has been a light to keep me smiling and sharing, learning and growing.

To Arianna, Francesca, Lucrezia, Zelan, Zoreh, Amelia, for being the best colleagues and friends I could have shared the worktime with. The laughs and all the lessons I got from your company are worth as gold. Thank you also to all the Master's students who came under my supervision and collaborated with the RICORDACI project; you have offered this work your great skills and ideas to help perfecting the final product.

To Salvatore and Gianluca. For your constant and faithful friendship, laughs and lightness; your constant presence and your warmth have made my life in Ravenna very fun.

To Bianca, Graziano, Dajana, Chiara, Oliver, Jan, Marco, Giulia, etc., and all whom I have loved during these three years; as well as the dear friends and more than friends. Even if not all have remained and some are far, your presence or passing through my life has added something of value; be it kindness, love, friendship or facing all those negative emotions that helped me grow, believe in myself, overcome obstacles and learn from my mistakes. I keep inside me a bit of you.

Finally, I thank the people of Italy, for giving me so much.

Abstract

This thesis is the result of the RICORDACI project, a three-year European-funded initiative which involved the collaboration between the University of Bologna and the restoration laboratory of the Cineteca di Bologna, *L'immagine Ritrovata* s.r.l, which aimed to find innovative solutions for the preservation of cinematographic film heritage.

Film conservation differs from the requirements of other types of cultural heritage, as it is mainly focused on guaranteeing the preservation of the content recorded on the film and ensuring its fruition. This is often hindered by the intrinsic instability of the filmic supports, in particular the cellulose derivatives employed as polymeric bases.

The physical-chemical decay of the cellulose acetate (CA) and cellulose nitrate (CN) polymeric film bases follow similar autocatalytic processes. In both cases, deformation and mechanical instability affects the film, and degradation leads to deposition of unwanted substances on the film surface, making it difficult or even impossible to unwind and digitize the affected rolls. In addition, degradation acts in the emulsions that contain the image, which becomes increasingly altered, and the image is eventually lost.
These three years of research have led to the development of new methods and technologies for the preservation of cinema films. In particular, this thesis presents the development of new analytical methodologies to exploit two types of portable miniaturized Near Infrared spectrometers working in Diffuse Reflectance mode over the Short Wave Infrared (SWIR) range, to study the near infrared (NIR) spectral behavior of film base materials for an accurate, non-invasive and fast characterization of the polymer type; and for films with cellulose acetate supports, they can be employed as a diagnostic tool for monitoring the Degree of substitution (DS) affected by the loss of acetyl groups. The proposed methods offer non-invasive, fast, inexpensive and simple alternatives for the characterization and diagnosis of film bases to help the strategic planning and decision-making regarding storage, digitalization and intervention of film collections.

Secondly, the text includes the evaluation of new green cleaning systems and solvents for the effective, fast and innocuous removal of undesired substances from degraded cinematographic films bases; these tests compared the efficiency of traditional systems and solvents against the new proposals. Firstly, the use of Deep Eutectic Solvent formulations for removing softened gelatin residues from cellulose nitrate bases, and secondly; the employment of green volatile solvents with different application methods, including the use of a new electrospun nylon mats, for avoiding the dangerous use of friction for the removal of Triphenyl Phosphate crystal blooms from the surface of cellulose acetate bases.
The research on cleaning involved the employment of Fourier Transform Infrared Spectroscopy (FTIR), Optical microscopy for sample surface documentation and cross section observation. The results obtained will help improving the efficiency of the interventions needed before the digitalization of historical cinematographic films and will pave the way for further investigation on the use of green solvents for cleaning polymeric heritage objects.
The text also includes a review of the analytical precedents on the study of cinematographic films,

focusing around the basic notions of film history, technical advances, materials and stratigraphic structure of cinematographic films, and the chemical characteristics of film materials, addressing in particular the emulsion, polymeric bases and their additives, as well as their degradation processes.

Keywords: Cinematographic film conservation and restoration, Near Infrared Spectroscopy (NIR), Short-Wave Infrared (SWIR), calibration function, Degree of Substitution (DS), Optical Microscopy, µATR-FTIR, Triphenyl Phosphate (TPP), plasticizer bloom cleaning, gelatin cleaning, cellulose derivatives, Cellulose Acetate (CA), Cellulose Nitrate (CN), Deep Eutectic Solvents (DES), electrospun nylon mats, Green Solvents, Conservation Science, Cultural Heritage.

Contents

Part I: *Precedents and state of the art*

Chapter 1 Photographic film: A historical background

A review of the history, technical developments and chemical processes that brought about modern photography is presented here, aiming to provide a minimal background that allows to adequately understand how photographic film materials were invented and successively improved, making emphasis on cinematographic film, its constitutive materials, structure and photochemical processing.

1.1 The invention of cameras and projection devices

Cinematographic film owes itself to still photography, its immediate predecessor. Photography as a concept traces its roots back to the invention of the *Camera oscura*, an ingenious device which first allowed to project an image of its surroundings onto the flat surface of a dark inner environment. The origins of the *camera oscura* can be dated back as far as 1000 d.C. With time, the instrument was provided with optical lenses and filters to focus, straighten and reflect the image, and it became smaller and more practical.

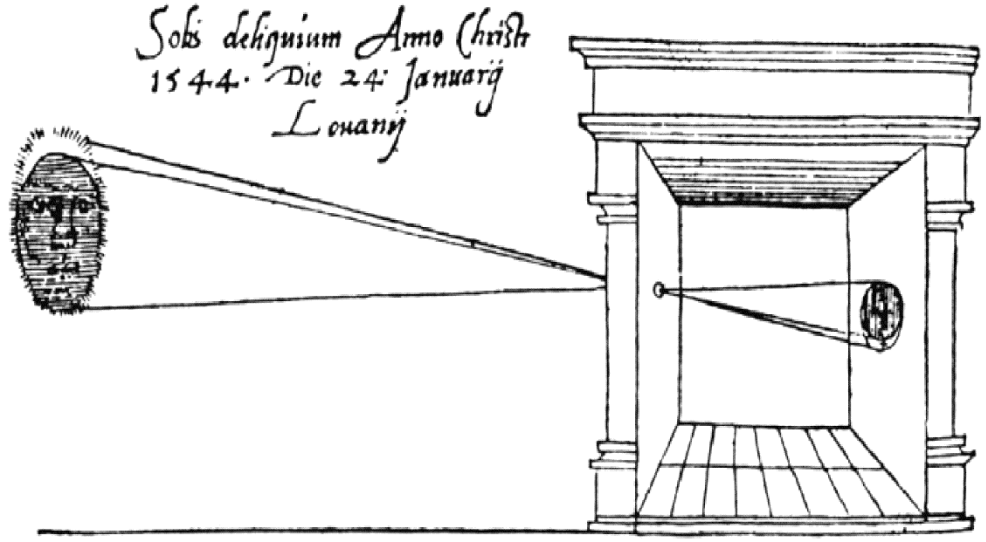

Fig. 1. Illustration a *Camera oscura* in Gemma Frisius, *De radio astronomico et geometrico liber*, 1554, collection of the National Science and Media Museum; reproduced by Silverman, 2015[1].

In 1646, German mathematician Athanasius Kircher published the *Ars Magna Lucis et Umbrae* ("The Great Art of Light and Shadow"[2]), which laid the foundation for the invention of the “magic lantern”, a small optical system which allowed to project images on transparent glass plates, using a light source and one or more lenses. These precedents would lend inspiration to the Lumière brothers three centuries later for their invention of the first cinematographic film projector and the conduction of the first commercial public screening on December 28th, 1895, thus marking the birth of cinema as we know it[3].

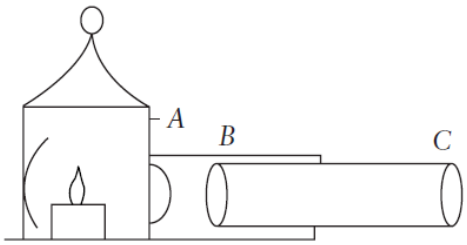

Fig. 2. Edited version of the first sketch of a magic lantern, in a letter by Petit in a letter to Huygens (28th November 1662), included in *Oeuvres complétes de Christiaan Huygens*, La Haye, 1880–1950, iv,p. 269 Koninklijke Hollandsche Maatschappij der Wetenschappen. The light of a candle is intensified by the concave mirror; the tube (BC) with two convex lenses magnifies the picture painted on a slide (A). Reproduced by Vermeir, 2005[4].

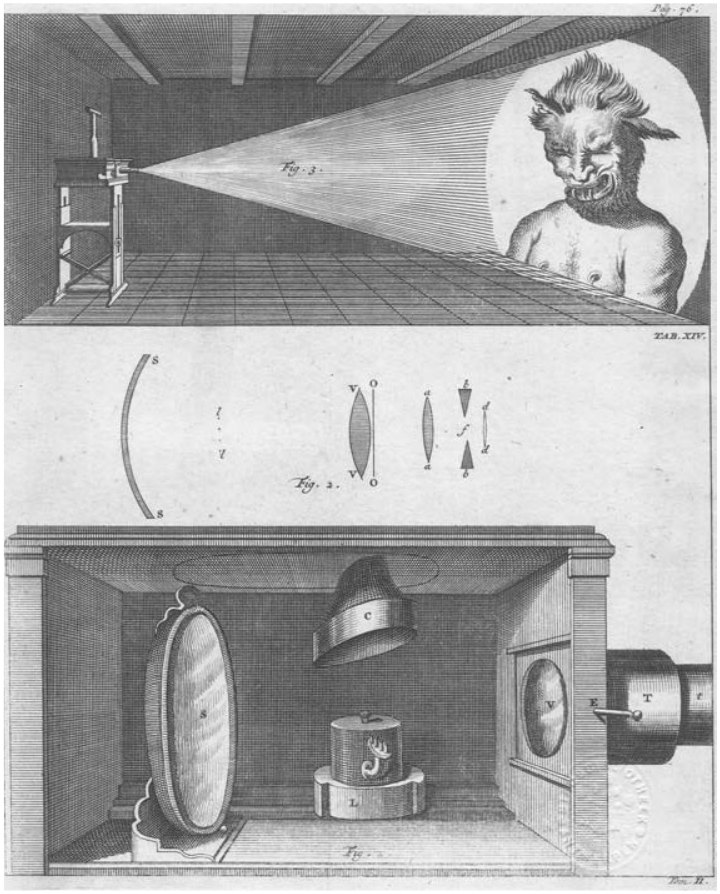

Fig. 3. Illustration of a magic lantern in W. J. S. van Gravesande, *Physices elementa mathematica, experimenta confirmata,* 2 tomes in 1 vol., Leyden, 1721–5, ii, 76 (Plate 14). Collection: Stadsbibliotheek Antwerpen. Reproduced by Vermeir, 2005[4].

1.2 Image recording materials and emulsions

Besides the invention of cameras and projectors, cinema and photography depended on the technical improvements that allowed to record the resulting light image. Until the 17th century, the projected images had to be drawn and painted manually (e.g., Vermeer most likely painted the imaged produced with a *camera oscura*[5]). This changed when in 1827 French lithographer Joseph Niépce (1765-1833) invented heliography, a term that derives from Greek ήλιος (*hēlios*) «sun» and

γραφέιν (graphéin) «to draw»[6], [7], which refers to the use of asphalt bitumen to print a light image. However, Niépce's first recorded required an eight-hour exposition.
Upon the discovery of photosensitive materials, such as silver chloride (AgCl) and silver nitrite ($AgNO_3$), and following the collaboration between Niépce and painter Jacques Louis Mande Daguerre (1787-1851), led the later to create in 1837 a more practical photographic system, the *daguerreotype*[7], which allowed to register images on silver-coated cupper plates previously exposed to iodium vapors. The *daguerreotype* dramatically reduced the required exposure times to only 20 minutes, and it required final treatments with mercury vapors and an immersion in a sodium chloride solution to fix the image.

Daguerreotypes created single, non-reproducible and unstable images. The stabilizing of the image over time was possible only after Sir John Herschel, an English chemist, applied a "fixing" Sodium hyposulfite (Na_2SO_2) to eliminate the remaining unexposed silver salts.
Finally, William Henry Fox Talbot (1800-1877) became aware of the existence of the latent image[8], and invented *calothopy*, from Greek καλός (kalòs) «fair», the first photographic developing method as it is understood nowadays, through a technique that included the immersion of a paper sheet in a silver nitrate ($AgNO_3$), potassium iodide (KI), acetic acid (CH_3COOH) and gallic acid ($C_6H_2(OH)_3COOH$) solution. The sheet thus prepared had to be exposed for a few minutes and then fixed by immersion in Sodium hyposulfite (Na_2SO_2) (Figure 1.3.1), which rendered a negative image capable of being indefinitely reproduced into positive prints. It was during this period that the term *photography,* likely coined by John Herschel[3], became widely diffused. It comes from the Greek vocables φώς, φότος (phòs, phòtos) «light» and γράφειν (graphéin) «to draw».

It was from the second half of the nineteenth century onwards that photography was greatly developed; Talbot's method was perfected, the waxed paper negative was invented, and new photosensitive supports were diffused, including salt paper, albuminate paper and collodion, a suspension of photosensitive silver salts suspended in a nitrocellulose matrix over glass slides, which could then be exposed. This last method allowed to reduce exposure times and costs respect to previous techniques[3], and it stayed in fashion from 1850 to 1880, when it was finally substituted by modern photographic emulsions, created by a mixture of silver halides suspended in an animal gelatin matrix.
The first successful attempt to produce a dry photosensitive gelatin emulsion was by Richard L. Maddox in 1871[9], consisting on a mix of silver bromide (AgBr) salts suspended in animal gelatin, which was then applied over glass supports and developed with pyrogallic acid ($C_6H_3(OH)_3$).

1.3 Employment of flexible polymeric films as photographic bases

Glass was used as support for photographic materials until 1889, when transparent and thin polymeric sheets were employed for the first time as base for industrial photographic negatives upon which the image-forming emulsion is coated, due to the advantageous flexibility and mechanical resistance of film respect to glass[3]; it is from these that modern-day photographic films are derived.
Photographic images supported on a flexible polymeric film revolutionized the way and ease in

which the world could be recorded[7]. A mere 14 years later, the invention of continuous film rolls allowed to register not only still images, but also motion by means of a continuous sequence of photographic images; such was the birth of cinematographic motion film.

In particular, different polymers have been employed throughout history to create flexible film bases. Chronologically, Cellulose derivates were used first, with Cellulose Nitrate (CN) being preferred during the first years of motion film production, going roughly from 1889 to 1951[10], [11].

The production of CN films was possible thanks to the discovery of camphor-plasticized CN, a mixture known as celluloid, first synthesized in 1869 by John Wesley Hyatt (1837-1920)[12]. The first photographic film over this kind of support was produced by Hannibal Goodwin (1822-1900), who registered a patent in 1887[7], [13], [14]. It was over this kind of film that George Eastman, founder of the Kodak company, created the first black and white film.
However, it was quickly acknowledged that CN supports were highly flammable; and their emissions of NO_2, noncombustible in itself, accelerates however the burning of combustible materials.
Even if CN films continued to be used until 1950, alternatives were sought for in the meanwhile in order to overcome the flammability hazard. At the beginning of 1909, new and less flammable cellulosic polymer films were introduced: Cellulose Acetate (CA) film bases, called “safety film” in the photographic industry, came into use since 1923 and (in the case of Cellulose Triacetate, CTA) they are still in use today. These included Cellulose Diacetate, Cellulose Acetate Propionate, Cellulose Acetate Butyrate, and since 1940, also Cellulose Triacetate (CTA)[7], [15], which has >2.7 acetylations per monomer unit, being also more soluble in organic solvents such as chloroform ($CHCl_3$) and dichloromethate (CH_2Cl_2)[16], and for its properties it has been adopted as the acetate derivative of choice for professional film bases throughout history[17]. Even if the employment of different CA species as film base overlapped over the years, CTA dominated the photographic film market from 1950 onwards, and still is the predilected base material for film negatives[18].
Lastly, since 1955 and especially after the 90’s[7], [15], [19], Polyethylene Terephthalate (PET) came into scene as a safer and more resistant film base than cellulose derivates, and is used particularly for print distribution copies and intermediate elements. In comparison to cellulose nitrate and cellulose acetate films, PET has as the advantage of permitting the manufacture of thinner films due to its superior tear resistance, flexibility, chemical and dimensional stability[7].
Polyethylene terephthalate films can be prepared by catalytic ester interchange reaction between dimethyl terephthalate and ethylene glycol, followed by catalytic polymerization under vacuum of the resulting dihydroxyethylene terephthalate monomer; and the final polymer is then cast as a film.

Chapter 2 Photographic film: Stratigraphy

Historic photographic negatives and cinematographic film technologies are very varied and their stratigraphy may be complex; however, the layout of film materials (Figures 4 and 5) always include a thick, transparent and flexible polymeric base coated with the film emulsion. The emulsion is the

layer employed to record the image, and in already developed films it consists of a colloidal suspension of dark silver particles and color dyes (if the film was colored), fixed in a matrix of photographic-grade gelatin[20]. Sometimes, a thin intermediate adhesive or “subbing” layer was applied to guarantee the adhesion between the emulsion and the polymeric base. Thin filters and coatings may be present between or above the aforementioned layers.

Fig. 4.- Black and White (B&W) developed film stratigraphy. 1) Protective overcoat or UV filter, 2) Gelatin and silver particle emulsion, 3) Antihalation layer, 4) “Subbing” adhesive layer, 5) Cellulose ester film base and 6) Anticurl layer[21].

Fig 5.- Chromogenic tripack color film stratigraphy after development. 1) Protective overcoat or UV filter, 2) Blue-sensitive layer of the emulsion (containing yellow dye), 3) Blue radiation filter, 4) Green-sensitive layer of the emulsion (containing magenta dye), 5) Red-sensitive layer of the emulsion (containing cyan dye), 6) Antihalation layer, 7) "Subbing" adhesive layer, 8) Cellulose ester film base and 9) Anticurl layer[21].

Photographic films are constituted by a particular stratigraphy. As portrayed in Figure 2.1, the most common layers are, from the top to the bottom, the gelatin emulsion layer, the so-called subbing layer, the polymeric support and the anticurl and antihalation layers.

Among the group of thinner secondary layers, anti-curl layers can be found on the back of the polymeric film, they are usually composed of gelatin and seek to prevent film deformation by counteracting the mechanical efforts exerted by the different layers upon humidity changes. Anti-halation layers instead can be found either below the emulsion or coated over the back side of the polymeric base. Antihalation layers are made of gelatin matrix containing instead color compounds (e.g., acid fuchsine or malachite) which prevent light to be reflected during exposure, thus blocking the creation of haloes in the image.

Finally, subbing layers consist in a thin overcoat whose function is to adhere the emulsion to cellulose acetate bases. Little information may be found regarding the materials used for subbing; and these include the use of a mixture of gelatin, cellulose acetate, cellulose nitrate and a solvent[22], [23]. Ciliberto et al.[15] reports that emissions of emissions of nitrostyrene from a positive B&N cinematographic CA film sample are due to this layer. No studies seem to have been publishing on the characterization of subbing layers, which from stratigraphic observation are not always present in films.

2.1 Photographic gelatin emulsions

The emulsion layers are constituted of a gelatin matrix. In the case of black and white films, this matrix contains silver halide particles, which are light-sensible and allow to record the image[15]. Instead, in most recent photographic color films, emulsions are often divided in three different gelatin sublayers containing a suspension of silver halide crystals together with yellow, magenta and cyan dye precursors respectively.

Most of the time, photographic gelatin corresponds to alkaline or type-B gelatin, which is produced from alkaline treatment of demineralized cattle bone, ossein[24]. Ossein is mostly made up of type I collagen, an heterotrimer collagen formed by three polypeptide chains, two α1(I) chains and one α2(I) chain, associated in a triple helix configuration except for the short non-helical terminal regions. The three strands are united by a ladder of intermolecular backbone N H···O C hydrogen bonds links, occurring transversally to the helical axis[25]. Both types of sub α-chain follow a repetitive Gly-X-Y sequence, in which every third amino acid position is occupied by a glycine residue (Gly) and the X and Y positions are preferentially occupied by imino acids proline (Pro) or 4-hydroxyproline (Hyp) (Figure 6), differing slightly in the amino acid distribution occurring at such positions[25].

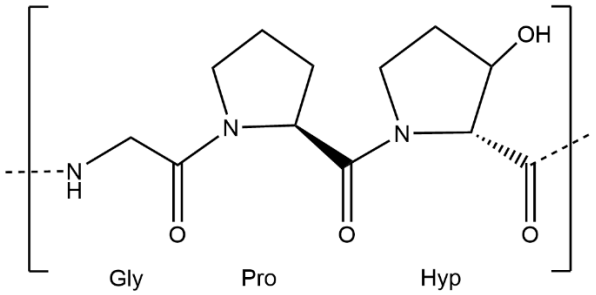

Fig. 6. Schematic representation of the preferred amino acid triplet sequence Gly-X-Y along the α-chains in collagen and gelatin, with the scheme showing as example Proline and Hydroxyproline at the X and Y positions.

Having a tendency for polar and non-polar residues to be distributed distinctly along the chain, collagen has differential hydrophobic and hydrophilic regions[24]. Intermolecular covalent cross-linking between neighboring lysine (Lys) or hydroxylysine (Hyl) residues in terminal telopeptides or along the helix stabilize and render parent collagen chains insoluble in water[24].

Through the hydrated lime slurry treatment, type-B gelatin is produced from parent collagen by destroying the crosslinking between collagen strands, making it soluble and purifying it from unwanted components also found in bones, such as mucopolysaccharides and non-collagenous proteins such as albumin and globulin[24].

This process also denatures the triple helix, causing the hydrolysis of some of the peptide bonds in collagen, so the superhelical structure and further supramolecular structures are destroyed, retaining only the primary amino acid sequence of the α-chains and the secondary structures of α-helices and random-coil fragments, which become organized as unordered single strands[25], [26], [27]. However, gelatin has the unique capacity for a limited renaturation of the collagen-like triple helices under certain conditions and gel formation[27].

Photographic gelatin should have high gelling power and viscosity, obtained through a high average molecular weight, being a mixture of polypeptide/polymer chains with very large macromolecules of different molecular weights: The major fraction is in the region of 100 000 g mol^{-1}, which corresponds to the intact polypeptide α-1 and α-2 chains (ca. 100 000 Da); this is accompanied by their fragments and oligomers found covalently cross-linked in doublets and triplets, called β- (ca. 200 000 Da) and γ-chains respectively (ca. 300 000 Da) [27], [28], as well as by bigger, more complex and branched oligomers made of five, eight or more α-chain units, which may surpass the 400 000 Da[29] [24]. Oligomers of three α-chains tend to be found as intact triple helices, but a certain amount exist as extended α-polymers bonded randomly by end-to-end or side-to-side bonds.

Gelatins have roughly the same amino acid composition as the parent collagen, thus a high content of Gly (33%) and imino acids Pro and Hyp (22%)[24]. However, the alkali treatment causes type-B gelatin to contain more acidic than basic groups in its molecule[30], as it partially hydrolyses many of the original amide groups of asparagine (Asn) and glutamine (Gln) in the protein by releasing ammonia. These reactions increase the content of aspartic acid (Asp) and glutamic acid (Glu), and increase the number of carboxyl groups. Furthermore, in more prolonged treatments a slow rate Conversion of arginine (Arg) into ornithine occurs by removal of an urea group from the Arg side-chain. Both processes result in an overall decrease in amide-nitrogen content, which lowers the isoelectric point to a range of pH from 4.7 to 5.6[28] or narrower[24], [22], at which the gelatin

molecule is most tightly coiled because of the equal number of charge attractions, being the least soluble in water[30].
Furthermore, type-B gelatin is characterized by containing lower amounts of aromatic, sulfur-bond forming and other trace amino acids than the parent collagen, such as sulfur-containing cysteine (Cys), hydrophobic tyrosine (Tyr), leucine (Leu), phenylalanine (Phe), isoleucine (Ile), polar serine (Ser), etc., as they are lost during cross-link cleavage[31], [32].
Overall, the presence of both basic amino groups and acidic hydroxy and carboxylic acid groups account for most of the water solubility of gelatin, as well as for its amphoteric properties[30]. However, it is important to consider that gelatin emulsions were commonly hardened by application of cross-linkers agents to the melted emulsion immediately before it was coated to the polymeric base. These agents react with gelatin through various mechanisms analogous to those occurring during the tanning of hides into leather, causing cross-linking between the amino acid chains of gelatin, thus increasing its viscosity and its resistance to swelling and solubilization in water[22], [33], [34]. Inorganic hardeners include metal cations of chromium[24], aluminum and iron, which create stable chromium/carboxyl cross-links. Organic hardeners include many compound families, such as aldehydes (formaldehyde in the first place), acetaldehydes, propionaldehydes, phenolic compounds (which form irreversible C-N or C-S bonds with amino or sulfhydryl groups of the protein structure, or the intermediate formation of resonance-stabilized free radicals, which can then react with Tyr, Lys and Cys residues) such as tannic acid, catechin and gallic acid; ketones, etc.[28].

2.1.1 Modern black and white emulsions

All cinematographic films possess an image-holding emulsion layer, coated over the supporting polymeric base. In both color and black and white modern film emulsions, this gelatin emulsion always contains photosensitive silver halides AgI, AgBr and AgCl, naturally sensitive to the UV and blue region of the electromagnetic spectrum, and sensitized to register lower wavelengths by the addition of dye sensitizers, such as chalcocarbocyanines and merocyanines, so image can be registered by exposing them to light[22], [35].
The silver halide crystals which are hit by photons create what is known as the “latent image”, undistinguishable to the naked eye, so further on, the film is subjected to a “developing bath”, which has the main objective of gradually reducing the exposed silver halide grains into dark metallic silver particles, rendering the image visible.

This developing bath is an aqueous solution containing as most important solute the developer agent. This developer donates electrons to the silver ions, becoming itself oxidized, and the silver becoming metallic. There is a small variety of classes of organic substances which have historical importance as developers (Figure 7); mainly t-hydroquinone, catechol, pyrogallol, p-aminophenol and its derivatives, as well as p-phenyl diamine and its derivatives[17].

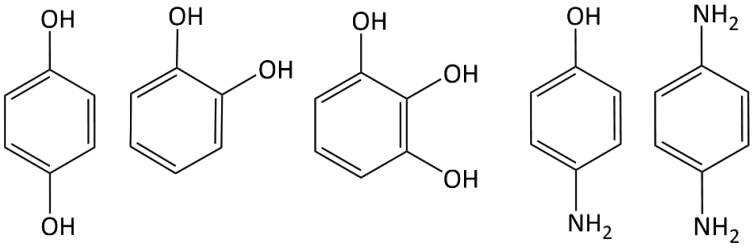

Fig. 7. Classical organic developing agents: t-hydroquinone, catechol, pyrogallol, p-aminophenol, and p-phenyl diamine.

The phenolic developing substances derived from the first four basic structures had been abandoned from 1975 onwards in favor of toluenediamines, due to the increasing international standardization in photographic technologies, (which would give rise to common commercial developing processes known as CD3 and CD4 processes), but before this period phenolic substances were commonly employed as film developers[22], [35].
Unreacted developers and their oxidized products are rinsed away from the film by successive processing baths.

2.1.2 Color emulsions: chromogenic tripack emulsions and dye couplers

In the beginning, color was in achieved by treating black and white films by hand or stencil coloring, as well as by chemical treatment of the exposed emulsion, including toning and tinting processes. It was only later that photographic emulsions started to be produced with separate sublayers containing different dye precursors in addition to the photosensitive silver halide crystals, which are at the base of modern “Integral chromogenic tripack” emulsions, the most popular and diffused color film emulsion technology, based in chromogenic processes for dye formation[36].
In films possessing this structure, the emulsion is divided in three layers (See layers 2, 4 and 5 in Fig. 5), each of which contains silver halide particles, sensitized to a particular region of the visible spectrum (blue, green or red, according to the layer), and each one of these layers contains also a different dye precursor or “coupler” suspended in the gelatin. Upon exposure, the silver halides in each one of these three sub-layers register a latent image corresponding to only one particular light color frequency, which can then be developed into dark metallic silver by the developing bath as previously described.
After the developing reaction, the now-oxidized developer agent (present only in the areas of previously-exposed halide crystals, now reduced into metallic silver), can then react with the color coupler in each layer, producing the final yellow, magenta or cyan color dyes, whose concentration is proportional to the original latent image density. In general, in tripack emulsions the dark silver particles get “bleached” away after dye formation by dissolving them in successive baths, leaving in the emulsion only the color dye clouds, which are then the sole responsible of producing the final image by color subtractive addition.
Dye coupler substances possess a wide structural variety, but share in all cases the presence of active methylene or methane groups. Common final dye families[37]–[39] are indamines, indophenols, indoanilienes (including yellow acylacetanilide dyes and 1-hyroxy-2naphthamide cyan dyes) and azomethines (including magenta cyclic chain pyrazolone dyes, created by a coupler with active methylene compounds into an open or cyclic chain); the last two groups were the most relevant

couplers since the 60’s onwards. There are many structural possibilities for any of these three dye types, as much as charge location exist[35].

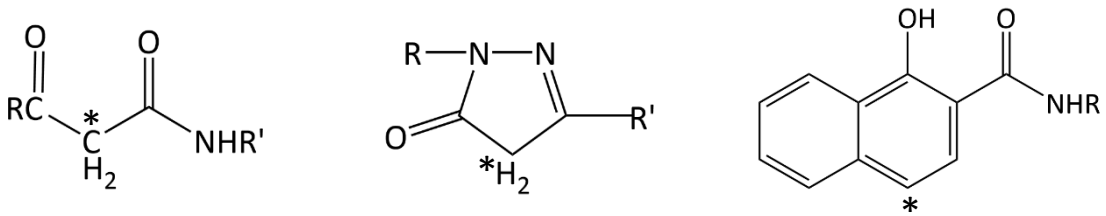

Fig. 8. Generic structures of photographic couplers: (for yellow dye formation), Pyrazolone (for magenta dye formation) and 1-Hydroxy-2-napthamides (for cyan dye formation).

In tripack films, dyes had to be immobilized into each one of the three emulsion sublayers in order to prevent them to be washed away or to pass from one sublayer into another; this was sometimes achieved by the increase in molecular rigidity of the final dye in respect to the dimension of its precursors. More often however, immobilization was ensured by a right balance in hydrosolubility, adjusted by including hydrophilic substitute groups (such as -COOH and -HSO_3) in the dye molecule, as well as by the presence of hydrophobic oily ballasting substances (usually hydrocarbons of 12 to 18 carbon length), thus ensuring the non-diffusivity of the dye through the swollen gelatin layers during aqueous bath processing[22].

Chapter 3 Physicochemical characteristics of cellulosic materials employed as photographic bases

Physicochemical properties of cellulose are briefly reviewed here, to help understand the characteristics of the derivates used as film bases.

3.1 Cellulose

Cellulose, a linear polysaccharide, is a chiral homopolymer composed by repeating D-anhydro glucose (D-anhydroglucopyranose) monomeric units, which assume a chair conformation, and are linked one to the next after a 180° rotation through a β-1,4, glycosidic bond. This conformation allows to minimize steric repulsion. Cellulose is insoluble in both water and main organic solvents, with the exception of some ionic liquids.
Further properties such as the degree of polymerization (DP, the term that describes the length of the polymeric chain)[40] depend on the source an extraction process. Cellulose is mainly obtained from wood and cotton pulp primary sources[40]–[42], being the most abundant biopolymer on earth, renewable and biodegradable. Cellulose extracted from natural sources has a DP ranging from 100 to 1000 units depending on the source and extracting method[43].

In cellulose, each polymeric chain is asymmetrical and has two monomeric units, a reducing and a non-reducing one: the first one possess a hemiacetal functional group in C1 position, whereas the second one has an hydroxyl group in C4 position (Figure 9).
Three of the carbon atoms in ach monomer group are linked to an hydroxyl group (OH), being these

primary carbon C6 and secondary carbons C2and C3. Hydroxyl groups are located in an equatorial position respect to the middle plane of the monomeric unit, whereas H atoms are placed in an axial position. Hydrogen bonds can be easily created between linear cellulose chains (Figure 9).

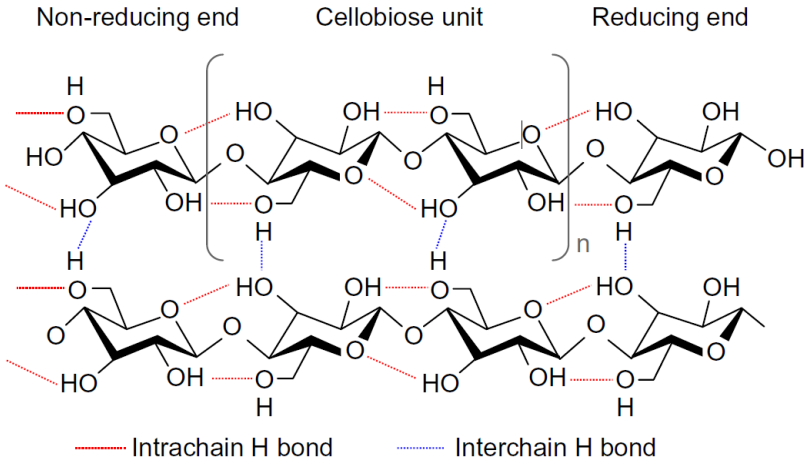

Fig. 9. Chemical structure of the intra and inter cellulose chain hydrogen bond network, highlighting reducing and non-reducing ends [44].Figure taken from Jones and Brischke, 2017[45].

The physicochemical characteristics of cellulose can be modified depending on the distribution of the inter- and intra-chain hydrogen bonds. Due to this bond network, cellulose chains aggregate in microfibril arrangements, which then group into fiber forms (Figure 10)[40].

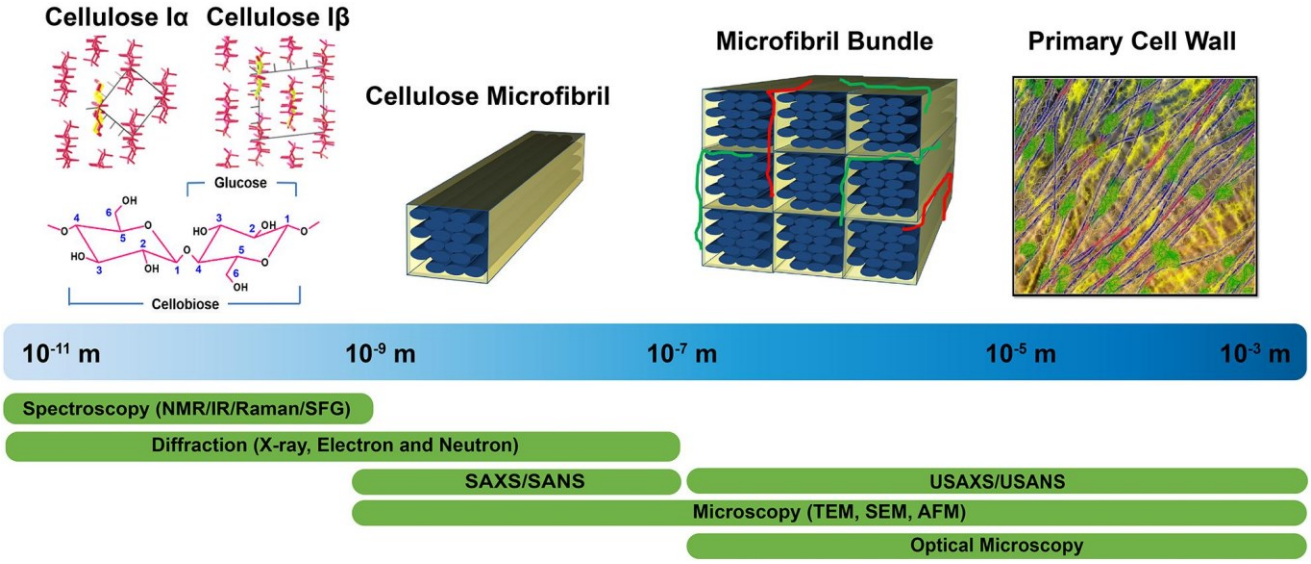

Fig. 10. Structural hierarchy of cellulose organization divided by scale. Figure taken from Rongpigi et al., 2019 [46].

Furthermore, non-covalent inter-chain interactions, such as hydrogen bonds and Van der Waals interactions, induce cellulose chains to assume ordinate or disordinate conformations, respectively called crystalline or amorphous regions (Figure 11).

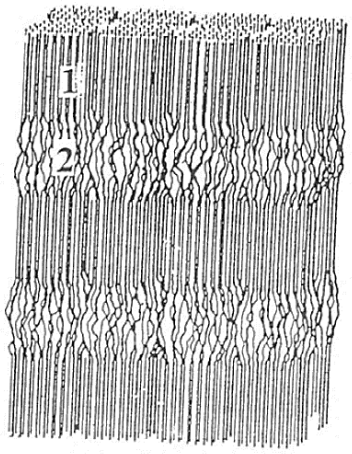

Fig. 11. Schematic representation of crystalline (1) and amorphous (2) cellulose chain regions in native cellulose microfibrils. Image taken from Ioelovich, 1999 [47].

Crystalline cellulose exists in several polymorphic forms, which differ in dimension of the unitary cells, geometry, chain orientation and polarity[40]. In nature, cellulose is found in the crystalline cellulose I form, a mixture of cellulose Iα (triclinic structure) and cellulose Iβ (monoclinic structure)[48].

Cellulose I can be irreversibly transformed into cellulose II, a more thermodynamically stable form, by means of an alkaline treatment using a concentrated NaOH solution or by precipitation from solution (regeneration). Other four cellulose polymorphisms exist, III_I, III_{II}, IV_I e IV_{II}, obtainable through different treatments[40], [49]. Cellulose derivates are easier to use and manipulate in respect to the natural polymer. All cellulose derivates are obtained from substituting one or more hydroxyl groups with a different function.

The average number of substitute groups per monomeric unit is called Degree of Substitution or DS, which ranges from zero in cellulose, to three for completely substituted cellulose[41].

3.2 Cellulose nitrate

Cellulose Nitrate (CN) is the derivate of cellulose where hydroxyl groups O-H in the anhydro glucopyranose ring are substituted by nitrate groups $O\text{-}NO_2$ (Figure 12).

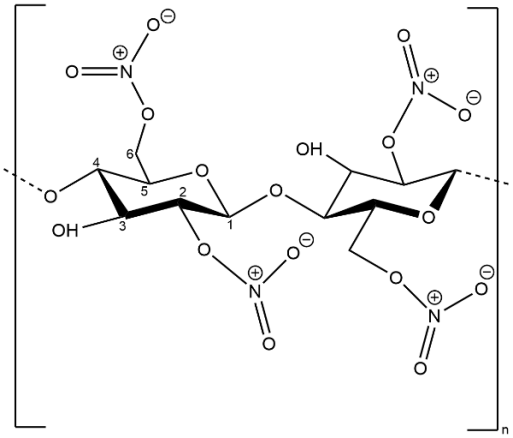

Fig. 12. CN repeating structure (DS:2).

CN was initially the most important and common inorganic derivate of cellulose employed for commercial purposes due to its physical properties and low cost[50]. However, due to its high flammability, its use for photographic film production was progressively reduced and then abandoned. CN is a colorless, mechanically resistant but flexible polymer if a plasticizer is added to it[21]. CN resoftens at 80-90°C, becomes liquid at 150°C and burs in air at 160°C. CN solubilizes easily in most polar solvents and swells in aromatic hydrocarbons, but it is resistant to water and is relatively unsensitive towards diluted acids and bases. Also, CN is no compatible with most natural resins[50].

To indicate the nitration degree of CN in the industrial sector, the nitrogen percentage is used: a nitrogen content of approximately 14% equals a DS of 3.0, whereas circa 11% of nitrogen corresponds to a DS of 2.0. Cellulose nitrate is a very unstable and explosive material, therefore, the most commercially used CN species is cellulose dinitrate, which although non-explosive, is still highly flammable, with nitrogen content of 10.7-12.2 %. The flammability of CN can be deduced from the DS[50]–[52]. Cellulose nitrate is synthesized from cellulose by nitration: cellulose fibers are immersed into an aqueous solution of nitric acid (HNO_3) and sulfuric acid (H_2SO_4) at 20-40°C[50]. Nitration of cellulose is a kind of esterification reaction towards equilibrium (Scheme 1):

$$R\text{-}OH + 2HONO_2 \leftrightarrows R\text{-}ONO_2 + H_2O + HONO$$

Scheme 1. Nitration of cellulose.

The reaction is reversible in water and the hydrolysis of nitrocellulose can be a competitive reaction which can determine the degradation of the polymer, depending on the direction towards which the equilibrium is inclined. Sulfuric acid favors nitration reaction, by swelling cellulose fibers, allowing for an easier penetration of nitric acid in the chain[14], [52]. The concentration of nitric acid influences the obtainable degree of nitration.

After washing the product to remove the acid excess, CN is stabilized by immersion in a boiling sodium carbonate solution (Na_2CO_3)[52]. Initially, CN was employed for producing military explosives, since it showed high flammability in humid environments[21], [51]. It was only until it was discovered that CN could be adequately stabilized by the addition of camphor in a 4:1 proportion to produce a mixture called celluloid, that it started to be employed to produce photographic film supports. This more stable plastic mixture was obtained mixing camphor, ethanol and cellulose nitrate[51].

Camphor has excellent plasticizing properties towards CN due to its deep-penetration capabilities; however, it shows a high volatility, as it changes phase from solid to a gas without becoming liquid (it sublimates) at room temperature[11], [14], [53]. Camphor is a resin derivate from evergreen *cinnamomum camphora*[14], and its primary structure is 1,7,7-trimethylbicicle (2,2,1) epta-2-one. From a chemical point of view, it belongs to the family of terpenoids (Figure 13)[14], [51].

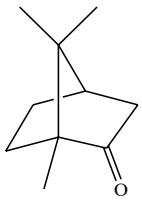

Fig. 13. Chemical structure of Camphor.

3.3 Cellulose acetates

Cellulose acetate (CA) is the organic derivate of cellulose in which the hydroxyl OH groups have been substituted by acetyl groups $O\text{-}(C{=}O)CH_3$ (Figure 14).

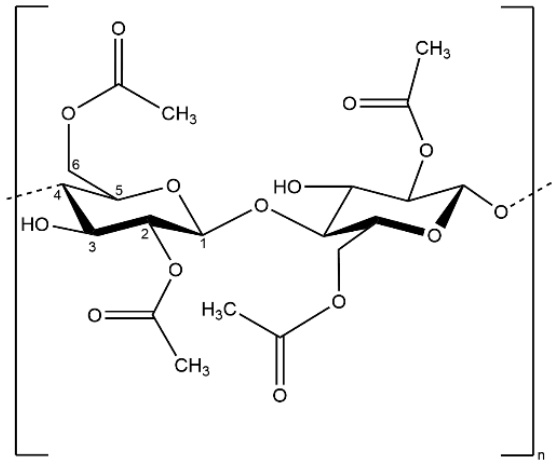

Fig. 14. Cellulose acetate repeating structure (DS: 2).

At an industrial level, CA is produced by homogenous or heterogeneous acetylation of cellulose using acetic anhydride $(CH_3CO)_2O$ and sulfuric acid (H_2SO_4)[54], [55]. Historically, CA was produced though three industrial processes which differ by the solvent of choice: The acetic acid process, the methylene chloride process and the heterogenous process. Among these, the acetic acid method is the most employed one for producing commercial CA. The process includes two main phases: acetylation of cellulose (Scheme 2) and cellulose triacetate hydrolysis (Scheme 3.3.2). For obtaining the best results from acetylation, primary cellulose must be subjected to an activation pretreatment which includes mechanical disintegration, reswell in acetic acid and mixing with sulfuric acid. Such pretreatment allows for more homogenous accessibility to hydroxyl groups. This is followed by the acetylation phase, consisting in an esterification reaction[41], [55].

$$R\text{-}OH + H_2SO_4 + (CH_3CO)_2O \rightarrow R\text{-}(OSO_2OH) + 2CH_3COOHR(OSO_2OH) + (CH_3CO)_2O$$

$$\leftrightarrows$$

$$R\text{-}(OSO_2O)^- + CH_3CO_2O(H^+)\,(CH_3CO)_2O(H^+) + R\text{-}OH \rightarrow R\text{-}OCOCH_3 + CH_3COOH$$

Scheme 2. General mechanism of cellulose acetylation.

The hydrolysis of cellulose acetate occurs mainly in acid conditions, and is interrupted according to the desired degree of substitution (DS), i.e., the average number of acetyl groups per anhydrous glucose unit (Scheme 3).

$$R\text{-}OCOCH_3 + H_3O^+ \leftrightarrows R\text{-}OH + CH_3COOH$$

Scheme 3. Cellulose acetate hydrolysis.

When the desired product is obtained it must be precipitated, washed and dried. Simultaneously, part of the acetic acid can be recovered and recycled for a new synthesis[41].

CA is characterized by low toxicity and flammability when compared to CN; it shows also moderate mechanical resistance and low production costs. Thanks to these properties, it has been employed for a wide variety of applications including cigarette filters, textile fivers, surface covering, films for food packaging, LCD screens and photographic film bases[41], [54], [56], [57].
The characteristics of CA, and therefore its applications, depend on its structural factors, such as degree of polymerization DP [42] and degree of substitution (DS)[41], [55].
Table 1 reports on DS and the corresponding value of the percentage content of acetyl groups and acetic acid according to each CA species.

Compound	DS	Acetyl content	Acetic acid content
Cellulose	0	0.0%	0%
Cellulose Monoacetate	1	21.1%	29.4%
Cellulose Diacetate (CDA)	2	34.9%	48.8%
Cellulose Triacetate (CTA)	3	44.8%	62.5%

Table 1. Cellulose acetate's DS, acetyl group and acetic acid concentration[41].

Equation 1 shows that DS is directly proportional to percentage content of acetyl groups[41].

$$DS = \frac{162 \times \%_{Acetyl}}{(43 \times 100) - \left[(43 - 1) \times \%_{Acetyl}\right]} \quad (1)$$

where:

- 162 is the molecular weight of the cellulose monomer;

- 43 is the molecular weight of the acetyl group;
- $\%_{Acetyl}$ is the weight content of acetyl groups.

Compared to cellulose, CA possesses a less crystalline structure: acetyl groups alter the structural organization (constitutional conformational and configurational regularity) of cellulose, modifying inter and intra chain interaction. As acetyl groups increase, crystallinity decreases, and volume increase[41], [54], [58]. CA is therefore characterized by an important network of polar interactions, constituted by hydrogen bonds and dipole-dipole interactions, though which the polymer is stabilized (Figure 15). The strength and density of the network of hydrogen bonds depend on the quantity of hydroxyl groups O-H, whereas the strength and density of the network of dipolar interactions are strongly influenced by the amount of acetyl groups $O\text{-}COCH_3$, defined by the DS[41], [55].

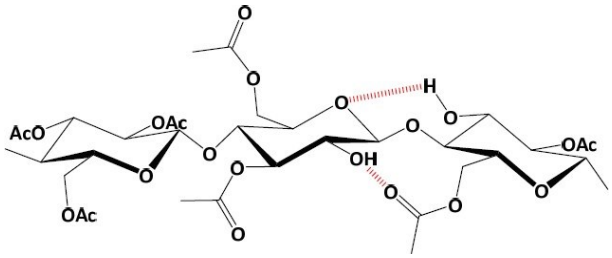

Fig. 15. Chemical structure of the intra-chain hydrogen bond network of cellulose acetate (DS:2.45)[41]

3.3.1 Additives for cellulose acetate

CA is a semicrystalline polymer, and to be thermically manipulated it needs additives such as plasticizers and flame retardants, because its fusion temperature (T_m) is too close to its decomposition temperature (T_d)[59].

Plasticizers

Plasticizers are generally molecules of low molecular weight added to the polymer to make it more flexible, durable and workable, by lowering its glass transition temperature (T_g)[60]. The glass transition temperature (T_g) of the plasticized polymer depends on the amounts and T_g of the respective components of the formula[41].

An ideal plasticizer must be highly compatible with the polymer, it must grant enough flexibility to the material for a wide temperature range, it must be colorless, chemically stable, lightfast, must not suffer from migration, lixiviation, nor induce acidity in the mixture, and it must be inexpensive and eco-friendly[41], [61].
Experimentally, it has been observed that the plasticizer interacts only with the amorphous phase of polymers by placing itself between the chains, creating different kinds of polymer-plasticizer interactions and increasing the free volume of the system (Figure 16), whereas the crystalline phase remains unaltered[41], [53] .

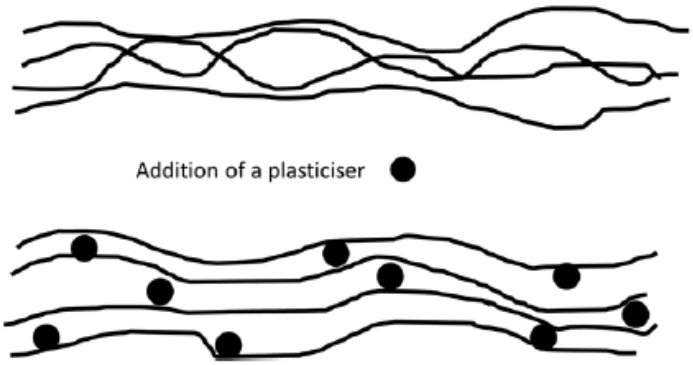

Fig. 16. Representation of plasticizer molecules (●) distribution among the polymer chains. Taken from Lambert and Wagner, 2017 [62].

Depending on whether the interaction between polymer and plasticizer is covalent or not, plasticizers can be divided into two categories, internal or external. Sometimes, internal and external plasticizers are used in binary or tertiary mixtures in order to improve their efficiency and reduce production costs[41], [63].

Cellulose acetate is often plasticized with 10-40% weight of plasticizer for producing film and sheets[55].Typical plasticizers compatible with cellulose acetate are citrates, triglycerids, and most importantly, phthalates and phosphates.

3.3.1.1 Phthalate esters

Phthalate esters are a class of organic compounds with chemical formula $C_6H_4(COOR)_2$, widely used as additives to confer durability and flexibility to a polymeric material. Dimethyl phthalate (DMP), diethyl phthalate (DEP) and dibutyl phthalate (DBP) belong to this class [64].

Plasticizers from the phthalate kind were widely used for producing CA objects, in particular dimethyl phthalate, diethyl phthalate and butyl phthalate. These compounds, being very volatile, are easily detected by SPME: they have been reported for example by Mousviasl in CA cinematographic film bases[65], by Curran et al.[66]and by Mitchell et al.[67]as the one of the highest emissions in tridimensional CA objects and thin sheets, and their presence can also be deduced by detection of their degradation products, benzoic acid methyl ester.
Phthalates with higher molecular weight such as di-ethylhexyl phthalate (DEHP), dioctyl phthalate, diisobutyl phthalate, as well as their degradation products, could be present too in these kind of objects[68]. Kemper and Lichtblau[63] used GCMS after solvent extraction to detect them in a set of 16 acetate sheets, X-ray and motion picture film rolls with different grades of degradation dating from 1948 to 2016. Instead, Mitchell et al.[67], after analyzing the headspace of mid-century developed photographic negatives, reported 1-hexanol 2-ethyl as sign of DEHP plasticizer, without reporting the detection of the actual plasticizer nor the remaining basic structure of the phthalate after breakdown.

Diethyl phthalate is one of the most employed phthalic esters for the production of plastics, with a wide range of applications in agriculture, industry and domestic spaces. It was one of the mot common plasticizers for CA until the end of the 20th century; however, due to its toxicity its industrial use has been progressively reduced, favoring instead more eco-friendly plasticizers.

Indeed, many studies show that DEP can cause serious environmental and health problems, as polluting and irritating agent[41], [69]–[71]. DEP is a low molecular weight compound (222 g/mol), found at room temperature as a colorless oily liquid with a characteristic smell. It mixes well with organic solvents, partially mixes with aliphatic solvents and cannot be mixed with water at 25°C. It shows a density equivalent to 1.12 g/cm^3 and a vapor pressure of 0.002 mmHg at 25°C, a fusion point of -3°C and a boiling point of 295°C[41], [61], [72]. From a chemical viewpoint, it is the diester of phthalic acid and ethanol, and it is constituted by an aromatic ring in which two hydrogen atoms in ortho position are substituted by two chains of esterified carboxylic acids (Figure 17).

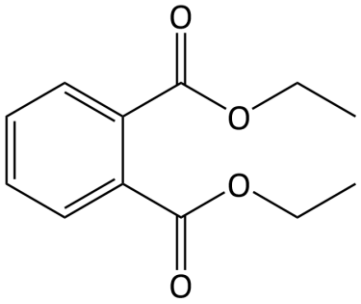

Fig. 17. Chemical structure of diethyl phthalate

CA films can contain around 20-40% weight of diethyl phthalate[64]. Experimentally, it is known that when the weight content of DEP increases, T_g of the plasticized cellulose acetate tends to decrease. However, in previous studies it has been reported that at concentrations higher than 25% in weight, two different T_g occur due to a separation phase that is created between plasticizer and polymer, while at concentrations lower than 25% in weightdiethyl phthalate shows high compatibility with the polymer and it is absorbed by active sites in it resulting in a single T_g being observed [41], [57], [73].

Dipolar interactions are created between cellulose acetate and phthalate ester plasticizer molecules, through hydrogen-accepting carbonyl groups (C=O) and the hydroxyl groups (OH)of the involved species. These interactions and the hydrophobic character of DEP influence locally the molecular mobility and hinder the access of water molecules to lateral acetyl groups, reducing humidity absorption in cellulose acetate films [59], [73].

Flame retardants

Most substances catch fire if exposed to high thermal stress [74] and many polymers, including CA, can burn at high temperatures or feed the combustion when they come in contact with flames. To avoid this, flame retardants are used, to increase the polymer's resistance to combustion.

A flame retardant is not expected to keep the material from catching fire, but to slower the propagation of flames and avoid long burning times; this is achieved by reducing at least one of three elements necessary for fire to appear, i.e., fuel, heat and oxygen[53]. An external source of heat is necessary to burn CA: the heat leads the high molecular weight polymer to thermally

decompose, through a radical mechanism, and release increasingly small volatile compounds which act as fuel for the fire. These species mix with the oxygen in the air and oxidize, to form a burnable mix while the material is combusting[74].

Some flame retardants act throughout the inhibition of radicals in gas phase by releasing acids during combustion, such as halogens. Other type of retardants produce non-combustible gases and dilute the amount of fuel or oxygen. Yet another kind of flame retardants reduce the speed of heat release during combustion, influencing the path of heat transfer towards the polymeric substrate; whereas some flame retardants form a layer of foamy carbon over the surface of the burning material to reduce the propagation of the flame. Carbon reduces both the heat transfer throughout the polymer, as the diffusion of oxygen and fuel, delaying combustion.

An ideal flame retardant should be thermically stable at working temperature, have long term compatibility with the polymer matrix, keep or improve the mechanical properties of the polymer, and not represent any health risk[74].

3.3.1.2 Phosphate esters

Phosphate esters are a group of organic phosphates with general formula $P=O(OR_3)$[75], which are mainly employed as fireproofing and flame retarding agents[53]. Some of the compounds which belong to this family of phosphoric acid esters are triethyl phosphate (TEP) and triphenyl phosphate (TPP), the resorcinol bis(diphenyl phosphate) (RDP) and bisphenol A bis(diphenyl phosphate) (BDP)[64], [74].

At the early twentieth century, TPP was employed as plasticizer and flame retardant for CN films replacing camphor, and later on, it was also used as additive for CA films[75], [76]. TPP is found at room temperature in crystal form as a transparent solid with a characteristic smell, typical for aromatic substances[76].

From a chemical point of view, TPP is the triester of phosphoric acid and phenol, and it is constituted by a phosphate group (PO_4^{3-}) to which three aromatic rings are bonded (Figure 18).

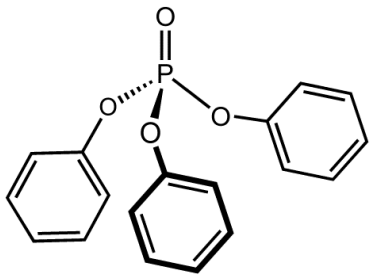

Fig. 18. Chemical structure of Triphenyl Phosphate (TPP).

Owing to its chemical structure, TPP is soluble in non-polar solvents such as benzene and chloroform, soluble in polar solvents like acetone, moderately soluble in alcohols, and it is not water-soluble. It has a molecular weight of 326 g/mol, a density of 1.2 g/cm^3, a vapor pressure of 0.000002 mmHg at 25°C, a melting point of 49-50°C and a boiling point of 244°C[61], [72], [75].

TPP starts to decompose at 600°C, generating aromatic hydrocarbons such as naphthalene, phenanthrene and anthracene; as well as oxygenated aromatic compounds such as phenol and phosphoric esters[77]. TPP, as all flame retarding agents containing phosphorus, catalyzes the formation of carbon, which isolates the surface of the polymer from both oxygen and fire heat, and slows down the release of volatile products which may act as fuel[53]. TPP is also employed as co-plasticizer to stabilize more volatile plasticizers such as DEP or DMP.
CA films can contain 10-20% weight of TPP[64]. Weak interactions can be created between CA and TTP plasticizer molecules. Several flame retardants are strong hydrogen bonding agents: when at higher temperatures water content boils, the bonding medium between hydroxyl groups of the cellulosic material becomes the flame retarding agent, which stabilizes the polymer reducing its volatility and thus its burnability[74].

The intermolecular hydrogen bond includes the O-H and P=O functional groups of CA and TPP respectively, through the electron-accepting phosphor. These interactions quickly diminish with the increase of the TPP concentration; this may be due to the difficulty for the relevant functional groups to organize themselves in immediate vicinity. Dipole-dipole interactions involve polarizable functional groups such as C=O and P-O-Ph, and are amplified with the increase of carbonyl groups present in the polymer. In CTA these interactions are quite strong, giving rise to a high compatibility with the polymer even when the number of centers of H bonding such as OH groups, are present in a lower quantity [78].

3.3.1.3 Butylated hydroxytoluene (BHT)

Among the additives employed for the manufacture of cellulose ester films during history[13], sterically hindered phenols were used as antioxidant agents; Butylated Hydroxytoluene (BHT, figure 19) is the main one amog these class of varied substances, with other common examples being hydroxyanisole (BHA), tertiary-butylhydroquinone (TBHQ) and gallates. BHT antioxidant and its degradation products have been reportedly detected from cellulose acetate emissions by SPME-GCMS[67], [68].

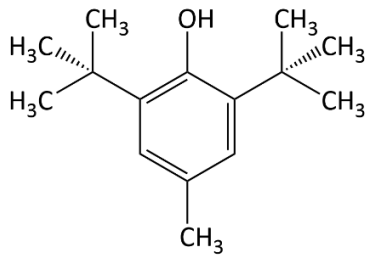

Fig. 19. Butylated Hydroxytoluene (BHT)

BHT and other hindered phenols represenatives undergo similar reactions[79] (Figure 20): Each BHT molecule can convert up to 2 peroxyl radicals coming from the photooxidation of cellulose acetate, turning them into hydroperoxides, and inhibiting the autooxidation of the polymer. The resulting oxytoluene radical products are very unreactive towards polymer chains due to steric hindrance, and

instead undergo a number of other degradation reactions. Ultimately all oxytoluene radicals are transformed into dimethylbenzoquinone or other quinonoid structures.

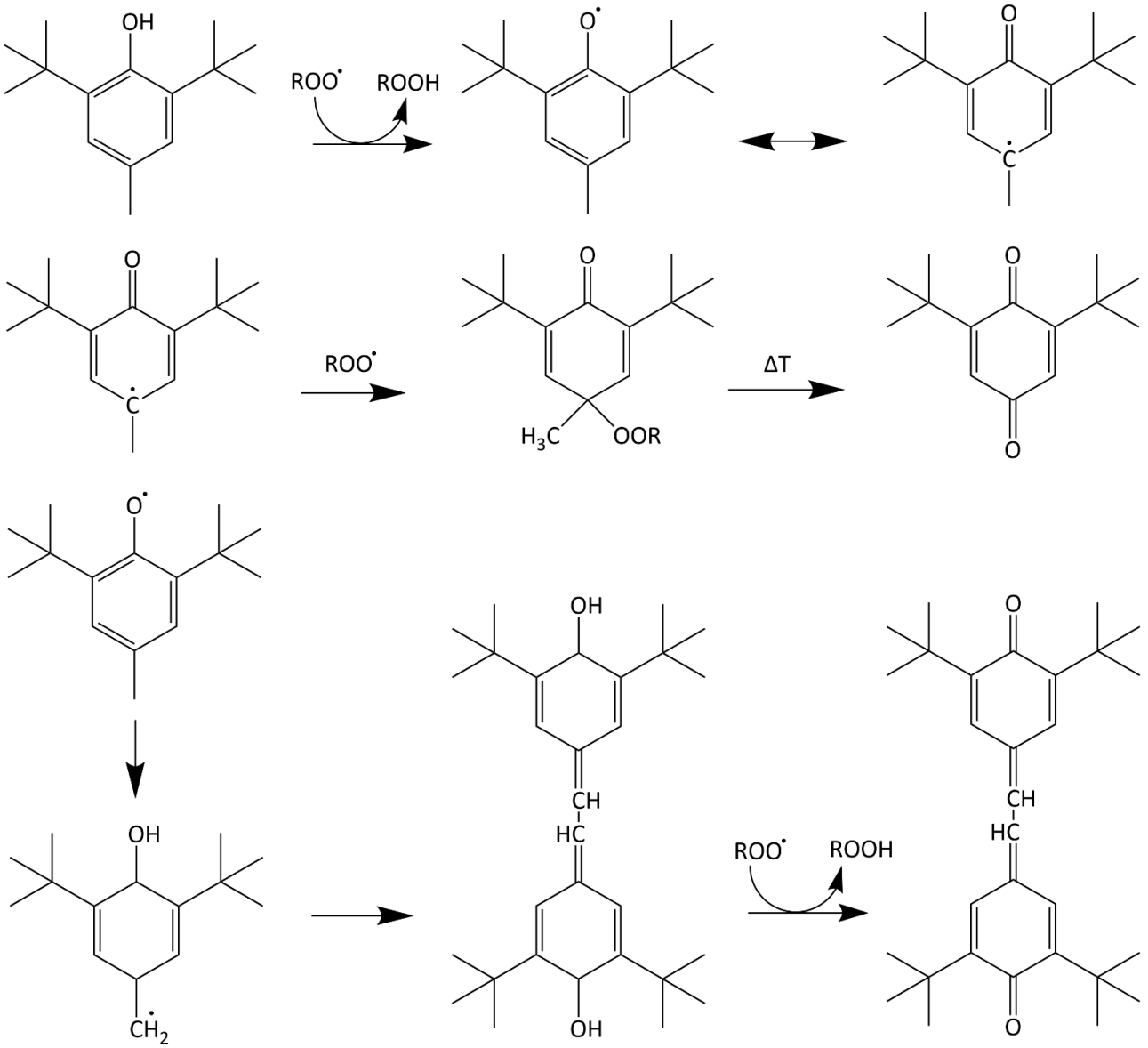

Fig. 20. Main reactions mechanism of BHT and other sterically hindered phenols[79].

Chapter 4 Degradation causes of cellulosic film base materials: State of the art

Over time, cinematographic films with cellulosic supports suffer from inevitable decay processes, caused by their intrinsic chemical constitution, the environmental conditions existing during their storage, and their story of use and conservation.

Therefore, to allow an accurate diagnosis and to propose adequate conservation and restoration measures for films, it is necessary to understand in depth the causes and mechanisms of degradation, as well as the macro and microscopical alteration effect occurring on these materials. Most common degradation pathways for cinematographic films are now described, in order to explain the physicochemical changes observed in the support, as well as the apparition of typical degradation products which should then be removed to ensure the better conservation of the

object.
These changes constitute the core topics addressed during the research lines regarding the non-invasive diagnosis of the film base conditions, and the development of green cleaning methodologies for removing alteration products from these artefacts.

4.1 Cellulose nitrate degradation

Photographic and cinematographic films materials over CN bases are known to be not only flammable, but also intrinsically unstable, mainly due to those degradation mechanisms triggered the by thermal, photocatalytic and hydrolytic loss of nitro substitutive groups of the CN base[23]. These processes are due to endogenous reasons (the liability of the N-O bond in nitro groups of CN), but depend also on exogenous conditions, so they may develop quickly under uncontrolled storage conditions. Particularly, unventilated environments showing high temperature and humidity or the presence of light may induce the thermal, hydrolytic and photocatalytic degradation respectively.

Hydrolysis implies the heterolytic scission of the N-O bond in the presence of humidity, and any eventual presence or residues of acid may catalyze it[50], [51]. Hydrolysis implies the loss of nitrate lateral groups with the resulting decrease of molecular weight of the polymer.

Regarding thermal and photochemical degradation, Selwitz affirms that homolytic scission of the N-O bond may occur at temperatures above 120°C and when the molecule is exposed to UV/visible radiation[51]. Photochemical or thermal degradation of cellulose nitrate consists in a radical mechanism, through which the N-O bond is homolytically broken, with the formation of very reactive radical species (Figure 21).

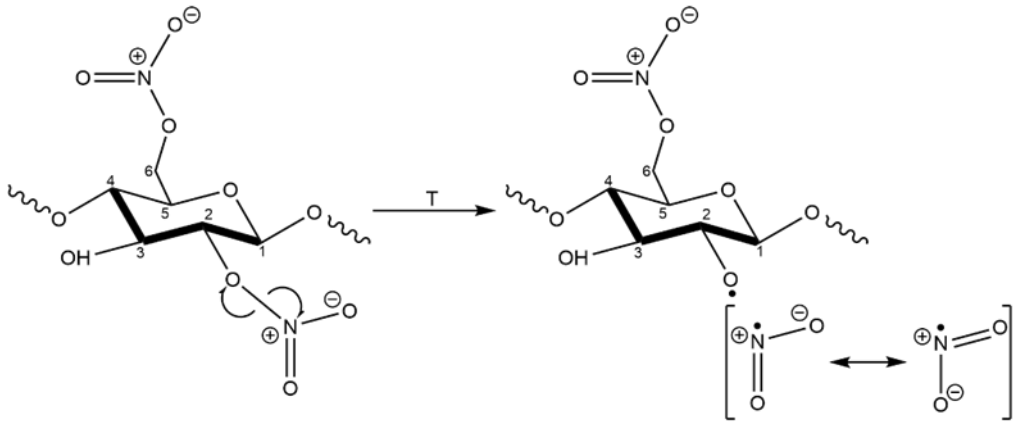

Fig. 21. CN's homolytic thermal breakdown mechanism.

One of the first products of thermal degradation is nitrogen dioxide, $NO_2\bullet$, among the most reactive and toxic oxidizing agents there are. It can be identified by yellowish vapors and characteristic smell [14], [16], [23], [50], [52].
Thermal decay is autocatalytic, in the sense that decay products tend to aggravate the condition of CN. The first N-O bonds to be broken are those involving secondary nitrate groups, i.e., those linked to carbon atoms C_2 and C_3, whereas primary nitrate groups, bonded to carbon atom C_6, break up with

temperatures over 135°C[50].

Regarding its light sensibility, CN is particularly vulnerable towards radiation with wavelengths between 360 and 400 nm. CN's photochemical degradation is similar to its thermal degradation and, according to some publications, it leads to the formation of carbonyl groups (Scheme 4, 2a, 4) [14], [23]; whereas at shorter wavelength (higher energy) radiation, cellulose ring disintegrates too[14], [51].

(1) $RR'CHO—NO_2 + h\nu \rightarrow RR'CH—O\bullet + NO_2\bullet$

(2)

(2a) $RR'CH—O\bullet \rightarrow R\bullet + R'CHO$

(2b) $RR'CH—O\bullet + RR'CHO—NO_2 \rightarrow RR'CH—OH + RR'CO\bullet—NO_2$

(3) $NO_2\bullet + RR'CHO—NO_2 \rightarrow$ breakdown

(4) $RR'CO\bullet —NO_2 \rightarrow RR'C=O + NO_2\bullet \rightarrow$ breakdown

Scheme 4. Radical breakdown mechanism of cellulose nitrate.

Yellowing and color change of the polymeric base are typical symptoms of photochemical degradation, attributable to the formation of conjugate structures, such as polyenes and double carbon-carbon bonds conjugated to carbonyl or aromatic groups. Along photodegradation, the number of conjugate structures increases and color change occurs from transparent to yellow, to orange, to red, to brown and black, as radiation at longer wavelengths are increasingly absorbed[50].

After all those processes involving the loss of CN's nitro groups, the resulting NO_2 gases can then react with water from the surrounding environment, leading to the production of nitric acid (HNO_3) as well as nitrous acid (HNO_2) (Scheme 5)[14], [23]. These acids continue to catalyze the hydrolytic loss of nitro groups in the CN polymer and further degrade the film.

$$2NO_2\bullet + H_2O \rightarrow HNO_3 + HNO_2$$

Scheme 5. Acid formation upon loss of nitrate lateral groups from CN.

In the end, film bases affected by such degradation mechanisms become increasingly deformed, frail and brittle. The frailty of CN bases may be aggravated by the loss of camphor plasticizer from the film, as camphor tends to gradually recrystallize in proximity of microfractures, impurities, and to be expelled into the surface, where it sublimates at room temperature. Eventually, degraded CN films break down to dust[80].

To avoid the complete loss of the images recorded on these films, their timely scanning and digitalization is a priority for cinematheques, libraries and other institutions safeguarding such audiovisual archives[81].

However, films which have already underwent some degree of hydrolytic degradation of their CN

bases may suffer also from the softening of their gelatin emulsions, which constitutes a serious drawback for their scanning. The softening of gelatin occurs due to a decrease on the pH to conditions more acidic than the isoelectric point of type-B gelatin in the photographic emulsion. At this point, the gelatin molecule becomes positively charged, and repulsion forces between charges slightly uncoils the molecule, facilitating gelatin solubilization[30]. Nguyen *et al*. have suggested also that NO_2 species promote the hydrolysis of hardened (cross-linked) and unhardened photographic gelatins, lowering their molecular weight and their viscosity[29].

Gelatin emulsion softening is a serious drawback, because upon becoming more fluid this material can easily migrate laterally when the film is pressured, and it may adhere to any surface in contact with it. This often affects the back side of the subsequent coils of the same film (Figure 1.3), causing the loss of images in the first coil and gelatin accumulation on the back of the second. The adhesion of convolutions, known as blocking, ultimately transforms the film into a solid unit which cannot be unrolled, a condition that due to its similarities in consistency to said object, is called the "hockey puck" state[80].

4.2 Cellulose acetate degradation

Just like photographic and cinematographic films with CN bases, films with CA bases shows spontaneous and progressive chemical degradation mechanisms. These processes are determined by the chemical properties of the plastic components themselves as endogenous causes, and as exogenous causes the environmental conditions towards which CA is exposed, with humidity, temperature, atmospheric oxygen and light radiation as main determining factors which can promote CA's chemical degradation[82].

The main degradation pathways for CA have been summarized by Nunes et al., and considers what had been previously proposed in literature by Ram [83], [84]Edge, and Allen [85], as well as calculations by Knight[86] and Ahmad et al. [87].

The first and most common degradation path is hydrolytic, and it involves the side chain ester bonds undergoing hydrolysis in the presence of humidity and an acid environment, in which heterolytic bond cleavage prevails. This mechanism may be triggered by residues coming from the manufacture process of the polymer, such as acetic acid (CH_3COOH) or sulfuric acid (H_2SO_4) [55] .
In particular, the process starts by the protonation of the ester carbonyl, leading to bond cleavage, the release of volatile acetic acid and the formation of an hydroxyl group, with the corresponding decrease in the DS of CA, which progressively reverts back into cellulose[76].
Therefore, the continuous formation of hydronium ions and acetic acid is said to be autocatalytic, as they repeatedly catalyze the deacetylation of the CA chain, making it easier for the heterolytic scission of ester bond (O=C)-O to occur, thus promoting the formation of more acetic acid. This phenomenon (Figure 22), typically characteristic of CA polymers, is commonly known as the "vinegar syndrome", for it causes the diffusion of a characteristic vinegar smell.

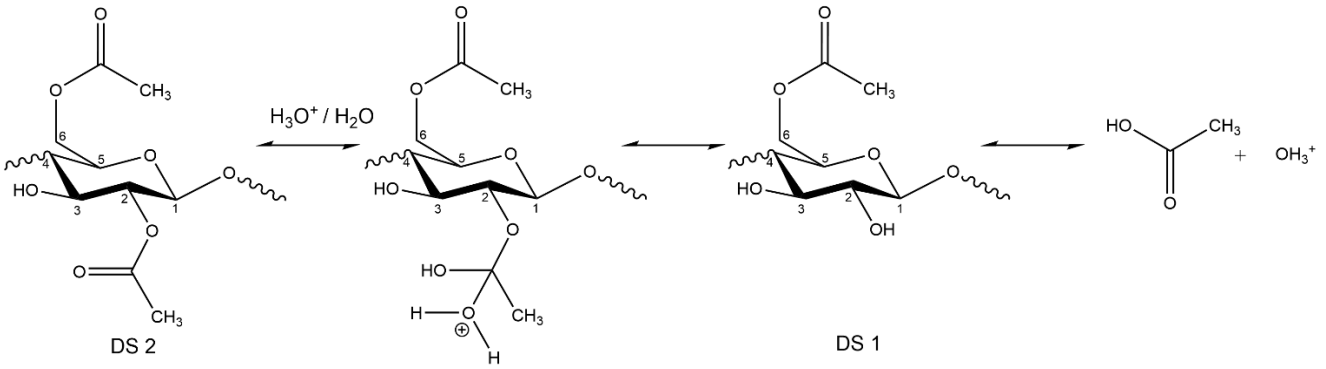

Fig. 22. The most common acid-catalyzed hydrolysis mechanism of cellulose acetate (DS:2).

Acetic acid would be the main volatile released from the first hydrolytic degradation mechanism of CA bases, which lose the acetate functional groups; acetic acid indeed has been reported to be the main emission from CA objects[66], [67], [88].
Interestingly enough, Curran et al. [10] detected also ethyl acetate as secondary emission around 12 minutes of retention. Probably this product comes from the loss of the acetate side group linked to non-cyclic C_5 and C_6 carbon atoms in CTA.

Acid hydrolysis may also cause the breaking of the β-1,4 glycosidic bond, causing chain depolymerization[23], [76], [89]. In this second hydrolytic decay mechanism, the breakage of the ether glycosidic bond of the polymeric backbone takes place (with maximum reaction rates at pH ≤ 4.) The hydronium ions cause the scission of the main chain and the formation of hydroxyl groups at C1 and C4, with further production of hydronium ions. This reaction is also autocatalytic.

Regarding CA's hydrolytic degradation, it has been hypothesized that Diphenyl Phosphate (DPP), a strong acid originating from the acid degradation of additive TPP, could act as catalyst for the CA acidic hydrolysis reaction's, although this is contested.[55], [57], [76], [90] (see Figure 24 below, in the section corresponding to additive loss).

Photochemical decay of CA can occur instead in the presence of oxygen and far (highly energetic) UV radiation; in case the polymer contains substances that act as photosensitizers, photodegradation may occur also in the presence of radiation with a wavelength (λ) ≥ 275 nm[91].
This reaction produce peroxide substituents in CA as intermediate product, which on their turn catalyze further degradation of the polymer[92]. This process consists in a step-wise radical mechanism, by the formation of very reactive species of low molecular weigh and increasingly oxidative power, such as alkyd radicals (RO•), peroxides (ROO•), and aldehydes (RCHO), as the polymer structure breaks apart[23], [55].

$CA\bullet + O_2 \rightarrow CA\text{-}OO\bullet$
$CA\text{-}OO\bullet + CA \rightarrow CA\text{-}OOH + CA\bullet$
$CA\text{-}OOH \rightarrow$ chain scission and generation of degradation products

Scheme 6. later stages of CA photooxidation

Macroscopically, the polymer begins to yellow and discolor as photodegradation advances. It has been hypothesized that an oxidative attack on CA at advanced stages of degradation would create formic acid, oxalic acid, and aldehydes[55]

It has also been found by previous studies that degraded cellulose esters emit furfural as a by-product of polymer backbone decay; having detected such volatiles from artificially degraded CA samples exposed to high temperature and humidity conditions[93].

As side note, other cellulose ester bases used only for a relatively short period [68] for cinematographic film base production, such as Cellulose Acetate Propionate (CAP) and Cellulose Acetate Butyrate (CAB), would release propyl and butyl acid by hydrolytic loss of their corresponding side groups.

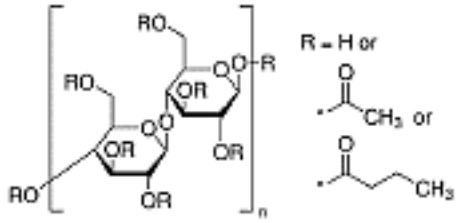

Fig. 23. Cellulose Acetate Butyrate (CAB)

Another symptom of decay of CA film bases is their loss of plasticizer and flame retarding additives[55]. Due to deacetylation in the CA chain, and depending on the kind of interaction that links the additive towards the CA polymer, as well as its volatility, its structural and chemical characteristics, plasticizers and flame retardants may spontaneously migrate from the polymer bulk towards the surface at the back of the film base (or become trapped between the CA base and the layers above, creating bubbles, emulsion detachments and other problems). In the case of phthalates, migration may cause oily and sticky residues over the film, capable of accumulating dirt and dust, whereas TPP migration creates acicular crystal blooms on the surface[73], which may appear macroscopically whitish and shiny.

Plasticizer loss changes the physical properties of the CA polymeric base, which shrinks, stiffens, and eventually becomes very fragile, and hinders the digitalization of the film's content due to the apparition of superficial material deposits that interfere with its proper observation.

The loss of plasticizer may be caused by different factors. Structural changes in the CA polymer and its chemical environment may compromise the stability of the plasticizer; and a plasticizer no longer compatible with the new chemical properties of the polymer bulk may migrate towards the base surface to crystallize or evaporate[57], [90], [94]. McGath suggest that the decay of CA films containing TPP seems to be amplified by the mechanical stresses exerted upon recrystallization of the additive[76].
Researches concerning food packaging have found that phthalate plasticizer migration depend on

pH, with low pH being a stimulating factor for the migration of these plasticizers[73], [95].
At room temperature, TPP in acid solutions is hydrolyzed very slowly to produce phenol and Diphenyl Phosphate (DPP; see Figure 24)[77]. DPP is a strong acid, which could contribute in accelerating the acid hydrolysis of CA[55], [57], [76], [90].

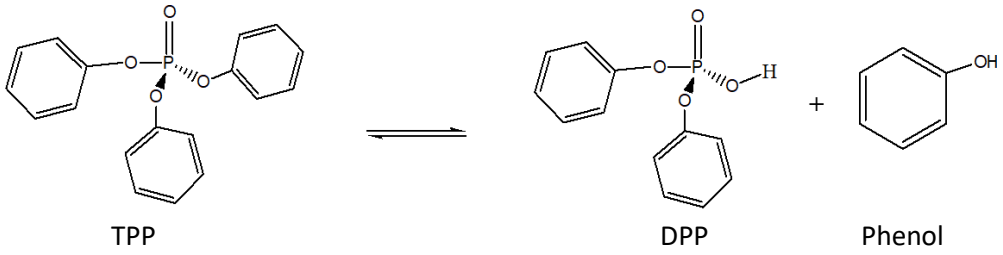

Fig. 24. TPP hydrolysis reaction.

Part II: Aim of the thesis

The RICORDACI project aimed to identify innovative solutions for the preservation of film heritage, in collaboration with the restoration laboratory of the Cineteca di Bologna *L'immagine Ritrovata*, putting particular emphasis on films possessing cellulose-derivative polymeric bases.

The research had as objectives to develop effective, accessible, fast, accurate non-invasive and non-destructive analytical methods for the characterization of cinematographic film bases, as well as for monitoring their condition. In particular, it aimed at testing two miniaturized portable spectrometers working at different portions in Short Wave Infrared (SWIR) range to identify the kind of polymeric base with the aid of multivariate analysis of the data; and employ them to create a diagnostic tool to measure the Degree of Substitution (DS) of cellulose acetate (CA) film bases as a method for monitoring their conservation state.

The work also aimed to prove the effectiveness and safety towards the object and the operator of new green methods to clean the surface of polymeric film supports allow their scanning; these included the use of Deep Eutectic Solvents (DES) for the removal of softened gelatin residues from cellulose nitrate (CN) film supports, as well as the application of green volatile solvents and new electrospun nylon fiber mats for the safe removal of triphenyl phosphate blooms CA film bases

These research lines involved the study and treatment of real historic cinematographic film samples of different typologies, as well as pure analytical reference standards of their constitutive materials, which were characterized by complementary techniques, principally Microscopy and Mid-Infrared Fourier Transformed Spectroscopy (FTIR).

Part III: *Experimental part*

Chapter 1 A new miniaturized short-wave infrared (SWIR) spectrometer for on-site cultural heritage investigations[1]

1.1 Abstract

This chapter shows the capabilities of a new miniaturized shortwave infrared (SWIR) spectrometer for the analysis of cinematographic film samples. This spectrometer is a prototype characterized by its small dimensions (45.0 mm in diameter x 47.5 mm in height x 60 g weight), so it can be easily handled and transferred out of a research laboratory. The prototype allows the acquisition of spectra in the SWIR range (1200–2200 nm), something uncommon among portable spectrometers. This spectral range allows the detection of several combination and overtone bands, which grants it significant diagnostic power. The present study helps for the development of monitoring and identification strategies based on miniaturized NIR spectrometers working in the SWIR spectral range for the characterization of polymeric bases in cinematographic and photographic films, safeguarded in cultural heritage institutions such as archives, museums and cinematheques. The analytical performance of the new spectrometer was assessed on a corpus of real cinematographic films. The accurate characterization of the polymeric film base in valuable historical films such as the ones selected as case studies faces challenging conservation issues not yet properly addressed, as the analysis of such kind of films usually require to be performed onsite, far from benchtop laboratory equipment, desirably in a non-invasive way. The data acquired with the tested prototype, combined with a multivariate data analysis approach, show the possibility to differentiate between the materials used as a support for cinematographic film bases, namely cellulose nitrate (CN), cellulose acetates (CA) and polyethylene terephthalate (PET), as well as for assessing the state of conservation of the cellulose acetate films. The prototype enabled rapid information acquisition to guide conservation storage and digitalization strategies, which need to be supported in real time by quick and easy-to-implement analytical procedures.

1.2 Introduction

In general terms, cinematographic films are made up of a thick, transparent polymeric base, which supports the thinner sub-layers that contain the recorded image and/or sound. Three general types of materials are used to produce the bases for film: cellulose nitrate (CN), cellulose acetates (CA), and polyethylene terephthalate (PET). CN and CA film bases are intrinsically unstable, tending to lose their acetyl and nitro functional groups via hydrolysis[84], [96]. Such phenomena, together with the decomposition of gelatin and the plasticizer migration, are the most important causes of cinematographic film degradation. To slow down the film's degradation rate, controlled storage conditions need be adopted, according to the type of polymeric base (such as the freezing of CN

[1] The work reported in this chapter has been extracted from the already published research article: E. Catelli *et al.*, "A new miniaturised short-wave infrared (SWIR) spectrometer for on-site cultural heritage investigations," *Talanta*, vol. 218, p. 121112, Oct. 2020, doi: 10.1016/j.talanta.2020.121112

elements). However, this may drastically increase the cost of the conservation of film collections. Thus, accurate identification of the film base is important for the most rational resource management of a movie archive.

The traditional approach for identifying film bases consists in a simple visual examination of the film's inscriptions and an empirical assessment of its structural characteristics. However, this can sometimes lead to an erroneous identification. Chromatographic techniques have also been proposed for characterizing the polymers used both in animation cells and cinematographic films [15], [97]. However, chromatographic analyses in most cases are costly, long, and require complex instrumentation and reagents, and they are invasive, requiring samples[98]. In comparison, spectroscopic analyses are a simpler and more accessible way to characterize film and animation cell bases: Raman spectroscopy[96], [99], FTIR spectroscopy in Transmission and Attenuated Total Reflection (ATR) modes[97], [99], [100] and NIR spectroscopy have been proposed. However, these techniques involve several drawbacks such as the non-portability of the instruments, the danger of damaging the sample during the analysis, or the occurrence of fluorescence in Raman spectra.

Portable NIR sensors are a promising alternative for film base studies, as they require much less analysis time and less expensive instruments. They can also be used on-site in a completely non-invasive way.

In order to offer a suitable diagnostic tool for film base identification, the performance of our new NIR prototype system was evaluated.

In cultural heritage research, the use of NIR spectroscopy (1000–2500 nm) has had a late and slow introduction, and only in the last decades portable NIR spectrometry has been employed in the non-invasive study of works of art in galleries or museums, without requiring precious objects to be moved or sampled.

NIR molecular investigation has been carried out on stones[101], paintings[102]and illuminated manuscripts[103], [104] using optical fiber spot reflectance spectroscopy. The spectral range used for the single point analysis varies according to the type of sensor spectrometer used, which usually are: 400–1000 nm (Visible-NIR range), 780–1000 (NIR range), 1050–1700 nm and 1050–2500 nm (Short-Wave-IR ranges)[105]. More recently, research has also focused on NIR hyperspectral imaging which provides chemical images, simultaneously obtaining information on the molecular composition and spatial distribution of the constituents[106], [107].

The miniaturization of vibrational spectrometers and sensors has revolutionized the analytical field and has led to portability, to a simplified use through automation, and to a reduction in time and costs for the analyses[108].

Miniaturized spectrometers represent a new generation of portable diagnostic systems[109], which can be associated with an easy interpretation of the results even by non-specialist technicians. Near infrared (NIR) spectrometers are used for developing miniaturized analytical strategies where no sample preparation is required, so measurements are fast and completely non-invasive[110]. NIR spectrometers have already been widely used in industry for quality control via data processing methods, in agro-food [111], [112] and pharmaceutical research[113], [114], as well as for diagnostic studies in forensic fields[115].

Miniaturized NIR spectrometers could also represent a turning point in the chemical investigation of cultural heritage. Although the importance of scientific analyses in the conservation field is largely acknowledged, the related cost, time and expertise required are often not feasible.
In this chapter we assess the potential of a new miniaturized SWIR prototype for the qualitative on-site investigation of historical cinematographic films. The prototype is very small (45 mm in diameter x 47.5 mm in height), weighs very little (60 g) and uses a simple method based on bringing the sensor into contact with the surface to be analyzed. The prototype exploits a SWIR range of 1200–2200 nm, an unique feature for miniaturized NIR devices, which usually have a limited range between 900 and 1700 nm[116]–[118]. The analysis guarantees the good diagnostic power of the data in heterogeneous artwork samples, exploiting a spectral range characterized by a high number of combination and overtone bands[119].
We believe that this is the first time that a miniaturized NIR spectrometer working in the SWIR spectral range has been proposed for the characterization of cinematographic film.
in an attempt to address challenging conservation issues for cinematographic heritage conservation, we considered the specific need for simple, accurate and non-invasive strategy for the study of film bases, that to date have not been studied sufficiently. For most of the analyzed films selected as case studies there was the particular need for analysis to be performed on-site at the film restoration laboratory, a place that is not easily accessible to scientists.
The NIR prototype enabled rapid information acquisition to guide conservation strategies, which needed to be supported in real time by quick and easy analytical procedures. We thus implemented appropriate tailored-data processing methods for the identification of the materials.

1.3 Materials and methods

1.3.1 Miniaturized NIR spectrometer and data elaboration

The NIR prototype was designed by Viavi Solutions (JDSU Corporation, Milpitas, CA)[3,6]. The system measures the diffuse reflectance in the spectral region of 1208–2160.5 nm (8278–4629 cm^{-1}). It is controlled by a portable computer via USB port. A linear-variable filter (LVF) is used as the dispersing element. LVF is directly connected to a 128-pixel linear Indium Gallium Arsenide (InGaAs) uncooled detector, which results in a compact device. Two tungsten light bulbs were used as the radiation source. The spot of analysis is approximately 3 mm in diameter. All the collected spectra were recorded at a nominal spectral resolution of 7.68 nm. Spectralon was used as the NIR-reflectance standard with 99% diffuse reflectance.
The spectrum acquisition was performed with an integration time of 3 ms and 1000 scans resulting in a measurement time of 3 s per sample. The MicroNIR Pro software (JDSU Corporation, Milpitas, CA) was used for data acquisition.

Multivariate data processing was performed by means of in-house Matlab routines (The Mathworks Inc., Natick, USA). Suitable row pretreatments were selected and applied in an attempt to minimize unwanted systematic variations, which could affect the signals. In more details, standard normal variate (SNV) transform was selected to correct for both baseline shifts and global intensity variations, while first Savitzky-Golay derivation was applied to enhance details within complex

spectral features (e.g., unresolved broad band shape). Afterwards, the spectra range considered was 1369.3–2122.1 nm. Column centering was performed prior to principal component analysis (PCA).

1.3.2 Cinematographic films

A total of 79 developed cinematographic film rolls or roll sections characterized by different polymeric bases (cellulose nitrate - CN -, cellulose acetates - CA - and polyethylene terephthalate - PET -) were analyzed. Samples belonged to different typologies (black and white, color, negative, positive and intermediate elements) and manufacturing companies (Eastman Kodak©, Agfa©, 3M©, Ferrania©, Pathe©, Orwo© and Fuji©). Preliminary information about the polymeric base composition was obtained by films inscriptions and conventional mechanical and visual film examination. According to their state of conservation film samples were broadly grouped in "well-preserved" (10 CN samples, 19 CA samples, and 13 PET samples) and "degraded" (16 CN samples, 11 CA samples, and 10 PET samples).
At least five spectra from each sample were recorded by placing the film between the spectrometer and the gold-coated glass holder. All films were analyzed directly in contact with the polymeric base.

1.4 Results and discussion

1.4.1 Historical cinematographic films

Spectra of the three classes of polymers used as film bases showed particular spectral profiles in the NIR region between 1200 and 2200 nm, which enabled them to be identified (Table 2, Fig. 25.A).
CN features diagnostic bands at 1423 nm (1st overtone of OH stretching), and at 1707 nm (1st overtone of CH stretching)[120]. CA samples can be easily identified and differentiated from the nitrocellulose-based films due to the characteristic double band at 1677 nm (1st overtone stretching of CH)[120] and at 1723 nm (1^{st} overtone of CH stretching)[121]. Finally, the different chemical nature of PET bases led to a NIR spectrum that was very dissimilar from the previous ones and characterized by a very strong band at 1661 nm that can be attributed to the 1st overtone of CH stretching[122]. PET spectra were also characterized by a band at 2138 nm due to the combination band of aromatic CH stretching and ring vibration[123].
This simple identification of the diagnostic band thus differentiates among the film bases. The data obtained were processed with principal component analysis (PCA) in order to assess the robustness and the discriminatory power of the method. Chemometric tools may also enable simple analysis methods to be developed that can support conservators and archive staff in interpreting the results. The resulting score scatter plot clearly shows three different clusters associated with the three classes of cinematographic film bases (Fig. 25.C). The interpretation of the loadings scatter plots (Fig. 25.D) enables the variables involved in the sample separation to be clearly identified. The diagnostic bands at 1423 and 1707 nm (in the loading plot variables at around 1690 nm and 1400 nm related to bands after derivative correction) played a crucial role in the separation of CN samples, as expected.

On the other hand, CA samples were characterized by bands at 1723 and 1907 nm (variables around 1707 and 1892 related to bands after derivative correction), while the PET basis can be clustered thanks to the presence of bands at 1661 and at 2138 nm (corresponding to bands with a derivative-like shape at about 1638 and 2114 nm).

The correct identification of film bases is even more important in degraded and partially altered films, which usually require urgent conservation actions together with appropriate storage. The performance of the micro NIR prototype was therefore also evaluated on degraded samples belonging to the three different classes. Degraded films are characterized by a reduced mechanical resistance, embrittlement, distortion and shrinkage, plasticizer exudation, dye fade, gelatin decomposition, delamination and “channeling” of the emulsion[94].

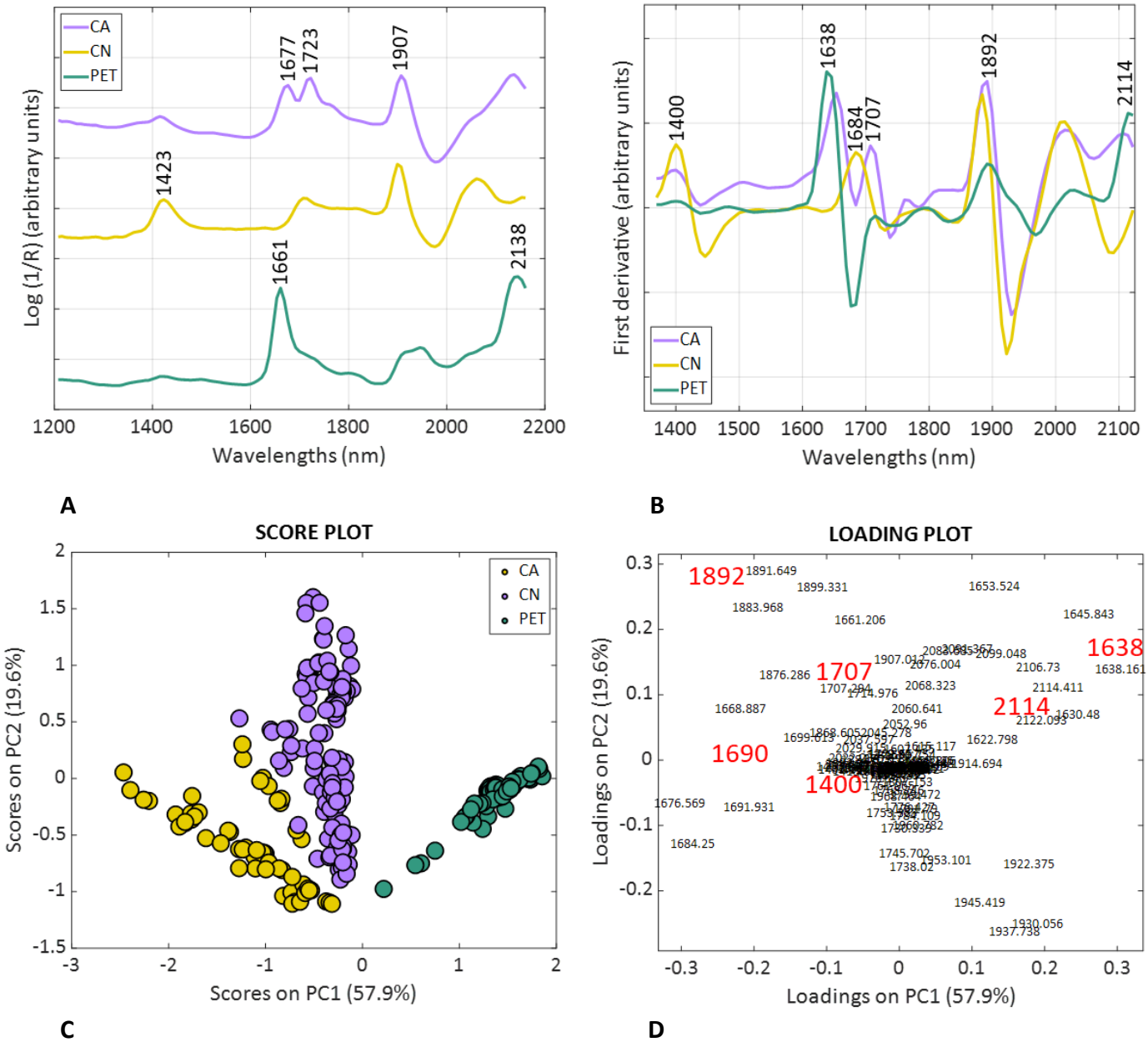

Fig. 25. Analysis of well-preserved cinematographic film samples: A.- representative spectra of cinematographic film support cellulose acetates (CA), cellulose nitrate (CN) and polyethylene terephthalate (PET); B.- first derivative spectra of cellulose acetates (CA), cellulose nitrate (CN) and polyethylene terephthalate (PET); C.- score plot of CA, CN and PET samples; D.- loading plot of CA, CN and PET.

Wavelength (nm)			Assignment
Cellulose nitrate	Cellulose acetate	Polyethylene terephthalate	
1423	1415		1st overtone of OH stretching[124]–[126]
		1415	1st overtone of OH stretching[127]
	1677	1661	1st overtone of CH stretching[120], [122], [127]–[129]
1707	1723	1707	1st overtone of CH stretching[121], [126], [127], [130]
		1799	–
1899			1st combination of OH stretching and bending[130]
	1907	1915	1st combination of OH stretching and bending [123], [124], [130] 2nd overtone C=O stretching[126], [127], [131]
		1945	2nd overtone of C=O stretching[123], [132]
2021			–
	2137	2138	Combination band of aromatic CH stretching and ring vibration[123]

Table 2. Absorption bands in the NIR region of cellulose nitrate (CN), cellulose acetates (CA) and polyethylene terephthalate (PET).

Spectra collected from CA degraded samples showed a strong decrease in the bands at 1661 and at 1723 nm. Conversely, a broad band appeared at 1462 nm which was attributed to the 1st overtone of free OH (Fig. 26.A). These outcomes may be related to the hydrolytic degradation observed in CA degraded materials[55]. To test the discrimination ability of the unsupervised model, a new dataset was created, including both well-preserved and degraded samples, and then submitted to PCA. The resulting plot described three main clusters associated with the three different types of polymers,

each containing well-preserved and degraded samples (Fig. 26.C). The limited dispersion of samples belonging to the same class led to a good discrimination among the various polymeric classes. The loadings plot (Fig. 26.D) confirmed the diagnostic role of bands at 1661, 1707, 1723 and 2138 nm, as previously described. Our NIR prototype is thus suitable for the identification of the film support irrespectively of the state of conservation.

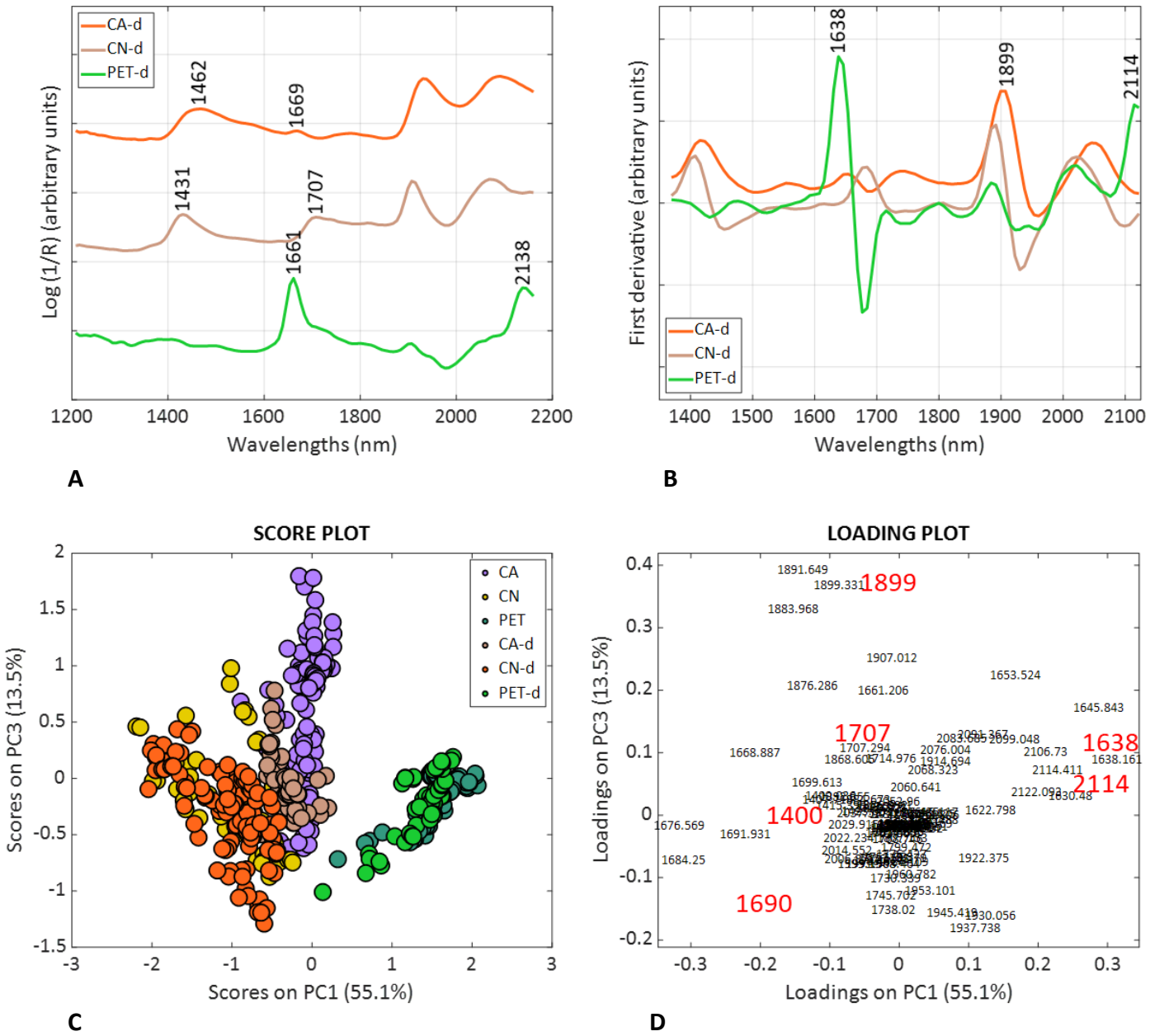

Fig. 26. Analysis of degraded and well preserved cinematographic film samples: A.- representative spectra of cinematographic film support cellulose acetates (CA), cellulose nitrate (CN) and polyethylene terephthalate (PET); B.- first derivative spectra of cellulose acetates (CA), cellulose nitrate (CN) and polyethylene terephthalate (PET); C.- score plot of CA, CN and PET samples; D.- loading plot of CA, CN and PET.

1.4.2 Conclusions

We have proposed a new SWIR portable prototype (1200–2200 nm) in combination with multivariate data analysis. This instrument is at the cutting edge of the development of

miniaturized devices, and it can be used as an on-situ, rapid, non-invasive methodology for identifying and differentiating between different support materials used for the production of historical cinematographic films. The spectral range employed proved to be well suited for the analysis of the whole set of historical films selected as case study, as they all presented characteristic overtone or combination bands.
We believe that the results obtained using our methodology have important implications for the study and preservation of photographic and cinematographic film collections. The differentiation between film materials with different supports can help conservation professionals to safely classify the films. This would improve the resource management of a movie archive regarding the choice of safety measures and storage environments needed for their film collection according to their different chemical composition, therefore reducing safety and degradation risks.

The advantages of the device in terms of cost, portability, ease of use could be exploited not only by conservation scientists but also conservators and conservator-restorers. To this aim, further efforts will be devoted to the development of new chemometric approaches for the automatic data processing and interpretation.

Chapter 2 A non-invasive diagnostic tool for cellulose acetate films using a portable miniaturized near infrared spectrometer

2.1 Introduction

Cellulose Acetate (CA) is a cellulose derivative where hydroxyl groups in the glucopyranose ring have been substituted by acetate groups CH_3COO^-. The average number of OH groups substituted by acetate groups is known as Degree of Substitution (DS).

Once mixed with significant amounts of plasticizer (phosphates and phthalates, to name the most relevant ones), CA was employed for producing sunglasses, combs, brooches and jewelry cases, often imitating expensive materials like mother-of-pearl, ivory or tortoiseshell[53]. Since 1909, and specially from 1948 onwards[133], CA was also used for producing transparent and flexible bases for photographic supports, called "safety films" due to their lower flammability when compared to Cellulose Nitrate (CN) supports[20]. Therefore, CA is a very abundant material in cinematheques and photographic archives.

Unfortunately, CA is also intrinsically unstable and hence, its use has been progressively reduced and substituted with more stable plastics, such as Polyethylene Terephthalate (PET)[134]. CA objects pose serious threats to museum collections, as this polymer shows thermal, photocatalytic and hydrolytic deterioration mechanisms which trigger the heterolytic scission of acetate substitutive groups from the CA chain[23] (Figure 27). The resulting CH_3COO^- gases react with environmental water, producing acetic acid, which further catalyze the scission of acetate groups and the hydrolytic reduction of the molecular weight of the polymer; affecting sensible materials in the vicinity too.

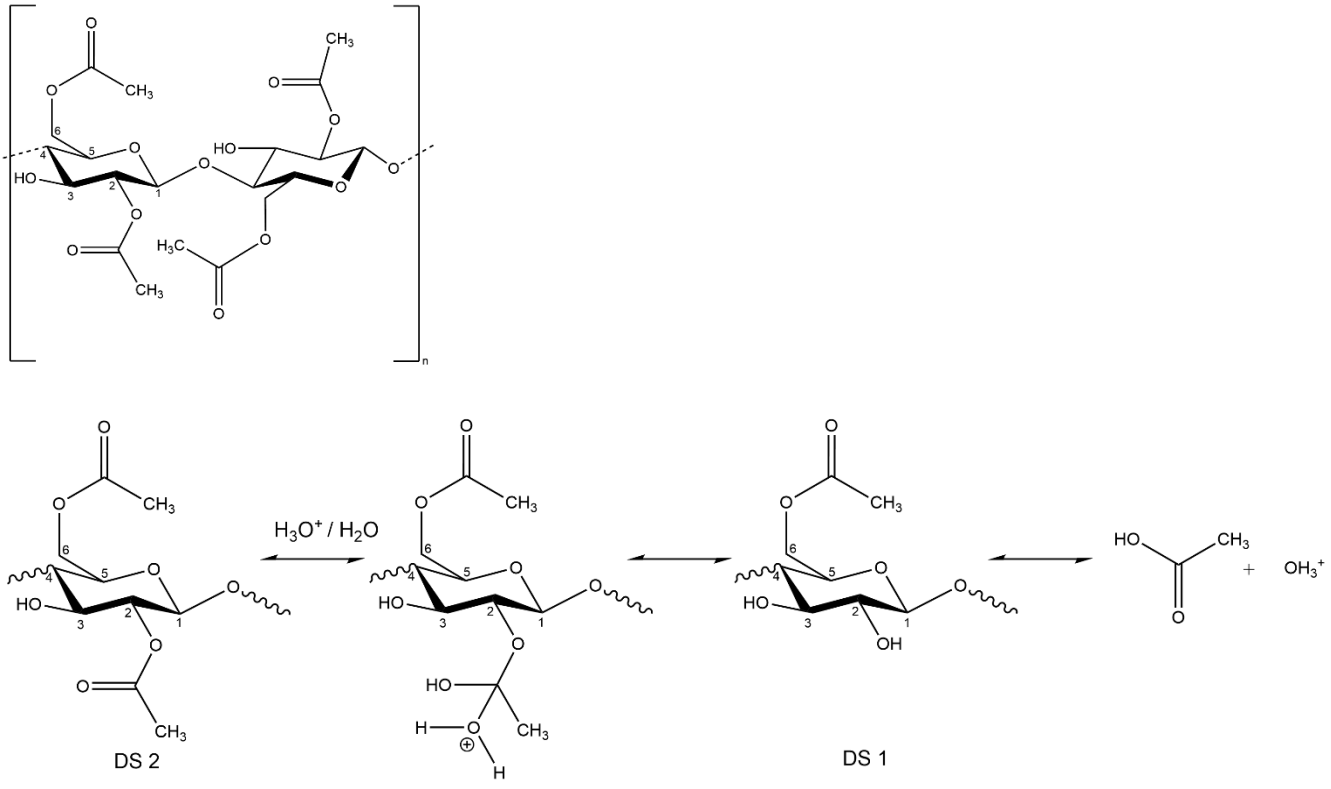

Fig. 27. The repeating structure of CA (up) and the polymer's hydrolytic breakdown mechanism (below).

These mechanisms develop quickly under uncontrolled storage conditions, particularly in unventilated environments with high temperature and relative humidity. As a consequence, CA objects may shrink and become distorted, frail and brittle; until the object finally crumbles down to dust[135]. Therefore, to prevent the loss of CA artifacts and film bases, their accurate condition assessment and monitoring are key for heritage institutions, as they allow to design suitable conservation strategies regarding display and storage conditions (e.g., for choosing separate, cool or cold storages)[10].

Usually, conservators identify the condition of CA objects from their superficial appearance (luster and texture), their expected degradation effects, and their smell. However, naked-eye observation alone is often unreliable because each object may render a wide variety of finishing appearances.

Considering that the DS of CA correlates well with the condition of the artifact, being hydrolysis its primary degradation mechanism, the measurement of DS in CA objects has been proposed as a method to diagnose their condition[23].

However, the evaluation of DS within a real historical object may be challenging. DS may be accurately measured by titration after alkaline hydrolysis of ester bonds to ascertain the percentage of combined acetic acid[121]. Nuclear Magnetic Resonance (NMR) and chromatographic techniques such as Gas Chromatographic Analysis (GC) and Ion Chromatography (IC) have been reported to accurately quantify DS in CA by measuring acetic acid content after removing any plasticizers by solvent extraction[136], [137]. However, all these techniques require (sometimes considerable) sampling, and such invasiveness is often unsuitable for the analysis of heritage objects. Furthermore, the required sample pretreatment and experimental set-ups are sophisticated and therefore, not readily available for every museum in the world.

In previous researches[23], [54], Fourier Transform Infrared (FTIR) spectroscopy both in transmission and macro Attenuated Total Reflectance (ATR) acquisition modes was used to calculate the DS of CA.

This was done by analyzing Microcrystalline Cellulose (MCC) and Cellulose Diacetate (CDA) standards, as well as their mixtures, to record the spectroscopic results equivalent to different DS. Calibration curves were then prepared by plotting DS as a function of the ratio between a reference band, such as COC stretching (vCOC), and that of a probe peak, like OH stretching (vOH), not affected by the presence of plasticizers.

Afterwards, these curves were applied to quantitatively calculate the values of DS in CA historical artifacts, and the DS thus calculated correlated well with the different conditions of the artifacts when assessed from their degradation effects (i.e., amount of shrinking, rigidity, fragility and distortion)[23].

In particular, ATR mode posed the advantage of providing diagnostic information without the need of sampling. However, this analysis introduces the risk of creating marks in the surface of heritage objects due to the pressure applied by the tip of the ATR crystal during measurement.

Also, ATR analysis is restricted to the study of flat surfaces, in order to ensure good contact between the crystal and the object and obtaining good quality spectra. Furthermore, the sensibility of the ATR-FTIR technique is constrained to approximately one micron depth from the surface[138], and thus it

may lead to less representative results if the degradation of an historic artefact varies at different depths.

Near Infrared (NIR) spectroscopy allows to register overtone and combination bands related to a few functional group molecular vibrations in the near-infrared region (4000 to 12500 cm^{-1}, i.e. 800 to 2500 nm)[139], thus enabling the chemical characterization of both organic and inorganic materials. NIR spectroscopy is an extremely fast and cost-effective way to conduct molecular investigation of polymers, particularly when applied in Diffuse Reflectance acquisition mode, and it is now widely employed for plastic waste classification at recycling facilities[140].

However, despite its low cost and ease of application, this technique has not yet been widely implemented in the context of heritage institutions, due to the inherent complexity of the broad and poorly resolved overtone and combination bands, which often overlap each other, being less specific for substance mixtures and harder to interpret when compared to the more-straightforward spectra obtained from fundamental bands in the Mid-infrared range (4000-400 cm^{-1}).

Nevertheless, in our previous paper (Catelli et al., 2020), NIR results proved useful for classifying heterogeneous artwork samples, showing highly specific responses for polymers in cinematographic film bases, which allowed for their identification[81]. The same research proved that, specifically for film bases constituted of CA, NIR possessed diagnostic power for differentiating degraded CA films from better-preserved ones, showing promising capabilities as a tool for monitoring the molecular condition of this polymer, with the advantages of being a non-invasive technique and requiring inexpensive and relatively simpler instrumentation than FTIR spectroscopy.

For this reason, and aiming to obtain a fast and inexpensive way to monitor the condition of CA cinematographic and photographic films in heritage collections, we hereby propose an accurate, non-invasive method for diagnosing CA film bases, based on the measurement of their DS, by employing a NIR calibration function built with a commercially-available, portable and miniaturized NIR spectrometer. This method exploits the hypsochromic shift experienced by the first overtone band of the OH stretching mode (2νOH) in cellulose acetate esters, which follows a decrease in DS.

The NIR spectrometer employed operates in Diffuse Reflectance over a range between 900 and 1700 nm (Short-Wave-IR), and being a small and light equipment (45 mm in diameter, 47.5 mm in height, and 60 g of weight), it allows for on-site measurements to be performed directly on the object without sampling, by simply bringing the surface of the artifact in contact with the sensor.

Before its application, the proposed NIR diagnostic method was validated by comparison to a well-accepted micro-invasive technique in the Mid-infrared range, Attenuated Total Reflectance Fourier Transform Infrared Microscopy (μATR-FTIR).

To ensure the robustness of the method, both NIR and FTIR calibration functions were built by performing replicate measurements on three separately-prepared standards sets.

Finally, sixteen historical cinematographic film samples with CA supports were diagnosed using both techniques, obtaining comparable results.

2.2 Aim of study

The first objective of the research is to generate a non-invasive calibration function for calculating the DS of CA cinematographic and photographic film bases, allowing for their accurate diagnosis, specifically by using the Diffuse Reflectance response of a portable and commercially available NIR spectrometer. This protocol will be useful for identifying the current condition of CA objects, for the early detection of degrading CA materials, and for evaluating the performance of cold and cool storage procedures intended to slow hydrolytic deacetylation.

The second objective is to validate the response of the NIR function by comparing the DS thus calculated, to the DS calculated with a μATR-FTIR calibration function built by following the methodology proposed by Nunes et al.[23]. Confirmation of the robustness of both NIR and μATR-FTIR calibration functions will be ensured by performing several measurements on separately prepared standard set replicates.

The applicability and effectiveness of the proposed NIR calibration function will be finally tested on several naturally-aged CA cinematographic films. This will be done by siding different NIR and μATR-FTIR measurements to separately calculate their DS, comparing both results and linking them to the macroscopic condition of the films.

2.3 Materials and methods

2.3.1 Reference materials

Cellulose Triacetate (CTA, Fluka, DS 2.97) and Triphenyl Phosphate (TPP, Sigma-Aldrich, ≥ 99%) in pellet presentation; Cellulose Diacetate (CDA, Sigma-Aldrich, DS 2.31) and Microcrystalline Cellulose (MCC, Sigma-Aldrich) in powder presentation; as well as Diethyl Phthalate (Alfa Aesar, 99%) in liquid presentation were purchased as standards.

With the exception of DEP, all reference materials were characterized by using μATR-FTIR and NIR after being pressed into pellets. DEP was instead imbibed into KBr and then pressed into a pellet before being submitted to NIR and transmission FTIR analysis.

The resulting spectral bands of MCC, CDA and CTA were attributed using bibliographic references.

The spectra of TPP and DEP, the most common additives used for cinematographic film production for plasticizing and flame retardant purposes, were analyzed to confirm that their contribution did not affect the FTIR and NIR response in the regions of interest for DS calculation in CA: For the Mid-infrared, the regions at 3330 cm^{-1} (for the νOH probe band) and ca. 1030 cm^{-1} (for the νCOC reference band); and in the near infrared, the range between 1410-1479 nm related to the 2νOH band.

2.3.2 Preparation of reference standards

In order to produce a μATR-FTIR calibration curve tailored to our FTIR spectrometer following the methodology of Nunes et al.[23], and for preparing the new NIR calibration function, three separate sets of 6 standard pellets each were prepared using CDA (DS 2.31) and MCC (DS 0) powders.

Each set of 6 standard pellets contained one reference made of pure CDA, one made of pure MCC, and the remaining four references were prepared by mixing CDA and MCC to reproduce the spectroscopic results equivalent to four different DS (i.e., 0.5; 1.0; 1.5 and 2.0), measuring the weight ratios according to the equation reported in literature[23]. The reagents for the reference standards were weighted with a Discovery DV215CD Ohau Corporation® analytical balance.

To prepare the standards, CDA and MCC powders were carefully and thoroughly grinded in an agate mortar in order to obtain homogeneous mixtures. After grinding, the references were pressed under 2 tons for 1 minute to obtain compact pellets, which were kept for 24 hours in a desiccator before performing μATR-FTIR and NIR measurements. Additionally, one CTA piece was analyzed in a flat area without any sample pretreatment, employing the same methodology used for the pressed pellet references.

2.3.3 NIR analyses, data elaboration and calibration function

All pressed standard references and the CTA pellet were analyzed by placing them between the spectrometer and a gold-coated glass holder. In all cases, 9 measurements per standard were taken at the same area of analysis. The spectra coming from each standard were then compared, and an interpretation of the observed trends was proposed following a bibliographic research. Pretreatment of the data was also performed before this comparison by applying a Quadratic Detrending transform using in-house Matlab routines (The Mathworks Inc., Natick, USA). This aimed to correct for both baseline shifts and exponential global intensity variations which could affect the signals.

For the function calculations that followed, the raw spectra were used as such without any pretreatment.

The average 2νOH band maximum wavelength (λ, in nm) per standard pellet was subtracted to the 2νOH band maximum λ in the CTA reference spectrum (registered at 1416 nm) to calculate its average 2νOH band shift.

The average 2νOH band shift of the three pellets with the same DS was then averaged. The NIR calibration functions were built by plotting the final shift values against the DS as a linear and 2^{nd} degree polynomial regression using Microsoft Excel™. The most satisfactory function was chosen by observing the trend of the data, and ensuring a high coefficient of determination (R^2).

Afterwards, the NIR calibration function was validated by comparing the DS estimated with the NIR for each standard pellet against the DS calculated with a μATR-FTIR calibration curve created with the same standards.

Additionally, a more detailed examination of the 2νOH signal was carried out by subjecting a representative spectrum of each reference to a 2^{nd} derivative for the region 1290-1670 nm, which allowed to identify the position of the most important components present in this range, which we tried to define by performing a peak deconvolution using the Peak Resolve function of Omnic software, assuming that each component had Gaussian distribution, without any baseline correction.

2.3.4 µATR-FTIR analyses and calibration function

At least 6 µATR-FTIR spectra were acquired per pressed reference pellet and for the CTA pellet. The spectra were then used without any correction or further manipulation, to calculate the ratio between the absorbance of the νOH band at 3330.6 cm^{-1} (probe band) and the absorbance of the νCOC band at 1020-1039 cm^{-1} (reference band, with the point of the band maximum variating slightly depending on the sample), using the procedure reported by Nunes et al.[23].

The absorbances of the probe and reference bands were measured using the peak heigh tool of the Omnic 7.2® Software (Thermo Fisher Scientific™), delineating both baselines and measuring the absorbance from the maximum of the band to the corresponding baseline. The baseline for the νCOC band was drawn between the points at 1517.8-1508.1 and 848.6-746.3 cm^{-1}, and the baseline for the νOH band was defined between the points at 3700.9 and 3178.2-3099.2 cm^{-1}.

The average νOH/νCOC ratio per standard reference was calculated, and the resulting ratio was then averaged with the average of the other 2 pellets with the same DS.

Afterwards, DS was plotted as a linear and 2nd degree polynomial regression of the final νOH/νCOC ratios using Microsoft Excel™. The most satisfactory function was chosen by observing the trend of the data and preferring a high coefficient of determination (R^2).

2.3.5 Miniaturized NIR spectrometer

NIR measurements were collected with a portable NIR spectrometer by Viavi Solutions (JDSU Corporation, Milpitas, CA), a compact device controlled by a portable computer via USB port, registering the diffuse reflectance in the spectral range of 908.1–1676.2 nm (11013.2 –5966.6 cm^{-1}) at a nominal spectral resolution of 6.2 nm. The system is equipped with a Linear-Variable Filter (LVF) as dispersing element, directly connected to a linear 128-pixel Indium Gallium Arsenide (InGaAs) uncooled detector, and employs two tungsten light bulbs as radiation source. The instrument allows for an analysis spot of ca. 3 mm diameter.

For the acquisition, first the dark current (D) was measured by placing the spectrometer carefully distant from any surface; then, a raw reflectance reference measurement was acquired from a Spectralon NIR-reflectance standard S(λ) with known 99% diffuse reflectance values s(λ). Raw reflectance measurements were then recorded from the reference pellets or real films T(λ) by using 100 scan iterations and an integration time of 10.1 ms, resulting in a total of 1.01 second analysis time per measurement. The dark current and reference spectra were kept under 1 minute age, and the sensor temperature stayed between 36° and 40°C for all measurements. The MicroNIR Pro software (JDSU Corporation, Milpitas, CA) was used for data acquisition.

2.3.6 Benchtop FTIR spectrometer

µATR-FTIR measurements were acquired from the same areas previously analyzed by NIR, using a Thermo Scientific® Nicolet iN 10MX spectrometer fitted with a mercury–cadmium–telluride (MCT) A-type detector cooled with liquid nitrogen, and an X–Y–Z motorized stage with 1 µm incremental steps. Spectra were recorded in the 4000 to 675 cm^{-1} range using a spectral resolution of 4 cm^{-1}, employing a Ge ATR crystal with an optical aperture of 400x400 µm in all cases (except for some real

films, where an aperture of 150x150 was employed), integrating 64 scans for each measurement and for the background, which was acquired before each measurement.

Instead, the KBr pellet imbibed with the DEP reference was analyzed in transmission FTIR by using a Nicolet iS50 spectrometer fitted with a Deuterated L-alanine-doped Triglycene Sulphate (DLaTGS) detector operating at room temperature. Spectra were recorded in the 4000 to 400 cm^{-1} range with a spectral resolution of 4 cm^{-1}.

2.3.7 Real Cinematographic films diagnosed with NIR and FTIR functions

Sixteen developed cinematographic film rolls or film sections, all with CA polymeric bases of 35 mm gauge, were kindly provided by the Fondazione Cineteca di Bologna (Table 3). Their DS was calculated by using the NIR and μATR-FTIR calibration functions, without any sample preparation.

These 16 samples corresponded to different element typologies (black and white, color, negative and positive elements), manufacturing companies, and covered gradual stages of degradation. Preliminary information about the polymeric base composition was obtained by film inscriptions, as well as conventional mechanical and visual film examination. The macroscopic state of conservation of the film samples was assessed by registering their degradation effects.

Sample name	***Element typology***	
CA1	Positive	Color
CA4	Positive	Color
CA6	Positive	Black & White
CA7	Negative	Color
Time0	Negative	Color
AA1	Unknown	Color (transparent)
AA4	Negative	Color
AA5	Positive	Color
CT4	Positive	Color
CT5	Positive	Color
CT10	Positive	Color
CT11	Positive	Color
CT12	Positive	Color
CT21	Positive	Color
CT24	Positive	Color
PSATCT-roll3	Positive	Color

Table 3. Description of the real cinematographic film samples analyzed

For each film sample, at least 3 μATR-FTIR spectra were acquired, and 9 to 15 NIR measurements were registered on the same area. Regarding the NIR, all real cinematographic film samples were analyzed directly in contact with the CA polymeric base by placing them between the spectrometer and a gold-coated glass holder (Fig. 28). For black and white films, NIR analyses were performed in regions where the emulsion at the opposite side of the film appeared clear, therefore containing low silver particle presence to avoid distortion of the NIR spectra.

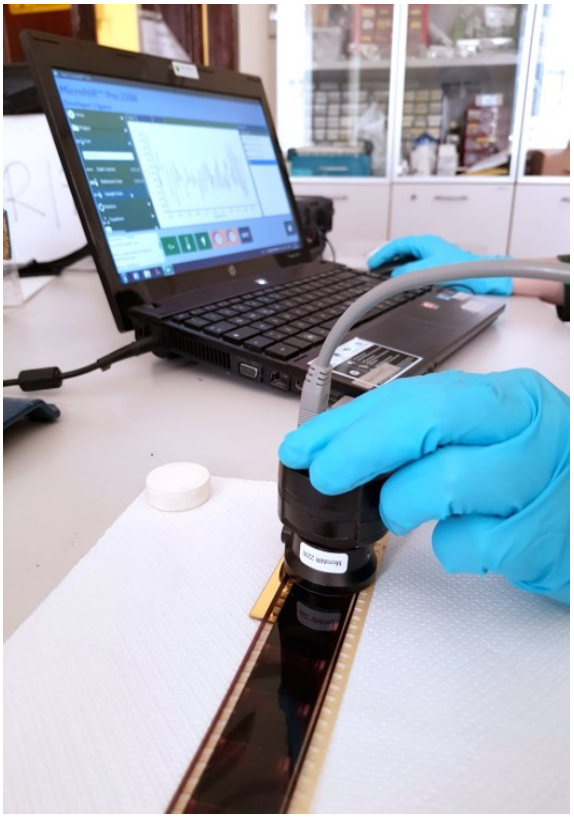

Fig. 28. NIR analysis of a real CA cinematographic film.

The resulting spectra were employed without performing any pretreatment or correction to calculate the average 2νOH band shift (NIR) and average νOH/νCOC ratio (μATR-FTIR) per film. These results were then employed for calculating the DS of the CA base in each film by solving the corresponding NIR and μATR-FTIR calibration functions. The DS values calculated by the NIR and the μATR-FTIR techniques were compared, and the percentual difference calculated.

2.4 Results and discussion

2.4.1 NIR characterization of the standard materials

A first overview of the NIR spectra of the seven reference corresponding to different DS, showed particular spectral profiles in the NIR region between 900 and 1700 nm, in which overtone and combination bands of CH and OH and appear (Fig. 29).

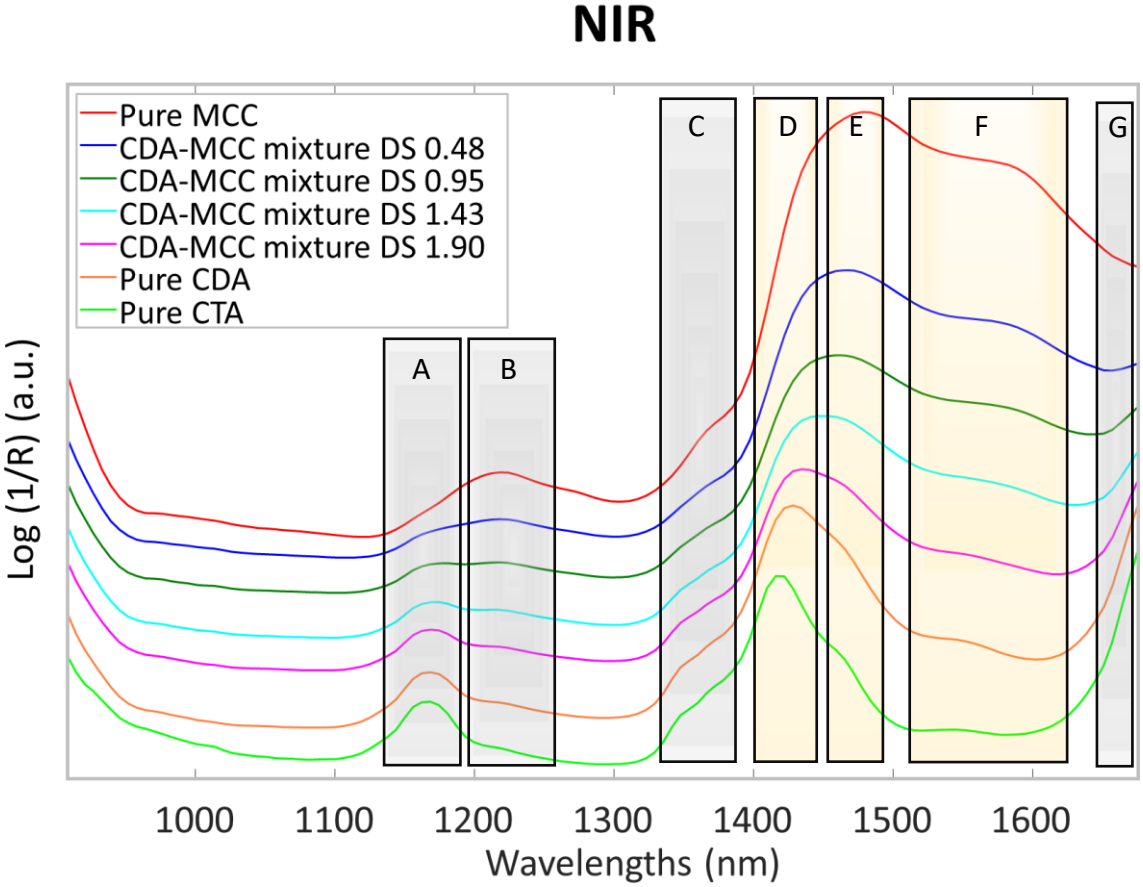

Fig. 29. Selected untreated spectra for each of the 7 standard reference materials. The frames indicate the regions (A to G) where different signals appear (assignment is given in Table 4). Regions D to F (highlighted in yellow), corresponding to OH vibrations, were employed for building the calibration functions.

The assignment of the bands in each region of the spectra is shown in Table 4. In particular for the region 1270-1670 nm, deconvolution of the spectra (see Figures SMI.1 to SMI.7) allowed to identify the most important components, following the approach of the NIR studies of hydrated cellulose performed by Cichosz and Masek [141] and the studies of untreated, heated and acetylated wood by Mitsui et al.[142].

Wavelength (Region by letter, peak maxima in nm)	Assignment
A.1162-1181	2nd overtone of CH_3 stretching[143]
B. 1218-1273	2nd overtone CH, CH_2 stretching[125], [126], [143], [144]
C. 1348 & 1367	1st overtone of CH_3 stretching and bending [118], [126], [143]

D.1416-1429	1st overtone of OH stretching, amorphous region [81], [125], [126], [141]–[147]
E.1466-1478	1st overtone of OH stretching[118], [144], [147] in semi-crystalline region[126], [141], [143], [146]-
F. 1551-1553, 1577-1603 and 1631-1639	1st overtone of OH stretching[125], [126], [145] affected by intra and inter chain hydrogen bonds (3OH···O5 and 2OH···O6) in the crystalline region[118], [141]–[143], [146], [148]
G.1670	1st overtone of CH stretching[81], [125], [126], [143], [144], [148]

Table 4. Interpretation of the NIR spectra for the seven standards shown in Figure 29, divided by regions (letters A-G)

All standards are divided in two main regions where two different types of diagnostic bands appear, namely, the region between 1100 and 1400 nm, which corresponds to overtones of CH vibrations; and the region between 1400 and 1660 nm, which is related to the 1st overtone of OH stretching. Furthermore, our spectrometer partially detected the contribution of the 1st overtone of CH stretching, which is known to appear from 1670 nm[81].

The changes in the spectra followed specific trends as DS increased, and we first sought to interpret this behavior in order to exploit it as a suitable diagnostic tool for film base condition assessment.

From the comparison of the spectra corresponding to each reference, one of the most outstanding features was the behavior of the signals at ca. 1162-1181 nm and 1218-1273 nm, both attributed to the second overtone of the stretching of CH substitutive groups. In particular, as the DS increased, the intensity of the band at 1218-1273 nm decreased too, and the intensity of the band 1162-1181 nm increased instead. The attributions found in literature suggest that, in particular for cellulose and cellulose acetate esters, the signals in the 1162-1181 nm range are mostly related to the contribution of methyl group (CH_3) vibrations, whereas those at the 1218-1273 nm interval are related instead to methine and methylene groups (CH, CH_2). The NIR spectral behavior of the analyzed standards therefore accurately suggest a decrease in CH_3 abundance with the decrease of DS, and a stronger contribution of CH and CH_2 groups.

Another important trend, and the one exploited for our proposed diagnostic method, is the one related to the changes of the bands appearing between 1400 and 1660 nm. This region is usually attributed to the first overtone of the OH stretching (2νOH), and for cellulose samples, different components and their attributions have been proposed by previous researches[141], [142]. In our standards samples, as DS decreases, the maximum registered of the bands in this region shifts to

higher wavelengths (lower frequencies), acquiring also higher relative intensity. A deconvolution of these bands allowed to better understand the changes in the contribution of the different components.

The prevalence of the signal at 1416-1429 nm corresponds to a higher contribution of hydroxyl groups in amorphous regions of the polymer; a maximum signal at 1466-1478 nm reflects a higher abundance of hydroxyl groups in semi-crystalline regions, whereas the increase of the signals at 1551-1639 nm is related to more hydroxyl groups involved in intra molecular hydrogen bonds in crystalline regions of the polymer[118], [141]–[143], [146], [148].

This accurately reflects the fact that the cellulosic chain decreases in crystallinity with the increase of DS, as acetyl groups alter its degree of structural organization, modifying also inter and intra chain interactions[54]. In fact, it is known that the influence of hydrogen bonding seem to contribute to the shift of the vOH fundamental band in the Mid-infrared region to lower wavenumbers[42], [59], and this could explain the corresponding shift of the 2vOH band in the NIR range to higher wavelengths. Finally, the increase in relative intensity of the 2vOH bands with decrease of DS reflects the higher abundance of hydroxyl groups in the cellulosic chain.

Cellulose acetate film bases may contain from 20-40% in weight of Diethyl Phthalate (DEP) and from 10 to 20% in weight of Triphenyl Phosphate (TPP)[64]. CA molecules are supposed to stablish mainly weak interactions with DEP, ruled by van der Waals forces[149] and dipolar interactions[59], [150], although some have suggested that hydrogen bonding occurs as well as between carbonyl groups in DEP, which act as hydrogen-acceptors, and hydroxyl groups in CA, the hydrogen donors[41]. Instead, hydrogen bonds are formed between O-H in CA and P=O groups in TPP, and weak interactions are formed as well between C=O in CA and P-O-Ph in TPP[78].

NIR spectra of Pure TPP exhibits its strongest signal at 1131 nm, attributed to the second overtone of aromatic CH stretching [123], [147]. As secondary signals, pure TPP showed also a series of bands at 1342, 1373, 1404 and 1428 nm.
Pure DEP showed instead two signals of similar intensity at 1137 and 1181 nm, the first of which may be attributed to the second overtone of aromatic CH stretching and the second overtone of methylene stretch respectively[123], [147], [151]. Both spectra are shown in Figure SMI.8.

Even if both plasticizers show responses overlapping the region related to the first overtone of the OH stretching in Cellulose and its acetate derivatives, we assumed that their contribution is low as these additives are present in relatively minor amounts in cinematographic film supports, specially taking into account the characteristics the NIR spectrometer, which enables to perform a bulk analysis where the response of the most abundant material, in this case Cellulose acetate, would overcome the response of materials present in lower quantities, such as the gelatin emulsion layers or the plasticizers. However, as it will be seen later, only the analysis of plasticized historical cinematographic samples would confirm this hypothesis.

2.4.2 µATR-FTIR characterization of the standard materials

Reference materials were characterized by µATR-FTIR, and the attribution of the bands of CTA, CDA and CTA pure standards is shown in table SMI.1.

In the µATR-FTIR spectra (Figure 30), we observe an intensity increase and a shift to lower wavenumbers of the OH stretching band (vOH, 3500-3330 cm^{-1}) with the decrease of DS. The increased intensity of the band has been attributed to the increased amount of free OH groups in samples with lower DS, whereas the red shift of the peak relates to hydrogen bonding affecting the OH groups involved. The intensity changes and wavelength shift of the OH band observed in the Mid-infrared range follow the same trend observed in the SWIR range, and therefore they must be explained by the same factors[152].

The µATR-FTIR spectrum of Pure TPP (Figure SMI.9) exhibits its strongest signals at 1588, 1484, 1293, 1174, 1160, 1008, 946, 784, 768, 753 and 689 cm^{-1}, as well as a series of smaller peaks at 3098, 3060, 3020, 1455, 1232, 1192, 1070, 1022, 964, 932 and 914 cm^{-1}.

The µATR-FTIR spectrum[1] of Pure DEP (Figure SMI.10) shows its strongest bands at 1724, 1281, 1123, 1073 and 744 cm^{-1}, as well as minor signals at 3073, 2984, 2929, 2905, 2875, 1600, 1580, 1447, 1391, 1367, 1173, 1040, 1017, 864 and 705 cm^{-1}. A proposed band assignment for the Mid-infrared response of TPP and DEP is given in table SMI.2. As it has been highlighted by previously, both additives of have either low or no contributions in the regions of the probe and reference bands used for the calculation of DS though FTIR calibration functions.

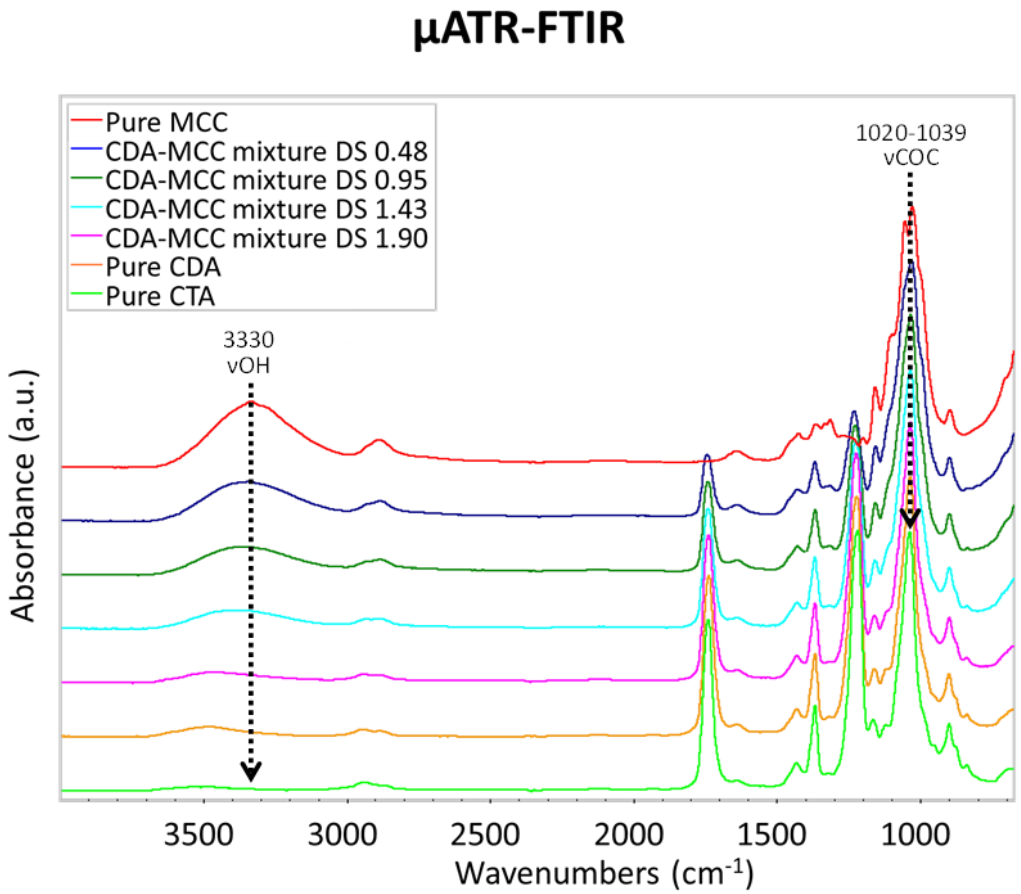

Fig. 30. Selected spectra of each reference standard used to build the calibration functions.

2.4.3 NIR and µATR-FTIR calibration functions

As portrayed in Figure 31, the NIR data followed a linear trend with increasing DS. Formula 2 shows the obtained NIR calibration function for Quantification of the DS:

$$y = -0.0474x + 2.9282$$

(2)

where *y* is the wavelength shift (in nm) of the maximum of the 2vOH band in the analyzed sample respect to the wavelength registered for the same band for the CTA reference.

For µATR-FTIR results, the data followed an non-linear but ascending quadratic curve with DS increase. Formula 3 is the resulting µATR-FTIR calibration function for quantification of the DS:

$$y = 78.592x^2 - 30.109x + 2.9022$$

(3)

where *y* is the ratio between the absorbance of the OH stretching at 3330.6 cm^{-1} (probe band) and of the COC stretching at ca. 1030 cm^{-1} (reference band).

It was interesting to note that measuring the ratio for high DS samples was difficult, due to the reduced sensibility of the Ge crystal in the region around 3000 cm^{-1}, which rendered low signal-to-noise ratio in the area related to the OH stretching.

Both resulting functions obtained a high coefficient of determination (R^2), over 0.97 for and over 0.99 for NIR, therefore they were considered to be robust enough to test their reliability for the analysis of real samples.

2.4.4 Diagnosis of 16 historical cinematographic films

16 cinematographic film samples were analyzed. An initial overview of their macroscopic appearance allowed us to classify ten of them in overall good condition (showing no color changes in their emulsion, good flexibility, resistance and absence of blooming or vinegar odor), four in intermediate condition (with dye fading, rigidity, distortion) and one sample as heavily degraded (fragmentary and frail, brittle, with yellowish base).

By µATR-FTIR analysis, it was confirmed that in all cases they corresponded to CA bases plasticized with TPP.

After calculating the DS with both functions, the absolute and percentual difference (being DS of 3 equal to 100%) between both was assessed. This allowed us to ensure that the DS calculated with the NIR was consistent. The data used for calculation and comparison is summarized in table SMI.3.

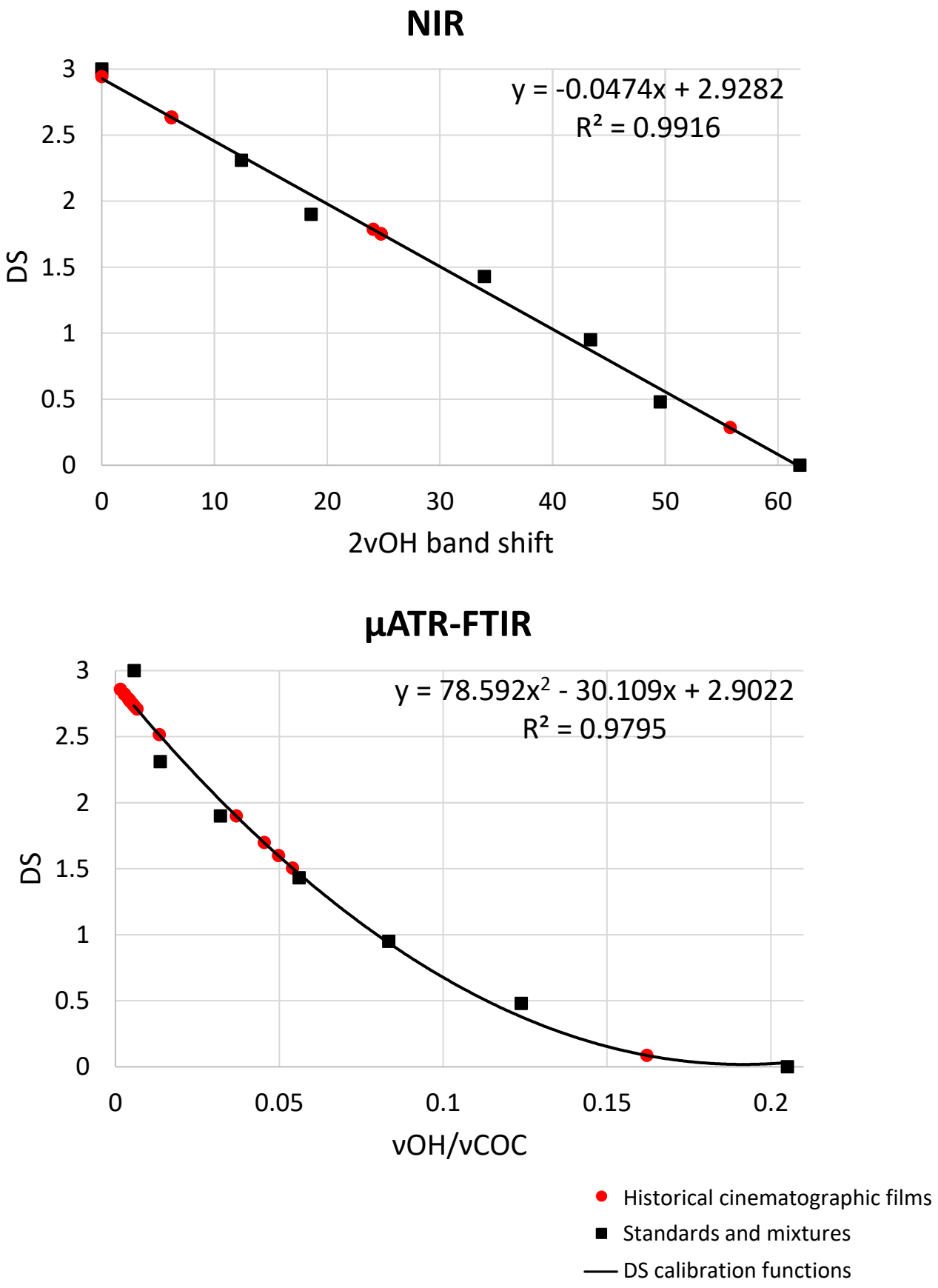

Fig. 31. DS calibration functions. Above: NIR; below: µATR-FTIR. Black squares stand for standards and mixtures, red dots for historical cinematographic films

2.5 Conclusion

A new diagnostic method for DS measurement of CA film bases using a NIR calibration function was found to be reliable, and its results comparable to those obtained by FTIR in the Mid-infrared range. In particular, a new version of a previously proposed Mid-infrared calibration curve was performed using µATR-FTIR with a Germanium tip, and it was proven that the NIR function shows higher reliability for DS measurements in samples with high DS, due to its higher sensibility towards the 2vOH vibrations when compared to the sensitivity of the µATR Ge tip towards vOH vibrations.

Even if the NIR method showed that the abundant presence of silver particles on the emulsion of cinematographic films may interfere with the signal to noise ratio of the spectra, it nevertheless showed excellent results for color and B&W elements where lower concentration of silver particles was observed.

This method constitutes a simple, fast, inexpensive and non-destructive way to diagnose cellulose acetate bases in cinematographic films and photographic negatives, and seems to have the potential to be employed to other kind of tridimensional CA artifacts.

2.6 Supplementary Material I

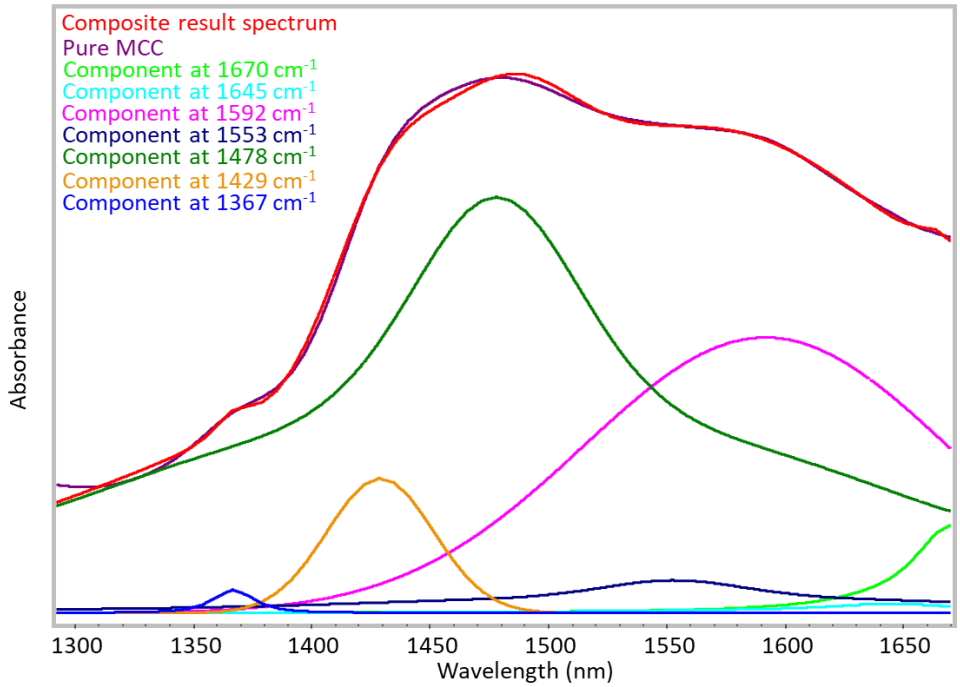

1

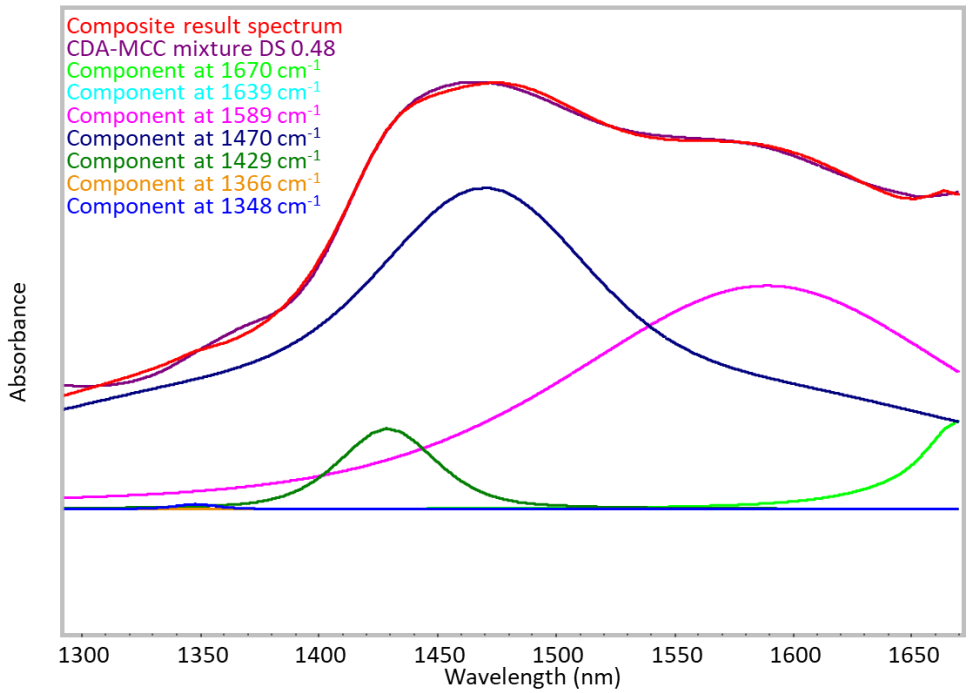
Composite result spectrum
CDA-MCC mixture DS 0.48
Component at 1670 cm-1
Component at 1639 cm-1
Component at 1589 cm-1
Component at 1470 cm-1
Component at 1429 cm-1
Component at 1366 cm-1
Component at 1348 cm-1
Absorbance
1300
1350
1400
1450
1500
1550
1600
1650
Wavelength (nm)

2

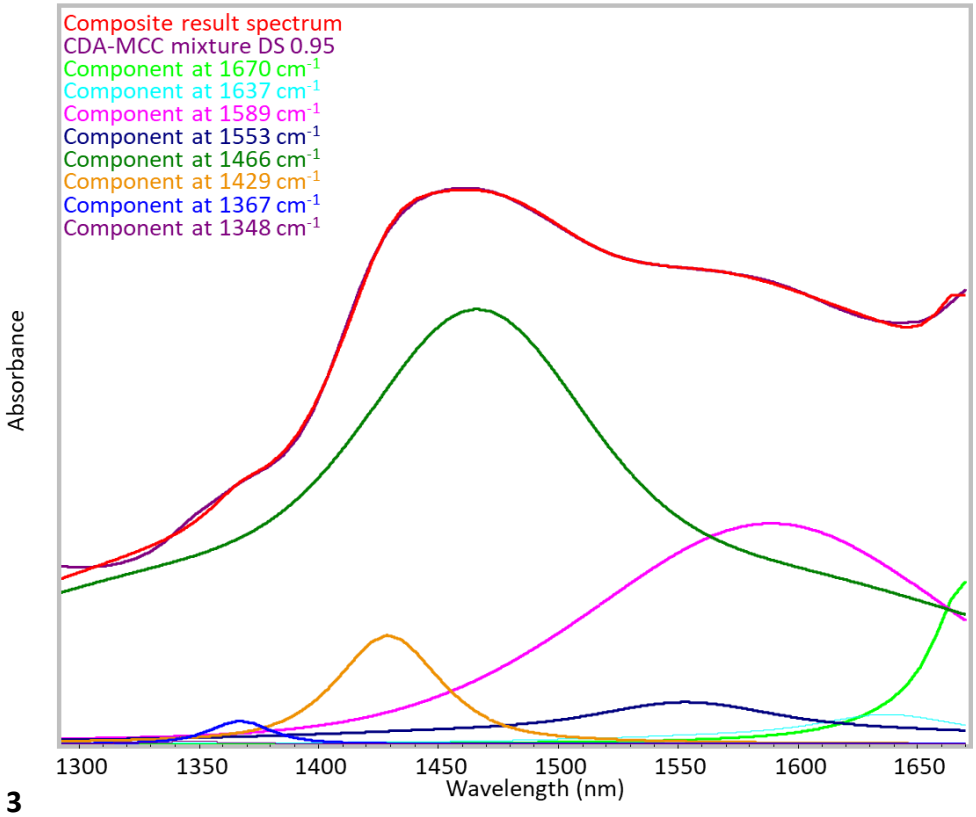
Composite result spectrum
CDA-MCC mixture DS 0.95
Component at 1670 cm-1
Component at 1637 cm-1
Component at 1589 cm-1
Component at 1553 cm-1
Component at 1466 cm-1
Component at 1429 cm-1
Component at 1367 cm-1
Component at 1348 cm-1
Absorbance
1300
1350
1400
1450
1500
1550
1600
1650
Wavelength (nm)

3

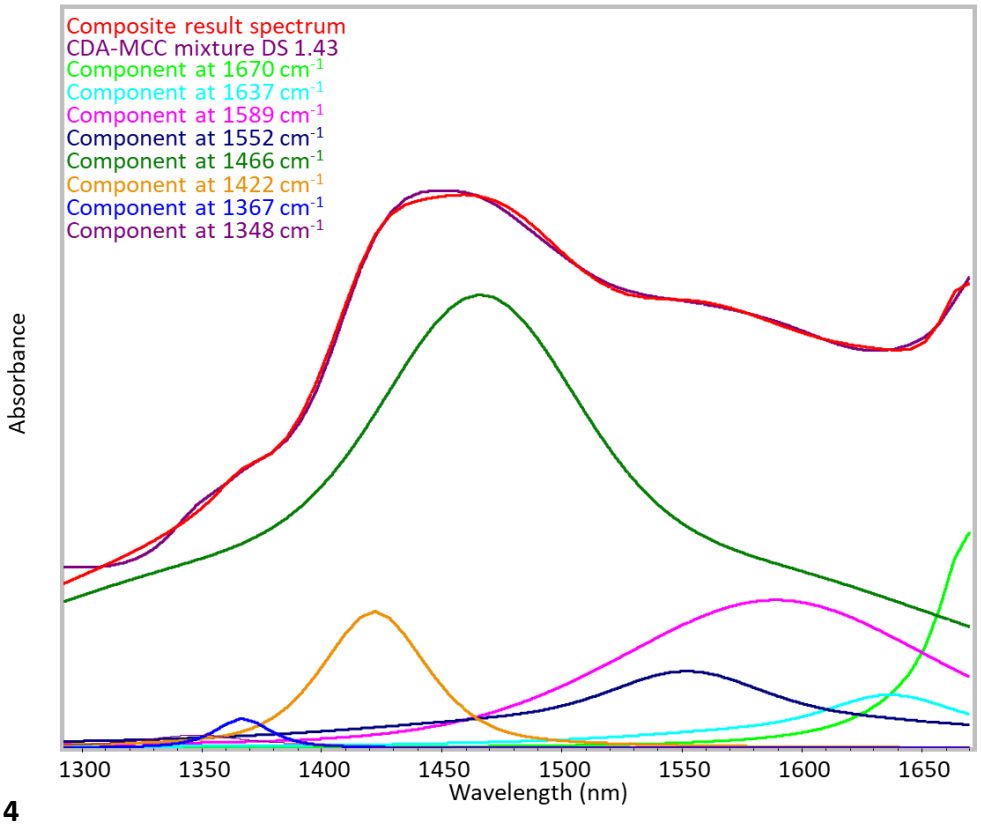
Composite result spectrum
CDA-MCC mixture DS 1.43
Component at 1670 cm-1
Component at 1637 cm-1
Component at 1589 cm-1
Component at 1552 cm-1
Component at 1466 cm-1
Component at 1422 cm-1
Component at 1367 cm-1
Component at 1348 cm-1
Absorbance
1300
1350
1400
1450
1500
1550
1600
1650
Wavelength (nm)

4

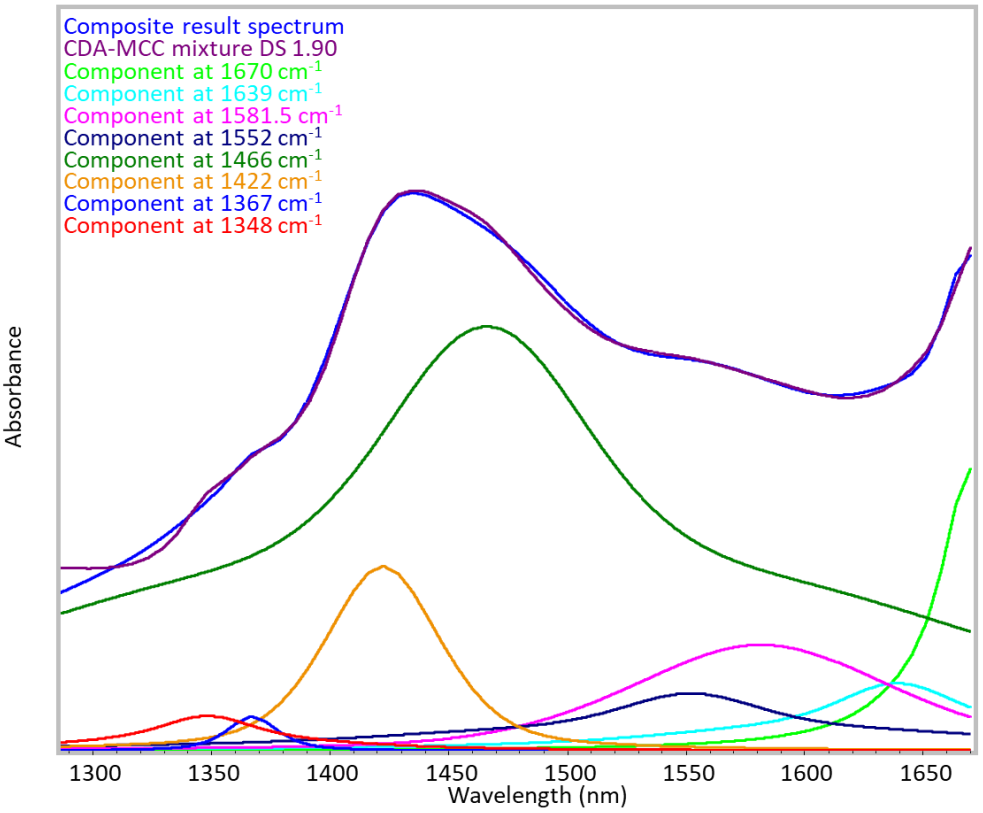
Composite result spectrum
CDA-MCC mixture DS 1.90
Component at 1670 cm-1
Component at 1639 cm-1
Component at 1581.5 cm-1
Component at 1552 cm-1
Component at 1466 cm-1
Component at 1422 cm-1
Component at 1367 cm-1
Component at 1348 cm-1
Absorbance
1300
1350
1400
1450
1500
1550
1600
1650
Wavelength (nm)

5

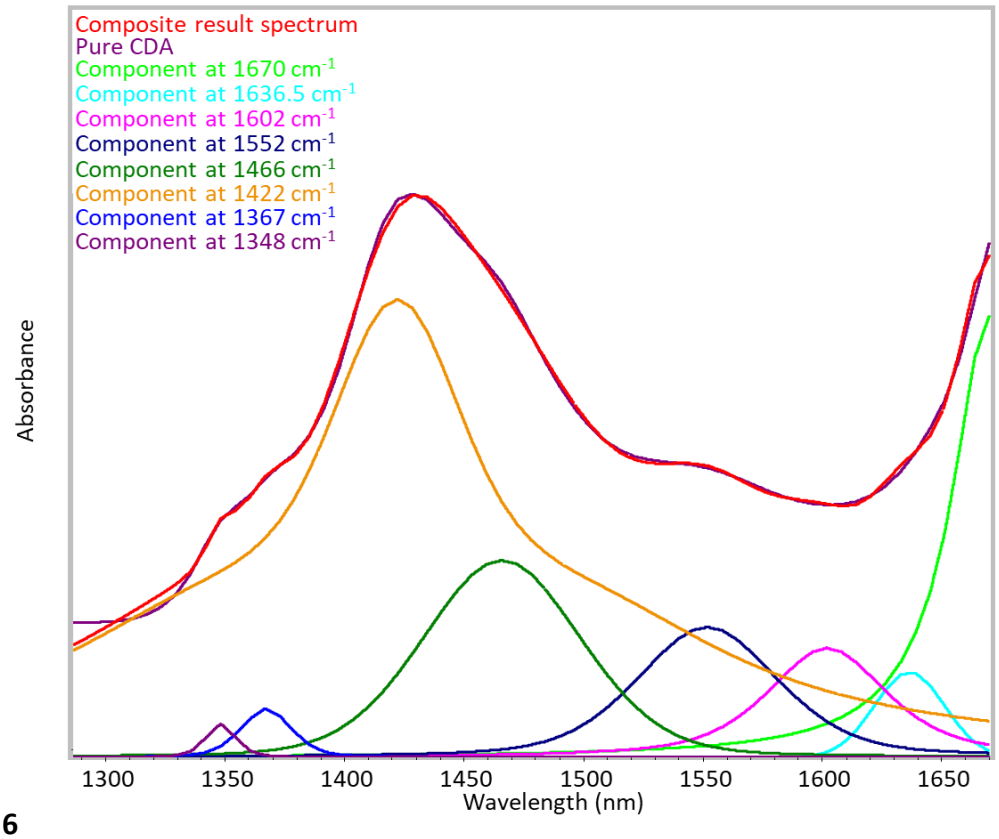

6

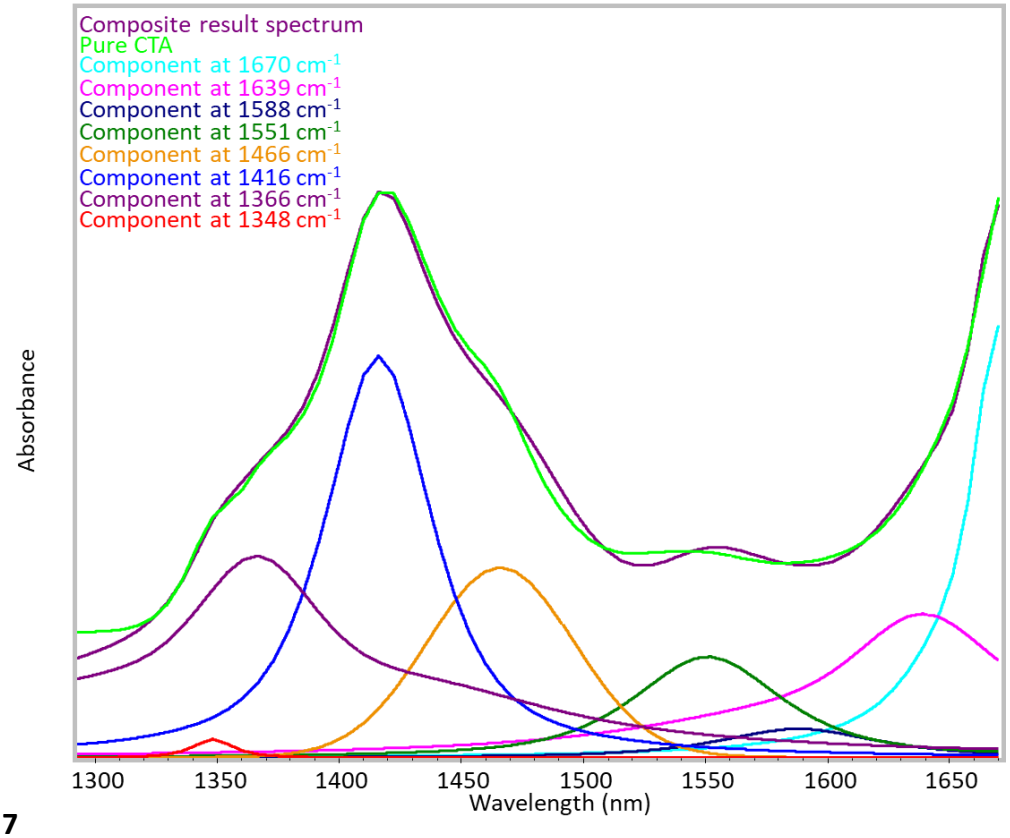

7

Fig. SMI.1-7 Deconvolution of selected NIR spectra from each of the seven standards used for building the DS calibration functions (From first to last: Pure MCC; CDA-MCC mixtures equivalent to DS 0.48, 0.95, 1.43, 1,90; pure CDA and Pure CTA).

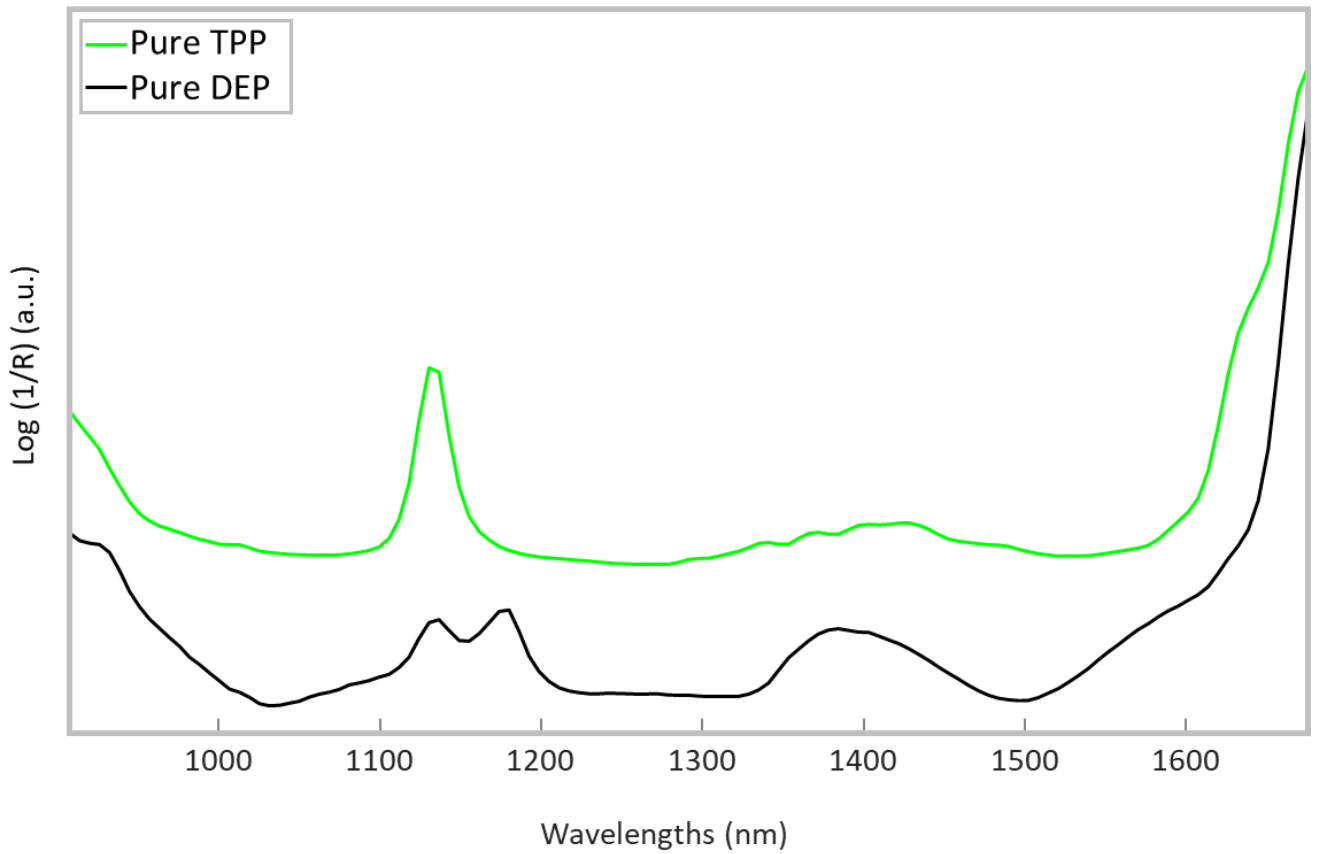

Fig. SMI.8 NIR spectrum of the Triphenyl Phosphate (TPP) and Diethyl Phthalate (DEP) standards.

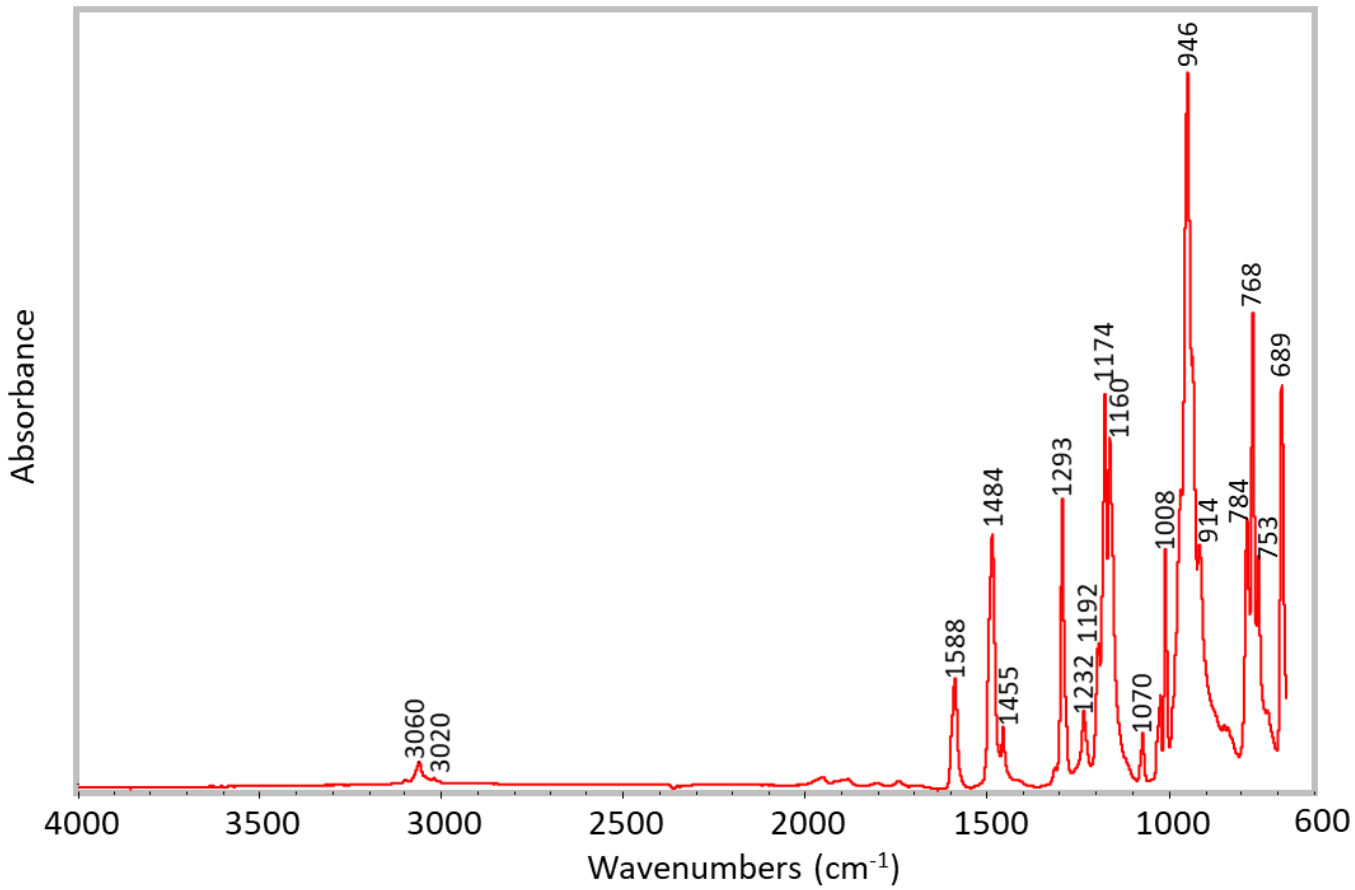

Fig. SMI.9 µATR-FTIR spectrum of the TPP standard.

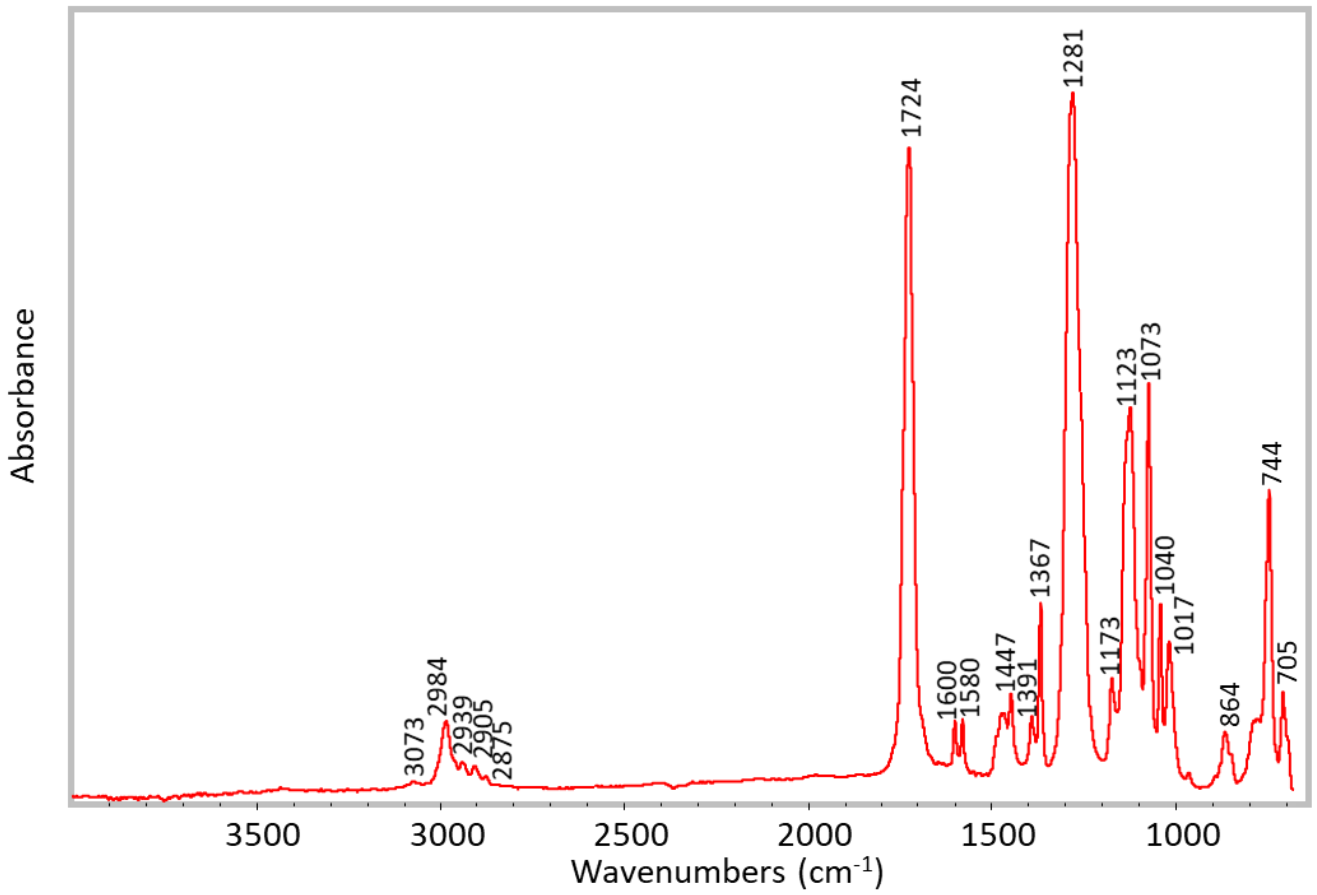

Fig. SM.10 μATR-FTIR spectrum of the DEP standard.

Wavenumber (cm^{-1})			Assignment
Pure CTA	**Pure CDA**	**Pure MCC**	
3496	**3479**	**3339**	**ν_sOH**[153]
2941	1943	---	νC-H[153] in CH_3[154]
2899	2889	2893	ν_aC-H in CH_2[153], [154], ν_sC-H in CH_3[155]
1741	1739	---	νC=O[68], [154], [156]
1644	1643	1646	ν_aC=O[154] and OH vibrations from crystallization water[153], [155]
1433	1433	1427	In plane δC-H[157] in CTA and CDA, $\delta_s CH_2$ at C–6 in MCC[158]
1367	1368	1369	δC-H in CH_3[89], [154], [156], [159], [160]
---	---	1335	In plane δOH[155]
---	---	1316	δCH_2 [155], [158] and δOH[155]
1219	1223	1202	ν_a(C-C-O)[89], [156]
1165	1162	1159	ν_a(C-O-C) at β-glucosidic linkage[154], [157]
1122	1121	1101	νCO[158]
1071	1071	1055	νC-O in pyranose ring[89], [155], [156], [158]
1038	**1037**	**1030**	**νCOC**[159], [160]
900	902	898	O.o. ring ν at C_1-O-C_4 β glucosidic bond[155], [157], δC-H[154]
839	841	---	---

* ν stretching vibration, ν_s symmetrical stretching vibration, ν_a asymmetrical stretching, δ bending vibration and δ_s scissoring, O.o.p. Out of plane

Table SMI.1 Assignments of the main infrared absorption bands of the pure standards used for building the DS calibration functions: CTA (Cellulose Tricetate, DS), CDA (Cellulose Acetate, DS), MCC (Microcrystalline cellulose, DS 0).

Wavenumber (cm^{-1})		Assignment
TPP standard	DEP standard	
3098	3073	
3060		vC-H[75], [161]
3020		vC-H[161]
	2984	Alkane vC-H[60]
	2929	
	2905	
	2875	
	1724	vC=O[60], [151], [162]
	1600	Aromatic vC-C[163]
1588	1580	Aromatic vC-C in DEP[163], vC=C in TPP[75], [161]
1484	1447	Methyl ($–CH_3$) vibrations[162] and aromatic vC-C in DEP[163]; vC=C in TPP[75], [161]
	1391	vs(OCO)[163]
	1367	
1293		vP=O[75]
	1281	vC-O[60]
1174	1173	In-plane δ(C-H) in TPP [75], [161], v(C-COO) in DEP[163]
1160		In-plane δ(C-H) in TPP[75]
	1123	
	1073	In-plane δ(C-H) bending[163]
	1040	
1008	1017	vP-O[75] and ring vibrations in TPP[161]
964		vP-O[75]
946		
932		
914		
	864	
784		Out of plane δC-H[75]
768		Out of plane δC-H[75]
753	744	Out of plane δC-H in TPP[75], aromatic CH vibration in DEP[73]
689	705	Out of plane δC-H in TPP[75]

* ν stretching vibration, ν_s symmetrical stretching vibration, ν_a asymmetrical stretching, δ bending vibration and δ_s scissoring

Table SMI.2 Assignments of the main Mid-infrared absorption bands of the TPP and DEP standards

Sample name	Element typology		2vOH band shift	DS calculated by NIR	$vOH_3/vCOC$	DS calculated by µATR-FTIR	DS Absolute difference	DS percentual difference
CA1	Positive	Color	6.194	2.6346044	0.00654121	2.70861346	0.07400906	2.466968672
CA4	Positive	Color	55.749	0.2856974	0.16208425	0.086719646	0.198977754	6.632591792
CA6	Positive	Black & White	0	2.9432	0.005785224	2.730643068	0.212556932	7.085231063
CA7	Negative	Color	6.194	2.6346044	0.004187106	2.777508301	0.142903901	4.76346335
Time0	Negative	Color	6.194	2.6346044	0.00275996	2.819699023	0.185094623	6.169820754
AA1	Unknown	Color (transparent)	6.194	2.6346044	0.004365565	2.77225502	0.13765062	4.588353998
AA4	Negative	Color	6.194	2.6346044	0.001465201	2.858252972	0.223648572	7.454952386
AA5	Positive	Color	6.194	2.6346044	0.003846154	2.787558757	0.152954357	5.09847858
CT4	Positive	Color	6.194	2.6346044	0.004483696	2.768780382	0.134175982	4.472532723
CT5	Positive	Color	6.194	2.6346044	0.002657059	2.822753466	0.188149066	6.271635549
CT10	Positive	Color	24.777	1.7537702	0.045355831	1.698256927	0.055513273	1.850442439
CT11	Positive	Color	24.777	1.7537702	0.049717818	1.599514759	0.154255441	5.141848029
CT12	Positive	Color	24.777	1.7537702	0.054026815	1.504908556	0.248861644	8.295388118
CT21	Positive	Color	6.194	2.6346044	0.01335495	2.51411305	0.12049135	4.016378321
CT24	Positive	Color	24.08877778	1.786391933	0.036877866	1.898727649	0.112335715	3.744523849
PSATCT-roll3	Positive	Color	6.194	2.6346044	0.005176527	2.748445946	0.113841546	3.794718201

Table SMI.3 Calculation of the DS of the 16 analyzed real cinematographic film samples by using the NIR and µATR-FTIR calibration functions, and comparison between the data obtained by both methods.

Chapter 3 Efficient Cleaning of Cellulose Nitrate Cinematographic Films Using Deep Eutectic Solvents

3.1 Abstract:

Historical photographic negatives and cinematographic films with cellulose nitrate (CN) supports are known to be intrinsically unstable. They show deterioration mechanisms related to the thermal, photocatalytic and hydrolytic loss of nitro substitutive groups from the CN chain. To prevent the disappearance of this heritage, its scanning and digitalization becomes a priority.

However, degradation may prevent the possibility to scan CN films. Since motion picture films are stocked as a reel, the backside of each frame is in contact with the front of another one. Due to degradation, the decrease in pH contributes to lowering the viscosity of gelatin and promoting its hydrolysis. In this way, the emulsion gets softer, so some residues may deposit on the back of the superimposed frames, and the gelatin may also spread over the film surface and come out from the edges.

Traditional approaches to clean gelatin residues from the surface of CN bases and from the sides of film rolls include mechanical removal with scalpels and the use of polar solvents. However, these methods are either slow, ineffective or could potentially damage the degraded CN support and the remaining gelatin emulsion at the other side of the film.

Accordingly, we have evaluated the performance of three choline chloride and betaine-based Deep Eutectic Solvent (DES) formulations. These DES are inexpensive, easy to prepare, green (non-volatile, safe towards operator and the environment), non-flammable and have been previously proposed for the extraction of proteinaceous material, but their use for the restoration of photographic negatives or cinematographic films has not been reported yet.

Selected areas over the frames of a real deteriorated CN cinematographic film were cleaned from gelatin accretions by rubbing a cotton swab soaked in DES. Isopropyl alcohol (IPOH) was then employed to remove the remaining DES residues.

To evaluate the cleaning performance, each area was characterized and documented before and after treatment using high-resolution Optical Microscopy (OM) in Bright and Dark Fields, Micro-Attenuated Total Reflectance Fourier Transform Infrared Spectroscopy (μATR-FTIR), and cross-section observation under visible and UV light.

All treatments using DES proved effective for the removal of gelatin residues and harmless towards the CN film supports at the selected application times, showing superior cleaning power compared to traditional methods. Thus, the proposed cleaning methods with DES are suitable for cinematographic and photographic film restoration.

3.2 Introduction

The layout of early film materials (Figure 32) include a thick, transparent and flexible Cellulose Nitrate (CN) base (c) coated with the film emulsion (a). The emulsion is the layer employed to record the image and, in already developed films, it consists of a colloidal suspension of dark silver particles and

color dyes (if the film was colored) fixed in a matrix of photographic-grade gelatin[20]. Sometimes, a thin intermediate adhesive or “subbing” layer (b) was applied to guarantee the adhesion between the emulsion and the polymeric base.

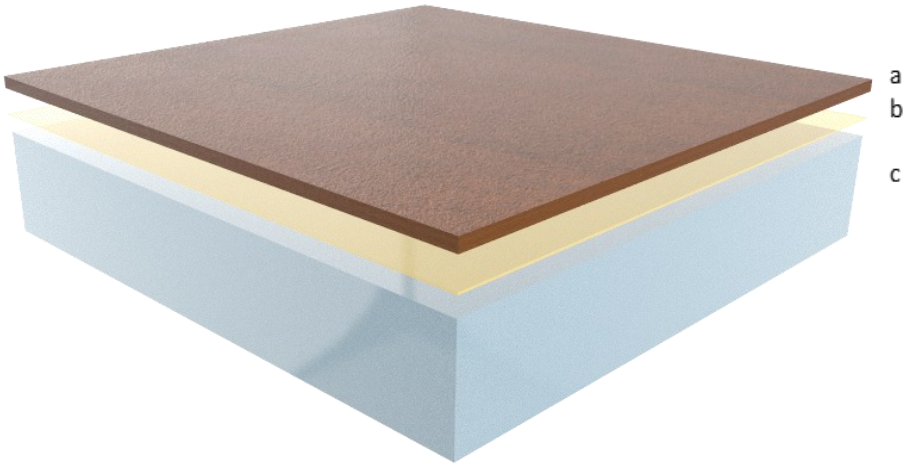

Fig. 32. Generic stratigraphy for a simple early-period CN film, showing the black and white (B&W) emulsion (a), in this case subjected to a red tinting process, an adhesive subbing layer (b) and the CN base (c). More complex films can include additional and thin layers such as an overcoat and an anti-curling layer, each one ≤1 μm thick, located over the emulsion, and below the base respectively.

CN is an inorganic cellulose derivate where hydroxyl groups in the glucopyranose ring have been substituted by nitrate groups O-NO_2.

Since 1889[10], [11], flexible polymeric films made of CN with a degree of substitution (DS) of around 2 were used as support for the first examples of cinematographic film.

Thanks to its low cost, CN was initially widely employed for producing film bases, but due to its high flammability, its use of was progressively reduced and then definitely abandoned in 1951[10], [11].

Cellulose nitrate photographic and cinematographic materials are known to be intrinsically unstable, mainly due to the degradation mechanisms triggered by thermal (Figure 33), photocatalytic and hydrolytic loss of nitro substitutive groups of the CN base[23]. This process occurs quickly under uncontrolled storage conditions, particularly unventilated environments showing high temperature and humidity.

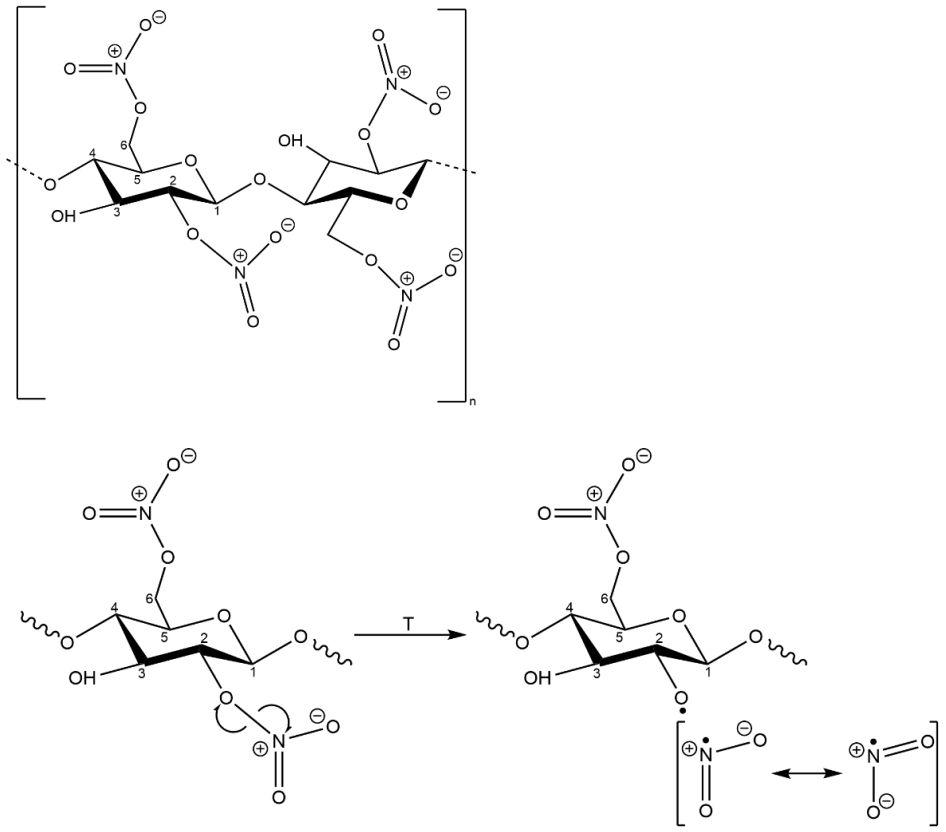

Fig. 33. Above: Repeating unit of CN polymer with Degree of substitution 2. Below: Scheme illustrating the polymer's homolytic thermal breakdown mechanism.

The resulting NO_2 gases react with environmental water producing nitric and nitrous acids, which catalyze further loss of nitro groups in the CN polymer and the reduction of the molecular weight of the backbone.

Eventually, the base deforms, becomes frail and brittle, and crumbles to dust[80]. To avoid the complete loss of the recorded images, their scanning and digitalization is a priority for cinematheques, libraries and other institutions safeguarding such audiovisual archives[81].

However, nitrate supports which have already underwent some degree of hydrolytic degradation of their bases can suffer from softening of their gelatin emulsions since the pH decreases to values lower than the isoelectric point of type-B gelatin (which goes from pH 4.7 to 5.6 or narrower [30][28] [24], [22]), where the gelatin molecule becomes positively charged, and the repulsion forces between positive charges slightly uncoil the gelatin molecule and facilitate its solubilization[30]. Nguyen et al. have suggested also that NO_2 species promote the hydrolysis of hardened (cross-linked) and unhardened photographic gelatins, lowering their molecular weight and their viscosity[29].

Photographic gelatin is most of the time alkaline or type-B gelatin, produced from the alkaline treatment of demineralized cattle bone, ossein[24]. Ossein is mostly made up of type I collagen, an heterotrimer collagen formed by three polypeptide α-chains associated in a triple helix configuration[25]. By treating parent collagen with an hydrated lime slurry, type B gelatin is produced, destroying the crosslinking between collagen[24]–[27].

Gelatin softening is a serious drawback, because upon becoming more fluid it can easily migrate laterally when it is pressured and adhere to any surface in contact with it. This often affects the back side of the subsequent coils of the same film (Figure 34), causing the loss of images in the first coil and gelatin accumulation on the back of the second. The adhesion of convolutions, known as blocking, ultimately transforms the film into a solid unit which cannot be unrolled, reaching the so-called “hockey puck” state[80].

Fig. 34. An early and tinted CN film exhibiting emulsion softening resulting in accretions and coil blocking.

Therefore, to allow the digitalization of the film and to avoid subsequent blocking when the reel is stored, it becomes mandatory to remove gelatin accretions.

Traditional cleaning approaches to eliminate gelatin residues from the side of film rolls include mechanical removal with surgical scalpels, and the use of polar solvents, such as distilled water, Ethanol (EtOH) and Isopropyl Alcohol (IPOH). However, the use of alcohols results in a slow, ineffective cleaning, whereas water may be potentially dangerous if it accidentally leaks towards the front of the frame when cleaning a section of the base. Furthermore, the use of organic solvents presents different drawbacks, since they are flammable, and the excessive emissions of volatile solvents can harm the environment and can pose health risks to the operator upon extended unprotected exposure.

To overcome these drawbacks, we have proposed, tested and evaluated the performance of three Deep Eutectic Solvent (DES) formulations which have been previously employed for the dissolution of proteinaceous[164], [165] and other organic materials, but to the best of the authors’ knowledge theyhave not been employed for the restoration of photographic negatives or cinematographic films. A different DES formulation has been previously applied in gel form to remove proteinaceous coatings in paintings[166]. We have proved that the three DES mixtures hereby proposed constitute a green, inexpensive, easy-to-prepare and effective alternative for the cleaning of gelatin accretions from CN photographic bases.

Deep Eutectic Solvents, first defined by Abbot et al. in 2003[167], are mixtures of a Hydrogen Bond Acceptor (HBA), commonly a quaternary ammonium salt, with an Hydrogen Bond Donor (HBD), like an amide, amine, alcohol or carboxylic acid. Electrostatic charge delocalization (through hydrogen

bonds and van der Waals interactions) between these two constituents lower the fusion point or glass transition temperature below that of the original components when both are present near a certain molar ratio[168], [169].

Choline Chloride (ChCl), Betaine (B) and Urea (U) (Figure 35) are biodegradable, environmentally friendly (being obtained from renewable sources), relatively cheap and non-toxic.

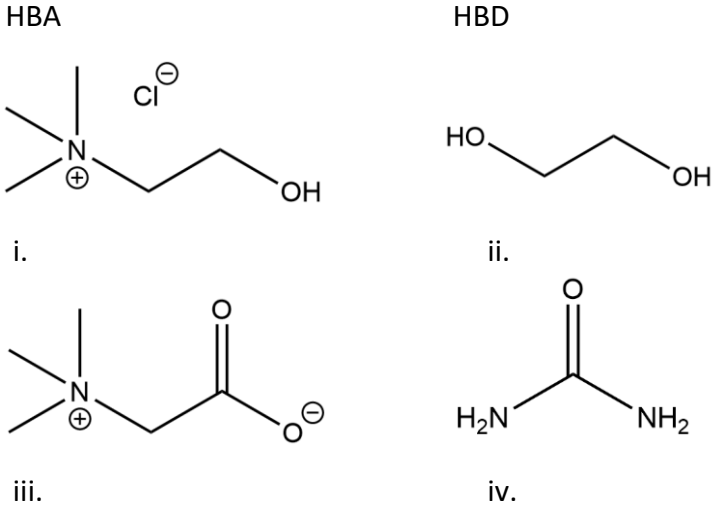

Fig. 35. Components of the tested DES mixtures: Choline Chloride (i.) and Betaine (iii.) as Hydrogen Bond Acceptors, and. Ethylene Glycol (ii.) and Urea (iv.) as Hydrogen Bond Donors.

Choline chloride is regarded as a B-complex vitamin and is extracted from biomass; betaine is the trimethyl derivative of glycine and is obtained as a metabolic oxidation product of choline in different organisms[170]. Betaine can be commercially retrieved by separation during sugar production from beets. Urea is the most commercialized nitrogenous fertilizer and is employed by mammals for processing nitrogen-containing compounds[171], [172].

Ethylene glycol (EG) instead, is a non-toxic compound commonly exploited as antifreeze, wetting and plasticizer agent in industrial processes[173].

By mixing choline chloride with ethylene glycol at a 1:2 molar proportion, a DES commonly called ethaline is obtained. This product has been widely studied due to its low viscosity and therefore high solubilizing power. Through computer modelling, it has been found that the HBD and HBA in this DES formulation form a supramolecular cage-like arrangement where the Cl^- anion becomes the central element interacting with five hydroxyl groups, one from the choline cation and four from both EG molecules[174]. Ethaline has been reported as capable of extracting collagen peptides from cod skins without destroying the peptide bonds in the process and also of being able to solubilize singular alanine, glutamic acid, lysine, glycine and hydroxyproline amino acids without creating new chemical bonds with them, so the solubilization process is probably based on intermolecular hydrogen bond formation between Cl^- and the amino and carboxyl groups[164].

When urea is used as HBD, it has been observed that relatively basic DES are obtained, owing to the presence of the amino group, and to the fact that a small fraction of ammonia is released through urea decomposition during DES preparation, rising the pH of the mixture[175].

The DES formed by mixing betaine and urea in a 1:2 ratio worked well for the extraction of bovine serum albumin protein, showing a low glass transition temperature. After FTIR studies, it was suggested that in this DES formulation not only hydrogen bonds but also Coulomb interactions are formed between HBD and HBA, so its intrinsic interactions and structure differ from those of choline chloride-based DES[176].

3.3 Aim of study

The objective of this research is to test three green DES formulations, i.e., choline chloride: ethylene glycol, betaine: ethylene glycol, and betaine: urea; as cleaning agents for cinematographic film cleaning, comparing their performance with that of traditional methods based on isopropyl alcohol (IPOH) and ethanol (EtOH), employed as conventional solvents, and evaluating their impact on the cellulose nitrate support.

3.4 Materials and methods

3.4.1 Chemicals

Reagents and solvents were acquired from Sigma-Aldrich and used without any further purification: Betaine ≥98%, choline chloride ≥98%, urea ACS reagent 99.0-1005%, ethylene glycol, 2-propanol (isopropyl alcohol) ACS reagent ≥99.8%, and ethyl alcohol 96.0-97.2%; distilled water.

An Amersham Protran® medical grade CN filter membrane with 0.45µm pore size, was used as CN analytical reference

3.4.2 Cinematographic film sample

Some coils of a CN 35 mm B&W positive print of the film *My Little Baby (La Principessa),* kindly donated by the Fondazione Cineteca di Bologna, were used for all testing. The emulsion showed an orange tinting treatment, and deterioration effects including emulsion softening and accretions. These softened gelatin residues accumulate on the back of the film base (Figure 36).

Fig. 36. Detail of the film sample appearance.

3.4.3 DES preparation

The DES mixtures were prepared by mixing the HBA with a HBD at a 1:2 molar ratio. For those DES based on betaine, a small amount of distilled water (10 wt% for B:EG and 30% wt% for B:U) was added to keep their viscosity low enough at room temperature (see Table 5).

DES abbreviation	HBA	HBD	Added distilled water content (%wt)
ChCl:EG	Choline Chloride (ChCl)	Ethylene Glycol (EG)	0%
B:EG	Betaine (B)	Ethylene Glycol (EG)	10%
B:U	Betaine (B)	Urea (U)	30%

Table 5. Constitution of tested DES formulations.

Mixing was performed in a Petri dish by stirring vigorously at 70-75°C until the components turned into a transparent fluid, then letting the glass dish stand still until the liquid cooled down.

3.4.4 Cleaning procedure

A small cotton swab (ctsw) soaked with ETOH, IPOH or the DES solvents was gently rolled over an area (ca. 0.7x0.7 cm) of the CN base surface, previously documented under Optical Microscopy (OM) and Micro-Attenuated Total Reflectance Fourier Transform Infrared Spectroscopy (µATR-FTIR), using minimal mechanical strength. Application time was 3 minutes when cleaning with pure IPOH and ETOH, whereas DES were applied for 1 minute and afterwards, non-volatile DES residues were removed from the surface by rolling 2 cotton swabs soaked with IPOH for 1.5 minutes. Total application time including intervals between ctsw change was 3 minutes; the final appearance of the cotton swabs was registered.

In total, 3 zones with comparable gelatin accretions were cleaned with each one of the 3 DES, one area was cleaned with pure IPOH, and a final area was cleaned with pure ETOH, for a total of 11 areas cleaned. Besides that, to evaluate the interaction with the support, each DES was applied with the same conditions directly in contact with the CN base in areas without gelatin residues.

3.4.5 Solubility tests

From the same degraded cinematographic film sample, eight rectangular pieces of similar size (approximately 6 mg each) were cut. After the removal of the gelatin emulsion with water the samples were dried for 2 days at room temperature.

The samples were weighted, their thickness measured with a Mutitoyo® MDC-25SX digimatic micrometer and their superficial appearance documented with Optical Microscopy (OM).

The samples were subsequently subjected to solubility tests using the same solvents employed for the cleaning, to assess their impact on degraded CN. This was done by immersing the CN samples into 100 µl of each solvent and sonicating them in sealed vials for 10 mins at room temperature. Two

of the CN samples were immersed in ChCl:EG, two in B:EG, and two in B:U, whereas one was immersed in IPOH and another one in EtOH. Afterwards, samples were oven-dried for two days. The samples immersed in the DES formulation were rinsed for 1 minute by immersion into 3 ml of IPOH and gently agitated before being put in contact with absorbing paper for removing eventual solvent residues, before allowing to dry for two days.

After drying, sample weights and thickness were measured again and the film surface condition documented with OM to check the changes or damages created during the procedure.

Weighting of samples used in the solubility tests was performed with a Discovery DV215CD Ohau Corporation® analytical balance. Sample weight was measured 3 to 4 times, each thickness 2 times, and averaged values were employed for comparison.

3.4.6 Evaluation of the cleaning performance

The performance of the cleaning procedure was evaluated using OM under different lightning conditions and μATR-FTIR on the film surface before and after the treatment.

In particular, evaluation of gelatin and DES residues presence, as well as the evaluation of the damage inflicted by the treatment on the CN base, was conducted by recording Bright Field (BF) and Dark Field (DF) surface microphotographs. μATR-FTIR allowed to check for the presence of characteristic DES and gelatin (amide II) bands. The extension and the thickness of collagen residues left over the CN base was evaluated by OM observation of cross sections prepared before and after the treatment.

3.4.6.1 Surface and Cross section observation at the Optical Microscope using visible and UV lights

Surface and cross section photomicrographs have been recorded with an Olympus DP70 cooled digital color camera directly connected to an Olympus BX51M Optical microscope with different magnification objectives (1.25-5x for surface and 5-50x for cross section photomicrographs) under visible and UV lights, respectively provided by a 100W halogen projection lamp and an Ushio Electric USH102D lamp. Surface photos were taken with visible light under DF (to enable real color observation) and BF (to enhance surface topography changes, transparent residue detection, and side differentiation), whereas cross section photos were taken in visible light (to record real color appearance) and UV fluorescence (to enhance material and layer differentiation).

3.4.6.2 Film surface photomicrograph blending

Surface photomicrographs from each cleaned area and each solubility test sample were stitched together using ImageJ Grid-stitching plugin based on the method published by Preibisch et al. 2009, using linear blending and maximum intensity blending modes[177] to obtain a single image covering the whole area of interest.

3.4.6.3 Cross section preparation

Cross sections of the treated film areas, useful to obtain information on the number and morphology of the layers present before and after cleaning, were prepared by embedding microsamples in KBr[178], [179]. To avoid the cracking of the pellet due to the thickness of the sample, we gently

pressed manually the first half of the pellet (300mg KBr), and after positioning the sample and adding the remaining 300 mg of KBr, the pellet was pressed at 2 tons for 1 minute.

3.4.6.4 FTIR spectroscopy

All FTIR spectra were acquired using a Thermo Scientific® Nicolet iN 10MX spectrometer fitted with a mercury–cadmium–telluride (MCT) type A detector cooled by liquid nitrogen and a X–Y–Z motorized stage with 1 µm incremental steps, except transmission spectra of pure reagents for DES production, which were acquired in transmission mode using a MidIR Agilent® Cary 630 using the same parameters. Spectra were recorded in the 4000 to 675 cm^{-1} range, using a spectral resolution of 4 cm^{-1}, applying 64 scans per measurement and 64 scans for the background, acquired before each measurement.

Characterization of surface materials and treatment evaluation were carried out using µATR-FTIR with a Ge ATR crystal and an optical aperture of 40x40 µm. RAS spectra of the DES mixtures were acquired on a thin DES layer over a gold-coated glass holder with an aperture of 80x80 µm.

FTIR spectra were automatically baseline corrected using OMNIC™ Software (Thermo Electron Corporaton™) after blanking out the 2300-2400 cm^{-1} region, related to νCO_2 signals.

µATR-FTIR measurements before cleaning were performed in 3 different spots, whereas µATR-FTIR analysis after cleaning was performed in 7 to 14 spots for each cleaning area to confirm the representativeness of the data. For the CN samples used in the solubility tests, three µATR-FTIR measurements were recorded per sample using 150x150 optical aperture on the dry samples at the same spots before and after the test.

3.5 Results and discussion

3.5.1 Characterization of the film sample:

By a visual examination of the film it can be noted that the support appears slightly warped and fragile, and the degraded emulsion from the front side has softened in many areas, so it has adhered to back side of the film base.

A fragment of the film sample has been embedded to evaluate the thickness of the gelatin residues. As reported in Figure 37, the CN base is about 124 µm-thick and is covered by a continuous layer of degraded gelatin with maximum thickness of 13.4 µm.

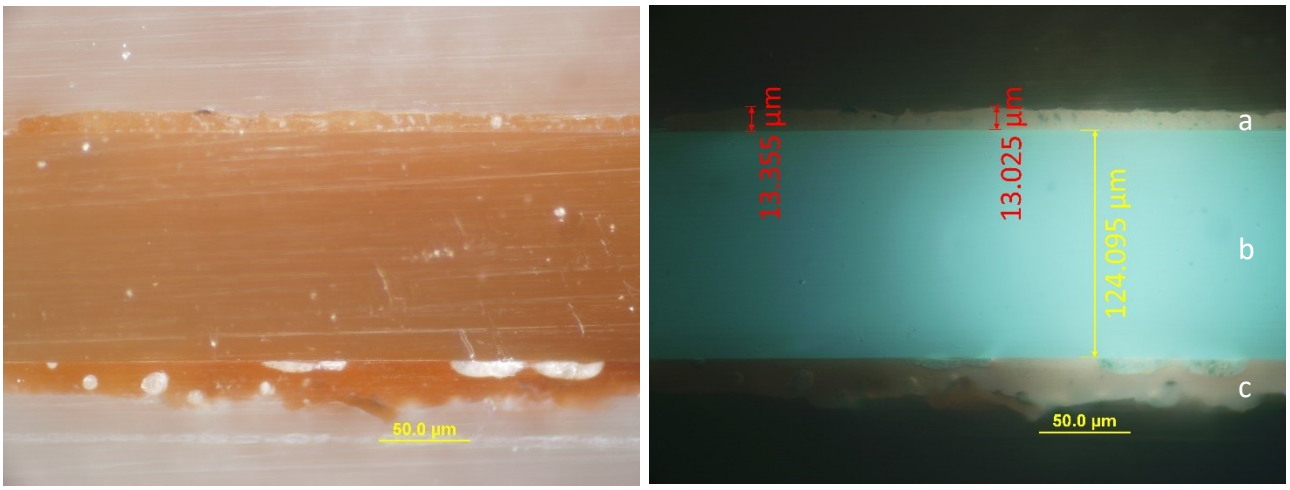

Fig. 37. 50x UV OM cross-sections photomicrographs of the film taken in a degraded point, highlighting the average depth of each of its layers: the red-tinted emulsion residues (a, depth in red) adhered to the back side of the film base, the CN base (b, depth in yellow), and the original emulsion layer at the front of the film (c). The treated side of the CN base is looking up.

The composition of the base and of the orange residues have been characterized by means of µATR-FTIR spectroscopy. Measurements performed on the base (Fig. SMII.1) present four strong absorption bands directly linked to the nitro group vibrations ascribable to cellulose nitrate (1640 cm^{-1}, 1276 cm^{-1}, 832 cm^{-1} and 750 cm^{-1})[89].

The band at 1728 cm^{-1} not present in the CN standard, is most likely related to the presence of camphor, commonly used as plasticizer for CN[89], [99], or to the presence of carbonyl intermediates (e.g. gluconolactones, gluconic and glucuronic acid) produced during scission of the CN chain at later degradation stages[23].

The broad band at 3426 cm^{-1} can be assigned to O-H stretching; the bathochromic shift of the band in comparison to the CN standard is a sign of the increase in hydrogen bonding between hydroxyl groups following hydrolytic loss of nitrate groups as a consequence of degradation[180].

The µATR-FTIR spectra registered on the orange-tinted emulsion residues over the CN base (Fig SMII.2) are quite similar to that of a gelatin glue standard. A shoulder at around 1727 cm^{-1} can be attributed to the C=O bond stretching, associated to camphor sublimating from the degrading film base or to plasticizers used in film emulsions themselves, such as oils[181], [99]. The peaks at 1340 and 825 cm^{-1} can be attributed to the presence of nitrates, which can be a residue of unreacted silver nitrate[182] or could derive from nitric and nitrous acids formed with the degradation of the CN base.

The strong characteristic band of Amide II of gelatin at ca. 1539 cm^{-1} does not overlap with other CN or DES bands, so they were used to detect remaining glue residues after the cleaning treatments.

3.5.2 Characterization of the DES solvents

The DES solvents were characterized by recording RAS-FTIR spectra. Table 6 reports the DES diagnostic bands which do not overlap with CN and gelatin signals, so they have been used to verify the presence of DES residues after the cleaning. The assignments of the bands are also reported.

Wavenumber (cm^{-1})			Assignment
ChCl:EG	B:EG	B:U	
---	1495	1491	ν_{as}H–C–H (CH_3) in betaine[183]
1479	1475	1472	δ_sC-H[174], δ_s CH_2, $\delta_s CH_3$, δ_sCOH[184] and ρCH_3[185] in choline chloride; $\nu_s COO^-$[183] and $\delta_a CH_3$ in betaine[186]; νCN in urea[187]
955	953 weak	955 weak	$\nu_a NC_4$, νC-C[184] and ν_aCCO[185], [187]in choline chloride; δC–C–N[183] and ν(CC)[188] in betaine
---	933	933	δ C–N–C[183] and ρ(CH_2) [186], [188] in betaine
883 medium	893	895 weak	ρC-H[173] and ρCH_2[189] in EG; νC–C[183] and ν_s(CCN)[186], [188] in betaine

* ν stretching, ν_s symmetrical stretching, ν_a asymmetrical stretching, δ bending, δ_s scissoring (for CH_2) and symmetrical deformation (for CH_3), δ_a asymmetrical deformation (for CH_3), ρ rocking

Table 6. Attribution of diagnostic FTIR bands useful for each DES detection

3.5.3 Solubility tests results

The effects of DES formulations on the degraded CN base were evaluated by comparing the thicknesses, weights and superficial appearance of samples before and after performing the solubility tests. The same tests were performed also with ethanol (EtOH) and isopropyl alcohol (IPOH) which are commonly employed for movie restoration.

Except for EtOH, none of the chosen solvents caused thickness differences of more than 3 μm in the CN samples, so such differences were not deemed conclusive.

EtOH completely solubilized the CN sample while IPOH caused a 0.5% decrease from the sample initial weight, letting unchanged the sample appearance.

ChCl:EG was the only DES solvent to clearly cause a change in the samples (see Fig. SMII.3), which became whitish and decreased in transparency, showing evident softening of the plastic and a weight loss of 3.15%. This was expected at such long treatment times since previous researches showed the capability of ChCl:EG and other Choline chloride-based DES to solubilize cellulose[190], [191].

B:EG induced a less pronounced whitish discoloration and loss of transparency, but no conclusive weight changes were observed on the samples. Finally, B:U seemed to have no effects on CN samples.

After observing the solubilization effects of each DES on fully immersed CN samples, their effect when applied directly on a clean CN film support with ctsw was assessed.

The surface OM photomicrographs (Fig. SMII.4) show that after applying all three DES, the treated areas did not have any distinctive changes on their surface.

The film depth variations measured by cross-section photos under UV light and the μATR-FTIR spectra (results not shown) indicated that the thickness of the films did not vary, and that no DES residues were found on the surface after the test.

3.5.4 Cleaning test results

The different treatments were applied to remove gelatin residues from the back side of the degraded movies described in section 4.1.

First, traditional cleaning systems (EtOH and IPOH) were tested and evaluated. OM surface photomicrographs (Fig. 38, I-IV) recorded after the treatment showed that IPOH practically did not remove the gelatin residues over the treated area, whereas EtOH showed a better performance, but still abundant gelatin residues remained covering wide areas of the surface after the treatment. Cross section photomicrographs (Fig38, V-VII) confirm that thicker gelatin residues remain after both treatments, with thicknesses up to 12.7 and 6.1 μm respectively, and μATR-FTIR analysis after both treatments (Fig 38, VIII) show strong Amide II signal at ca. 1539 cm^{-1} in several measurement points, confirming that the observed residues are constituted by gelatin.

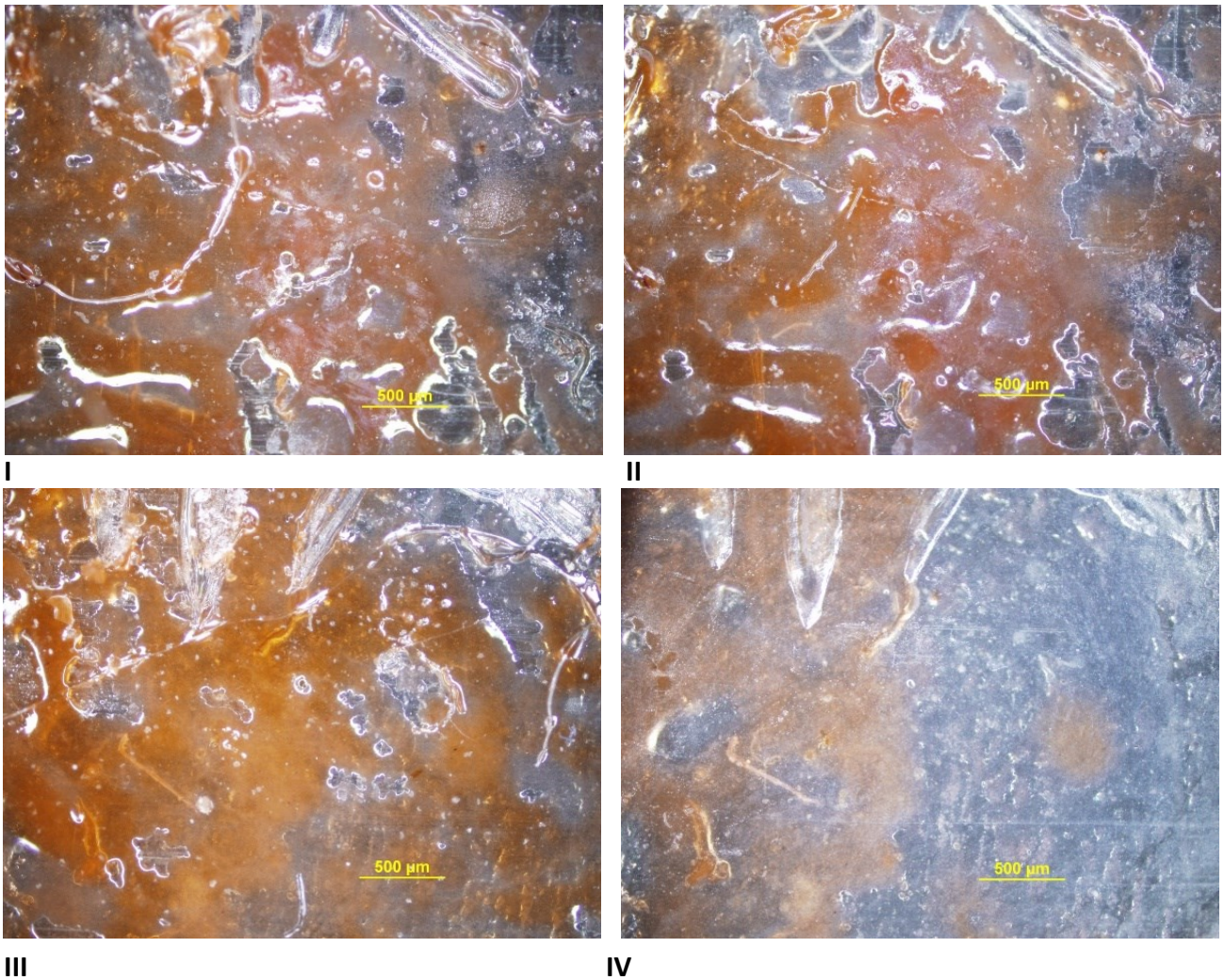

I **II**

III **IV**

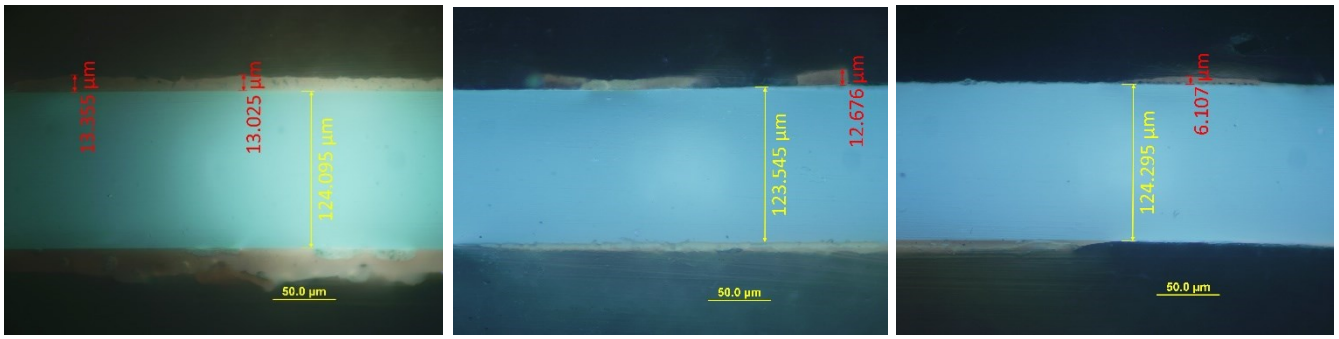

V VI VII

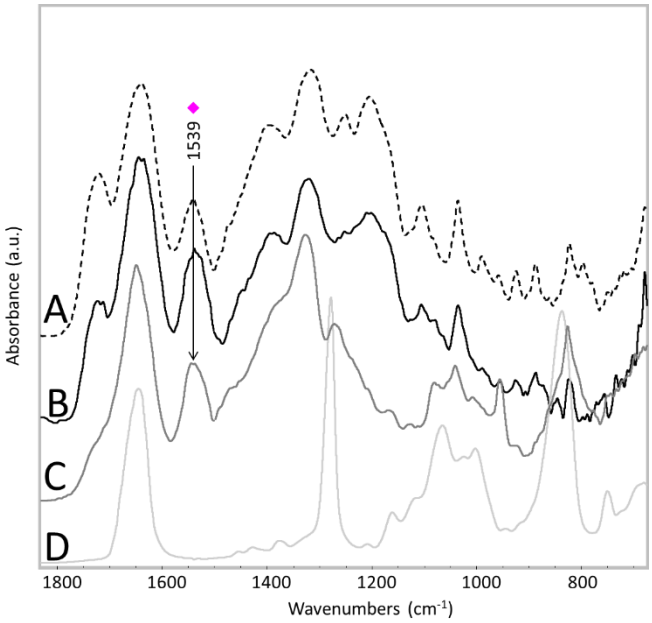

VIII

Fig. 38. Evaluation of cleaning performance using traditional solvents. I-IV: Dark Field 5x surface OM photomicrographs of selected film areas before (left) and after (right) being treated with IPOH (II) and EtOH (IV) using the same methodology as used with the DES. V-VII: 50x UV OM cross-section photomicrographs of the film before cleaning (left) and after cleaning with IPOH (center) and EtOH (right). The treated side of the CN base is looking up. VIII:µATR-FTIR spectra: Representative spectrum of gelatin residues before cleaning (A, dashed line), a representative spectrum of the film surface once cleaned with IPOH (B, black), and EtOH (C, dark gray); spectrum of an unplasticized CN standard reference (D, light gray). Diagnostic Amide II band due to gelatin presence is highlighted with a magenta diamond.

In comparison, cleaning tests using all the three DES formulations showed a much more efficient cleaning efficacy.

From figure 39, we can observe that after the treatments the extension of gelatin residues was considerably and homogeneously reduced. The surface topography showed that the remaining residues were hard to see even at higher magnification, having a small extension and being transparent due to their reduced thickness. We could not detect any resulting damage on the underlying CN surface, such as scratches following the circular cotton swab trajectory, gloss changes, etc. in any of the 9 cleaned areas. The only scratches visible after the cleaning are the typical horizontal ones ascribable to mechanical action derived by the movie transit through projection machines.

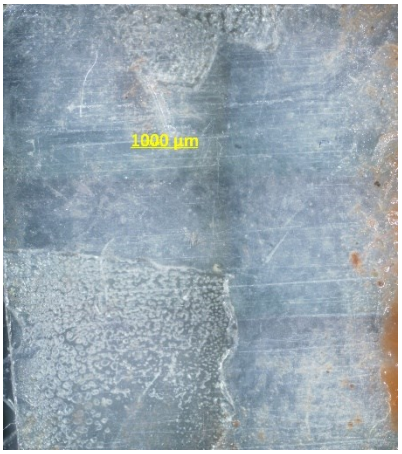

I

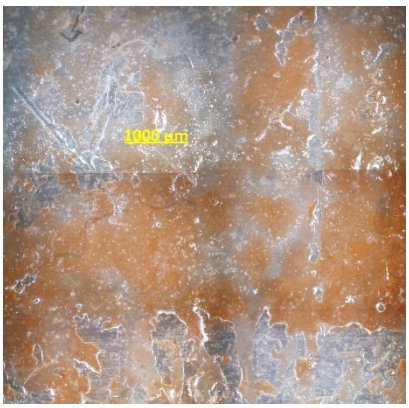

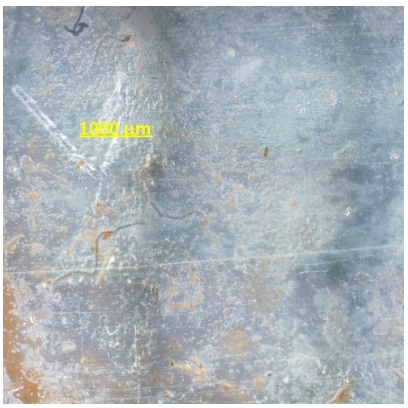

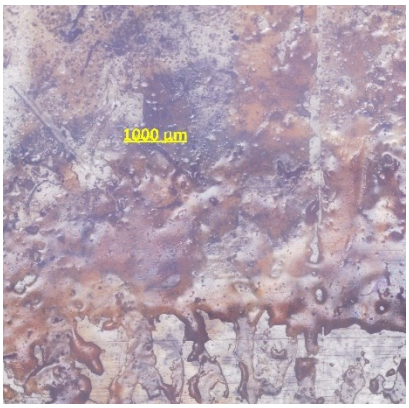

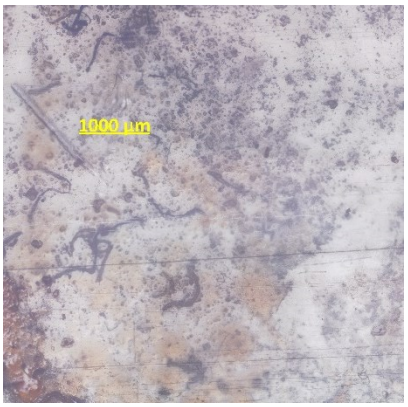

II

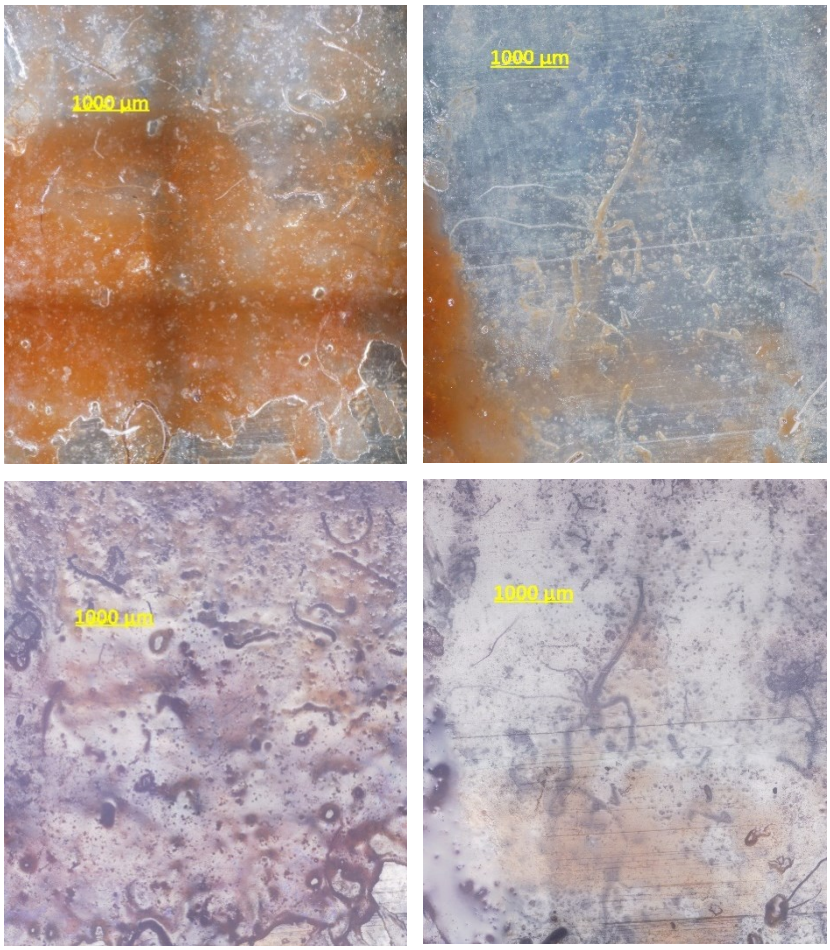

III

Fig. 39. Surface photomicrographs of selected film areas before (left) and after (right) being treated with ChCl:EG (I), B:EG (II) and B:U (III), taken in Dark Field (upper images) and Bright Field (lower images).

Cross sections from representative points of each cleaning area (Fig. 40) also prove that after treatment, the CN base shows uniform thicknesses of 122.4-125 µm, so no detectable thickness changes occurred on the CN base as compared to the cross section of an untreated area, with such minor differences being likely due to intrinsic base depth variability.

Cross section observation indicates also that after all the treatments, remaining residues are very punctual and much reduced in thickness, with average depths between 2.4 and 1.4 µm. These residues are not uniformly distributed, and generally show a lighter UV fluorescence over the CN base. Due to their transparence, thinness and punctuality, these residues are not detectable with the naked eyes. Therefore, it is less likely that they create a relevant impact during image scanning using transmitted light.

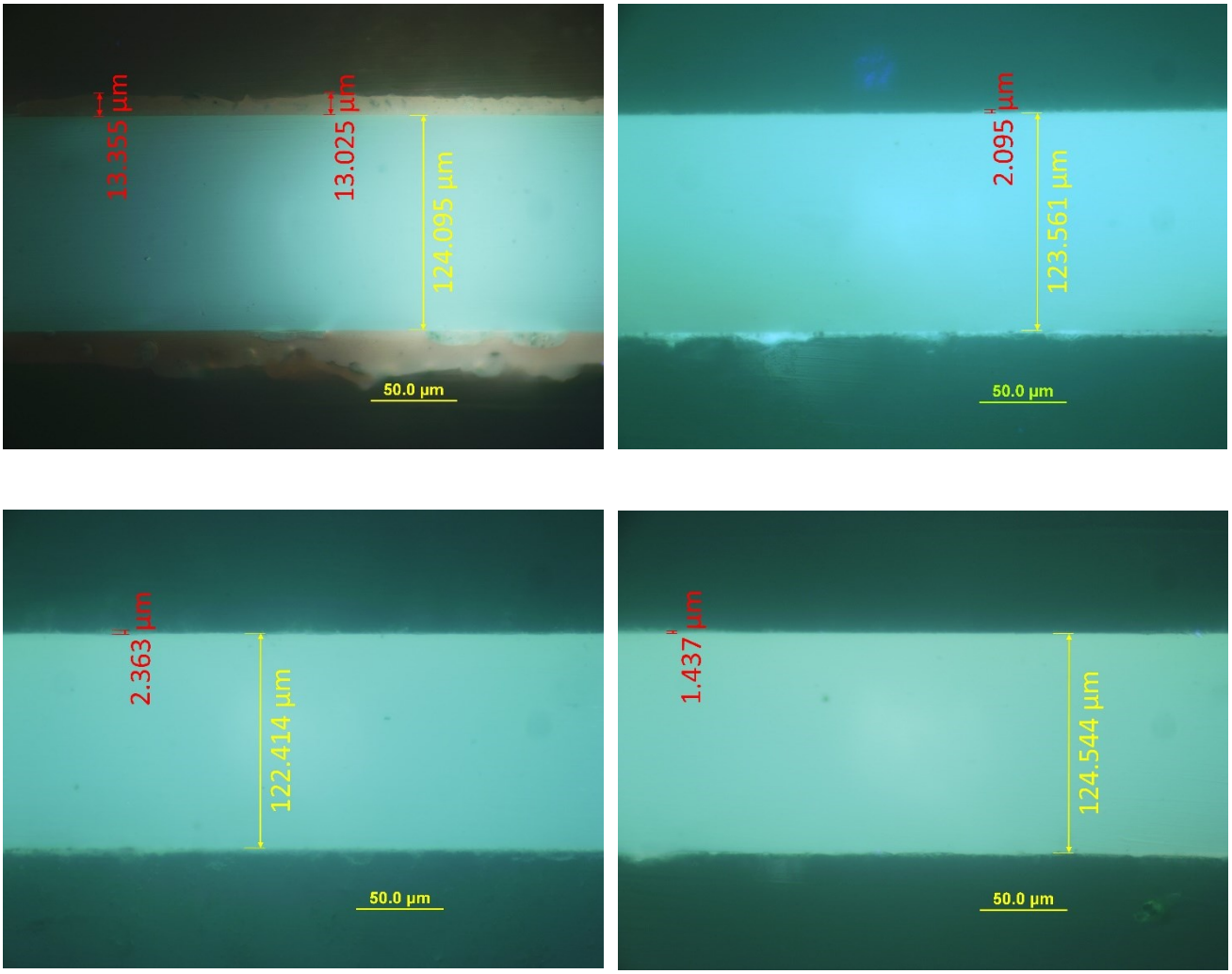

Fig. 40. 50x UV OM cross-sections photomicrographs of the film before cleaning (up left) and after cleaning with ChCl:EG (up right), B:EG (bottom left) and B:U (bottom right). The treated side of the CN base is looking up.

µFTIR-ATR spectra acquired in at least 7 randomly selected points along the center of each cleaned area, showed the same profile observed in untreated CN areas without gelatin residues (Fig. 41). In particular, the bands associated to gelatin and the ones related to the DES solvents are not present in the vast majority of the cleaned area, confirming that the treatment not only resulted overall effective in removing the gelatin, but also left no major solvent residues.

All remaining DES/gelatin residues were punctual and very constrained spatially over the cleaned surface. Most were transparent, and all had diameters of less than 0.39 mm.

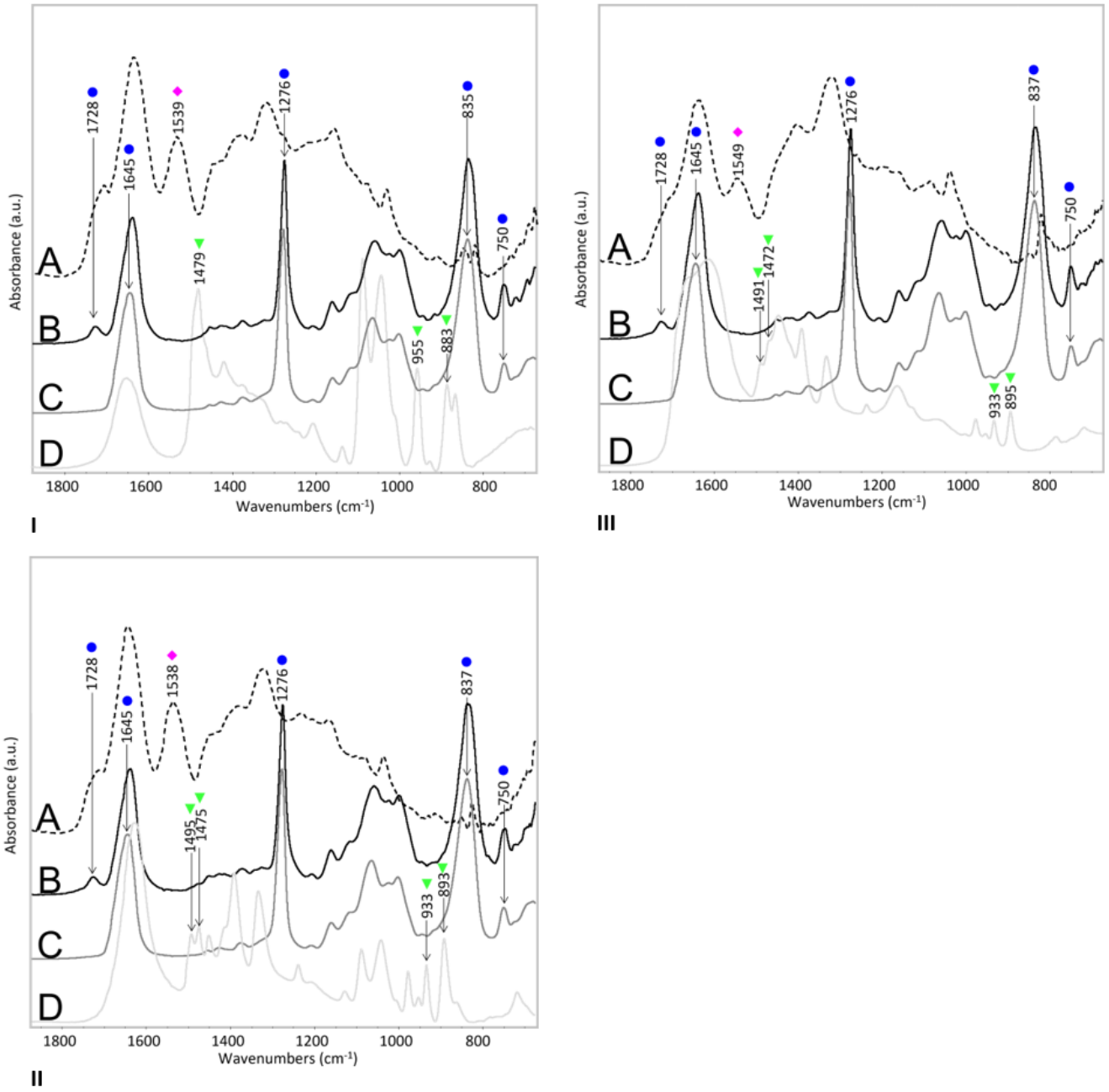

Fig. 41. FTIR spectra. Each figure shows: µATR-FTIR of the gelatin residues covering each area before cleaning (A, dashed line), a representative µATR of the film surface once cleaned (B, black), µATR-FTIR of an unplasticized CN standard (C, dark gray) and the reference RAS-FTIR of each DES employed (D, light gray: I. ChCl:EG; II. B:EG; III. B:U). Diagnostic FTIR bands due to the CN base and its plasticizer are accompanied with a blue circle; the one due to gelatin presence shows a magenta diamond, and the peaks attributable to DES presence are highlighted with green triangles.

Overall, all three DES show good cleaning action, however, ChCl:EG showed lower viscosity than the other DES, which made easier to control the area of application and to monitor the cleaning level during the treatment, whereas the more viscous Betaine-based DES tended to obscure the surface during treatment and made it difficult to asses the cleaning level until removal with IPOH.

3.6 5.Conclulsion

All the three formulations proved efficient in the removal of photographic gelatin residues from cinematographic CN bases using cotton swabs for application, so they are suitable for restoration purposes when followed by careful IPOH application for removal of DES residues. At short application times, DES seem innocuous towards polymeric film bases.

DES seem particularly promising or the treatment of heavily degraded CN film bases, and perhaps for separating glued cinematographic and photographic material which shows blocking to scan it before they arrive to the hockey puck state.

Further research is ongoing to test the applicability of these new solvents through the use of carrying semirigid absorbing materials, to remove the mechanical action of the cotton swab.

This research sets a precedent on the application of green solvent for the cleaning of polymeric cultural objects, a field that has not yet been studied in depth.

3.7 Supplementary Material II

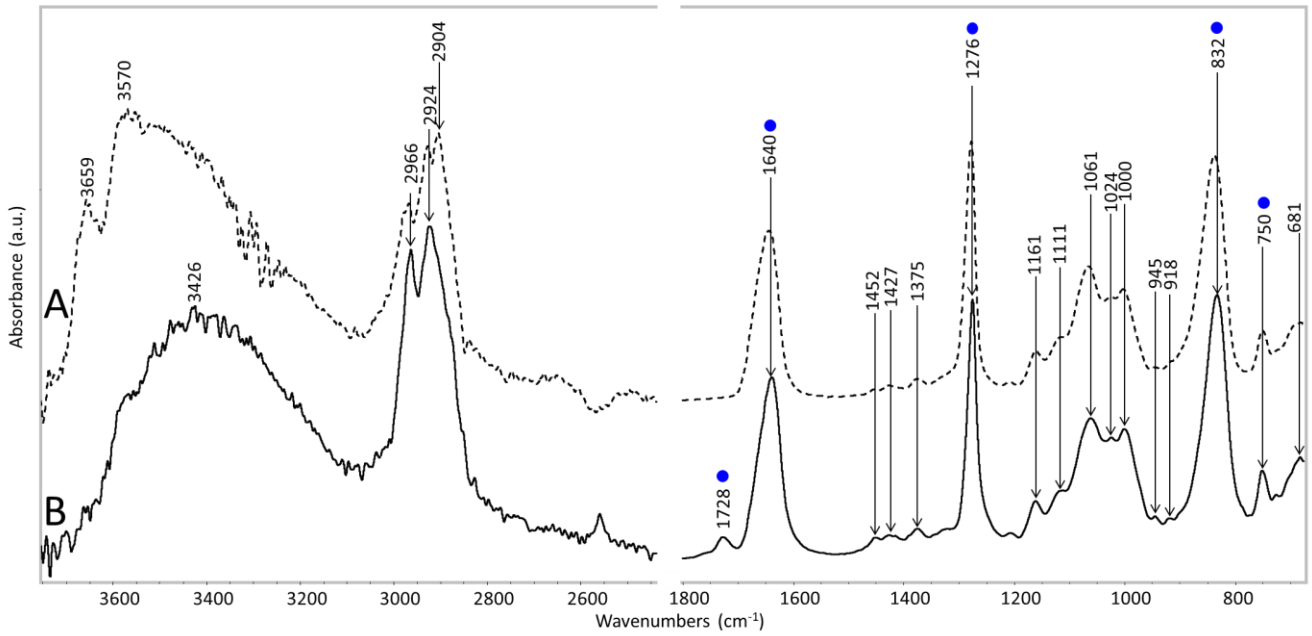

Fig. SMII.1 µATR-FTIR spectra of an unplasticized CN standard (A, dashed line) and of the studied film base without gelatin residues (B, black). Diagnostic FTIR bands due to the CN base and its plasticizer are accompanied with a blue circle.

Wavenumber (cm^{-1})		**Assignment**
Cellulose nitrate filter (reference)	Film base without gelatin residues in the studied sample	
3659		
3570	3426	νO-H (bound)
2966	2964	νC-H [89], [192]
2928	2924	ν_sC-H [89], [193]
2904		
	1728	νC=O[193], from camphor[89], [99], [156] or CN degradation products (e.g. glucolactone, gluconic and glucuronic acids) [192], [194], [195]
1645	**1640**	**ν_aO-NO_2** [89], [99]
1454	1452	δCH_2 [193]
1427	1427	δCH_2 [89]
1375	1375	δC-H [89]
1278	**1276**	**$\nu_s NO_2$** [89], [99], [156], [193]
1160	1161	ν_aO-C-C [156]
1115	1111	νCO in ring[89]
1065	1061	ν_a O-C-C attached to the nitro group[156]
1024	1024	νCO [193]
1002	1000	νC-O [193]
945	945	δ_sCH[193]
918	918	δ_sCH[193]
837	**832**	**ν-NO** [99], [156], [193]
750	**750**	**δO-NO_2** [89], [99], [193]
694	698	δO-NO_2 [89], [99], [193]
681	681	Pyranose[193]

* ν stretching vibration, ν_s symmetrical stretching vibration, ν_a asymmetrical stretching, δ bending vibration and δ_s scissoring.

Table SMII.1 Assignments of the main infrared absorption bands of the spectra in Figure SMII.1

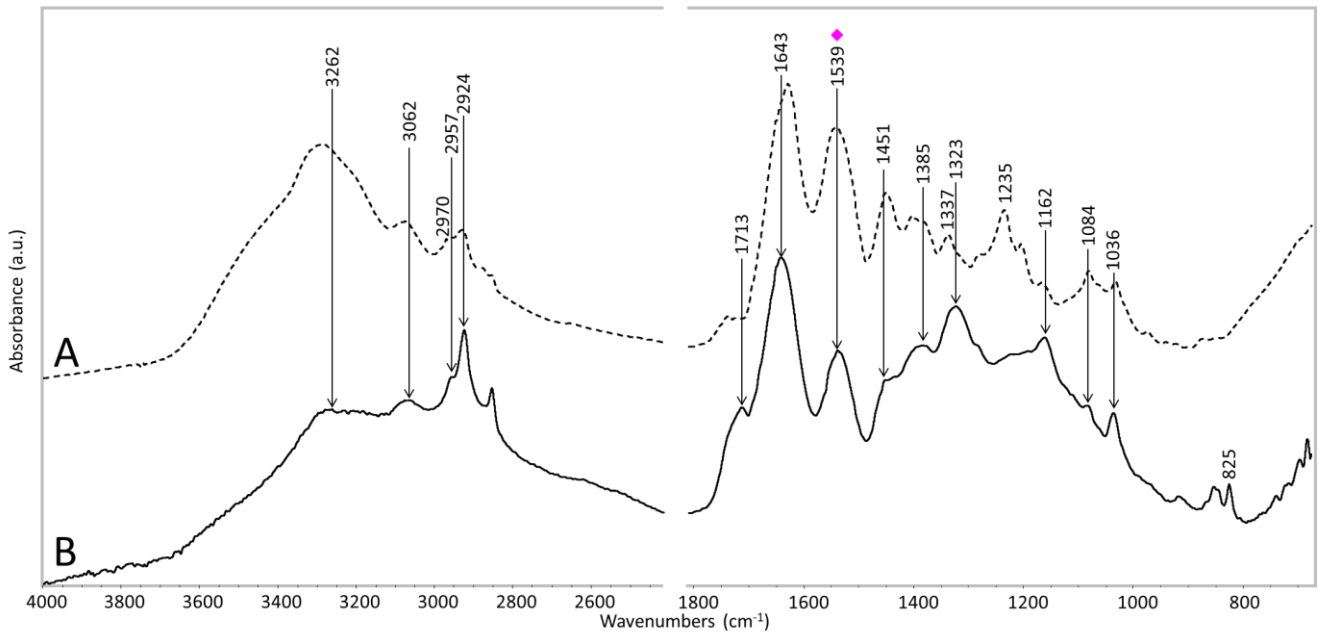

Fig. SMII.2 µATR-FTIR spectra of industrial bovine glue reference (A, dashed line) and of the gelatin residues found over the studied sample (B, black). The diagnostic FTIR band due to gelatin presence is highlighted with a magenta diamond.

Wavenumber (cm^{-1})		**Assignment**
Industrial calf glue adhesive	Softened emulsion residues over the film base of the studied sample	
3284	3262	Amide A (Fermi resonance of νNH and Amide I overtone)[196] [197]
3074	3062	Amide B (Fermi resonance of νNH and Amide I overtone)[196] [197]
2970	2957	νC-H[197]
2929	2924	
2854	2854	
1736	1713	νC=O from CN degradation products) or/and camphor[99]
1629	1643	Amide I (ν C=O 80%, ν C-N 10%, δ N-H 10%[197][196])[198]
1540	**1539**	**Amide II** (ν C-N 40%, δ N-H 60%)[197] [196]
1451	1451	δCH_2 and δCH_3 [197] [198]
1402	1385	δCH_2 and δCH_3 [198]
1337	1323	νCH_2, δC-H [197]and δCH_3 [198]
1235	1223	Amide III (νC-N, δN-H) [196][198]
1162	1162	
1082	1084	νC-O, νC-O-C [197]-
1032	1036	νC-O, νC-O-C,-[197]-; ν_a NO in NO_3^- ion [199]
---	825	ν Nitrate ion[199]

* ν stretching vibration, ν_s symmetrical stretching vibration, ν_a asymmetrical stretching, δ bending vibration and δ_s scissoring.

Table SMII 2. Assignments of the main infrared absorption bands of the spectra in Figure SM.2

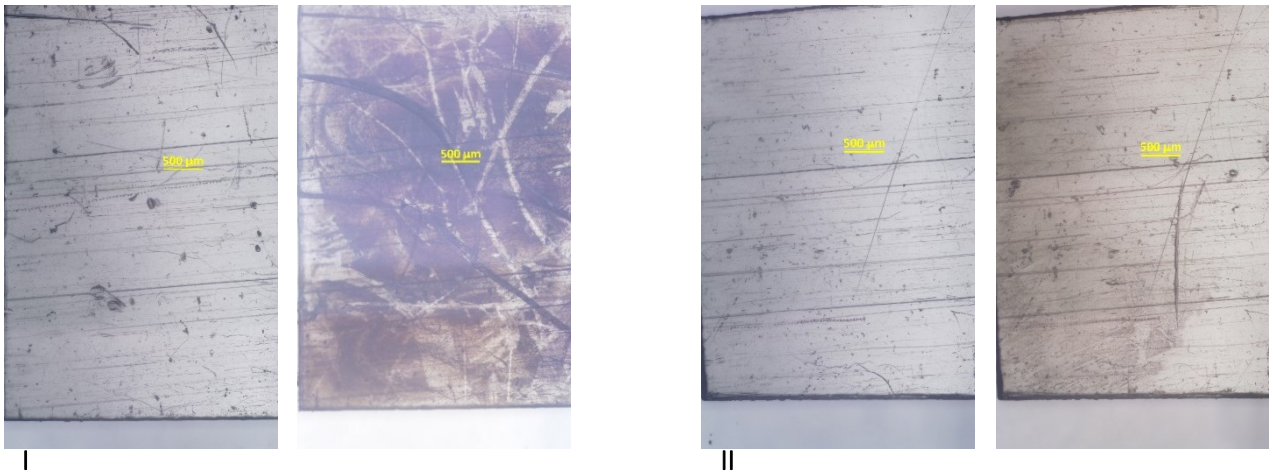

Fig. SM.3 Bright Field surface OM photomicrographs of CN base samples areas before (left) and after (right) being subjected to solubility tests inChCl:EG (I), B:EG (II) and B:U (III).

I

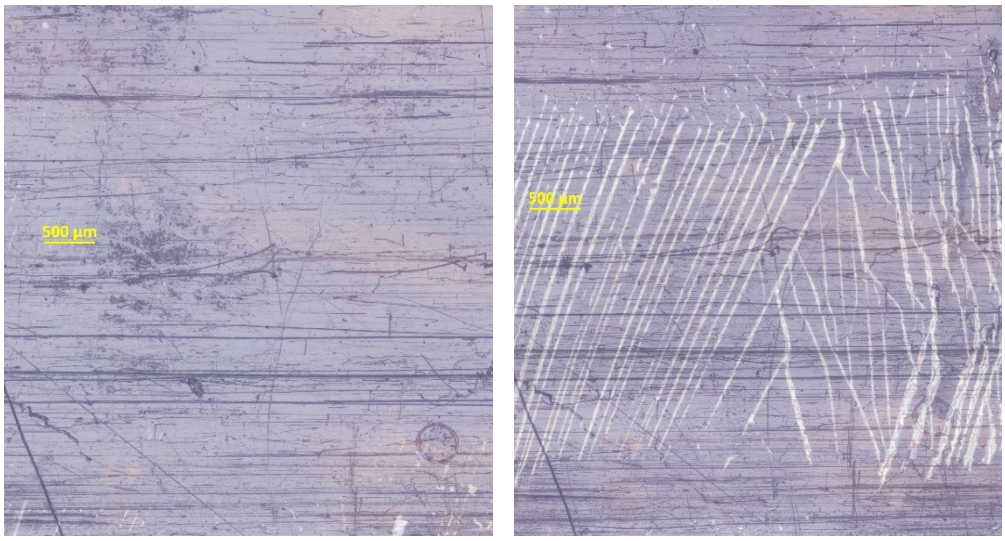

II

III

Fig. SMII.4 Bright Field surface OM photomicrographs of relatively clean film base areas before (left) and after (right) being treated with ChCl:EG (I), B:EG (II) and B:U (III) using the same methodology for removal of gelatin residues. Notice the absence of dark circular scratches due to cotton swab application. White lines instead reflect cracks in the gelatin emulsion at the other side of the film base, due to pressure applied by cotton swab treatment.

Chapter 4 Cleaning Triphenyl Phosphate (TPP) blooms from Cellulose Acetate film bases

4.1 Abstract:

Historical photographic negatives and cinematographic films with Cellulose Acetate (CA) bases contain from 10% to 20% weight of Triphenyl Phosphate (TPP, $C_{18}H_{15}O_4P$), an additive with fire retardant properties. Unfortunately, CA bases are intrinsically unstable, as they show deterioration mechanisms related to the thermal and hydrolytic loss of acetyl substitutive groups from the CA chain, which causes degradation effects such as shrinkage, embrittlement, detachment ("channeling") and buckling of the gelatin emulsion, as well as the migration and bloom of additives of the CA base to the film surface. Thus, scanning and digitalization is essential to preserve the information recorded on acetate films.

However, degradation may prevent the possibility to scan CA films. Since the loss of acetyl groups implies a reduction of carbonyl groups in the CA polymer, the dipolar interactions between P=O groups in Triphenyl Phosphate (TPP, $C_{18}H_{15}O_4P$) towards the polymer decrease, and such reduced affinity is responsible for the migration of TPP from the bulk of the polymer towards its surface, where it blooms in crystal form. TPP crystals disrupt any existing layer, and their presence over the surface of film frames prevents a clear projection of the image.

Traditional approaches to clean TPP residues from the back of CA film bases include mechanical removal with eyeglass-cleaning cloth and the use of polar solvents applied with cotton swabs. However, these methods are slow and ineffective, and dry cleaning can also create scratches on the surface of degraded CA supports.

Accordingly, we have evaluated the performance of isopropyl alcohol (IPOH) and green solvents isoamyl acetate (IAA), dimethyl carbonate (DMC), and diethyl carbonate (DEC); applied through cotton swabs and an innovative nylon (6,6) electrospun mat, with and without mechanical action, against the performance of the eyeglass-cleaning cloth when rubbed dry and solvent-soaked. Testing was performed by cleaning selected surface areas on the backside of a real deteriorated CA cinematographic film with TPP blooms. To the best of our knowledge, this is the first time electrospun mats are used for the restoration of photographic negatives or cinematographic films.

To evaluate the cleaning performance, each area was characterized and documented before and after treatment using high-resolution Optical Microscopy (OM) in Bright and Dark Fields, Micro-Attenuated Total Reflectance Fourier Transform Infrared Spectroscopy (μATR-FTIR), and cross-section observation under visible and UV light.

IPOH and DEC showed good capabilities for removal of TPP residues without the use of friction by employing the proposed electrospun nylon mats, thus bypassing the danger of employing mechanical action combined with solvent by rubbing cotton swabs or electrospun nylon mats, which are effective for the removal of TPP residues. The solvents appear harmless towards the deacetylated CA film support, and they show better cleaning power than conventional rubbing with dry eyeglass-cleaning cloth.

Cleaning by rubbing with solvent-soaked eyeglass-cleaning cloth demonstrated lower efficiency and has the disadvantage of causing the deposition of unwanted substances over the treated film area, whereas solvent-soaked nylon electrospun mats did not leave any residues.

Thus, the proposed cleaning methods employing IPOH and DEC applied by electrospun nylon mat with and without rubbing seem suitable and promising for cinematographic and photographic film restoration.

4.2 Introduction

Film materials (Figure 42) include a thick, transparent and flexible polymeric base (c) coated with the photographic-grade gelatin emulsion (a) where the image is recorded[20]. Sometimes, a thin intermediate adhesive or "subbing" layer (b) was applied to guarantee the adhesion between the emulsion and the polymeric base. Also, some films may show very thin coatings on the backside of the polymeric base, including antihalation and anticurl layers, which are useful to enhance image registration and prevent the deformation of the film, respectively. Usually, these layers are primarily composed by gelatin binders.

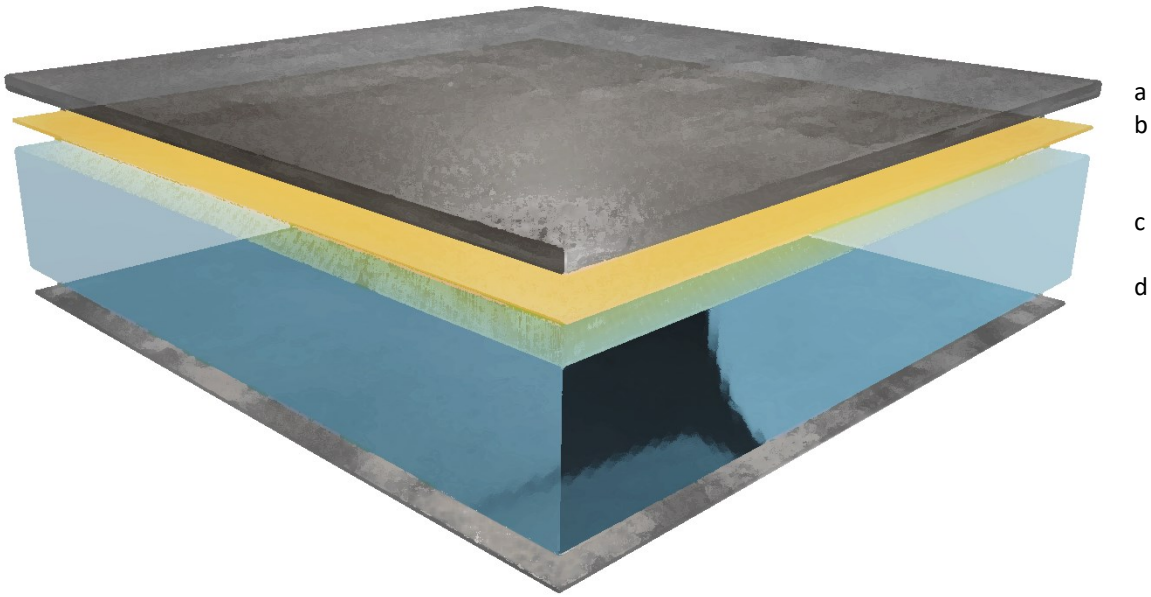

Fig. 42. Generic stratigraphy for a CA film, showing the black and white (B&W) emulsion (a), an adhesive subbing layer (b) and the CA base (c), which is coated on its backside by a thin antihalation layer (d) ≤2 µm thick.

Cellulose Acetate (CA) is a cellulose derivative where hydroxyl groups in the glucopyranose ring have been substituted by acetate groups CH_3COO^-, and it has been used for producing transparent and flexible bases for photographic supports since 1909, and specially from 1948 onwards[133], due to its lower flammability when compared to Cellulose Nitrate (CN) supports[20]. Therefore, CA "safety films" are a very abundant material in cinematheques and photographic archives.

For its employment as cinematographic and photographic film base, CA must be supplemented with significant amounts of plasticizers and flame-retardant additives. Triphenyl Phosphate (TPP, $C_{18}H_{15}O_4P$; Figure 43) is one of the most relevant of these additives, being added to CA bases from 10% to 20% in weight[64] for plasticizing and flame retardant purposes. CA molecules are supposed

to stablish mainly weak interactions between C=O in CA and P-O-Ph in TPP[78], although hydrogen bonds can also be formed between O-H in CA and P=O groups in TPP.

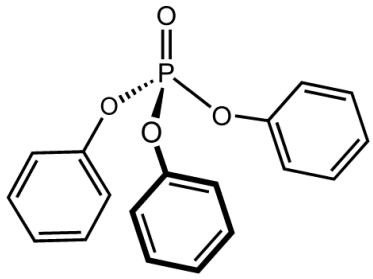

Fig. 43. Triphenyl phosphate (TPP).

Unfortunately, CA film bases show thermal and hydrolytic deterioration mechanisms, which involve the heterolytic scission of the acetate substitutive groups from the CA chain[23] (Figure 44). The resulting CH_3COO^- gases react with environmental water, producing acetic acid, which further catalyze the scission of acetate groups and the hydrolytic reduction of the molecular weight of the polymer, affecting sensible materials in the vicinity too.

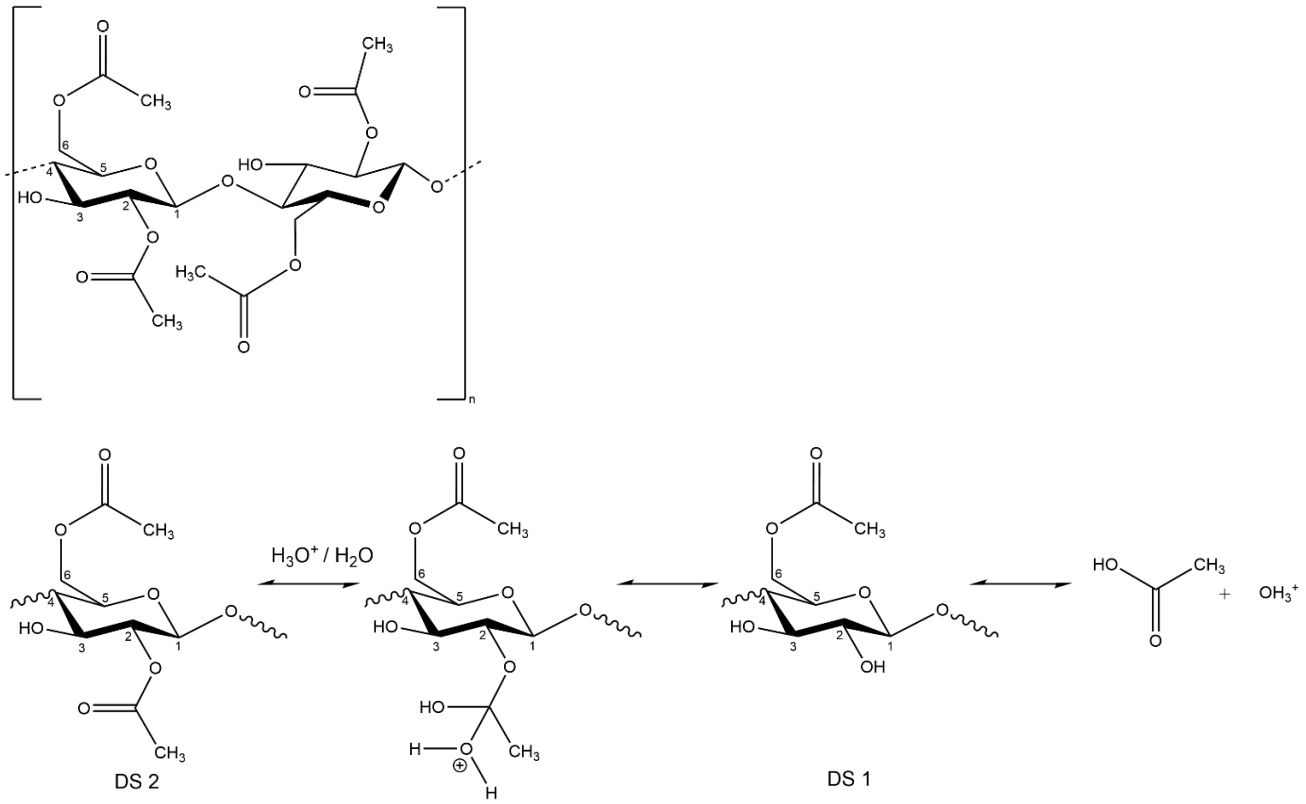

Fig. 44. Scheme illustrating the polymer's hydrolytic breakdown mechanism.

These mechanisms develop quickly under uncontrolled storage conditions, particularly in unventilated environments with high temperature and relative humidity. As a consequence, CA objects may shrink and become distorted, frail and brittle[135].

Furthermore, additives such as TPP are known to migrate to the surface of acetate films and objects as they degrade, forming disfiguring crystalline blooms or haloes, which can disrupt the continuity and stability of layers such as the emulsion or coatings on either side of the film[57], [73], [200]. In

particular, TPP blooms obscure the image and obstruct its copying or digitalization. Gas Chromatography Mass Spectroscopy (GC/MS) has been reported to accurately identify TPP in historical CA objects by solvent extraction[136].

Moreover, some have suggested that TPP can break down into diphenyl phosphate and hydroxyl-triphenyl phosphate (OH-TPP)[201], [202], a highly acidic species that would promote the hydrolysis of CA polymers. Due to their disfiguring effect and its potentially harmful effects, plasticizer residues must be removed from film materials before scanning.

However, cleaning of TPP from a real historical film may be challenging. Traditional cleaning approaches to eliminate TPP residues from the surface of CA films include mechanical removal by rubbing with dry microfiber eyeglass-cleaning cloth, and the use of polar solvents, such as Isopropyl Alcohol (IPOH), applied with cotton swabs. IPOH is a flammable colorless aliphatic alcohol hydrocarbon (chemical formula $CH_3CHOHCH_3$), prepared from propylene, with boiling point 82.3°C at 760 mm Hg, flash point 12°C and vapor pressure 45.4 mm Hg at 25°C[78].

Yet, the use of eyeglass-cleaning cloth results in a slow, ineffective cleaning, and it may create scratches on the film surface. Furthermore, the use of IPOH or other organic solvents by cotton swabs presents different drawbacks, since the excessive emissions of volatile solvents can harm the environment and can pose health risks to the operator upon extended unprotected exposure. Stiffening and deformation of the polymeric support is accentuated due to plasticizer migration and loss, and the film fragility increases the risk of creating damages over prolonged mechanical treatments.

Cleaning of cultural objects made of plastic remains largely an unexplored research area in Conservation Science. In particular for CA, mainly dry cleaning methods have been tested[203]; whereas for the removal of additive bloom from polymer surfaces, only some work has been published on the dry mechanical cleaning of plasticizer from PVC objects[204].

To overcome these drawbacks, we have compared the performance of IPOH as conventional cleaning agent against that of new green solvents isoamyl acetate (IAA), dimethyl carbonate (DMC), and diethyl carbonate (DEC) when employed for cleaning TPP bloom from CA cinematographic films.

IAA is a flammable but human consumption-safe solvent, being also water-miscible it is often employed as food flavoring additive for its characteristic banana aroma[205]. DMC is a flammable organic compound with the formula $OC(OCH_3)_2$, forms part of the carbonate ester family[206], constituting a non-polar aprotic solvent. It is synthesized by a green process using CO_2 as a building block, being characterized by a low toxicity and full biodegradability, so it is considered a green substitute for dimethyl sulphate and methyl halides, compared to other carboxylate (phosgene) or alkylate agents (methyl halides)[207]. In addition, DMC has a high vapor pressure (7.57 kPa at 25 °C), which guarantees a lower residual amount on the treated surface.

Finally, DEC (another alkyl carbonate) is a water-insoluble and environmentally friendly solvent, being low bio-accumulative and easily biodegradable [208]. It is insoluble in water and its lows toxicity allows it to be used as flavoring agents, although it is also a flammable liquid[209].

Solvent	Chemical Structure	Molecular Weight (g/mol)	Boiling point (at 760 mm Hg)	Vapor Pressure	Flash point
DMC[210]	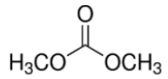	90.08	90 °C	42 mm Hg (at 20°C)	17°C
DEC[209]	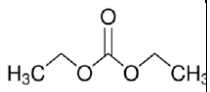	118.13	126 °C	10.8 mm Hg (at 25 °C)	25 °C
IAA[211]	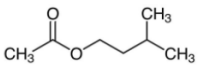	130.18	142°C	5.6 mm Hg (at 25 °C)	25 °C

Table 7. Properties of the green solvents tested for TPP cleaning.

Furthermore, we have evaluated the application of the tested solvents through new type of electrospun nylon 6,6 mat, which can be cut and then impregnated with the cleaning agent to be applied over the film. The interaction between fibers and solvent allows for retention and a controlled release of the cleaning agent, also limiting the evaporation rate of the volatile solvent. The increased thickness of the proposed mats (ca. 500 µm) and their big pore size allow for a big retention of solvent.

4.3 Aim of study

The objective of this research is to test isopropyl alcohol (IPOH), a conventional cleaning agent, and IAA, DMC DEC as new green alternatives for cinematographic film cleaning, for the removal of unwanted TPP bloom, a degradation product occurring after its migration from the CA substrate to the backside surface of the film base. This research compares the performance of IPOH when applied by traditional cotton swab, by commercial microfiber eyeglass-cleaning cloth, and by a new electrospun nylon mat as innovative application substrate system, evaluating the impact of each method towards the aged cellulose acetate support.

4.4 Materials and methods

4.4.1 Chemicals

Reagents and solvents were acquired from Sigma-Aldrich and used without any further purification: 2-propanol (isopropyl alcohol, IPOH) ACS reagent ≥99.8%, isoamyl acetate (IAA), dimethyl carbonate (DMC), and diethyl carbonate (DEC).

4.4.2 Electrospun fiber mats and commercial eyeglass-cleaning cloths

A 20% nylon 6.6 solution in Hexafluoroisopropanol (HFIP) was electrically charged to create a jet employing an needle connected to a cathode and an inversely charged anode connected to the collector[212]. The employed parameters were: 22 cm of distance from needle to the collector, the

0.015 ml/minute deposition rate of the solution, and 19kV voltage (ddp). This allowed to produce sheets of nonwoven fabric composed by long, continuous nanofibers with a diameter of 0.825 - 1.1 µm in a cost-effective way, which are characterized by interconnected and open porosity, high surface area, high liquid permeability, excellent flexibility, as well as good mechanical resistance.

Commercial eyeglass-cleaning cloths were characterized by µATR-FTIR to be a blend of PET and polyamide fibers by comparison against reference spectral libraries.

4.4.3 Reference standards materials

Triphenyl Phosphate (TPP, Sigma-Aldrich, ≥ 99%) and Cellulose Triacetate (CTA, Fluka, DS 2.97) in pellet presentation; and Microcrystalline Cellulose (MCC, Sigma-Aldrich) in powder presentation were used as analytical references for the FTIR studies.

The references were pressed under 2 tons for 1 minute to obtain compact pellets, which were kept for 24 hours in a desiccator before performing µATR-FTIR measurements for their characterization. Additionally, one CTA piece was analyzed in a flat area without any sample pretreatment, employing the same methodology used for the pressed pellet references.

The resulting spectral bands of TPP, CTA and MCC, and were attributed using bibliographic references.

4.4.4 Real Cinematographic film sample

Sections of a developed 16 mm B&W positive cinematographic film with a CA polymeric base were kindly provided by the Fondazione Cineteca di Bologna and were used for all testing. Preliminary information about the polymeric base composition and the crystal bloom on its surface was obtained by µATR-FTIR measurements. The macroscopic state of conservation of the film sample (Fig. 45) was assessed by registering its degradation effects.

Fig. 45. Details of the macroscopic appearance of the film sample.

4.4.5 Cleaning procedures

Areas of the sample film base of ca. 0.7x0.7 cm, showing comparable TPP bloom presence, were documented under Optical Microscopy (OM) and Micro-Attenuated Total Reflectance Fourier Transform Infrared Spectroscopy (µATR-FTIR) before being subjected to the cleaning treatments.

Afterwards, the final appearance of the cotton swabs and electrospun mats was registered, and the treatment performance was evaluated with OM, µATR-FTIR and by performing a cross section in a representative point.

Two zones were cleaned by rubbing a dry eyeglass-cleaning cloth on them, and another eight were treated by rubbing them with cotton swabs soaked with the four tested solvents (two areas per solvent). Other four areas were cleaned each with one of the four tested solvents applied through a nylon electrospun mats without any friction. The two most promising solvents (IPOH and DEC) were then applied through a nylon electrospun mats without any friction for longer application times.

Afterwards these two areas were treated by rubbing them with a square of eyeglass-cleaning cloth soaked respectively in IPOH and DEC, and finally two areas were treated by mechanically rubbing the surface with an electrospun nylon mat wet with IPOH and DEC. In total, 24 areas were cleaned. All treatments had a duration of 40 seconds, except two cleaning tests with electrospun nylon mats soaked in IPOH and DEC without applying any friction, which were left to act for 5 minutes.

A summary of the tests performed is presented in Table 8 below.

Cleaning system	**Cleaning solvent**	**Application time**	**Replicates**
Eyeglass-cleaning cloth with friction	Without solvent (dry)	40 seconds	2
Cotton swab	IPOH	40 seconds	2
	IAA	40 seconds	2
	DMC	40 seconds	2
	DEC	40 seconds	2
Electrospun nylon mat without friction	IPOH	40 seconds	2
	IAA	40 seconds	2
	DMC	40 seconds	2
	DEC	40 seconds	2
Electrospun nylon mat without friction	IPOH	300 seconds (5 minutes)	1
	DEC	300 seconds (5 minutes)	1
Eyeglass-cleaning cloth and friction	IPOH	40 seconds	1
	DEC	40 seconds	1
Electrospun nylon mat with friction	IPOH	40 seconds	1
	DEC	40 seconds	1

Table 8. Summary of the cleaning methodologies tested for the removal of TPP bloom.

For the procedure employing the eyeglass-cleaning cloth with solvent, the cloth was cut into a 0.7 x 0.7 squares, which were then weighted. The volume of IPOH to be added was calculated by the ratio defined as cloth square weight×1.2 (µl/mg), and the solvent was measured and applied with a micropipette. The wet cloth squares were rubbed over the test area for 40 seconds under the stereomicroscope.

For the procedures using solvents and electrospun nylon mats, the nylon sheets were cut into 0.7 x 0.7 square mats, which were then weighted. The volume of IPOH to be added was calculated by the ratio defined as mat weight×7 (µl/mg), and it was measured and applied with a micropipette.

The weight of each cloth square and electrospun mat was measured 3 times, its thickness measured 2 times, and average values were calculated. The thickness was registered with a Mutitoyo® MDC-25SX digimatic micrometer, whereas weighting was performed with a Discovery DV215CD Ohau Corporation® analytical balance.

4.4.6 Solubility tests

To evaluate the interaction of each solvent with the degraded CA support, eight rectangular pieces from the same cinematographic film sample were cut in similar sizes (1.7-2.5 mg each) and were treated under the stereomicroscope by rubbing them on both sides with cotton swabs soaked in distilled water, ethanol, and then scratching their surface with a surgical scalpel with the scope to remove completely the gelatin emulsion, subbing, antihalation and articurling layers, as well as any TPP bloom residues, to expose the CA base alone. Then, the samples were dried for 2 days at room temperature in a desiccator to allow any remaining water to evaporate.

The samples were weighted, their thickness measured, and their superficial appearance documented with Optical Microscope (OM) photographs in Bright and Dark field before the solubility test. Each weight was measured 3 times, each thickness 2 times, and average values were calculated for comparison. Finally, µATR-FTIR analyses were performed to register the intensity of the TPP bands and calculate the DS of the CA base using a calibration function prepared by following the procedure proposed by Nunez et al.[23] (see Chapter 2 “A non-invasive diagnostic tool for cellulose acetate films using a portable miniaturized near infrared spectrometer”).

The samples were subsequently subjected to solubility tests using the same solvents employed for cleaning, to assess their impact on CA. This was done by immersing the CA samples into 200 µl of each solvent and sonicating them in sealed vials for 10 mins at room temperature. Afterwards, samples were dried at room temperature in a desiccator for one day.

After drying, sample weights and thickness were measured again, and the film surface condition was documented with OM to check the changes or damages created during the procedure. The thickness of the solubility tests samples was registered with a Mutitoyo® MDC-25SX digimatic micrometer. Weighting of samples used in the solubility tests was performed with a Discovery DV215CD Ohau Corporation® analytical balance. µATR-FTIR analyses were repeated to evaluate changes in the film chemical condition following the treatment.

4.4.7 Evaluation of the cleaning performance

The performance of the cleaning procedure was evaluated using OM under different lightning conditions and µATR-FTIR on the film surface before and after the treatment.

Identification and quantification of TPP residues, as well as the evaluation of the damage inflicted by the treatment on the CA base was conducted by observation of changes in the extension, color and texture of residues and for topographic and texture changes (scratches, etc.) of the CA base surface by recording Bright Field (BF) and Dark Field (DF) surface microphotographs. µATR-FTIR allowed to check the presence of characteristic TPP bands. The extension and the thickness of collagen residues left over the CA base was evaluated by OM observation of cross sections prepared before and after the treatment.

4.4.7.1 Surface and Cross section observation at the Optical Microscope using visible and UV lights

Surface and cross section photomicrographs have been recorded with an Olympus DP70 cooled digital color camera directly connected to an Olympus BX51M Optical microscope with different magnification objectives (1.25-5x for surface and 5-100x for cross section photomicrographs) under visible and UV lights, respectively provided by a 100W halogen projection lamp and an Ushio Electric USH102D lamp. Surface photos were taken with visible light under DF (to enable real color observation) and BF (to enhance surface topography changes, transparent residue detection, and side differentiation), whereas cross section photos were taken in visible light (to record real color appearance) and UV fluorescence (to enhance material and layer differentiation).

4.4.7.2 Film surface photomicrograph blending

Surface photomicrographs from each cleaned area were stitched together using ImageJ Grid-stitching plugin based on the method published by Preibisch et al. 2009, using linear blending and maximum intensity blending modes[177] to obtain a single image covering the whole area of interest.

4.4.7.3 Cross section preparation

Cross sections of the treated film areas, useful to obtain information on the number and morphology of the layers present before and after cleaning, were prepared by embedding microsamples taken with a surgical scalpel. KBr was selected as non-fluorescent and MidIR-transparent embedding material following the method adapted from Mazzeo et al. 2007 and Prati et al. 2016[178], [179]. To avoid the cracking of the pellet due to the thickness of the sample, we gently pressed manually the first half of the pellet (300mg KBr), and after positioning the sample and adding the remaining 300 mg of KBr, the pellet was pressed at 2 tons for 1 minute.

4.4.7.4 FTIR analyses

All µATR-FTIR measurements were acquired using a Thermo Scientific® Nicolet iN 10MX spectrometer fitted with a mercury–cadmium–telluride (MCT) type A detector cooled with liquid nitrogen, and a X–Y–Z motorized stage with 1 µm incremental steps. Spectra were recorded in the 4000 to 675 cm^{-1} range using a spectral resolution of 4 cm^{-1} with a Ge ATR crystal, integrating 64 scans per measurement and 64 scans for the background, acquired before each measurement.

Characterization of surface materials and cleaning evaluation were carried out with an optical aperture of 150x150 µm. µATR-FTIR spectra of the reference materials and solubility tests samples were acquired instead using an aperture of 400x400 µm. Additionally, FTIR analysis were performed on the precipitates deposited after soaking an eyeglass-cleaning cloth with IPOH- over a gold-coated glass holder. The measurements were acquired in RAS mode with an aperture of 80x80 µm on the same spectrometer.

FTIR spectra were automatically baseline corrected using OMNIC™ Software (Thermo Electron Corporation™) after blanking out the 2300-2400 cm^{-1} region, related to vCO_2 signals.

µATR-FTIR measurements before cleaning were performed in 3 different spots, whereas µATR-FTIR analysis after cleaning was performed in 8 to 12 spots for each cleaning area to confirm the representativeness of the data.

4.5 4. Results and discussion

4.5.1 Characterization of the film sample:

An initial overview of the macroscopic condition of the film sample allowed us to classify it as heavily degraded (frail, brittle, with yellowish base). The film sample support shows deterioration effects including deformation of the base following the position the film stayed rolled up, detachment and channeling of the emulsion at the front side, as well as warping, shrinking, rigidity, fragility, brittleness, and yellowing of the CA base. Finally, the sample showed TPP accretions at the backside of the CA base.

A fragment of the film sample has been embedded to evaluate the stratigraphy and depth of the TPP residues. As reported in Figure 46, the CA base is about 93 µm-thick and is covered by crystal bloom of TPP with maximum thickness of 9.8 µm. Furthermore, between the crystal residues and the CA base, we can observe residues of thin (2 µm-thick maximum) layer characterized by the presence of dark particles. This layer is probably antihalation layer, whose residues are still on the film as result of a poor development process.

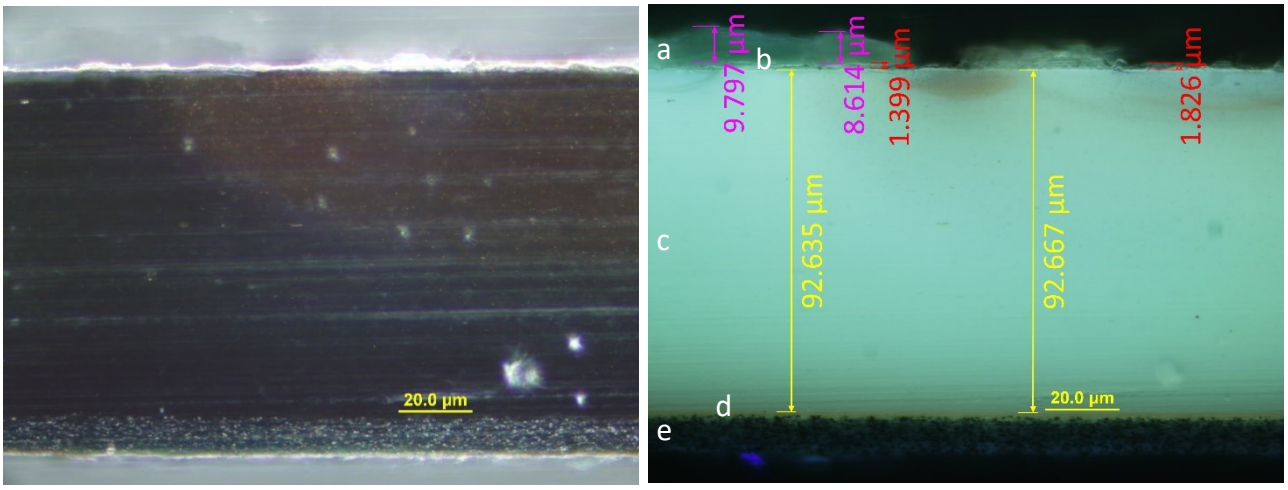

Fig. 46. 100x Visible (left) and UV (right) OM cross-sections photomicrographs of the film taken in a degraded point, highlighting the average depth of each of its layers: the TPP crystal bloom at the back side of the film base (a, depth in purple), the anticurling/antihalation layer (b, depth in red) the CA base (c, depth in yellow), the subbing layer (d) and the black and white emulsion (e). The treated side of the CA base is looking up.

4.5.2 µATR-FTIR characterization of the historical cinematographic film sample and TPP blooms

Before performing the cleaning tests, an initial µATR-FTIR characterization of the film base was performed, to identify the nature and condition of the cellulose derivate film in comparison to analytical standards. Reference materials and an area of the film sample base without TPP bloom were characterized by µATR-FTIR, and the attribution of the bands is shown in table SMIII.1.

Measurements performed on the polymeric base (Fig. 47) present the characteristic C-O stretching vibration due to carboxylate group at 1020 cm^{-1} as an evidence of the cellulose backbone in the material[29]. The spectrum shows also weak characteristic carbonyl stretching (νC=O) at 1728 cm^{-1} and CH bending bands (δC-H) at 1371 cm^{-1}, which can be used to confirm that the film substrate material is made of CA. The broad and strong band with maximum at ca. 3336 cm^{-1} can be assigned to O-H stretching (νOH). The reduction in the magnitude of the νC=O and δC-H bands and the growth in the O-H peak, renders a spectral response more similar to that of pure MCC than pure CTA. This proves that the deacetylation process of the CA base is at an advanced stage, which explains its severely degraded macroscopic condition. The loss of most of the acetate groups in the polymer reflect a spectral response where the CA has almost completely reverted back to cellulose[55].

Compared to the spectrum of standard CTA, the νOH absorption band in the film sample spectrum is broader and appears shifted toward lower wavenumbers. The bathochromic shift of the νOH band in the film sample corresponds to a cellulose derivate with low Degree of Substitution (DS), where the increased amount of free OH groups involves an increase in hydrogen bonding between hydroxyl groups following hydrolytic loss of acetate groups[42], [59].

The weak bands at 1589, 1487, 1296, 773 and 685 cm^{-1}, present in the film sample spectrum but not in the spectra of the CTA and MCC pure standards, are related instead to the presence of TPP additive, as can be confirmed by comparison to the pure TPP standard.

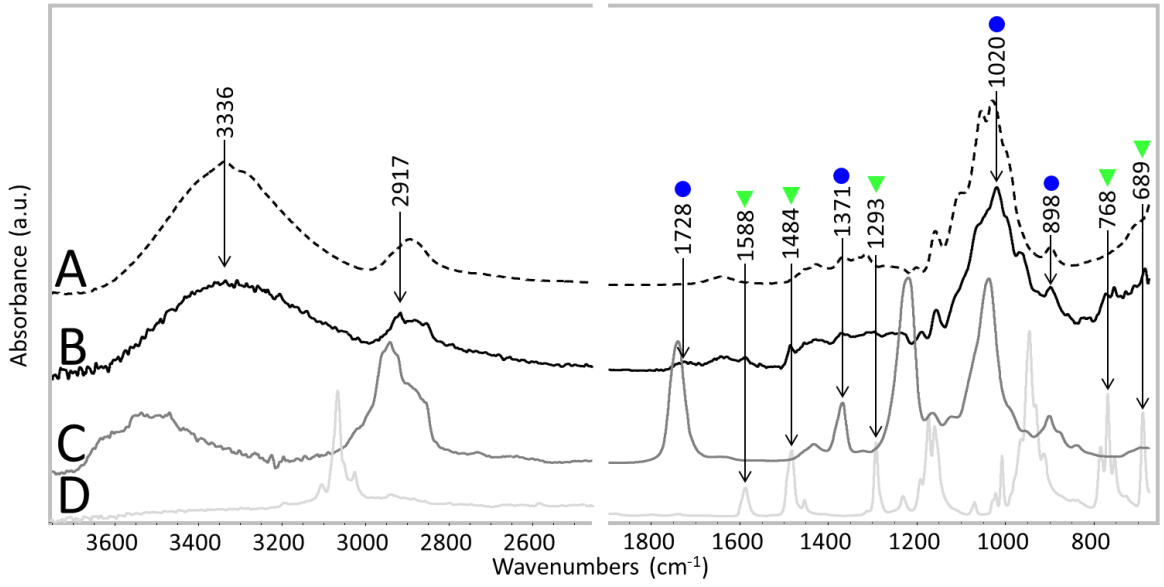

Fig. 47. µATR-FTIR spectra: Pure MCC standard (A, dashed line), an untreated area of the studied film base without any TPP bloom (B, black), a Pure CTA standard (C, dark gray) and pure TPP standard (D, light gray). Diagnostic FTIR bands due to the degraded cellulosic base are accompanied with a blue circle, and those related to TPP presence are highlighted with a green triangle.

The crystal bloom residues have also been characterized by means of µATR-FTIR spectroscopy. The µATR-FTIR spectrum of a crystal accretion from the film sample was compared with a TPP reference spectrum (Figure 48). The µATR-FTIR spectrum of Pure TPP exhibits its strongest signals at 1588, 1484, 1293, 1174, 1160, 1008, 946, 784, 768, 753 and 689 cm^{-1}, as well as a series of smaller peaks at 3098, 3060, 3020, 1455, 1232, 1192, 1070, 1022, 964, 932 and 914 cm^{-1}.

As the spectrum of the crystal bloom in the film and the reference spectrum of pure TPP are practically identical, and as both share the same bands weakly visible in the spectrum obtained from the film base in areas without crystal blooms, µATR-FTIR analysis allowed us to conclude that the film base under study corresponds to a heavily deacetylated CA film base containing TPP as additive.

The signals at around 1587 and 1487 cm^{-1} are the is due to aromatic C=C stretching of phenyl ring; the peak at 1293 cm^{-1} can be attributed to the P=O bond vibrations, whereas the one ca. 1232 corresponds to aromatic ring C-H vibrations. The absorption of the P-O bond occurs instead at ca. 964 cm^{-1}, which help confirm the presence of the phosphate group. A full band assignment for the Mid-infrared response of TPP is given in table SMIII.2.

As the strong bands of TPP at ca. 950 and cm^{-1} and 768 cm^{-1} do not overlap with other peaks from the polymeric film sample, they were used as main characteristic signals to detect TPP residues remaining after the cleaning treatments.

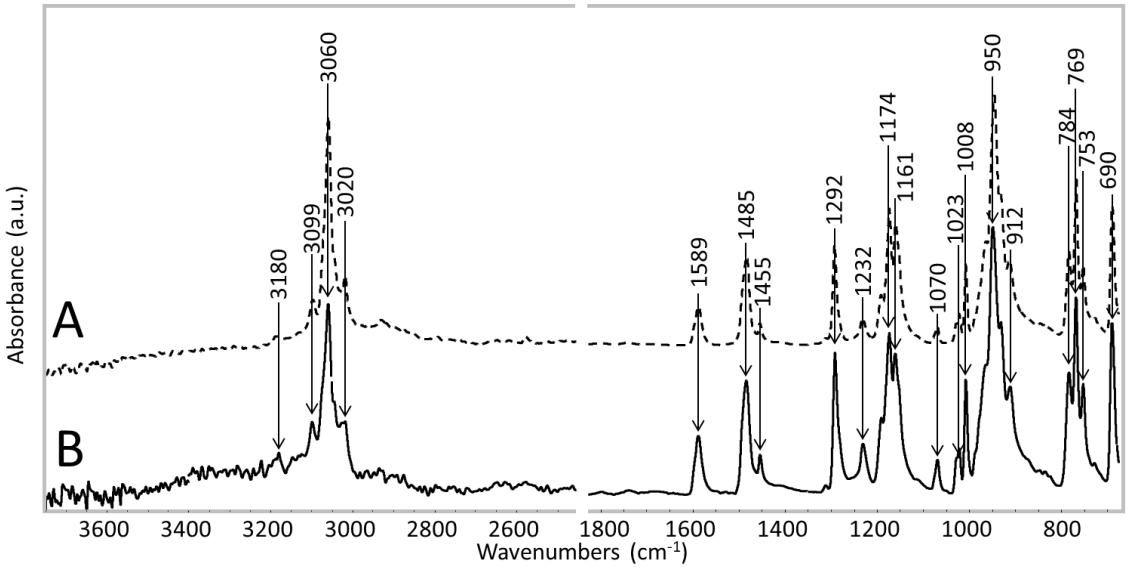

Fig. 48. µATR-FTIR spectra of a Pure TPP standard (A, dashed line), and of the TPP bloom over the studied film base (B, black).

The µATR-FTIR spectra registered on the base lacks the strong characteristic band of amide II at ca. 1539 cm^{-1}, expected to be detected before the cleaning treatment as sign of the gelatin binder of the antihalation layer. This shows how discontinuous the layer is, and how it has been disrupted by degradation processes, including the bloom of TPP crystals.

4.5.3 Solubility tests results

By comparing the thicknesses, weights, DS and superficial appearance of the CA samples before and after being immersed and sonicated in each solvent, the effects of each solvent on the degraded CA

were evaluated. A summary of the measured parameters is presented in Table SMIII.3, and photomicrographs before and after treatment of one sample per solvent are shown in Figure SMIII.1.

µATR-FTIR analysis showed that the DS of the exposed surface of the polymeric base before being subjected to the solvents was around 0.07, so very close to pure cellulose. After exposing the samples to the solubility tests, the calculated DS sometimes varied slightly, but it stayed always below 0.39. These relatively slight variations are most likely due to internal sample inhomogeneity. An averaged spectrum of the samples before and after being subjected to each of the solvents is shown in Figure SMIII.2.

It is noteworthy to say that before treatment, some µATR-FTIR measurements showed strong intensity of the TPP-related bands, even after cotton swab and mechanical preparation of the samples. The intensity of the TPP bands lowered after treatment to comparable levels among all samples.

None of the chosen solvents caused weight differences of more than 3.5%. Thickness variations did not correspond well to weight variations, being in general more erratic and not following a reproducible trend between test replicates. This is likely due to the uneven surface topology of the samples following their pretreatment with a surgical scalpel; therefore, thickness measurements were not taken in consideration. Finally, and most relevantly, surface photomicrographs showed that the samples remained relatively unaltered after treatment (Figure SMIII.1).

In conclusion, no relevant changes were relieved after immersing and sonicating for 10 minutes the degraded CA base into any of the tested solvents.

4.5.4 Cleaning test results

In general, cleaning tests using solvents showed a much more efficient cleaning than dry cleaning, as will be discussed. As tests performed in duplicate showed overall a similar final condition, only one area per kind of test is shown here for discussion.

4.5.4.1 Cleaning by rubbing a dry eyeglass-cleaning cloth

When a dry eyeglass-cleaning cloth was rubbed against the film, the removal of TPP bloom from the treated area seemed inefficient. OM surface photomicrographs (Fig. 49) showed that the dry cloth left many TPP residues over the treated area, whereas cross section photomicrographs (Fig. 50, II) confirm that thick TPP residues remain after treatment with the dry cloth, with thicknesses up to 9.5 µm.

µATR-FTIR analyses after the treatment (Fig. 51) detected the strong response of TPP at along several measurement points, confirming that observed residues are constituted by this substance.

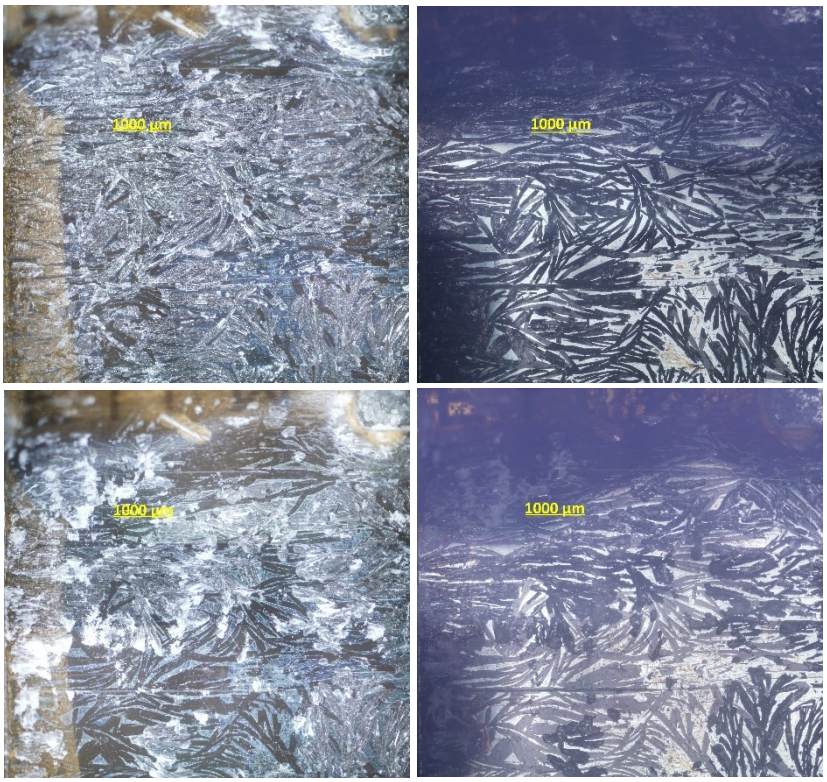

Fig. 49. Surface photomicrographs of a selected film area before (up) and after (down) being treated with traditional eyeglass-cleaning cloth in dry conditions; taken in Dark Field (left images) and Bright Field (right images).

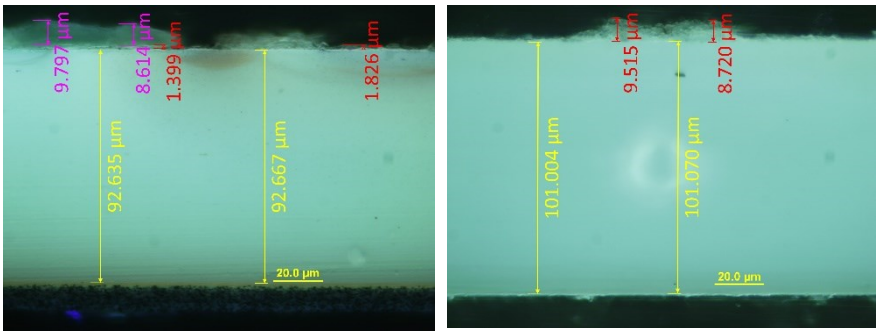

Fig. 50. 100x UV OM cross-sections photomicrographs of the film before cleaning (I), after being treated with eyeglass-cleaning cloth in dry conditions (II). The treated side of the CA base is looking up.

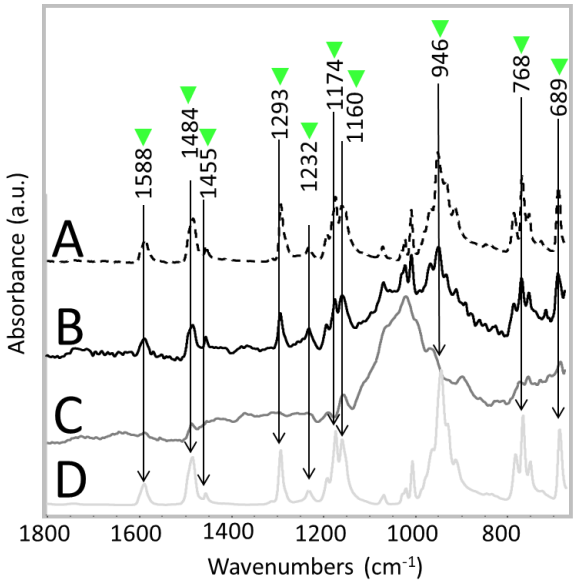

Fig. 51. µATR-FTIR spectra: Representative spectrum of TPP bloom before cleaning (A, dashed line); a representative spectrum of the film surface once cleaned with a dry eyeglass-cleaning cloth (B, black); a spectrum of an untreated area of the film without any TPP bloom (C, dark gray); and a reference spectrum of pure TPP. Diagnostic bands due to TPP presence are highlighted with a green triangle.

4.5.4.2 Cleaning by rubbing cotton swabs soaked in solvent

In comparison, cleaning with cotton swabs soaked in the four tested solvents (IPOH, IAA, DEC and DMC) led to better results. Regarding the visual appearance of the treated areas, OM surface photomicrographs (Fig. 52) showed that apart from some punctual points, the surface appeared overall flat and reflective, evidencing the removal of TPP crystals, except for the border of the area treated with DMC, where matte residues regions are still evident after the treatment (Fig. 52, IV).

Cross sections (Fig. 53) prepared from the center of the treated areas confirm that the depths of the TPP residues were considerably and homogenously reduced, except for the area treated with IAA, where thicker residues could still be found (Fig. 53, III).

Finally, µATR-FTIR analyses performed in the central region of the treated surfaces (Fig. 54) retrieved in all cases a response corresponding to the clean CA base (except one of the eight points of the area cleaned with DMC), confirming that the areas are overall clean.

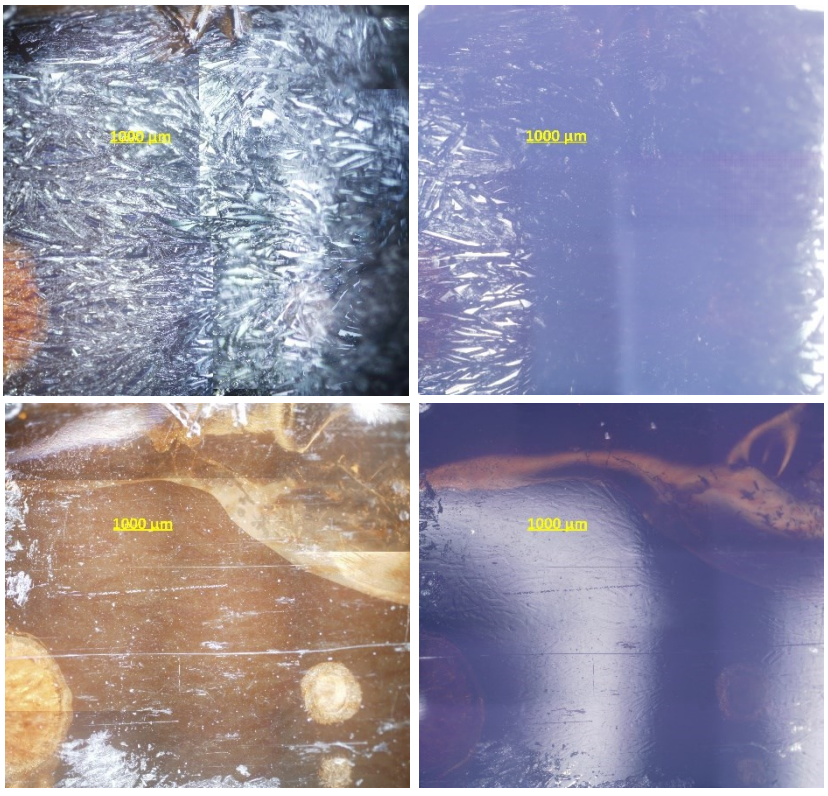

I

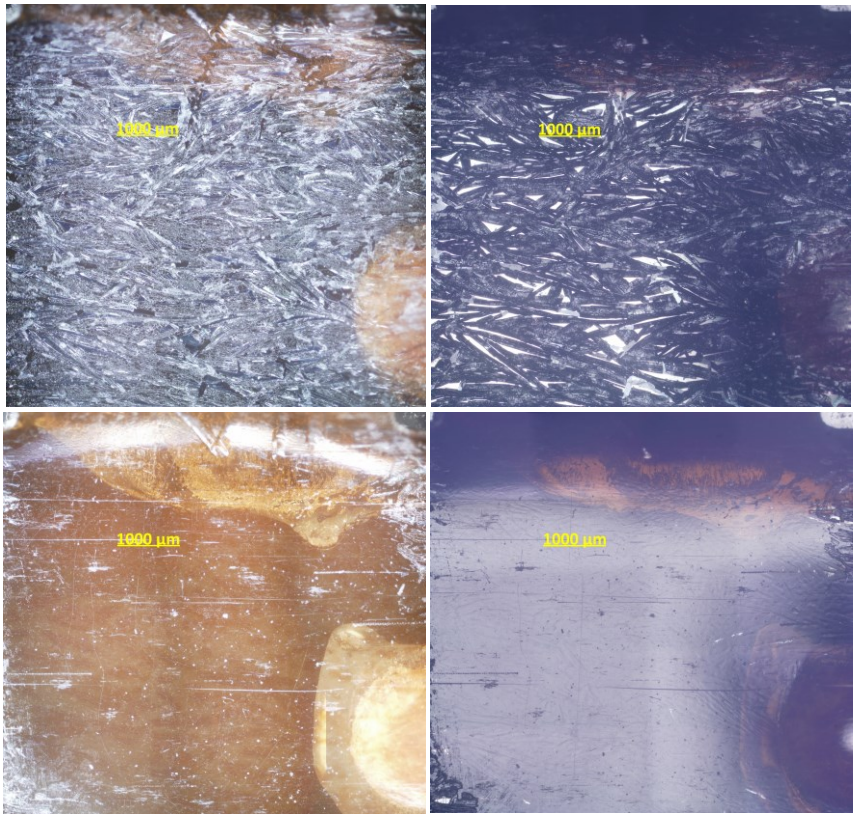

II

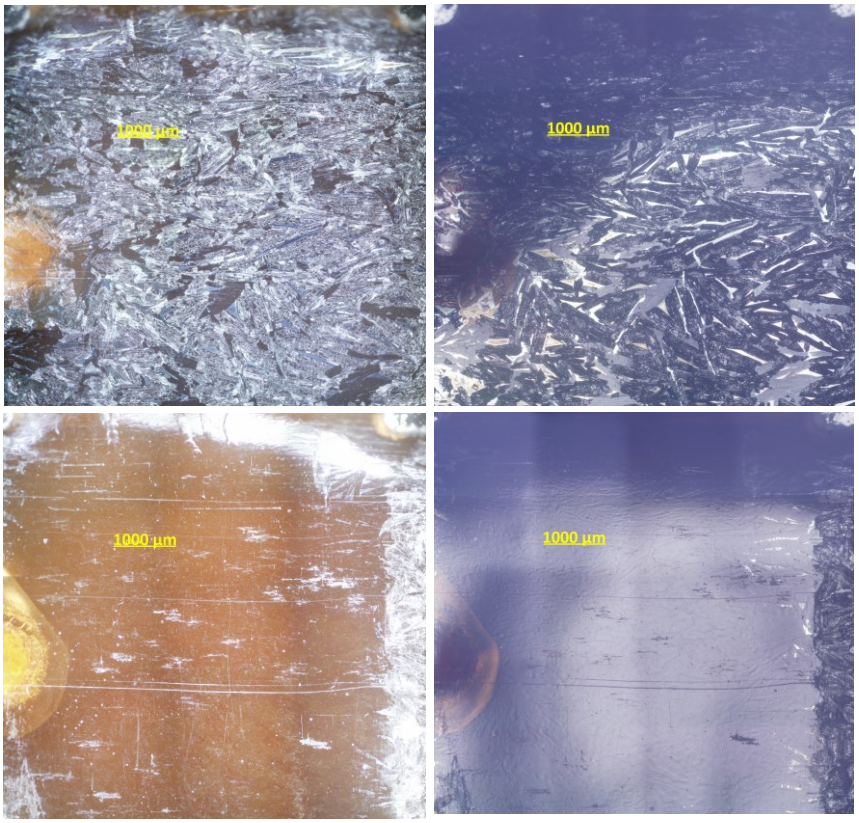

III

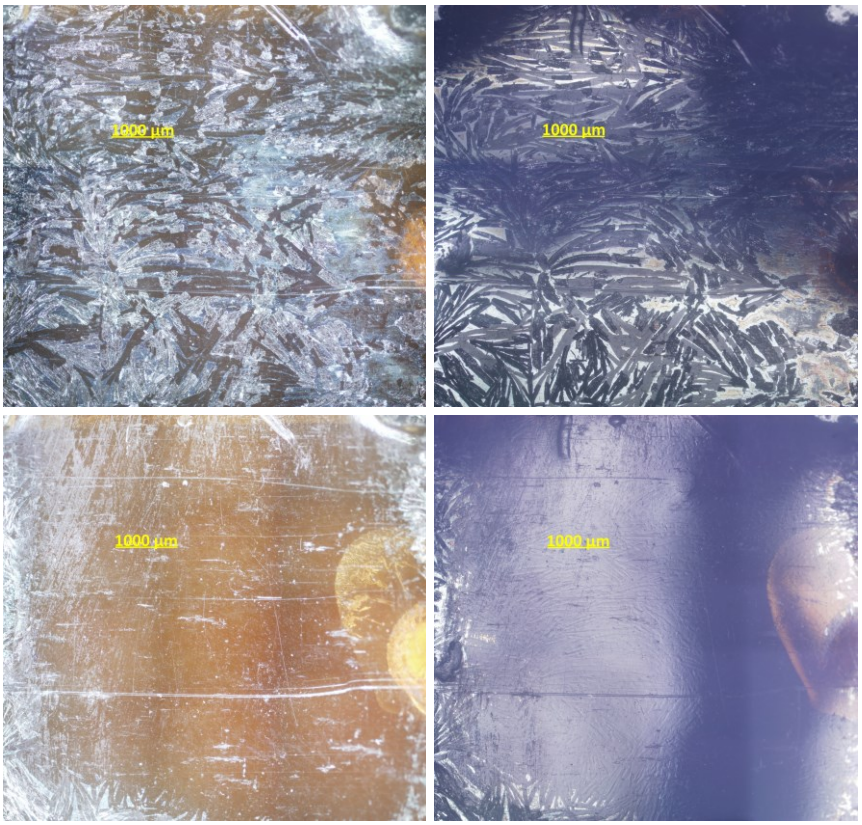

IV

Fig. 52. Surface photomicrographs of selected film areas before (up) and after (down) being rubbed with a cotton swab soaked with IPOH (I), soaked with IAA (II); soaked with DEC (III); and soaked with DMC (IV). Photos were taken in Dark Field (left images) and Bright Field (right images).

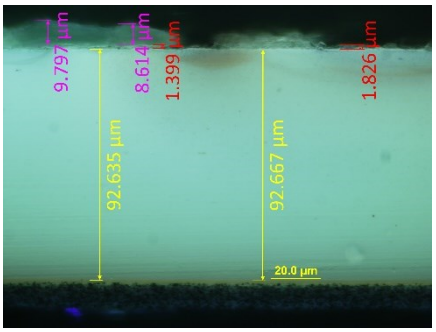

I

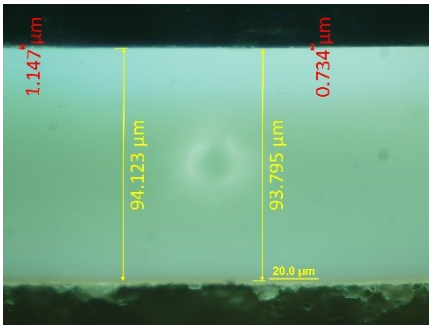

II

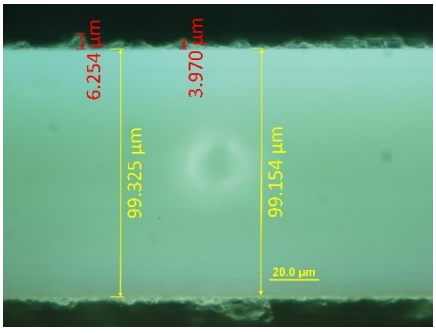

III

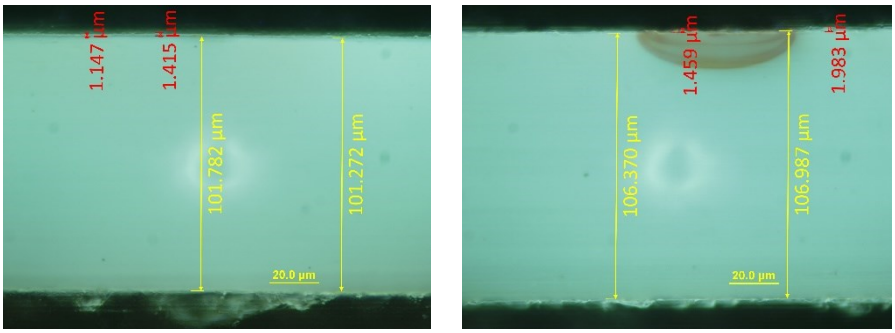

IV **V**

Fig. 53. 100x UV OM cross-sections photomicrographs of the film before cleaning (I), and after rubbing with a cotton swab soaked with IPOH (II), soaked with IAA (III), soaked wit DEC (IV) and soaked with DMC (V). The treated side of the CA base is looking up.

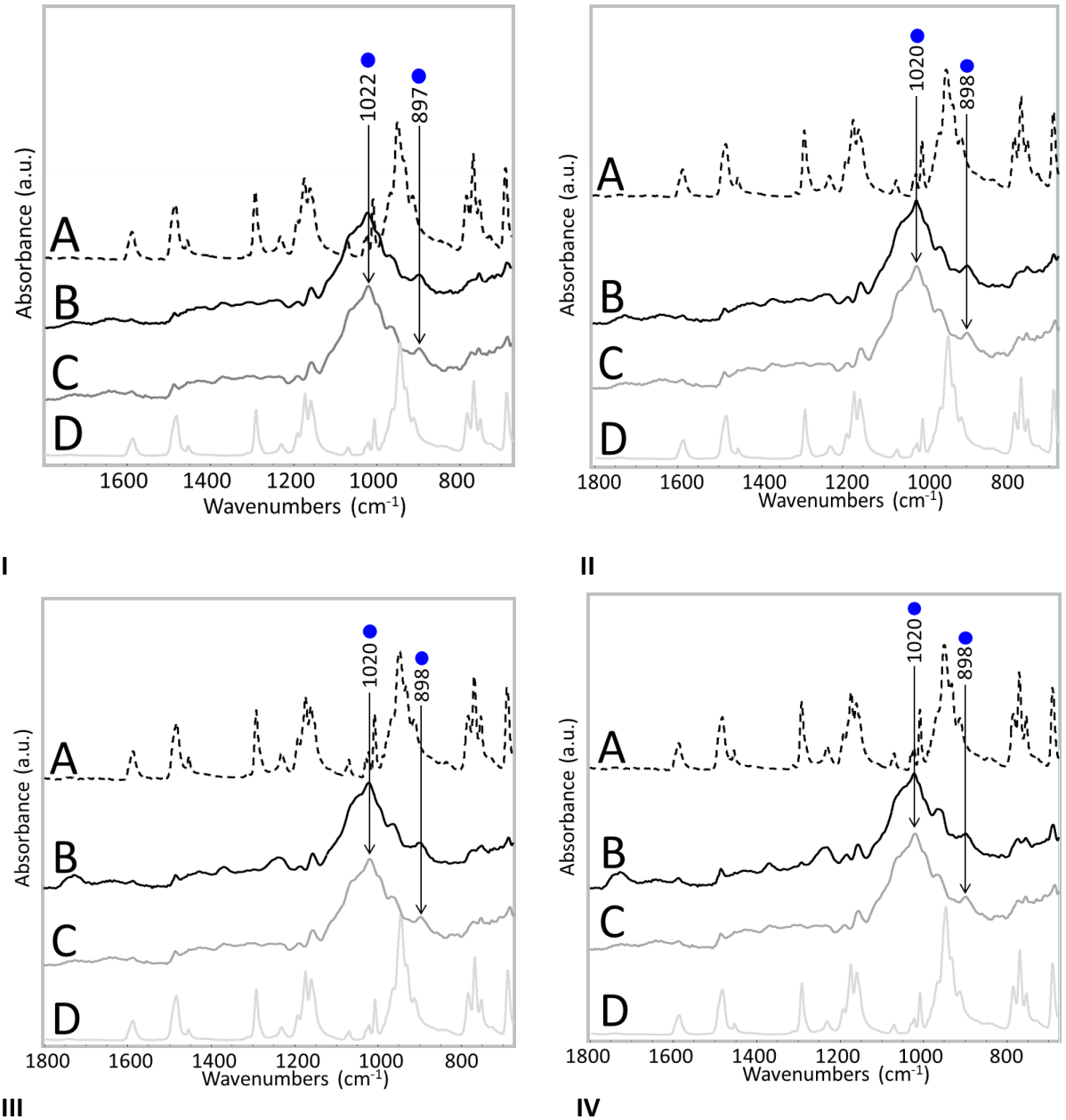

I **II**

III **IV**

Fig. 54. µATR-FTIR spectra: Representative spectrum of TPP bloom before cleaning (A, dashed line); a representative spectrum of the film surface once cleaned (B, black: I. By rubbing a cotton swab soaked with IPOH; II. By rubbing with a

cotton swab soaked with IAA; III. By rubbing with a cotton swab soaked with DEC; by rubbing with a cotton swab soaked with DMC); a spectrum of an untreated area of the film without any TPP bloom (C, dark gray); and a reference spectrum of pure TPP (D, light gray). The signals due to the degraded CA base with a blue circle.

4.5.4.3 Electrospun nylon mat cleaning with solvents and no mechanical action (40 second application)

The four solvents were then applied without any friction by means of electrospun nylon mats, to avoid risking the mechanical stresses caused by traditional cotton swab cleaning.

From the evaluation of the surface appearance after the treatments (Fig. 55), OM photomicrographs reveal that where the contact between the mat and the surface was ensured, the flatness and reflectivity of the surface was greatly recovered, specially for IPOH and DEC (Fig. 55, I and III). However, for those areas treated with IAA and DMC (Fig. 55, II and IV), a small percentage of the surface still exhibited rough and protruding residues.

Cross sections confirmed that nearly all residues were removed by the treatments with IPOH and DEC (Fig. 56, I and III), whereas thicker and more extended residues can be seen on the cross sections coming from areas treated with IAA and DMC (Fig. 56, II and IV).

Finally, µATR-FTIR measurements acquired after the cleaning treatments (Fig. 57) showed that, from all the test replicates using the four solvents, only one replicate obtained by IPOH and one by DEC reached a cleaning level where all the spectra from the central test area corresponded to the clean CA base. Instead, the remaining replicates from those solvents, as well as both tests using IAA and DMC, showed from 2 to 4 points out of 9 which corresponded to a strong TPP bloom presence.

From this set of trials, it was possible to conclude that when applied without friction for 40 seconds using an electrospun nylon mat, IPA and DEC performed better than IAA and DMC, so these two solvents were deemed more promising and further testing were undertaken with longer application time (5 minutes=300 seconds).

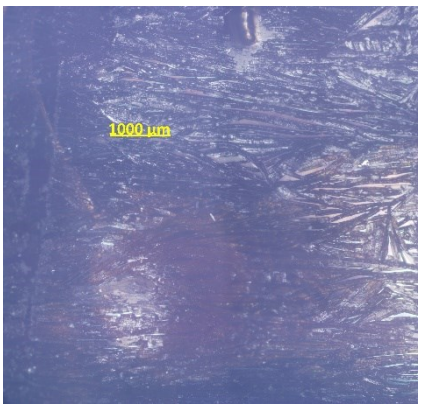

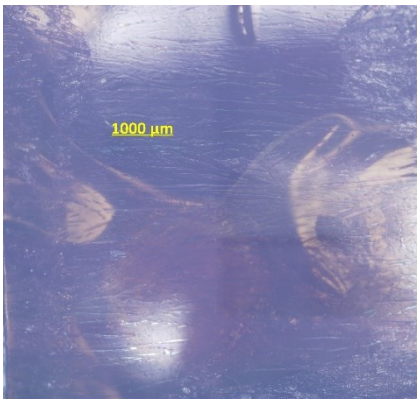

I

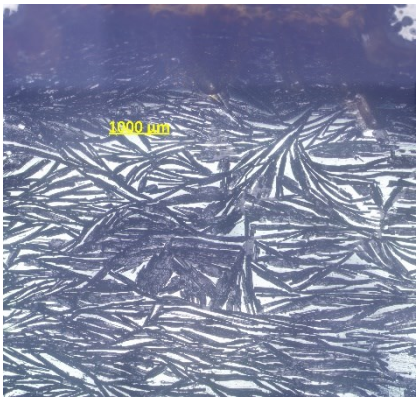

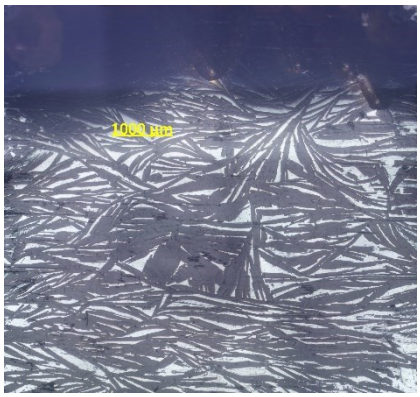

II

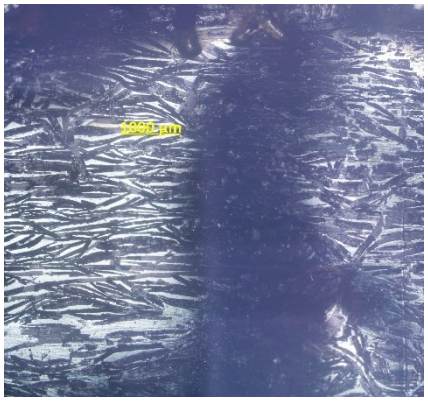

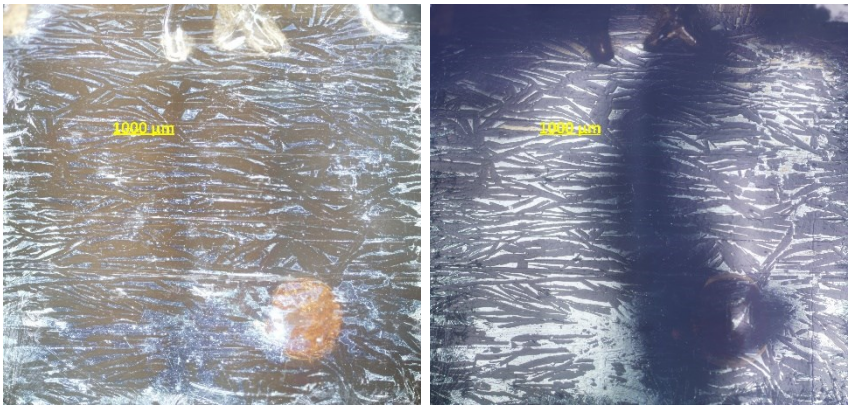

III

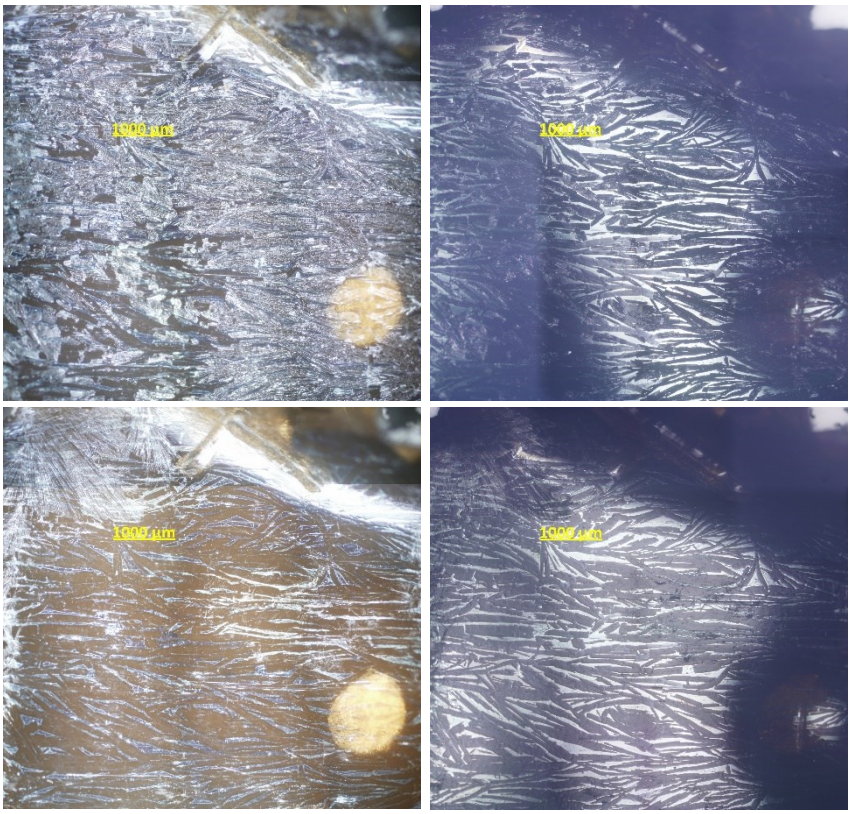

IV

Fig. 55. Surface photomicrographs of selected film areas before (up) and after (down) being cleaned without friction with an electrospun nylon mat soaked with IPOH (I), soaked with IAA (II); soaked with DEC (III); and soaked with DMC (IV). Photos were taken in Dark Field (left images) and Bright Field (right images).

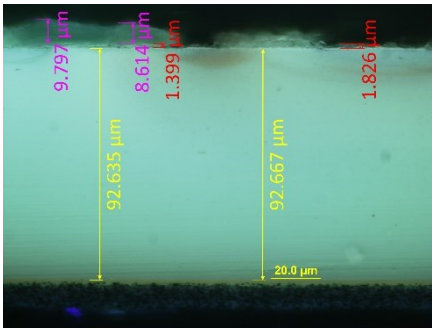

I

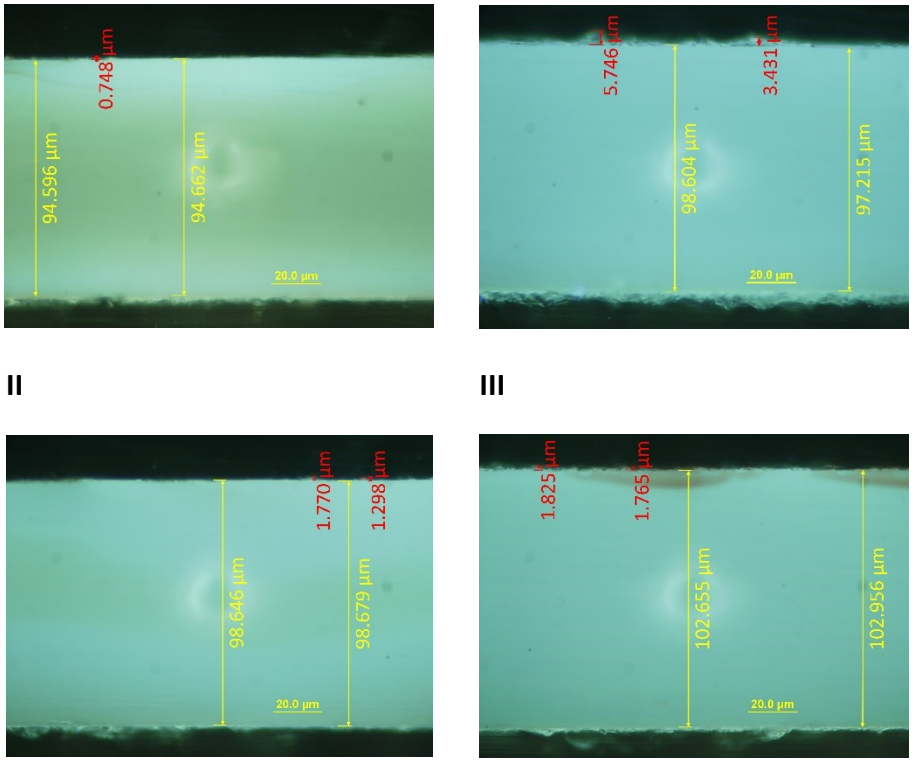

II III

IV V

Fig. 56. 100x UV OM cross-sections photomicrographs of the film before cleaning (I), and after being cleaned without friction with an electrospun nylon mat soaked with IPOH (II), soaked with IAA (III), soaked wit DEC (IV) and soaked with (DMC). The treated side of the CA base is looking up.

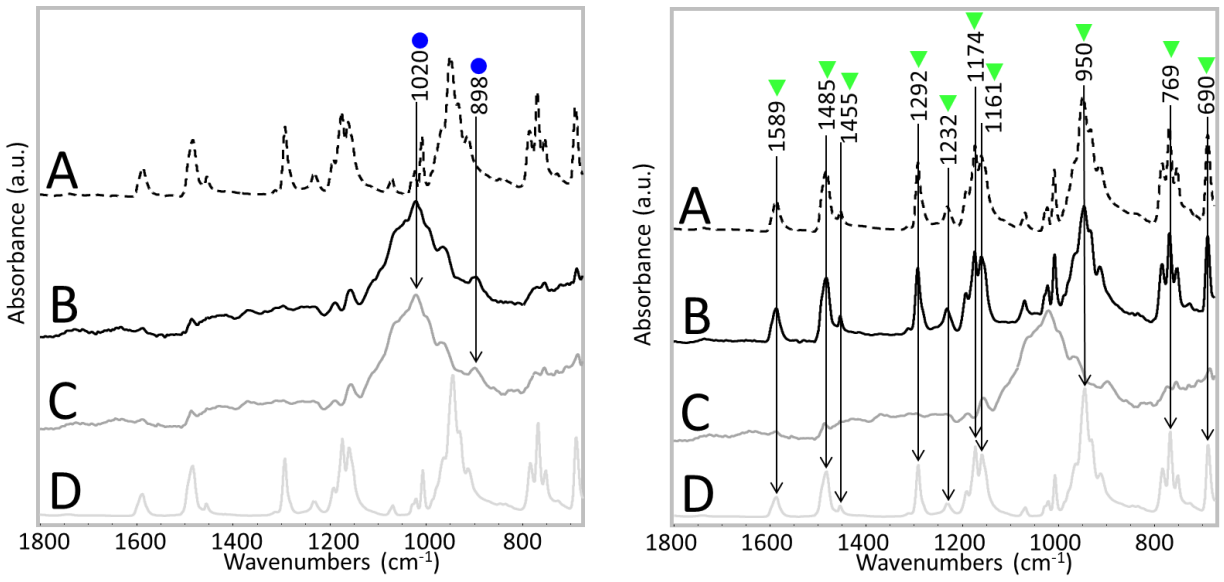

I II

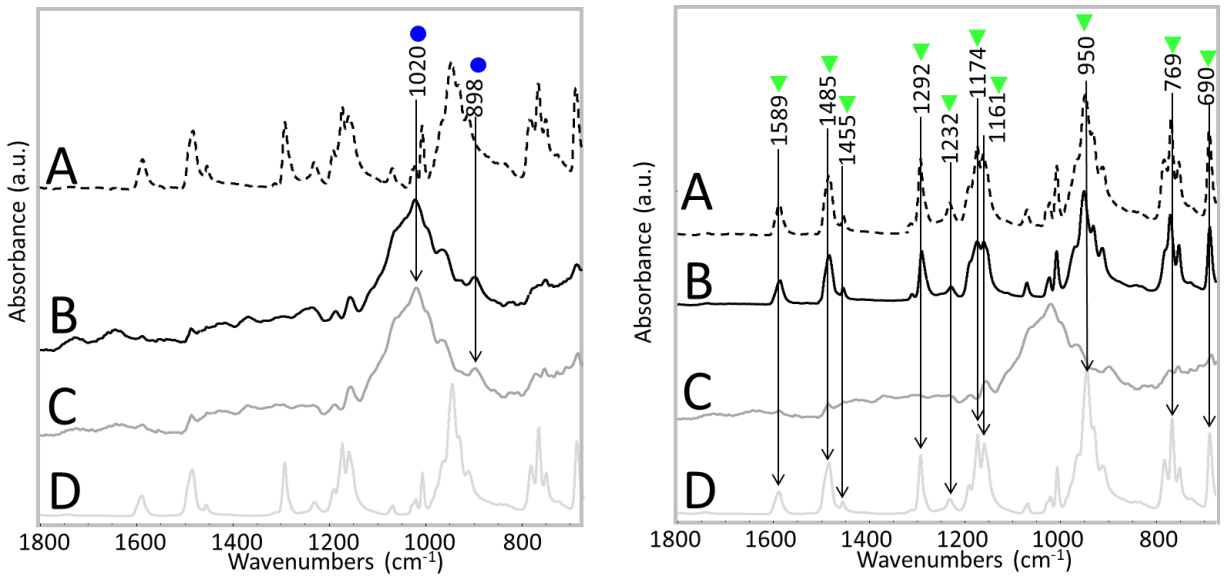

Fig. 57. µATR-FTIR spectra: Representative spectrum of TPP bloom before cleaning (A, dashed line); a representative spectrum of the film surface once cleaned without friction (B, black: I. with an IPOH-soaked electrospun nylon mat; II. with an IAA-soaked electrospun nylon mat; III. With a DEC-soaked electrospun nylon mat; IV. With a DMC-soaked electrospun nylon mat); a spectrum of an untreated area of the film without any TPP bloom (C, dark gray); and a reference spectrum of pure TPP (D, light gray). Diagnostic bands due to TPP presence are highlighted with a green triangle, those coming from the degraded CA base are shown with a blue circle.

4.5.4.4 Electrospun nylon mat cleaning with solvents and no mechanical action (5 minutes=300 second application)

IPOH and DEC, previously identified as the most promising of the four solvents tested for TPP removal, were further tested. A longer application of the solvent-wet electrospun nylon mats was carried out without friction, choosing 300 seconds (5 minutes) as application time after visually comparing the results of preliminary trials, and identifying the time needed for the evaporation of most of the solvent from the electrospun mats.

From the study of the OM surface photomicrographs (Fig. 58), it emerged that the extension of TPP crystals was greatly reduced in both test; however, little rough particles can still bee seen distributed over the film, and for the test with IPOH, the apparition of dendritic structures on the surface can be detected (Fig. 58, I).

Cross section analysis (Fig. 59). confirmed that even if the residues depths were considerably reduced by both treatments, relevant portions of the cross sections were still covered in residues ranging from 2.2 to 5.1 µm depth.

Regarding the µATR-FTIR analyses performed in the center of the treated areas, 4 measurements from the test with IPOH and 3 points from the test with DEC showed the strong response of TPP bloom residues (Fig. 60). In addition, for the test using IPOH (Fig. 60, I), three of the resulting spectra showed also the amide I and amide II bands, respectively at 1661 and 1545 cm^{-1}, characteristic for proteinaceous material presence[196]–[198]. This likely reflects the presence of the anticurling or antihalation gelatin layer which may swell and partially dissolve in alcohols like IPOH.

From this set of trials, it was possible to conclude that when applied with electrospun nylon mats for a long application time of 300 seconds, IPOH and DEC were not able to completely remove all TPP residues without the aid of friction.

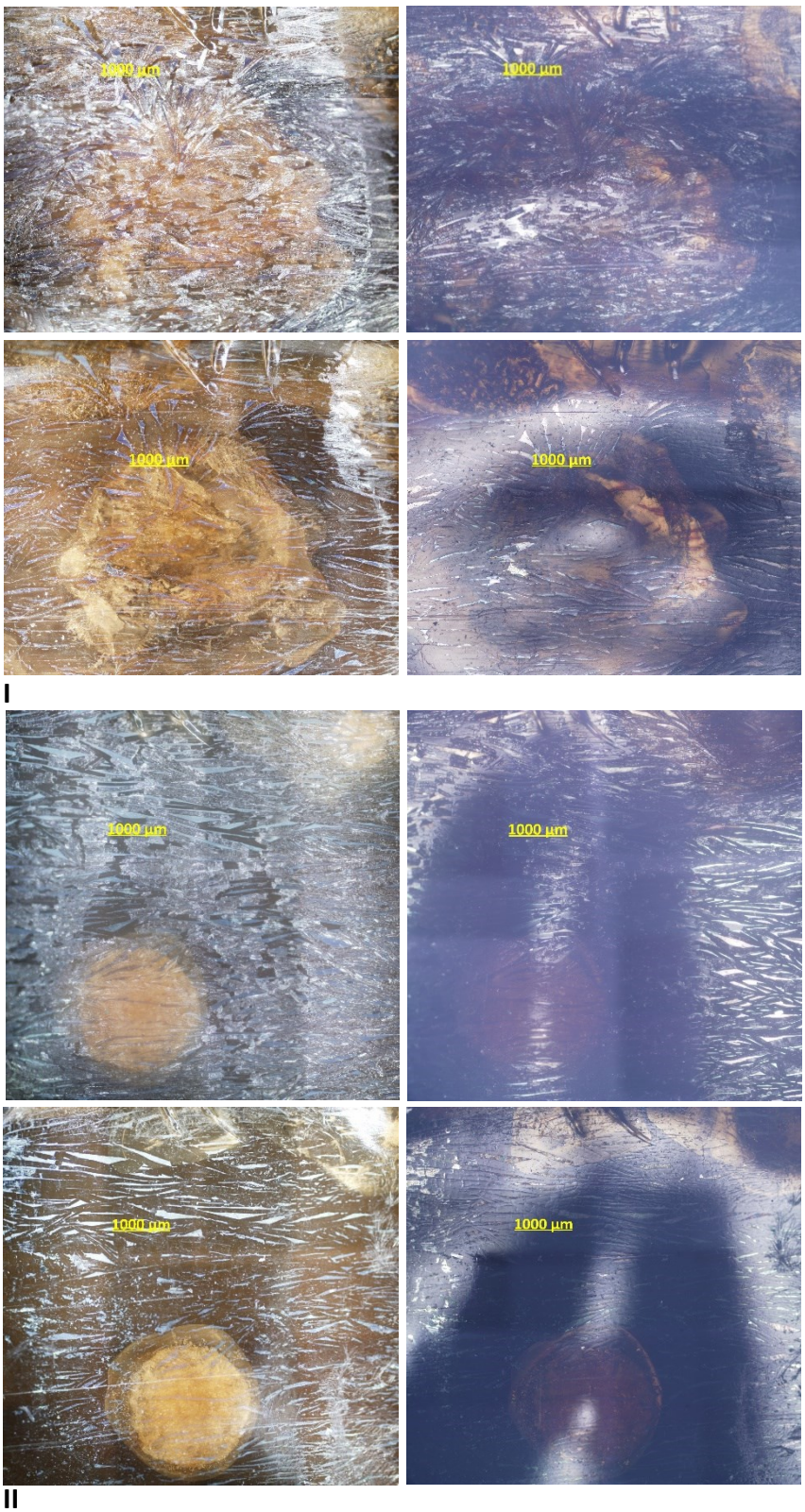

Fig. 58. Surface photomicrographs of selected film areas before (up) and after (down) being treated without any friction by applying for five minutes an electrospun nylon mat soaked in IPOH (I) or soaked in DEC (II), taken in Dark Field (left images) and Bright Field (right images).

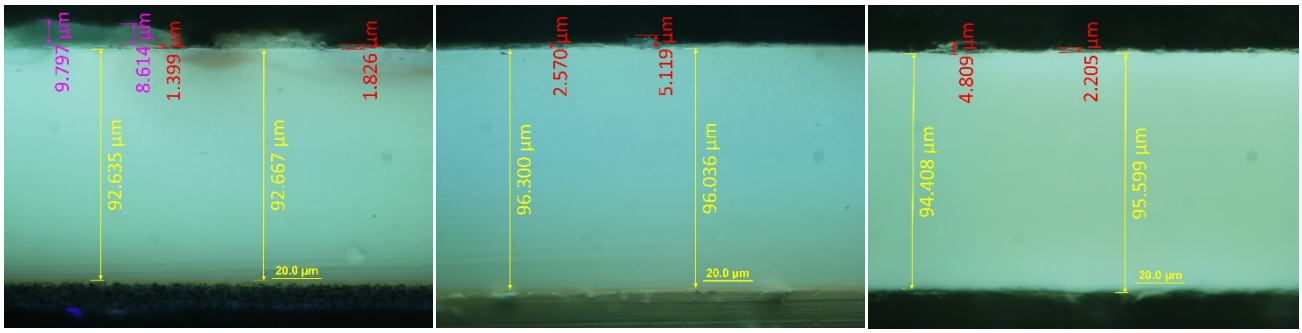

Fig. 59. 100x UV OM cross-sections photomicrographs of the film before cleaning (I), after being treated without any friction by applying for five minutes an electrospun nylon mat soaked in IPOH (II) or soaked in DEC (III). The treated side of the CA base is looking up.

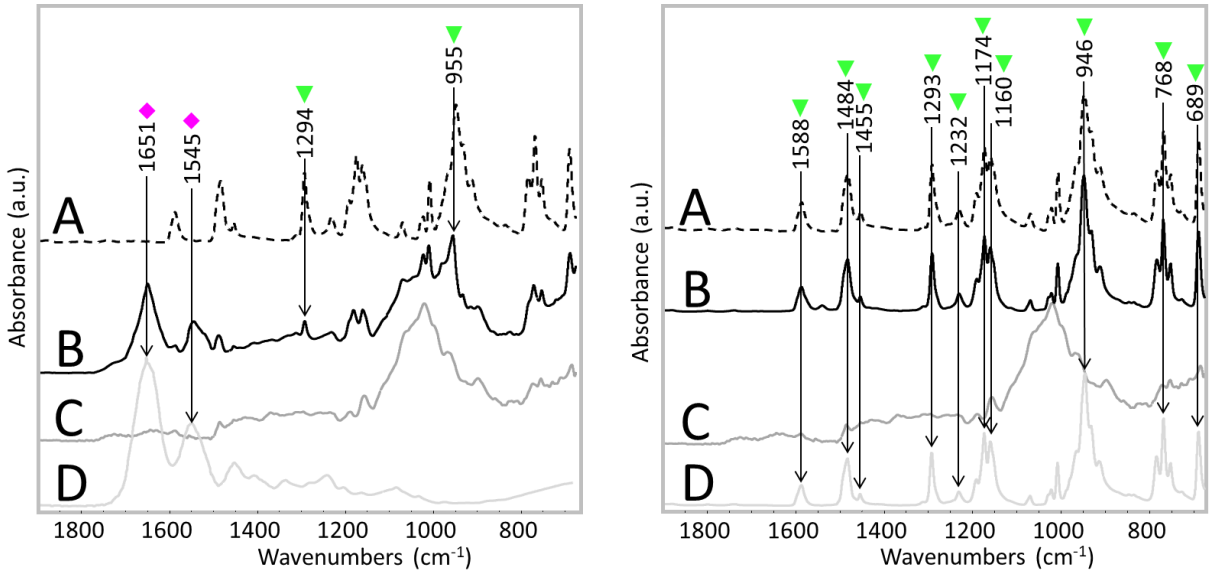

Fig. 60. µATR-FTIR spectra: Representative spectrum of TPP bloom before cleaning (A, dashed line); a representative spectrum of the film surface once cleaned (B, black: I. with an IPOH-soaked electrospun nylon mat; II. with a DEC-soaked electrospun nylon mat); a spectrum of an untreated area of the film without any TPP bloom (C, dark gray); and a spectrum of reference unwanted residues (D, light gray: I. FTIR of collagen reference; III. µATR-FTIR of pure TPP reference). Diagnostic bands due to TPP presence are highlighted with a green triangle, those coming from gelatin residues are shown with a magenta diamond.

4.5.4.5 Cleaning by rubbing eyeglass-cleaning cloth soaked in solvent

After the previous tests showed that friction was essential for the obtention of satisfactory cleaning results, two areas were treated by rubbing squares of eyeglass-cleaning cloth soaked in IPOH and DEC (the best performing solvents). These tests had the objective of reducing the amount of solvent needed when compared to more solvent-absorbing cotton swabs, and obtaining a procedure that could be applied over long extensions of film, as opposed to punctual cotton swab cleaning.

From OM surface observation (Fig 61), rubbing the eyeglass-cleaning cloth soaked in both solvents showed a better performance than applying the cloth in dry conditions, but considerable extensions of thin residues remained over the film surface after both treatments. For the test with IPOH, the

residues follow the path of application of the cloth (Fig 61, I), and for the test with DEC, these follow a dendritic pattern (Fig 61, II).

Cross sections show the presence of residues after treatment with the solvent-wet cloths, reaching thicknesses above 4 µm for both areas (Fig 62).

µATR-FTIR analysis after both treatments (Fig. 63) show along several measurement points a strong response of the bands related to TPP, specially the peak at 949 cm^{-1}, confirming that the observed residues are constituted by this substance. Additionally, cleaning with the IPOH-soaked cloth resulted in the presence of a substance with FTIR response at approximately 1572 and 1542 cm^{-1} (Fig. 63, I), observed also when performing RAS analysis on the precipitates resulting from soaking an eyeglass-cleaning cloth with IPOH over a gold-coated glass holder. These bands corresponds to the asymmetric stretching vibration of COO^- in a carboxylate[213], coming from the eyeglass-cleaning cloth, which becomes dissolved in IPOH and deposits over the film after the treatment.

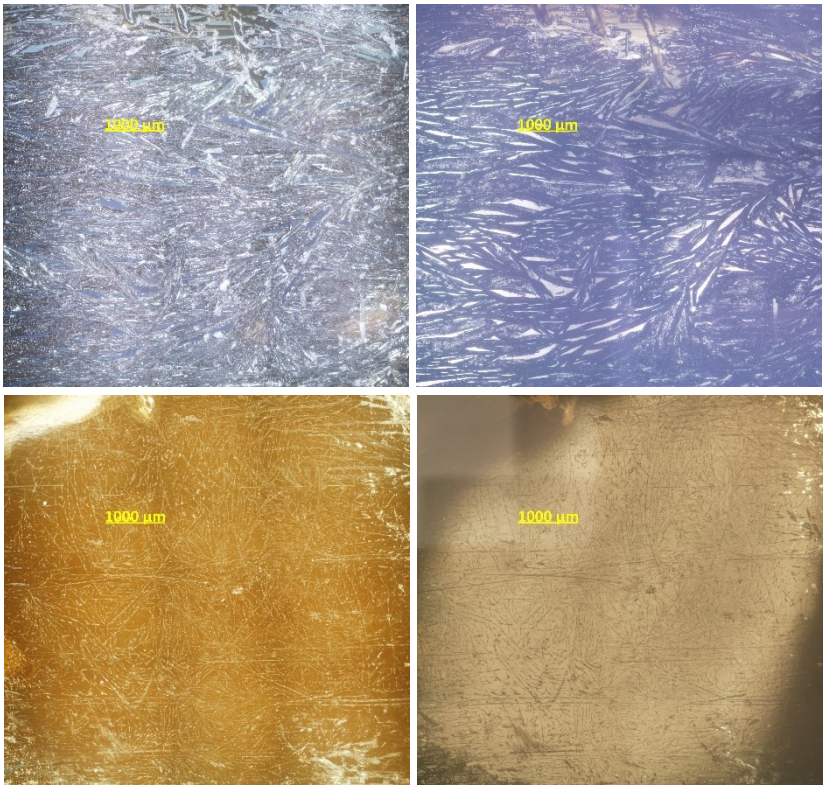

I

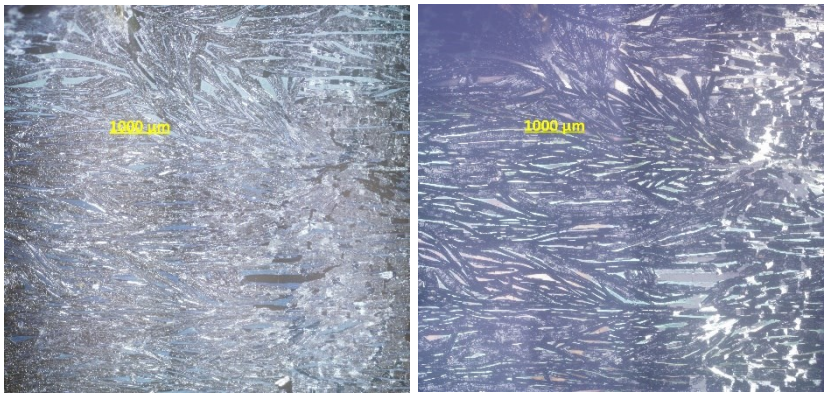

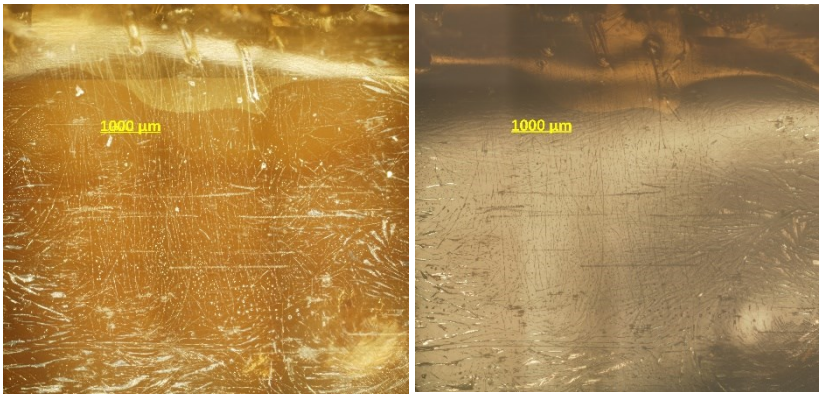

II

Fig. 61. Surface photomicrographs of selected film areas before (up) and after (down) being treated with an eyeglass-cleaning cloth soaked with IPOH (I) or soaked with DEC (II); taken in Dark Field (left images) and Bright Field (right images).

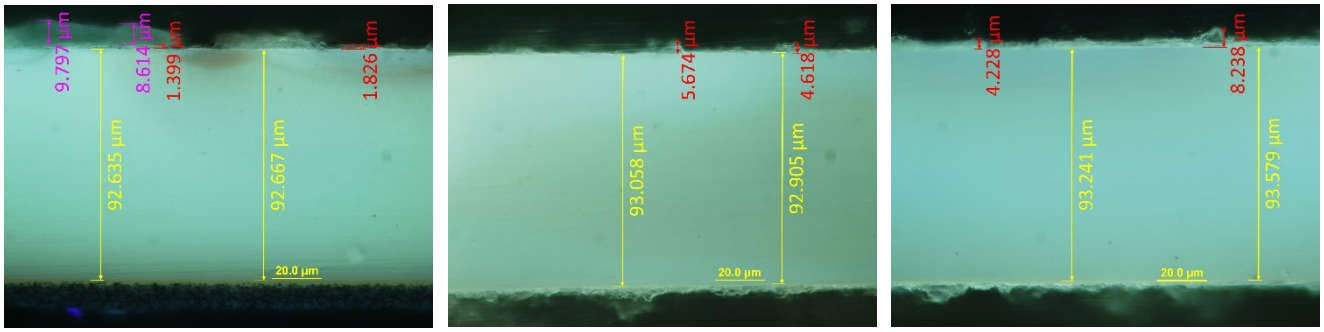

I II III

Fig. 62. 100x UV OM cross-sections photomicrographs of the film before cleaning (I), and after rubbing with an eyeglass-cleaning soaked with IPOH (II), and after rubbing with an eyeglass-cleaning cloth soaked with DEC (III). The treated side of the CA base is looking up.

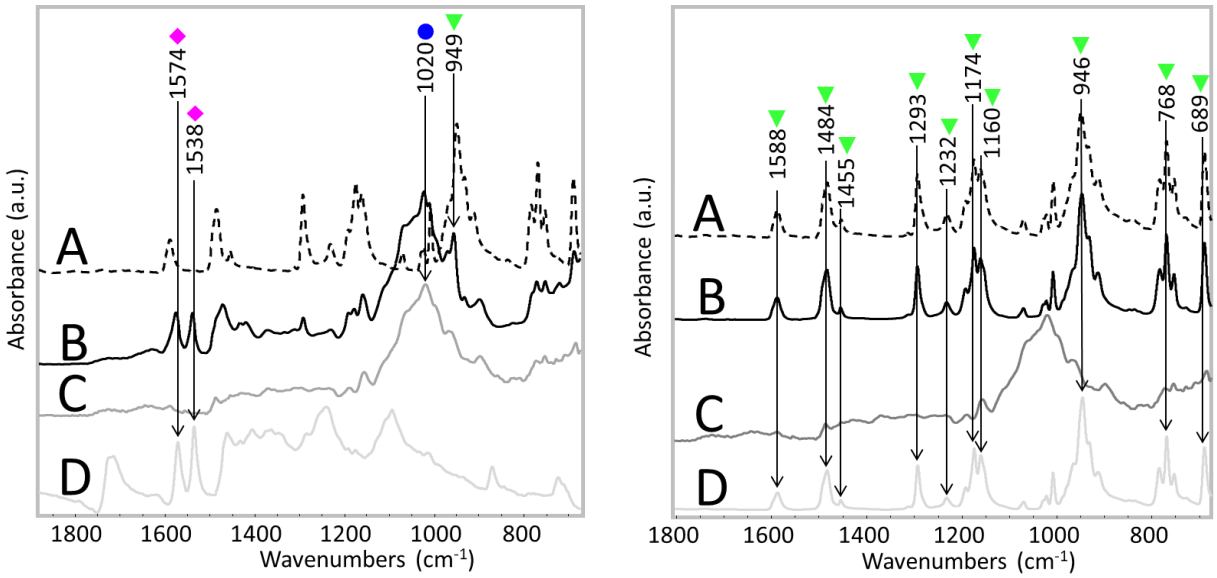

I II

Fig. 63. µATR-FTIR spectra: Representative spectrum of TPP bloom before cleaning (A, dashed line); a representative spectrum of the film surface once cleaned (B, black: I. By rubbing with an eyeglass-cleaning cloth soaked with IPOH; II. By rubbing with an eyeglass-cleaning cloth soaked with DEC); a spectrum of an untreated area of the film without any TPP

bloom (C, dark gray); and a spectrum of reference unwanted residues (D, light gray: I. FTIR-RAS spectrum of the precipitates left after soaking an eyeglass-cleaning cloth with IPOH; II. µATR-FTIR of pure TPP). Diagnostic bands due to TPP presence are highlighted with a green triangle, those due to precipitates coming from the eyeglass-cleaning cloth are shown with a magenta diamond, and the signals due to the degraded CA base with a blue circle.

4.5.4.6 Cleaning by rubbing electrospun mats soaked in solvent

In comparison, cleaning tests performed by rubbing an electrospun nylon mat soaked either with IPOH or DEC showed a much more efficient cleaning than rubbing the eyeglass-cleaning cloth soaked in the corresponding solvent.

From OM surface photomicrographs (Figure 64), it can be observed that after both treatments, the extension of TPP bloom was considerably and homogeneously reduced. No superficial damage resulted upon the CA surface, such as scratches following the circular cotton swab trajectory, gloss changes, etc. in either of the cleaned areas. The only visible damage after the cleaning by rubbing the electrospun nylon mat soaked with IPOH is an horizontal breakage in the lower part of the cleaning area (Figure 64, I), ascribable to the mechanical stress derived by the pressure of the treatment over the fragile and deformed film base.

Cross sections from representative points of both cleaning areas (Fig. 65) show that after the treatments, remaining residues are very much reduced in thickness, with average depths below 2 µm. These residues are not continuously distributed over the CA base, and from the homogeneity of their thicknesses and the color of their UV fluorescence, they could correspond to the antihalation layer. Due to their transparency, thinness and punctuality, these residues are not detectable in naked eye observation.

µATR-FTIR spectra acquired in at least 7 randomly selected points along the center of each cleaned area, showed the same profile observed in untreated CA areas without TPP residues (Fig. 66), confirming that both treatments resulted effective in removing the TPP bloom.

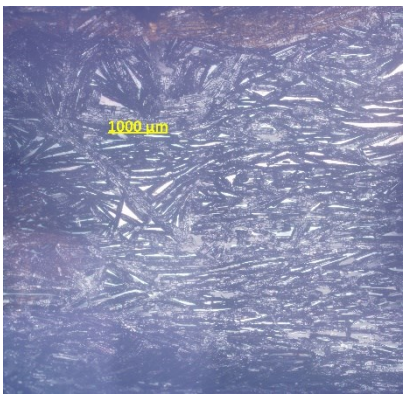

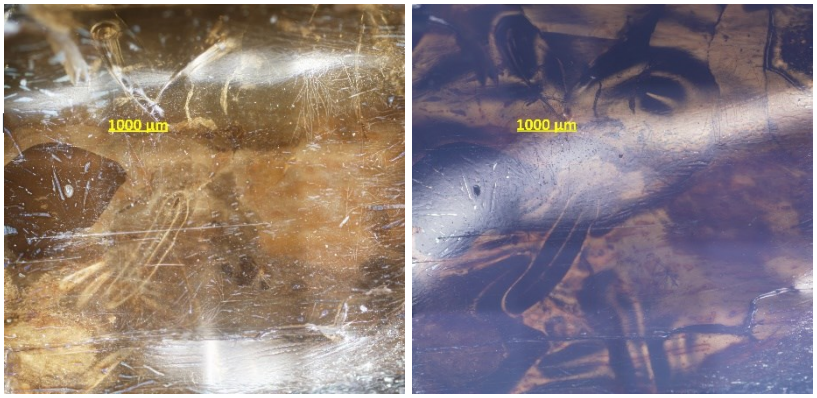

I

II

Fig. 64. Surface photomicrographs of selected film areas before (up) and after (down) being treated by rubbing an electrospun nylon mat soaked with IPOH (I) or an electrospun nylon mat soaked in DEC (II), taken in Dark Field (left images) and Bright Field (right images).

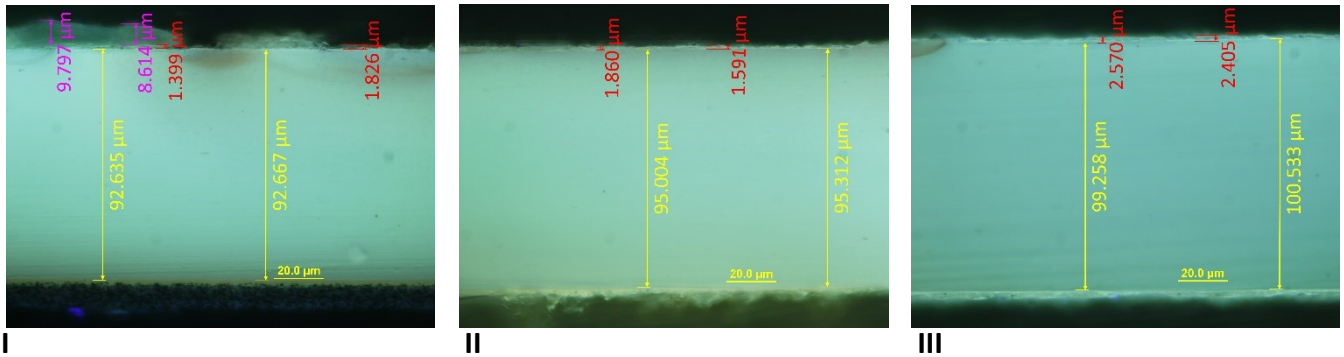

I II III

Fig. 65. 100x UV OM cross-sections photomicrographs of the film before cleaning (I), after cleaning by rubbing an

electrospun nylon mat soaked in IPOH (II), and after cleaning by rubbing an electrospun nylon mat soaked in DEC (III). The treated side of the CA base is looking up.

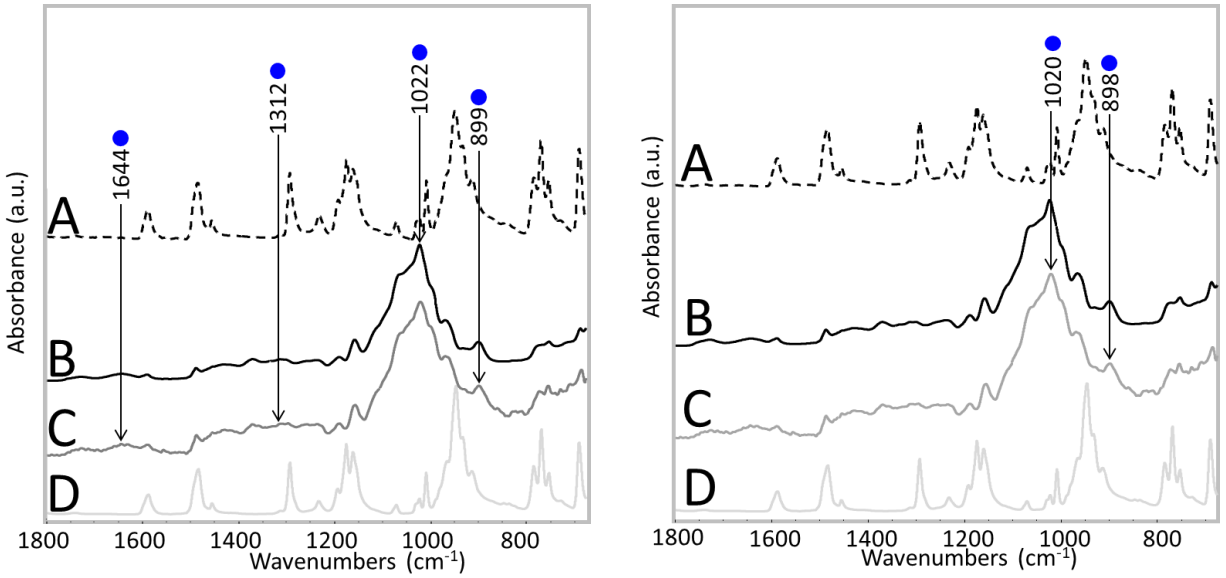

Fig. 66. FTIR spectra. Each figure shows: µATR-FTIR of the TPP bloom covering each area before cleaning (A, dashed line), a representative µATR-FTIR of the film surface once cleaned (B, black: I. by rubbing with an electrospun nylon mat soaked with IPOH; II. by rubbing with an electrospun nylon mat soaked in DEC); a spectrum of an untreated area of the film without any TPP bloom (C, dark gray); and a reference spectrum of pure TPP (D, light gray). Diagnostic FTIR bands due to the CA base are accompanied with a blue circle.

4.6 5.Conclulsion

We have found that when removing TPP bloom from degraded CA cinematographic film bases which have reverted to a DS close to 0, solvent cleaning is more effective than traditional mechanical cleaning with a dry eyeglass-cleaning cloth.

None of the four tested solvents (IPOH, IAA, DEC nor DMC) has produced any solubilization or damage to the cinematographic film base: OM photomicrographs have not relived any new scratches following the motion of cleaning devices, areas of gloss variation remain minimal and likely related to previous presence of a disruptive TPP crystal; whereas cross section photomicrographs of the CA base show uniform base topography and thicknesses between 92.6-107.0 µm. No detectable thickness changes occurred when compared to the cross section of untreated or dry-cleaned areas, with minor differences being likely due to intrinsic manufacture variability and differential shrinkage due to degradation. This conclusion is supported also by the fact that solubility tests did not lead to any relevant appearance or weight changes on exposed CA base samples after subjecting them to 10 minute sonication in each of the solvents.

Among the cleaning procedures involving the use of solvents, rubbing with solvent-soaked eyeglass-cleaning cloth left more TPP residues than rubbing with solvent- soaked cotton swabs or applying solvent-soaked electrospun nylon mats with or without friction. Furthermore, applying solvents with commercial eyeglass-cleaning cloths may cause the deposition carboxylates or other unwanted substances present in the cloths onto the treated film surface.

Among all the trials for the remotion TPP residues, excellent results were achieved by rubbing the film surface with solvent-soaked cotton swabs, rubbing with IPOH-soaked electrospun nylon mats, rubbing with DEC-soaked electrospun nylon mats; or cleaning without friction by applying electrospun mats soaked in IPH or DEC for short times (40 seconds). All tests resulting in similar cleaning levels.

Solvent cleaning without the use of friction by employing electrospun nylon mats showed that IPOH and DEC have the best cleaning performance from among the tested solvents; however, further testing may be necessary to asses why good cleaning levels were achieved at short application times whereas long application times (5 minutes) showed inferior to results. Parallel testing using electrospun mats produced with different parameters are desirable.

IPOH and DEC applied with electrospun nylon mats and mechanical action seem particularly promising for the treatment of CA film bases before their scanning, as they could be adapted for automated machine-cleaning procedures for long and continuous cinematographic films showing TPP bloom, thus improving the treatment speed when compared to cotton swab application, and diminishing the exposure of operators towards the volatile solvent.

The present study constitutes the first time the use of green solvents and electrospun fiber mats are employed for the cleaning of cellulose acetate substrates, and may constitute the foundation for implementing plasticizer cleaning methodologies on degraded tridimensional CA objects too.

4.7 Supplementary Material III

Wavenumber (cm^{-1})			**Assignment**
Pure CTA	**Pure MCC**	**Film sample polymeric base**	
3496	**3339**	**3336**	**ν_sOH**[153]
2941	---	2916	νC-H[153] in CH_3[154]
2899	2893	2883	ν_aC-H in CH_2[153], [154], ν_sC-H in CH_3[155]
1741	---	1728	νC=O[68], [154], [156]
1644	1646	1645	ν_aC=O[154] and OH vibrations from crystallization water[153], [155]
1433	1427	1429	In plane δC-H[157] in CTA and CDA, $\delta_s CH_2$ at C–6 in MCC[158]
1367	1369	1371	δC-H in CH_3[89], [154], [156], [159], [160]
---	1335	---	In plane δOH[155]
---	1316	1311 &1296	δCH_2 [155], [158] and δOH[155]
1219	1202	---	ν_a(C-C-O)[89], [156]
1165	1159	1157	ν_a(C-O-C) at β-glucosidic linkage[154], [157]
1122	1101	1111	νCO[158]
1071	1055	1063	νC-O in pyranose ring[89], [155], [156], [158]
1038	**1030**	**1020**	**νCOC**[159], [160]
900	898	898	O.o.p. ring ν at C_1-O-C_4 β glucosidic bond[155], [157], δC-H[154]
839	---	---	---

* ν stretching vibration, ν_s symmetrical stretching vibration, ν_a asymmetrical stretching, δ bending vibration and δ_s scissoring, O.o.p. Out of plane.

Table SMIII.1 Assignments of the main bands in the μATR-FTIR spectra of the pure CTA (Cellulose Tricetate) and pure MCC (Microcrystalline Cellulose) standards, and the polymeric base of the treated film sample.

Wavenumber (cm^{-1})		Assignment
TPP standard	**Crystal bloom on film sample**	
3098	3099	
3060	3060	vC-H[75], [161]
3020	3026 & 3018	vC-H[161]
1588	1588	vC=C in TPP[75], [161]
1484	1485	vC=C in TPP[75], [161]
	1455	
1293	1292	vP=O[75]
	1232	
1174	1174	In-plane δ(C-H) in TPP [75], [161]
1160	1161	In-plane δ(C-H) in TPP[75]
	1070	
	1023	
1008	1008	vP-O[75] and ring vibrations in TPP[161]
964	964	vP-O[75]
946	950	
932	932	
914	912	
784	784	O.o.p. δC-H[75]
768	769	O.o.p. δC-H[75]
753	753	O.o.p. δC-H in TPP[75]
689	690	O.o.p. δC-H in TPP[75]

* v stretching vibration, v_s symmetrical stretching vibration, v_a asymmetrical stretching, δ bending vibration and δ_s scissoring, O.o.p. Out of plane.

Table SMIII.2 Assignments of the main bands in the µATR-FTIR spectra of the pure TPP (Triphenyl Phosphate) standard and the crystal bloom cleaned from the backside of the treated film sample.

Solvent	Sample	Weight before treatment (mg)	Weight after treatment (mg)	Weight change (mg)	Weight change %	Thickness before treatment (µm)	Thickness after treatment (µm)	Thickness change (µm)	Thickness change %	DS before treatment	DS after treatment	DS change	DS change %
IPOH	2	2.453	2.477	+0.023	+0.95%	102.50	119.50	+17.00	+16.59%	0.048	0.241	+0.193	+6.45%
	1	2.297	2.300	+0.003	+0.15%	114.00	109.50	-4.50	-3.95%	0.067	0.381	+0.314	+10.46%
IAA	5	2.000	1.933	-0.067	-3.33%	106.00	100.50	-5.50	-5.19%	0.068	0.019	-0.049	-1.62%
	3	2.677	2.683	+0.007	+0.25%	111.00	109.00	-2.00	-1.80%	0.026	0.032	+0.006	+0.21%
DMC	6	1.870	1.890	+0.020	+1.07%	107.00	106.50	-0.50	-0.47%	0.054	0.034	-0.020	-0.67%
	4	2.513	2.500	-0.013	+- 0.53%	105.50	096.00	-9.50	-9.00%	0.128	0.023	-0.105	-3.50%

DEC	7	1.647	1.683	+0.037	+2.23%	95.00	81.5	-13.50	-14.21%	0.059	0.089	+0.030	+1.00%
	8	1.840	1.873	+0.033	+1.81%	111.00	MISSING DATA	MISSING DATA	MISSING DATA	0.156	0.194	+0.039	+1.28%

Table SMIII.3 Averaged values of weight, thickness and DS measured of the studied CA base before and after being subjected to solubility tests in the four solvents employed for cleaning.

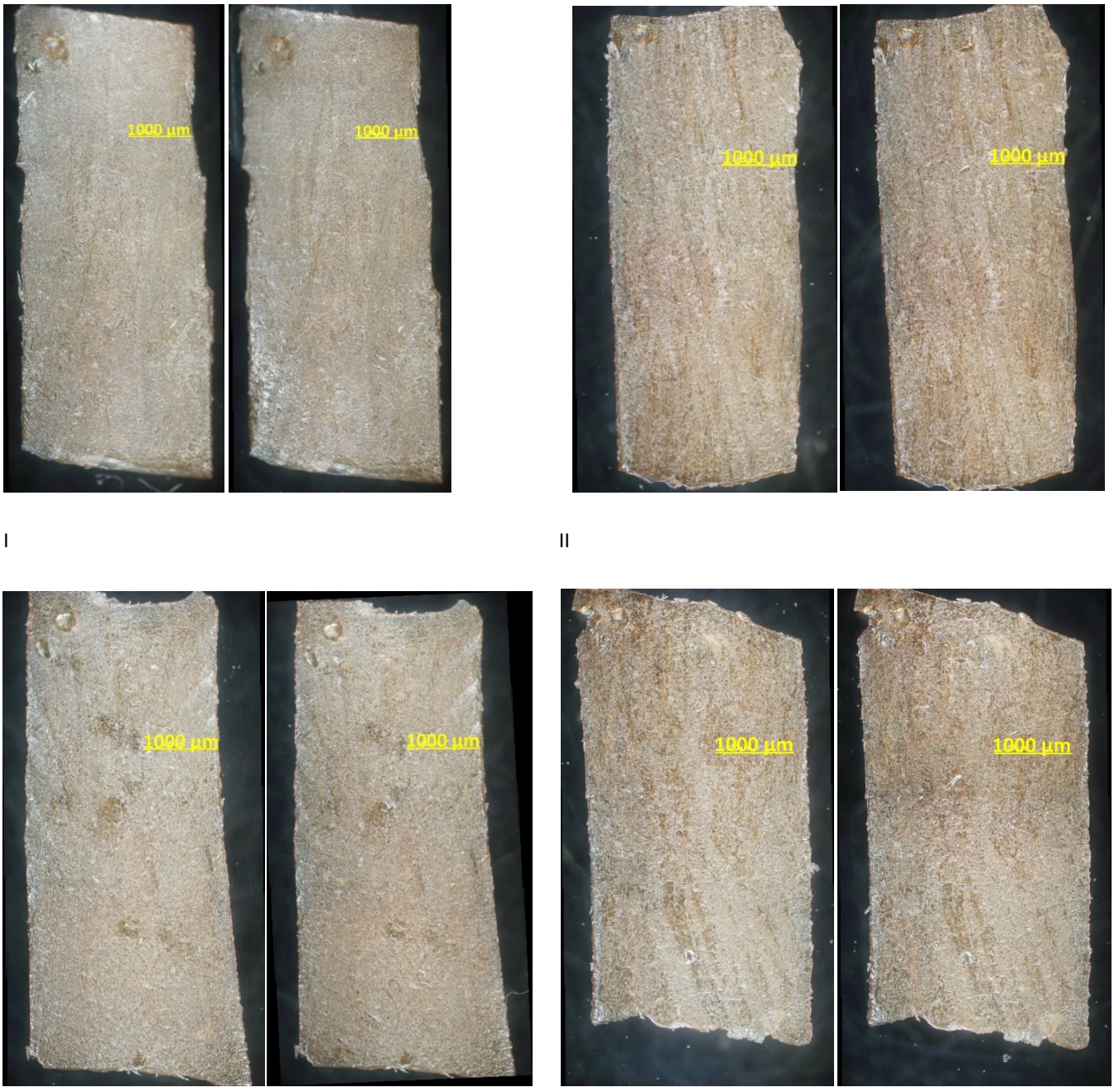

I II

III IV

Fig. SMIII.1 Dark Field surface OM photomicrographs of selected CA base samples before (left) and after (right) being subjected to solubility tests in IPOH (I), IAA (II), DMC (III) and DEC.

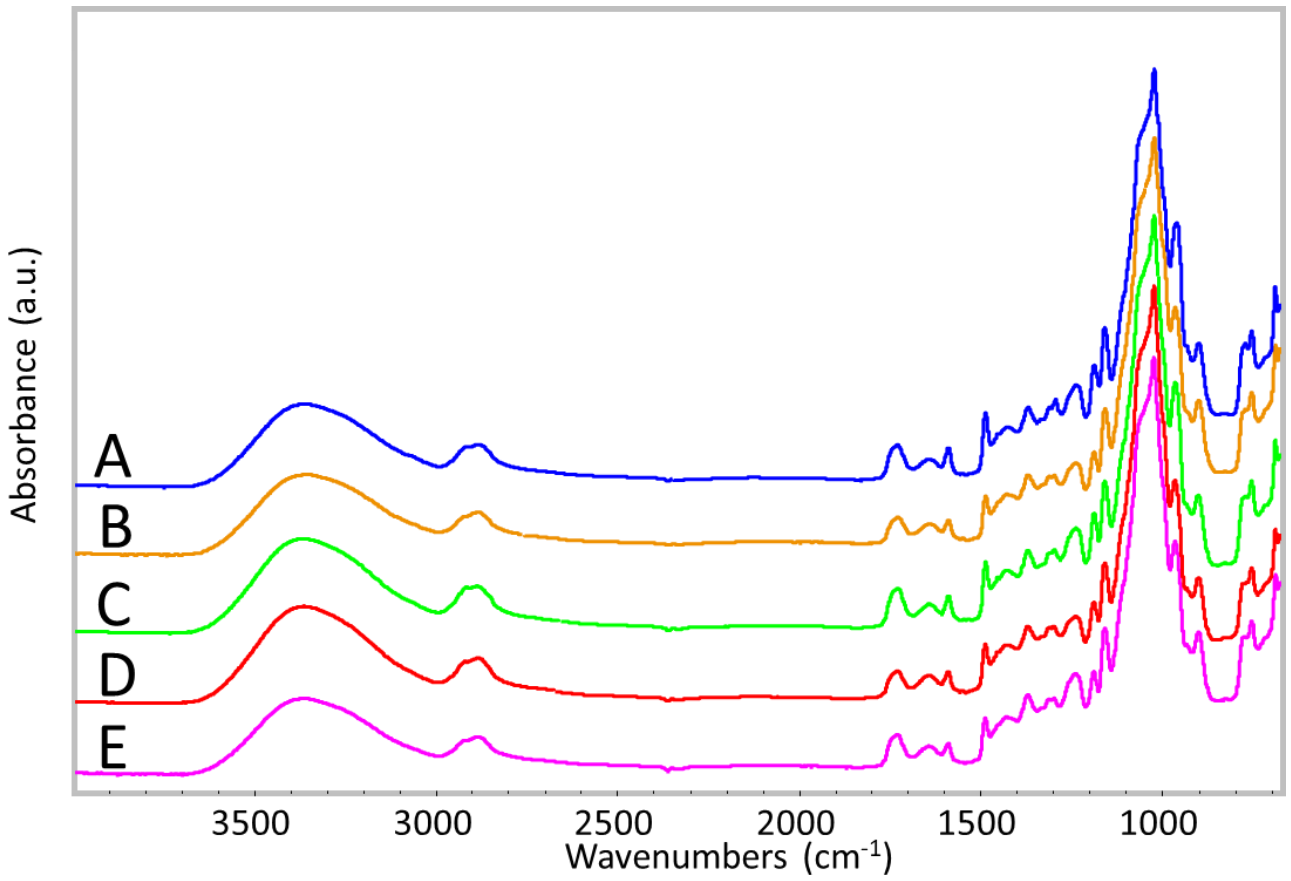

Fig. SMIII.2 Averaged µATR-FTIR spectra of the pretreated and exposed CA base of the studied film sample I. before being subjected to solubility tests (A, blue), after sonication in IPOH(B, yellow), after sonication in IAA (B, green), after sonication in DMC (D, red) and after sonication in DEC (E, magenta).

Part IV: *Acknowledgements and funding*

I want to give my special thanks to my supervisor Silvia Prati, to my co-supervisors Giorgia Sciutto and Rocco Mazzeo, for their guidance and support through this perios, and for having put your confidence in me. Thank you for your constant support in all my academic endeavors.

I heartily thank the Fondazione Cineteca di Bologna as well as the specialists past and preset, from L'Immagine Ritrovata S.R.L., in particular Marianna De Sanctis, Maura Psichedda, Fabiana Appicciafuoco and Lara Nobili, for supporting the research, coordinating activities, for providing the studied samples and commercial eyeglass-cleaning cloths, as well as for granting access to their facilities for all the necessary testing. I thank as well Cristiano Valorosi, Elena Taylor, Andrea Mangano, and the rest of the staff who enriched my vision and understanding on film conservation.

I would like to acknowledge the support of my co-supervisor, professor Chiara Samorì from the UNIBO campus Ravenna, for providing the DES reagents, the green solvents at the initial testing state, and for facilitating the use of the laboratories at the Environmental Sciences Faculty. I thank also to all the academics with whom I have collaborated along the project, for having allowed me to learn and increase my skills, even if the work did got included in the final version of this thesis: Francesco Zerbetto and Jacopo Fadanni from the Giacomo Ciamician Chemistry Department of UNIBO, to introducing me to the study of machine learning on RGB images for digital restoration

purposes, and to Roberto Paolesse from the University of Tor Vergata, Rome, for the SPME-GCMS analysis performed on CA samples and films.

In particular, I thank Professor Maria João Melo and Artur Neves, from the Conservation and Restoration Department of the Faculty of Science and Technology from the NOVA University di Lisbon (Caparica campus), for kindly providing the analytical standards used in this research and for the fruitful discussions we shared regarding Infrared analyses of cellulose esters.

Funding: This work was supported by the Emilia-Romagna Region [European Social Fund Scholarship for PhD Research Projects; 2014/2020 program. Project title: *RICORDACI-Ricerca sulla conservazione, restauro e diagnosi di film cinematografic*i, approved DGR 886/2016].

Part V: Bibliography

[1] K. Silverman, *The Miracle of Analogy, or, The History of Photography, Part 1*. Stanford, California: Stanford University Press, 2015.

[2] A. Kircher, *Athanasii Kircheri Fuldensis Buchonii ... Ars magna lucis et umbrae, in 10. libros digesta*. 1671. Accessed: Jan. 15, 2022. [Online]. Available: http://archive.org/details/viae001105_to085_cor-26051_0000000

[3] A. Gilardi, *Storia sociale della fotografia*. Pearson Italia S.p.a., 2000.

[4] K. Vermeir, "The magic of the magic lantern (1660–1700): on analogical demonstration and the visualization of the invisible," *Br. J. Hist. Sci.*, vol. 38, no. 2, pp. 127–159, Jun. 2005, doi: 10.1017/S0007087405006709.

[5] P. Steadman, *Vermeer's Camera: Uncovering the Truth Behind the Masterpieces*. Oxford University Press, 2002.

[6] F. D. Giammatteo, *Storia del cinema*. Marsilio, 2005.

[7] Eastman Kodak Company, *The essential reference guide for filmmakers*. New York: Eastman Kodak Company, 2007.

[8] M. Daniel, "William Henry Fox Talbot (1800–1877) and the Invention of Photography," *The Met's Heilbrunn Timeline of Art History*. Oct. 2004. Accessed: Jan. 26, 2022. [Online]. Available: https://www.metmuseum.org/toah/hd/tlbt/hd_tlbt.htm

[9] S. Calixto, N. Ganzherli, S. Gulyaev, and S. Figueroa-Gerstenmaier, "Gelatin as a Photosensitive Material," *Molecules*, vol. 23, no. 8, p. 2064, Aug. 2018, doi: 10.3390/molecules23082064.

[10] A. Bereijo, "The conservation and preservation of film and magnetic materials (1): film materials," *Libr. Rev.*, vol. 53, no. 6, pp. 323–331, Aug. 2004, doi: 10.1108/00242530410544411.

[11] Edward Chauncey Worden, *Nitrocellulose Industry*. 1911. Accessed: Apr. 24, 2020. [Online]. Available: http://archive.org/details/in.ernet.dli.2015.163826

[12] H. W. Schütt, “David v. Goliath: the patent infringement case of Goodwin v. Eastman,” *Hist. Photogr.*, vol. 7, no. 1, pp. 1–5, Jan. 1983, doi: 10.1080/03087298.1983.10442740.

[13] I. Baker, “Celluloid,” in *Fifty Materials That Make the World*, Cham: Springer International Publishing, 2018, pp. 23–27. doi: 10.1007/978-3-319-78766-4_6.

[14] J. A. Reilly, “Celluloid Objects: Their Chemistry and Preservation,” *J. Am. Inst. Conserv.*, vol. 30, no. 2, pp. 145–162, 1991, doi: 10.2307/3179527.

[15] E. Ciliberto, P. Gemmellaro, V. Iannuso, S. La Delfa, R. G. Urso, and E. Viscuso, “Characterization and Weathering of Motion-picture Films with Support of Cellulose Nitrate, Cellulose Acetate and Polyester,” *Procedia Chem.*, vol. 8, pp. 175–184, 2013, doi: 10.1016/j.proche.2013.03.023.

[16] A. Hamrang, “Degradation and stabilisation of cellulose based plastics & artifacts.,” Ph.D., Manchester Metropolitan University, 1994. Accessed: Jun. 08, 2020. [Online]. Available: https://ethos.bl.uk/OrderDetails.do?did=1&uin=uk.bl.ethos.240556

[17] P. Zugenmaier, “4. Characteristics of cellulose acetates— 4.1 Characterization and physical properties of cellulose acetates,” *Macromol. Symp.*, vol. 208, no. 1, pp. 81–166, Mar. 2004, doi: 10.1002/masy.200450407.

[18] National Film Preservation Foundation, Ed., *The film preservation guide: the basics for archives, libraries, and museums*. San Francisco, Calif: National Film Preservation Foundation, 2004.

[19] B. Lavédrine, J.-P. Gandolfo, M. Frizot, and S. Monod, *Photographs of the Past: Process and Preservation*. Getty Publications, 2009.

[20] P. Read and M.-P. Meyer, *Restoration of motion picture film*. Oxford: Butterworth-Heinemann, 2000.

[21] E. A. Carter, B. Swarbrick, T. M. Harrison, and L. Ronai, “Rapid identification of cellulose nitrate and cellulose acetate film in historic photograph collections,” *Herit. Sci.*, vol. 8, no. 1, p. 51, May 2020, doi: 10.1186/s40494-020-00395-y.

[22] C. E. K. Mees, T. H. James, A. Kocher, and C. R. Berry, *The theory of the photographic process*, 3rd ed. New York: Macmillan, 1966. Accessed: Jan. 09, 2019. [Online]. Available: https://trove.nla.gov.au/version/12386604

[23] S. Nunes *et al.*, “A diagnostic tool for assessing the conservation condition of cellulose nitrate and acetate in heritage collections: quantifying the degree of substitution by infrared spectroscopy,” *Herit. Sci.*, vol. 8, no. 1, p. 33, Dec. 2020, doi: 10.1186/s40494-020-00373-4.

[24] F. A. Johnston-Banks, “Gelatine,” in *Food Gels*, P. Harris, Ed. Dordrecht: Springer Netherlands, 1990, pp. 233–289. doi: 10.1007/978-94-009-0755-3_7.

[25] J. Bella, “Collagen structure: new tricks from a very old dog,” *Biochem. J.*, vol. 473, no. 8, pp. 1001–1025, Apr. 2016, doi: 10.1042/BJ20151169.

[26] I. A. Balakhnina, N. N. Brandt, A. A. Mankova, and A. Yu. Chikishev, “The problem of manifestation of tertiary structure in the vibrational spectra of proteins,” *Vib. Spectrosc.*, vol. 114, p. 103250, May 2021, doi: 10.1016/j.vibspec.2021.103250.

[27] S. R. Derkach, Y. A. Kuchina, A. V. Baryshnikov, D. S. Kolotova, and N. G. Voron'ko, "Tailoring Cod Gelatin Structure and Physical Properties with Acid and Alkaline Extraction," p. 17, 2019.

[28] R. Schrieber and H. Gareis, *Gelatine Handbook: Theory and Industrial Practice*, 1st ed. Wiley, 2007. doi: 10.1002/9783527610969.

[29] T.-P. Nguyen, B. Lavédrine, and F. Flieder, "Effects of N02 and S02 on the Degradation of Photographic Gelatin," *Imaging Sci. J.*, vol. 45, no. 3–4, pp. 239–243, Jan. 1997, doi: 10.1080/13682199.1997.11736417.

[30] G. M. Haist, *Modern Photographic Processing*. Wiley, 1979.

[31] W. F. Harrington and P. H. [Von Hippel, "The Structure Of Collagen And Gelatin," vol. 16, C. B. Anfinsen, M. L. Anson, K. Bailey, and J. T. Edsall, Eds. Academic Press, 1962, pp. 1–138. doi: 10.1016/S0065-3233(08)60028-5.

[32] J. E. Eastoe, "The amino acid composition of mammalian collagen and gelatin," *Biochem. J.*, vol. 61, no. 4, pp. 589–600, Dec. 1955.

[33] C. Tengroth, U. Gasslander, F. Andersson, and S. Jacobsson, "Cross-Linking of Gelatin Capsules with Formaldehyde and Other Aldehydes: An FTIR Spectroscopy Study," *Pharm. Dev. Technol.*, vol. 10, no. 3, pp. 405–412, Aug. 2005, doi: 10.1081/PDT-200065693.

[34] K. Tomšová, M. Ďurovič, and K. Drábková, "The effect of disinfection methods on the stability of photographic gelatin," *Polym. Degrad. Stab.*, vol. 129, pp. 1–6, Jul. 2016, doi: 10.1016/j.polymdegradstab.2016.03.034.

[35] Society of Photographic Scientists and Engineers, *SPSE Handbook of Photographic Science and Engineering*. Wiley, 1973.

[36] B. Flueckiger, "Timeline of Historical Film Colors." 2012. [Online]. Available: https://filmcolors.org/

[37] P. Bergthaller, "Couplers in colour photography—chemistry and function Part 1," *Imaging Sci. J.*, vol. 50, no. 3, pp. 153–186, Jan. 2002, doi: 10.1080/13682199.2002.11784403.

[38] P. Bergthaller, "Couplers in colour photography—chemistry and function Part 2," *Imaging Sci. J.*, vol. 50, no. 3, pp. 187–230, Jan. 2002, doi: 10.1080/13682199.2002.11784404.

[39] P. Bergthaller, "Couplers in colour photography—chemistry and function Part 3," *Imaging Sci. J.*, vol. 50, no. 4, pp. 233–276, Jan. 2002, doi: 10.1080/13682199.2002.11784405.

[40] D. Trache *et al.*, "Microcrystalline cellulose: Isolation, characterization and bio-composites application—A review," *Int. J. Biol. Macromol.*, vol. 93, pp. 789–804, Dec. 2016, doi: 10.1016/j.ijbiomac.2016.09.056.

[41] C. Y. Bao, D. R. Long, and C. Vergelati, "Miscibility and dynamical properties of cellulose acetate/plasticizer systems," *Carbohydr. Polym.*, vol. 116, pp. 95–102, Feb. 2015, doi: 10.1016/j.carbpol.2014.07.078.

[42] Y. Guo and P. Wu, "Investigation of the hydrogen-bond structure of cellulose diacetate by two-dimensional infrared correlation spectroscopy," *Carbohydr. Polym.*, vol. 74, no. 3, pp. 509–513,

Nov. 2008, doi: 10.1016/j.carbpol.2008.04.005.

[43] D. Klemm, B. Heublein, H.-P. Fink, and A. Bohn, “Cellulose: Fascinating Biopolymer and Sustainable Raw Material,” *Angew. Chem. Int. Ed.*, vol. 44, no. 22, pp. 3358–3393, May 2005, doi: 10.1002/anie.200460587.

[44] B. Lu, A. Xu, and J. Wang, “Cation does matter: how cationic structure affects the dissolution of cellulose in ionic liquids,” *Green Chem*, vol. 16, no. 3, pp. 1326–1335, 2014, doi: 10.1039/C3GC41733F.

[45] D. Jones and C. Brischke, Eds., “2 - Wood as bio-based building material,” in *Performance of Bio-based Building Materials*, Woodhead Publishing, 2017, pp. 21–96. doi: 10.1016/B978-0-08-100982-6.00002-1.

[46] S. Rongpipi, D. Ye, E. D. Gomez, and E. W. Gomez, “Progress and Opportunities in the Characterization of Cellulose – An Important Regulator of Cell Wall Growth and Mechanics,” *Front. Plant Sci.*, vol. 9, p. 1894, Mar. 2019, doi: 10.3389/fpls.2018.01894.

[47] M. Ioelovich, “Concept of the Native Cellulose Structural Organization,” *SITA*, vol. 1, pp. 68–77, Oct. 1999.

[48] J. Credou and T. Berthelot, “Cellulose: from biocompatible to bioactive material,” *J Mater Chem B*, vol. 2, no. 30, pp. 4767–4788, 2014, doi: 10.1039/C4TB00431K.

[49] R. H. Atalla and D. L. VanderHart, “Native Cellulose: A Composite of Two Distinct Crystalline Forms,” *Science*, Jan. 1984, doi: 10.1126/science.223.4633.283.

[50] Y. Shashoua, S. M. Bradley, and V. D. Daniels, “Degradation of Cellulose Nitrate Adhesive,” *Stud. Conserv.*, vol. 37, no. 2, pp. 113–119, 1992, doi: 10.2307/1506403.

[51] C. Selwitz, *Cellulose nitrate in conservation*. Marina del Rey, Calif: Getty Conservation Institute, 1988.

[52] C. W. Saunders and L. T. Taylor, “A review of the synthesis, chemistry and analysis of nitrocellulose,” *J. Energ. Mater.*, vol. 8, no. 3, pp. 149–203, Sep. 1990, doi: 10.1080/07370659008012572.

[53] Y. Shashoua, *Conservation of plastics: materials science, degradation and preservation*, 1. ed. Oxford: Elsevier, 2008.

[54] P. Fei, L. Liao, B. Cheng, and J. Song, “Quantitative analysis of cellulose acetate with a high degree of substitution by FTIR and its application,” *Anal. Methods*, vol. 9, no. 43, pp. 6194–6201, Nov. 2017, doi: 10.1039/C7AY02165H.

[55] D. Littlejohn, R. A. Pethrick, A. Quye, and J. M. Ballany, “Investigation of the degradation of cellulose acetate museum artefacts,” *Polym. Degrad. Stab.*, vol. 98, no. 1, pp. 416–424, Jan. 2013, doi: 10.1016/j.polymdegradstab.2012.08.023.

[56] X. Fan, Z.-W. Liu, J. Lu, and Z.-T. Liu, “Cellulose Triacetate Optical Film Preparation from Ramie Fiber,” *Ind. Eng. Chem. Res.*, vol. 48, no. 13, pp. 6212–6215, Jul. 2009, doi: 10.1021/ie801703x.

[57] L. Liu, D. Gong, L. Bratasz, Z. Zhu, and C. Wang, “Degradation markers and plasticizer loss of

cellulose acetate films during ageing," *Polym. Degrad. Stab.*, vol. 168, p. 108952, Oct. 2019, doi: 10.1016/j.polymdegradstab.2019.108952.

[58] S. Fischer, K. Thümmler, B. Volkert, K. Hettrich, I. Schmidt, and K. Fischer, "Properties and Applications of Cellulose Acetate," *Macromol. Symp.*, vol. 262, no. 1, pp. 89–96, Jan. 2008, doi: 10.1002/masy.200850210.

[59] A. Benazzouz, E. Dudognon, N. T. Correia, V. Molinier, J.-M. Aubry, and M. Descamps, "Interactions underpinning the plasticization of a polymer matrix: a dynamic and structural analysis of DMP-plasticized cellulose acetate," *Cellulose*, vol. 24, no. 2, pp. 487–503, Feb. 2017, doi: 10.1007/s10570-016-1148-y.

[60] Y. Wu, Y. Si, D. Zhou, and J. Gao, "Adsorption of diethyl phthalate ester to clay minerals," *Chemosphere*, vol. 119, pp. 690–696, Jan. 2015, doi: 10.1016/j.chemosphere.2014.07.063.

[61] C. R. Fordyce and I. W. A. Meyer, "Plasticizers for Cellulose Acetate and Cellulose Acetate Butyrate," *Ind. Eng. Chem.*, p. 8, 1940.

[62] S. Lambert and M. Wagner, "Environmental performance of bio-based and biodegradable plastics: the road ahead," *Chem. Soc. Rev.*, vol. 46, no. 22, pp. 6855–6871, Nov. 2017, doi: 10.1039/C7CS00149E.

[63] B. Kemper and D. A. Lichtblau, "Extraction of plasticizers: An entire and reproducible quantification method for historical cellulose acetate material," *Polym. Test.*, vol. 80, p. 106096, Dec. 2019, doi: 10.1016/j.polymertesting.2019.106096.

[64] K. Takahashi, M. Sasaki, H. Hayakawa, H. Yajima, and Y. Oda, "Composition of the white precipitate formed on the surface of damaged triacetyl cellulose-based motion picture films," *Sci. Rep.*, vol. 11, no. 1, p. 1502, Dec. 2021, doi: 10.1038/s41598-020-80498-5.

[65] S. Mousviasl, "Analytical methods for characterization of materials in motion picture films and their degradation," MSc in Science for the Conservation-Restoration of Cultural Heritage, University of Bologna, Italy, 2016.

[66] K. Curran, M. Underhill, L. T. Gibson, and M. Strlic, "The development of a SPME-GC/MS method for the analysis of VOC emissions from historic plastic and rubber materials," *Microchem. J.*, vol. 124, pp. 909–918, Jan. 2016, doi: 10.1016/j.microc.2015.08.027.

[67] G. Mitchell, C. Higgitt, and L. T. Gibson, "Emissions from polymeric materials: Characterised by thermal desorption-gas chromatography," *Polym. Degrad. Stab.*, vol. 107, pp. 328–340, Sep. 2014, doi: 10.1016/j.polymdegradstab.2013.12.003.

[68] M. Schilling, M. Bouchard, H. Khanjian, T. Learner, A. Phenix, and R. Rivenc, "Application of Chemical and Thermal Analysis Methods for Studying Cellulose Ester Plastics," *Acc. Chem. Res.*, vol. 43, no. 6, pp. 888–896, Jun. 2010, doi: 10.1021/ar1000132.

[69] N. Bensalah, S. Dbira, and A. Bedoui, "Mechanistic and kinetic studies of the degradation of diethyl phthalate (DEP) by homogeneous and heterogeneous Fenton oxidation," *Environ. Nanotechnol. Monit. Manag.*, vol. 11, p. 100224, May 2019, doi: 10.1016/j.enmm.2019.100224.

[70] Y. Tao *et al.*, "Metabolism of diethyl phthalate (DEP) and identification of degradation

intermediates by Pseudomonas sp. DNE-S1," *Ecotoxicol. Environ. Saf.*, vol. 173, pp. 411–418, May 2019, doi: 10.1016/j.ecoenv.2019.02.055.

[71] X. Zhang, M. Feng, R. Qu, H. Liu, L. Wang, and Z. Wang, "Catalytic degradation of diethyl phthalate in aqueous solution by persulfate activated with nano-scaled magnetic CuFe 2 O 4 /MWCNTs," *Chem. Eng. J.*, vol. 301, pp. 1–11, Oct. 2016, doi: 10.1016/j.cej.2016.04.096.

[72] PubChem, "Triphenyl phosphate." https://pubchem.ncbi.nlm.nih.gov/compound/8289 (accessed Jan. 13, 2022).

[73] E. Richardson, M. Truffa Giachet, M. Schilling, and T. Learner, "Assessing the physical stability of archival cellulose acetate films by monitoring plasticizer loss," *Polym. Degrad. Stab.*, vol. 107, pp. 231–236, Sep. 2014, doi: 10.1016/j.polymdegradstab.2013.12.001.

[74] A. L. Mohamed and A. G. Hassabo, "Flame Retardant of Cellulosic Materials and Their Composites," in *Flame Retardants*, P. M. Visakh and Y. Arao, Eds. Cham: Springer International Publishing, 2015, pp. 247–314. doi: 10.1007/978-3-319-03467-6_10.

[75] M. Kumar Trivedi, "Physicochemical and Spectroscopic Characterization of Biofield Treated Triphenyl Phosphate," *Am. J. Appl. Chem.*, vol. 3, no. 5, p. 168, 2015, doi: 10.11648/j.ajac.20150305.13.

[76] M. K. McGath, "Investigation of Deterioration Mechanisms of Cellulose Acetate Compounded with Triphenyl Phosphate," PhD, The University of Arizona, 2012.

[77] World Health Organization and I. P. on C. Safety, "Triphenyl phosphate," World Health Organization, 1991. Accessed: Jan. 14, 2022. [Online]. Available: https://apps.who.int/iris/handle/10665/40299

[78] A. L. Geddes, "The Interaction of Organo-phosphorus Compounds with Solvents and Cellulose Acetate," *J. Phys. Chem.*, vol. 58, no. 12, pp. 1062–1066, Dec. 1954, doi: 10.1021/j150522a003.

[79] F. Shahidi, P. K. Janitha, and P. D. Wanasundara, "Phenolic antioxidants," *Crit. Rev. Food Sci. Nutr.*, vol. 32, no. 1, pp. 67–103, Jan. 1992, doi: 10.1080/10408399209527581.

[80] "FilmCare.org." https://www.filmcare.org/vd_binder.php (accessed Apr. 30, 2021).

[81] E. Catelli *et al.*, "A new miniaturised short-wave infrared (SWIR) spectrometer for on-site cultural heritage investigations," *Talanta*, vol. 218, p. 121112, Oct. 2020, doi: 10.1016/j.talanta.2020.121112.

[82] M. da C. C. Lucena, A. E. V. de Alencar, S. E. Mazzeto, and S. de A. Soares, "The effect of additives on the thermal degradation of cellulose acetate," *Polym. Degrad. Stab.*, vol. 80, no. 1, pp. 149–155, Jan. 2003, doi: 10.1016/S0141-3910(02)00396-8.

[83] A. T. Ram and J. L. McCrea, "Stability of Processed Cellulose Ester Photographic Films," *SMPTE J.*, vol. 97, no. 6, pp. 474–483, Jun. 1988, doi: 10.5594/J02945.

[84] A. T. Ram, "Archival preservation of photographic films—A perspective," *Polym. Degrad. Stab.*, vol. 29, no. 1, pp. 3–29, Jan. 1990, doi: 10.1016/0141-3910(90)90019-4.

[85] M. Edge, N. S. Allen, T. S. Jewitt, and C. V. Horie, "The inhibition of oxidative and hydrolytic

degradation pathways in archival cellulose-triacetate base cinematograph films," *Polym. Degrad. Stab.*, vol. 29, no. 1, pp. 31–48, Jan. 1990, doi: 10.1016/0141-3910(90)90020-8.

[86] B. Knight, "Lack of evidence for an autocatalytic point in the degradation of cellulose acetate," *Polym. Degrad. Stab.*, vol. 107, pp. 219–222, Sep. 2014, doi: 10.1016/j.polymdegradstab.2013.12.002.

[87] I. R. Ahmad, D. Cane, J. H. Townsend, C. Triana, L. Mazzei, and K. Curran, "Are we overestimating the permanence of cellulose triacetate cinematographic films? A mathematical model for the vinegar syndrome," *Polym. Degrad. Stab.*, vol. 172, p. 109050, Feb. 2020, doi: 10.1016/j.polymdegradstab.2019.109050.

[88] K. Curran, A. Možir, M. Underhill, L. T. Gibson, T. Fearn, and M. Strlič, "Cross-infection effect of polymers of historic and heritage significance on the degradation of a cellulose reference test material," *Polym. Degrad. Stab.*, vol. 107, pp. 294–306, Sep. 2014, doi: 10.1016/j.polymdegradstab.2013.12.019.

[89] A. Quye, D. Littlejohn, R. A. Pethrick, and R. A. Stewart, "Investigation of inherent degradation in cellulose nitrate museum artefacts," *Polym. Degrad. Stab.*, vol. 96, no. 7, pp. 1369–1376, Jul. 2011, doi: 10.1016/j.polymdegradstab.2011.03.009.

[90] J. Tsang *et al.*, "Degradation of 'Lumarith' Cellulose Acetate," *Stud. Conserv.*, vol. 54, no. 2, pp. 90–105, Jan. 2009, doi: 10.1179/sic.2009.54.2.90.

[91] J. Puls, S. A. Wilson, and D. Hölter, "Degradation of Cellulose Acetate-Based Materials: A Review," *J. Polym. Environ.*, vol. 19, no. 1, pp. 152–165, Mar. 2011, doi: 10.1007/s10924-010-0258-0.

[92] K. Hosono, A. Kanazawa, H. Mori, and T. Endo, "Photodegradation of cellulose acetate film in the presence of benzophenone as a photosensitizer," *J. Appl. Polym. Sci.*, vol. 105, no. 6, pp. 3235–3239, Sep. 2007, doi: 10.1002/app.26386.

[93] K. Curran, M. Underhill, J. Grau-Bové, T. Fearn, L. T. Gibson, and M. Strlič, "Classifying Degraded Modern Polymeric Museum Artefacts by Their Smell," *Angew. Chem. Int. Ed.*, vol. 57, no. 25, pp. 7336–7340, Jun. 2018, doi: 10.1002/anie.201712278.

[94] N. S. Allen, M. Edge, J. H. Appleyard, T. S. Jewitt, C. V. Horie, and D. Francis, "Acid-catalysed degradation of historic cellulose triacetate, cinematographic film: Influence of various film parameters," *Eur. Polym. J.*, vol. 24, no. 8, pp. 707–712, Jan. 1988, doi: 10.1016/0014-3057(88)90002-X.

[95] L. Castle, A. J. Mercer, J. R. Startin, and J. Gilbert, "Migration from plasticized films into foods 3. Migration of phthalate, sebacate, citrate and phosphate esters from films used for retail food packaging," *Food Addit. Contam.*, vol. 5, no. 1, pp. 9–20, Jan. 1988, doi: 10.1080/02652038809373657.

[96] A. Neves, E. M. Angelin, É. Roldão, and M. J. Melo, "New insights into the degradation mechanism of cellulose nitrate in cinematographic films by Raman microscopy," *J. Raman Spectrosc.*, vol. 0, no. 0, p. 11, 2018, doi: 10.1002/jrs.5464.

[97] M. Truffa Giachet *et al.*, “Assessment of the composition and condition of animation cels made from cellulose acetate,” *Polym. Degrad. Stab.*, vol. 107, pp. 223–230, Sep. 2014, doi: 10.1016/j.polymdegradstab.2014.03.009.

[98] I. Bonaduce, E. Ribechini, F. Modugno, and M. P. Colombini, “Analytical Approaches Based on Gas Chromatography Mass Spectrometry (GC/MS) to Study Organic Materials in Artworks and Archaeological Objects,” *Top. Curr. Chem.*, vol. 374, no. 1, Feb. 2016, doi: 10.1007/s41061-015-0007-x.

[99] F. C. Izzo *et al.*, “Elucidating the composition and the state of conservation of nitrocellulose-based animation cells by means of non-invasive and micro-destructive techniques,” *J. Cult. Herit.*, Oct. 2018, doi: 10.1016/j.culher.2018.09.010.

[100] V. Knotek, P. Korandová, R. Kalousková, and M. Ďurovič, “Study of triacetate cinematographic films and magnetic audio track by infrared spectroscopy,” *Koroze Ochr. Mater.*, vol. 62, no. 1, pp. 26–32, Feb. 2018, doi: 10.2478/kom-2018-0005.

[101] M. Bacci, R. Chiari, S. Porcinai, and B. Radicati, “Principal component analysis of near-infrared spectra of alteration products in calcareous samples: An application to works of art,” *Chemom. Intell. Lab. Syst.*, vol. 39, no. 1, pp. 115–121, Nov. 1997, doi: 10.1016/S0169-7439(97)00063-4.

[102] M. Bacci, M. Picollo, G. Trumpy, M. Tsukada, and D. Kunzelman, “Non-Invasive Identification of White Pigments on 20Th-Century Oil Paintings by Using Fiber Optic Reflectance Spectroscopy,” *J. Am. Inst. Conserv.*, vol. 46, no. 1, pp. 27–37, Jan. 2007, doi: 10.1179/019713607806112413.

[103] J. K. Delaney *et al.*, “Use of imaging spectroscopy, fiber optic reflectance spectroscopy, and X-ray fluorescence to map and identify pigments in illuminated manuscripts,” *Stud. Conserv.*, vol. 59, no. 2, pp. 91–101, Mar. 2014, doi: 10.1179/2047058412Y.0000000078.

[104] M. Aceto *et al.*, “Characterisation of colourants on illuminated manuscripts by portable fibre optic UV-visible-NIR reflectance spectrophotometry,” *Anal. Methods*, vol. 6, no. 5, p. 1488, 2014, doi: 10.1039/c3ay41904e.

[105] S. Baronti, A. Casini, F. Lotti, and S. Porcinai, “Multispectral imaging system for the mapping of pigments in works of art by use of principal-component analysis,” *Appl. Opt.*, vol. 37, no. 8, p. 1299, Mar. 1998, doi: 10.1364/AO.37.001299.

[106] K. A. Dooley *et al.*, “Mapping of egg yolk and animal skin glue paint binders in Early Renaissance paintings using near infrared reflectance imaging spectroscopy,” *The Analyst*, vol. 138, no. 17, p. 4838, 2013, doi: 10.1039/c3an00926b.

[107] P. Ricciardi *et al.*, “Near Infrared Reflectance Imaging Spectroscopy to Map Paint Binders In Situ on Illuminated Manuscripts,” *Angew. Chem. Int. Ed.*, vol. 51, no. 23, pp. 5607–5610, Jun. 2012, doi: 10.1002/anie.201200840.

[108] Á. Ríos, M. Zougagh, and M. Avila, “Miniaturization through lab-on-a-chip: Utopia or reality for routine laboratories? A review,” *Anal. Chim. Acta*, vol. 740, pp. 1–11, Aug. 2012, doi: 10.1016/j.aca.2012.06.024.

[109] V. Gubala, L. F. Harris, A. J. Ricco, M. X. Tan, and D. E. Williams, “Point of Care Diagnostics: Status and Future,” *Anal. Chem.*, vol. 84, no. 2, pp. 487–515, Jan. 2012, doi: 10.1021/ac2030199.

[110] N. A. O’Brien *et al.*, “Miniature near-infrared (NIR) spectrometer engine for handheld applications,” Baltimore, Maryland, USA, May 2012, p. 837404. doi: 10.1117/12.917983.

[111] C. A. Teixeira dos Santos, M. Lopo, R. N. M. J. Páscoa, and J. A. Lopes, “A Review on the Applications of Portable Near-Infrared Spectrometers in the Agro-Food Industry,” *Appl. Spectrosc.*, vol. 67, no. 11, pp. 1215–1233, Nov. 2013, doi: 10.1366/13-07228.

[112] D. M. Friedrich, C. A. Hulse, M. von Gunten, E. P. Williamson, C. G. Pederson, and N. A. O’Brien, “Miniature near-infrared spectrometer for point-of-use chemical analysis,” San Francisco, California, United States, Mar. 2014, p. 899203. doi: 10.1117/12.2040669.

[113] A. Guillemain, K. Dégardin, and Y. Roggo, “Performance of NIR handheld spectrometers for the detection of counterfeit tablets,” *Talanta*, vol. 165, pp. 632–640, Apr. 2017, doi: 10.1016/j.talanta.2016.12.063.

[114] M. Alcalà *et al.*, “Qualitative and Quantitative Pharmaceutical Analysis with a Novel Hand-Held Miniature near Infrared Spectrometer,” *J. Infrared Spectrosc.*, vol. 21, no. 6, pp. 445–457, Dec. 2013, doi: 10.1255/jnirs.1084.

[115] K. Tsujikawa *et al.*, “Application of a portable near infrared spectrometer for presumptive identification of psychoactive drugs,” *Forensic Sci. Int.*, vol. 242, pp. 162–171, Sep. 2014, doi: 10.1016/j.forsciint.2014.05.020.

[116] C. Malegori, E. J. Nascimento Marques, S. T. de Freitas, M. F. Pimentel, C. Pasquini, and E. Casiraghi, “Comparing the analytical performances of Micro-NIR and FT-NIR spectrometers in the evaluation of acerola fruit quality, using PLS and SVM regression algorithms,” *Talanta*, vol. 165, pp. 112–116, Apr. 2017, doi: 10.1016/j.talanta.2016.12.035.

[117] R. Risoluti, G. Gullifa, A. Battistini, and S. Materazzi, “‘Lab-on-Click’ Detection of Illicit Drugs in Oral Fluids by MicroNIR–Chemometrics,” *Anal. Chem.*, vol. 91, no. 10, pp. 6435–6439, May 2019, doi: 10.1021/acs.analchem.9b00197.

[118] R. Risoluti, S. Materazzi, F. Tau, A. Russo, and F. S. Romolo, “Towards innovation in paper dating: a MicroNIR analytical platform and chemometrics,” *The Analyst*, vol. 143, no. 18, pp. 4394–4399, 2018, doi: 10.1039/C8AN00871J.

[119] D. A. Burns and E. W. Ciurczak, *Handbook of Near-Infrared Analysis*. CRC Press, 2007.

[120] C. E. Miller, “Near-Infrared Spectroscopy of Synthetic and Industrial Samples,” in *Handbook of Vibrational Spectroscopy*, J. M. Chalmers and P. R. Griffiths, Eds. Chichester, UK: John Wiley & Sons, Ltd, 2006. Accessed: Feb. 28, 2019. [Online]. Available: http://doi.wiley.com/10.1002/0470027320.s0106

[121] A. M. Senna, K. M. Novack, and V. R. Botaro, “Synthesis and characterization of hydrogels from cellulose acetate by esterification crosslinking with EDTA dianhydride,” *Carbohydr. Polym.*, vol. 114, pp. 260–268, Dec. 2014, doi: 10.1016/j.carbpol.2014.08.017.

[122] J. Zhang, K. Tian, C. Lei, and S. Min, “Identification and quantification of microplastics in table

sea salts using micro-NIR imaging methods," *Anal. Methods*, vol. 10, no. 24, pp. 2881–2887, 2018, doi: 10.1039/C8AY00125A.

[123] C. E. Miller and B. E. Eichinger, "Determination of Crystallinity and Morphology of Fibrous and Bulk Poly(ethylene terephthalate) by Near-Infrared Diffuse Reflectance Spectroscopy," *Appl. Spectrosc.*, vol. 44, no. 3, pp. 496–504, Mar. 1990, doi: 10.1366/0003702904086173.

[124] F. W. Langkilde and A. Svantesson, "Identification of celluloses with Fourier-Transform (FT) mid-infrared, FT-Raman and near-infrared spectrometry," *J. Pharm. Biomed. Anal.*, vol. 13, no. 4–5, pp. 409–414, Apr. 1995, doi: 10.1016/0731-7085(95)01298-Y.

[125] A. Wójciak, H. Kasprzyk, E. Sikorska, A. Krawczyk, M. Sikorski, and A. Wesełucha-Birczyńska, "FT-Raman, FT-infrared and NIR spectroscopic characterization of oxygen-delignified kraft pulp treated with hydrogen peroxide under acidic and alkaline conditions," *Vib. Spectrosc.*, vol. 71, pp. 62–69, Mar. 2014, doi: 10.1016/j.vibspec.2014.01.007.

[126] X. Li, C. Sun, B. Zhou, and Y. He, "Determination of Hemicellulose, Cellulose and Lignin in Moso Bamboo by Near Infrared Spectroscopy," *Sci. Rep.*, vol. 5, no. 1, p. 17210, Dec. 2015, doi: 10.1038/srep17210.

[127] E. W. Crandall and A. N. Jagtap, "The near-infrared spectra of polymers," *J. Appl. Polym. Sci.*, vol. 21, no. 2, pp. 449–454, Feb. 1977, doi: 10.1002/app.1977.070210211.

[128] C. Kradjel and K. A. Lee, "NIR Analysis of Polymers (27)," in *Handbook of Near-Infrared Analysis*, D. A. Burns and E. W. Ciurczak, Eds. CRC Press, 2007.

[129] A. Dantas de Oliveira, V. H. da Silva, M. F. Pimentel, G. M. Vinhas, C. Pasquini, and Y. M. B. de Almeida, "Use of Infrared Spectroscopy and Near Infrared Hyperspectral Images to Evaluate Effects of Different Chemical Agents on PET Bottle Surface," *Mater. Res.*, vol. 21, no. 5, Aug. 2018, doi: 10.1590/1980-5373-mr-2017-0949.

[130] F. Zapata, M. Ferreiro-González, and C. García-Ruiz, "Interpreting the near infrared region of explosives," *Spectrochim. Acta. A. Mol. Biomol. Spectrosc.*, vol. 204, pp. 81–87, Nov. 2018, doi: 10.1016/j.saa.2018.06.002.

[131] J. Yan, N. Villarreal, and B. Xu, "Characterization of Degradation of Cotton Cellulosic Fibers Through Near Infrared Spectroscopy," *J. Polym. Environ.*, vol. 21, no. 4, pp. 902–909, Dec. 2013, doi: 10.1007/s10924-013-0605-z.

[132] A. Alassali, S. Fiore, and K. Kuchta, "Assessment of plastic waste materials degradation through near infrared spectroscopy," *Waste Manag.*, vol. 82, pp. 71–81, Dec. 2018, doi: 10.1016/j.wasman.2018.10.010.

[133] C. R. Fordyce, "Improved Safety Motion Picture Film Support," *J. Soc. Motion Pict. Eng.*, vol. 51, no. 4, pp. 331–350, Oct. 1948, doi: 10.5594/J11731.

[134] L. Enticknap, *Film Restoration: the Culture and Science of Audiovisual Heritage.* Palgrave Macmillan, 2013. Accessed: Nov. 29, 2018. [Online]. Available: http://public.eblib.com/choice/publicfullrecord.aspx?p=1571902

[135] "FilmCare.org." https://www.filmcare.org/vd_embrittlement.php (accessed Dec. 16, 2021).

[136] J. Mazurek, A. Laganà, V. Dion, S. Etyemez, C. Carta, and M. R. Schilling, “Investigation of cellulose nitrate and cellulose acetate plastics in museum collections using ion chromatography and size exclusion chromatography,” *J. Cult. Herit.*, vol. 35, pp. 263–270, Jan. 2019, doi: 10.1016/j.culher.2018.05.011.

[137] H. Kono, H. Hashimoto, and Y. Shimizu, “NMR characterization of cellulose acetate: Chemical shift assignments, substituent effects, and chemical shift additivity,” *Carbohydr. Polym.*, vol. 118, pp. 91–100, Mar. 2015, doi: 10.1016/j.carbpol.2014.11.004.

[138] P. Luan and G. S. Oehrlein, “Characterization of Ultrathin Polymer Films Using p-Polarized ATR-FTIR and Its Comparison with XPS,” *Langmuir*, vol. 35, no. 12, pp. 4270–4277, Mar. 2019, doi: 10.1021/acs.langmuir.9b00316.

[139] H. W. Siesler, “Basic Principles of Near-Infrared Spectroscopy,” in *Handbook of Near-Infrared Analysis*, 3rd ed., CRC Press, 2007.

[140] S. Zhu, H. Chen, M. Wang, X. Guo, Y. Lei, and G. Jin, “Plastic solid waste identification system based on near infrared spectroscopy in combination with support vector machine,” *Adv. Ind. Eng. Polym. Res.*, vol. 2, no. 2, pp. 77–81, Apr. 2019, doi: 10.1016/j.aiepr.2019.04.001.

[141] S. Cichosz and A. Masek, “IR Study on Cellulose with the Varied Moisture Contents: Insight into the Supramolecular Structure,” *Materials*, vol. 13, no. 20, p. 4573, Oct. 2020, doi: 10.3390/ma13204573.

[142] K. Mitsui, T. Inagaki, and S. Tsuchikawa, “Monitoring of Hydroxyl Groups in Wood during Heat Treatment Using NIR Spectroscopy,” *Biomacromolecules*, vol. 9, no. 1, pp. 286–288, Jan. 2008, doi: 10.1021/bm7008069.

[143] M. Schwanninger, J. C. Rodrigues, and K. Fackler, “A Review of Band Assignments in near Infrared Spectra of Wood and Wood Components,” *J. Infrared Spectrosc.*, vol. 19, no. 5, pp. 287–308, Oct. 2011, doi: 10.1255/jnirs.955.

[144] B. Sun, J. Liu, S. Liu, and Q. Yang, “Application of FT-NIR-DR and FT-IR-ATR spectroscopy to estimate the chemical composition of bamboo (Neosinocalamus affinis Keng),” *Holzforschung*, vol. 65, no. 5, Aug. 2011, doi: 10.1515/hf.2011.075.

[145] K. Awa, H. Shinzawa, and Y. Ozaki, “An Effect of Cellulose Crystallinity on the Moisture Absorbability of a Pharmaceutical Tablet Studied by Near-Infrared Spectroscopy,” *Appl. Spectrosc.*, vol. 68, no. 6, pp. 625–632, Jun. 2014, doi: 10.1366/13-07273.

[146] T. Inagaki, H. W. Siesler, K. Mitsui, and S. Tsuchikawa, “Difference of the Crystal Structure of Cellulose in Wood after Hydrothermal and Aging Degradation: A NIR Spectroscopy and XRD Study,” *Biomacromolecules*, vol. 11, no. 9, pp. 2300–2305, Sep. 2010, doi: 10.1021/bm100403y.

[147] R. M. Correia *et al.*, “Portable near infrared spectroscopy applied to quality control of Brazilian coffee,” *Talanta*, vol. 176, pp. 59–68, Jan. 2018, doi: 10.1016/j.talanta.2017.08.009.

[148] L. R. Terra, J. V. Roque, C. C. Pola, I. M. Gonçalves, N. de F. F. Soares, and R. F. Teófilo, “Study of chemical compound spatial distribution in biodegradable active films using NIR hyperspectral imaging and multivariate curve resolution,” *J. Chemom.*, vol. 34, no. 1, Jan. 2020, doi:

10.1002/cem.3193.

[149] O. A. Fridman and A. V. Sorokina, “Criteria of efficiency of cellulose acetate plasticization,” *Polym. Sci. Ser. B*, vol. 48, no. 5, pp. 233–236, Oct. 2006, doi: 10.1134/S1560090406090028.

[150] V. J. McBrierty, C. M. Keely, F. M. Coyle, H. Xu, and J. K. Vij, “Hydration and plasticization effects in cellulose acetate: molecular motion and relaxation,” *Faraday Discuss.*, vol. 103, no. 0, pp. 255–268, Jan. 1996, doi: 10.1039/FD9960300255.

[151] A. Dubault, L. Bokobza, E. Gandin, and J. Halary, “Effects of molecular interactions on the viscoelastic and plastic behaviour of plasticized poly(vinyl chloride),” *Polym. Int.*, vol. 52, no. 7, pp. 1108–1118, Jul. 2003, doi: 10.1002/pi.1189.

[152] J. J. Workman, “Interpretive Spectroscopy for Near Infrared,” *Appl. Spectrosc. Rev.*, vol. 31, no. 3, pp. 251–320, Aug. 1996, doi: 10.1080/05704929608000571.

[153] R. G. Zhbankov, *Infrared Spectra of Cellulose and its Derivatives*. 1995. Accessed: Nov. 15, 2019. [Online]. Available: http://link.springer.com/openurl?genre=book&isbn=978-1-4899-2734-7

[154] F. Toja, A. Nevin, D. Comelli, M. Levi, R. Cubeddu, and L. Toniolo, “Fluorescence and Fourier-transform infrared spectroscopy for the analysis of iconic Italian design lamps made of polymeric materials,” *Anal. Bioanal. Chem.*, vol. 399, no. 9, pp. 2977–2986, Mar. 2011, doi: 10.1007/s00216-010-4323-2.

[155] C.-M. Popescu, P. T. Larsson, N. Olaru, and C. Vasile, “Spectroscopic study of acetylated kraft pulp fibers,” *Carbohydr. Polym.*, vol. 88, no. 2, pp. 530–536, Apr. 2012, doi: 10.1016/j.carbpol.2011.12.046.

[156] A. Pereira, A. Candeias, A. Cardoso, D. Rodrigues, P. Vandenabeele, and A. T. Caldeira, “Non-invasive methodology for the identification of plastic pieces in museum environment — a novel approach,” *Microchem. J.*, vol. 124, pp. 846–855, Jan. 2016, doi: 10.1016/j.microc.2015.07.027.

[157] J. Pajnik *et al.*, “Functionalization of polypropylene, polyamide and cellulose acetate materials with pyrethrum extract as a natural repellent in supercritical carbon dioxide,” *J. Supercrit. Fluids*, vol. 136, pp. 70–81, Jun. 2018, doi: 10.1016/j.supflu.2018.02.014.

[158] S. Y. Oh *et al.*, “Crystalline structure analysis of cellulose treated with sodium hydroxide and carbon dioxide by means of X-ray diffraction and FTIR spectroscopy,” *Carbohydr. Res.*, vol. 340, no. 15, pp. 2376–2391, Oct. 2005, doi: 10.1016/j.carres.2005.08.007.

[159] A. Pereira, A. T. Caldeira, B. Maduro, P. Vandenabeele, and A. Candeias, “Tortoiseshell or Polymer? Spectroscopic Analysis to Redefine a Purported Tortoiseshell Box with Gold Decorations as a Plastic Box with Brass,” *Appl. Spectrosc.*, vol. 70, no. 1, pp. 68–75, Jan. 2016, doi: 10.1177/0003702815615344.

[160] F. Bressan, R. Bertani, C. Furlan, F. Simionato, and S. Canazza, “An ATR-FTIR and ESEM study on magnetic tapes for the assessment of the degradation of historical audio recordings,” *J. Cult. Herit.*, vol. 18, pp. 313–320, Mar. 2016, doi: 10.1016/j.culher.2015.09.004.

[161] R. J. H. Clark, C. D. Flint, and A. J. Hempleman, “F.t.i.r. and Raman spectra of

triphenylphosphine, triphenylarsine, triphenylstibine, and dibenzylsulphide," *Spectrochim. Acta Part Mol. Spectrosc.*, vol. 43, no. 6, pp. 805–816, Jan. 1987, doi: 10.1016/0584-8539(87)80223-4.

[162] A. Marcilla, S. Garcia, and J. C. Garcia-Quesada, "Migrability of PVC plasticizers," *Polym. Test.*, vol. 27, no. 2, pp. 221–233, Apr. 2008, doi: 10.1016/j.polymertesting.2007.10.007.

[163] O. Klug and W. Forsling, "A Spectroscopic Study of Phthalate Adsorption on γ-Aluminum Oxide," *Langmuir*, vol. 15, no. 20, pp. 6961–6968, Sep. 1999, doi: 10.1021/la990105j.

[164] C. Bai, Q. Wei, and X. Ren, "Selective Extraction of Collagen Peptides with High Purity from Cod Skins by Deep Eutectic Solvents," *ACS Sustain. Chem. Eng.*, vol. 5, no. 8, pp. 7220–7227, Aug. 2017, doi: 10.1021/acssuschemeng.7b01439.

[165] N. Li, Y. Wang, K. Xu, Y. Huang, Q. Wen, and X. Ding, "Development of green betaine-based deep eutectic solvent aqueous two-phase system for the extraction of protein," *Talanta*, vol. 152, pp. 23–32, May 2016, doi: 10.1016/j.talanta.2016.01.042.

[166] Y. Jia *et al.*, "Deep eutectic solvent and agar: a new green gel to remove proteinaceous-based varnishes from paintings," *J. Cult. Herit.*, vol. 51, pp. 138–144, Sep. 2021, doi: 10.1016/j.culher.2021.08.001.

[167] A. P. Abbott, G. Capper, D. L. Davies, R. K. Rasheed, and V. Tambyrajah, "Novel solvent properties of choline chloride/urea mixtures," *Chem. Commun.*, no. 1, pp. 70–71, Jan. 2003, doi: 10.1039/B210714G.

[168] W. Li *et al.*, "Switching the basicity of ionic liquids by CO2," *Green Chem.*, vol. 10, no. 11, pp. 1142–1145, Nov. 2008, doi: 10.1039/B811624E.

[169] E. L. Smith, A. P. Abbott, and K. S. Ryder, "Deep Eutectic Solvents (DESs) and Their Applications," *Chem. Rev.*, vol. 114, no. 21, pp. 11060–11082, Nov. 2014, doi: 10.1021/cr300162p.

[170] J. C. Lin and N. Gant, "Chapter 2.3 - The Biochemistry of Choline," in *Magnetic Resonance Spectroscopy*, C. Stagg and D. Rothman, Eds. San Diego: Academic Press, 2014, pp. 104–110. doi: 10.1016/B978-0-12-401688-0.00008-2.

[171] M. Francisco, A. van den Bruinhorst, and M. C. Kroon, "Low-Transition-Temperature Mixtures (LTTMs): A New Generation of Designer Solvents," *Angew. Chem. Int. Ed.*, vol. 52, no. 11, pp. 3074–3085, 2013, doi: https://doi.org/10.1002/anie.201207548.

[172] I. Zahrina, M. Nasikin, and K. Mulia, "Evaluation of the interaction between molecules during betaine monohydrate-organic acid deep eutectic mixture formation," *J. Mol. Liq.*, vol. 225, pp. 446–450, Jan. 2017, doi: 10.1016/j.molliq.2016.10.134.

[173] Y.-C. Guo, C. Cai, and Y.-H. Zhang, "Observation of conformational changes in ethylene glycol–water complexes by FTIR–ATR spectroscopy and computational studies," *AIP Adv.*, vol. 8, no. 5, p. 055308, May 2018, doi: 10.1063/1.4995975.

[174] D. V. Wagle, C. A. Deakyne, and G. A. Baker, "Quantum Chemical Insight into the Interactions and Thermodynamics Present in Choline Chloride Based Deep Eutectic Solvents," *J. Phys. Chem. B*, vol. 120, no. 27, pp. 6739–6746, Jul. 2016, doi: 10.1021/acs.jpcb.6b04750.

[175] S. P. Simeonov and C. A. M. Afonso, “Basicity and stability of urea deep eutectic mixtures,” *RSC Adv.*, vol. 6, no. 7, pp. 5485–5490, Jan. 2016, doi: 10.1039/C5RA24558C.

[176] C.-X. Zeng, S.-J. Qi, R.-P. Xin, B. Yang, and Y.-H. Wang, “Synergistic behavior of betaine–urea mixture: Formation of deep eutectic solvent,” *J. Mol. Liq.*, vol. 219, pp. 74–78, Jul. 2016, doi: 10.1016/j.molliq.2016.02.076.

[177] S. Preibisch, S. Saalfeld, and P. Tomancak, “Globally optimal stitching of tiled 3D microscopic image acquisitions,” *Bioinformatics*, vol. 25, no. 11, pp. 1463–1465, Jun. 2009, doi: 10.1093/bioinformatics/btp184.

[178] S. Prati, G. Sciutto, I. Bonacini, and R. Mazzeo, “New Frontiers in Application of FTIR Microscopy for Characterization of Cultural Heritage Materials,” *Top. Curr. Chem.*, vol. 374, no. 3, p. 26, Apr. 2016, doi: 10.1007/s41061-016-0025-3.

[179] R. Mazzeo, E. Joseph, S. Prati, and A. Millemaggi, “Attenuated Total Reflection–Fourier transform infrared microspectroscopic mapping for the characterisation of paint cross-sections,” *Anal. Chim. Acta*, vol. 599, no. 1, pp. 107–117, Sep. 2007, doi: 10.1016/j.aca.2007.07.076.

[180] V. I. Kovalenko, R. M. Mukhamadeeva, L. N. Maklakova, and N. G. Gustova, “Interpretation of the IR spectrum and structure of cellulose nitrate,” *J. Struct. Chem.*, vol. 34, no. 4, pp. 540–547, 1994, doi: 10.1007/BF00753522.

[181] S. Noohi and H. Asadian, “Application of FTIR Microscopy to Identify Some Glass Plates of Golestan Palace Photo Archive,” *Nian Conserv. Sci. J.*, vol. 01, no. 01, pp. 48–53, Sep. 2017, doi: 10.30699/ics.journal.01.48.

[182] F. A. Miller and C. H. Wilkins, “Infrared Spectra and Characteristic Frequencies of Inorganic Ions,” *Anal. Chem.*, vol. 24, no. 8, pp. 1253–1294, Aug. 1952, doi: 10.1021/ac60068a007.

[183] M. Viertorinne, J. Valkonen, I. Pitkänen, M. Mathlouthi, and J. Nurmi, “Crystal and molecular structure of anhydrous betaine, (CH3)3NCH2CO2,” *J. Mol. Struct.*, vol. 477, no. 1, pp. 23–29, Mar. 1999, doi: 10.1016/S0022-2860(98)00613-9.

[184] K. Biernacki, H. K. S. Souza, C. M. R. Almeida, A. L. Magalhães, and M. P. Gonçalves, “Physicochemical Properties of Choline Chloride-Based Deep Eutectic Solvents with Polyols: An Experimental and Theoretical Investigation,” *ACS Sustain. Chem. Eng.*, vol. 8, no. 50, pp. 18712–18728, Dec. 2020, doi: 10.1021/acssuschemeng.0c08288.

[185] C. Du, B. Zhao, X.-B. Chen, N. Birbilis, and H. Yang, “Effect of water presence on choline chloride-2urea ionic liquid and coating platings from the hydrated ionic liquid,” *Sci. Rep.*, vol. 6, no. 1, p. 29225, Jul. 2016, doi: 10.1038/srep29225.

[186] J. Baran *et al.*, “Structure and polarised IR and Raman spectra of the solid complex betaine–trichloroacetic acid,” *J. Mol. Struct.*, vol. 550–551, pp. 21–41, Sep. 2000, doi: 10.1016/S0022-2860(00)00381-1.

[187] J. Grdadolnik and Y. Maréchal, “Urea and urea–water solutions—an infrared study,” *J. Mol. Struct.*, vol. 615, no. 1–3, pp. 177–189, Sep. 2002, doi: 10.1016/S0022-2860(02)00214-4.

[188] M. M. Ilczyszyn and H. Ratajczak, “Polarized vibrational spectra of betaine monohydrate single crystal,” *Vib. Spectrosc.*, vol. 10, no. 2, pp. 177–189, Jan. 1996, doi: 10.1016/0924-2031(95)00040-2.

[189] K. Krishnan and R. S. Krishnan, “Raman and infrared spectra of ethylene glycol,” *Proc. Indian Acad. Sci. - Sect. A*, vol. 64, no. 2, p. 111, Aug. 1966, doi: 10.1007/BF03047675.

[190] R. Häkkinen and A. Abbott, “Solvation of carbohydrates in five choline chloride-based deep eutectic solvents and the implication for cellulose solubility,” *Green Chem.*, vol. 21, no. 17, pp. 4673–4682, 2019, doi: 10.1039/C9GC00559E.

[191] M. Zdanowicz, K. Wilpiszewska, and T. Spychaj, “Deep eutectic solvents for polysaccharides processing. A review,” *Carbohydr. Polym.*, vol. 200, pp. 361–380, Nov. 2018, doi: 10.1016/j.carbpol.2018.07.078.

[192] G. Mitchell, F. France, A. Nordon, P. Tang, and L. T. Gibson, “Assessment of historical polymers using attenuated total reflectance-Fourier transform infra-red spectroscopy with principal component analysis,” *Herit. Sci.*, vol. 1, no. 1, p. 28, 2013, doi: 10.1186/2050-7445-1-28.

[193] D. S. Moore and S. D. McGrane, “Comparative infrared and Raman spectroscopy of energetic polymers,” *J. Mol. Struct.*, vol. 661–662, pp. 561–566, Dec. 2003, doi: 10.1016/S0022-2860(03)00522-2.

[194] S. Berthumeyrie, S. Collin, P.-O. Bussiere, and S. Therias, “Photooxidation of cellulose nitrate: New insights into degradation mechanisms,” *J. Hazard. Mater.*, vol. 272, pp. 137–147, May 2014, doi: 10.1016/j.jhazmat.2014.02.039.

[195] M. Edge, N. S. Allen, M. Hayes, P. N. K. Riley, C. V. Horie, and J. Luc-Gardette, “Mechanisms of deterioration in cellulose nitrate base archival cinematograph film,” *Eur. Polym. J.*, vol. 26, no. 6, pp. 623–630, Jan. 1990, doi: 10.1016/0014-3057(90)90218-S.

[196] J. Kong and S. Yu, “Fourier Transform Infrared Spectroscopic Analysis of Protein Secondary Structures,” *Acta Biochim. Biophys. Sin.*, vol. 39, no. 8, pp. 549–559, Aug. 2007, doi: 10.1111/j.1745-7270.2007.00320.x.

[197] G. Vyskočilová, M. Ebersbach, R. Kopecká, L. Prokeš, and J. Příhoda, “Model study of the leather degradation by oxidation and hydrolysis,” *Herit. Sci.*, vol. 7, no. 1, p. 26, Dec. 2019, doi: 10.1186/s40494-019-0269-7.

[198] K. Belbachir, R. Noreen, G. Gouspillou, and C. Petibois, “Collagen types analysis and differentiation by FTIR spectroscopy,” *Anal. Bioanal. Chem.*, vol. 395, no. 3, pp. 829–837, Oct. 2009, doi: 10.1007/s00216-009-3019-y.

[199] G. Ritzhaupt and J. P. Devlin, “Infrared spectra of nitric and hydrochloric acid hydrate thin films,” p. 6.

[200] “FilmCare.org.” https://www.filmcare.org/ (accessed Jul. 11, 2019).

[201] R. Hou, X. Luo, C. Liu, L. Zhou, J. Wen, and Y. Yuan, “Enhanced degradation of triphenyl phosphate (TPHP) in bioelectrochemical systems: Kinetics, pathway and degradation mechanisms,” *Environ. Pollut.*, vol. 254, p. 113040, Nov. 2019, doi:

10.1016/j.envpol.2019.113040.

[202] Y. Shinagawa, M. Murayama, and Y. Sakaino, “Investigation of the Archival Stability of Cellulose Triacetate Film: The Effect of Additives to CTA Support.,” *Spec. Publ. R. Soc. Chem.*, no. 105, pp. 138–150, 1992.

[203] B. Lavédrine, A. Fournier, and G. Martin, *Preservation of Plastic Artefacts in Museum Collections*. Comité Des Travaux Historiques Et Scientifiques, 2012.

[204] C. Morales Muñoz, “Surface modification of plasticized PVC by dry cleaning methods: Consequences for artworks,” *Appl. Surf. Sci.*, vol. 256, no. 11, pp. 3567–3572, Mar. 2010, doi: 10.1016/j.apsusc.2009.12.156.

[205] G. Wypych and A. Wypych, *Databook of green solvents*. Toronto: ChemTec Publ, 2014.

[206] J. Yiming *et al.*, “A new bio-based organogel for the removal of wax coating from indoor bronze surfaces,” *Herit. Sci.*, vol. 7, no. 1, p. 34, Dec. 2019, doi: 10.1186/s40494-019-0276-8.

[207] F. Aricò and P. Tundo, “Dimethyl carbonate as a modern green reagent and solvent,” *Russ. Chem. Rev.*, vol. 79, no. 6, pp. 479–489, Aug. 2010, doi: 10.1070/RC2010v079n06ABEH004113.

[208] K. Shukla and V. C. Srivastava, “Diethyl carbonate: critical review of synthesis routes, catalysts used and engineering aspects,” *RSC Adv.*, vol. 6, no. 39, pp. 32624–32645, 2016, doi: 10.1039/C6RA02518H.

[209] PubChem, “Diethyl carbonate.” https://pubchem.ncbi.nlm.nih.gov/compound/7766 (accessed Oct. 12, 2020).

[210] PubChem, “Dimethyl carbonate.” https://pubchem.ncbi.nlm.nih.gov/compound/12021 (accessed Oct. 12, 2020).

[211] PubChem, “Isoamyl acetate.” https://pubchem.ncbi.nlm.nih.gov/compound/31276 (accessed Oct. 12, 2020).

[212] S. Ramakrishna, Ed., *An introduction to electrospinning and nanofibers*. Hackensack, NJ: World Scientific, 2005.

[213] Y. Foucaud *et al.*, “Adsorption mechanisms of fatty acids on fluorite unraveled by infrared spectroscopy and first-principles calculations,” *J. Colloid Interface Sci.*, vol. 583, pp. 692–703, Feb. 2021, doi: 10.1016/j.jcis.2020.09.062.